Funded by
DFG Deutsche Forschungsgemeinschaft
German Research Foundation

JG|U UNIVERSITÄTSmedizin. MAINZ

ANALYSIS OF SENESCENCE IN GLIOBLASTOMA CELLS EXPOSED TO TEMOZOLOMIDE

A study for the identification of senescence maintaining pathways and novel senolytic agents

Dissertation for the degree of doctor of natural sciences
at the faculty of biology
of the Johannes Gutenberg-University Mainz

Submitted by
Lea Constanze Beltzig
born 07.12.1991 in Seeheim-Jugenheim

Mainz, 2023

Dean: Univ.-Prof. Dr. Eckhard Thines

1. Assessor: Prof. Dr. Bernd Kaina

2. Assessor: PD Dr. Anne Régnier-Vigouroux

Date of oral defence:

Content

Abstract IV
Zusammenfassung VI
1. Introduction 1
1.1. Brain Cancer: Glioblastoma 1
1.1.1. Classification 1
1.1.2. Incidences and causes 3
1.1.3. Diagnosis 4
1.1.4. Treatment 5
1.2. Temozolomide 6
1.2.1. Genotoxic effects of temozolomide 8
1.2.2. DNA damage induced by O^6methylguanine 10
1.2.3. Cytotoxicity induced by O^6methylguanine 13
1.2.3.1. Induction of apoptosis 13
1.2.3.2. Induction of senescence 16
1.3. CCNU 18
1.4. Methadone 20
1.5. Senolytic agents 21
1.5.1. Artesunate 21
1.5.2. Curcumin 22
1.5.3. Fisetin 23
1.6. Aim of the study 24
2. Materials 25
2.1. Chemicals and consumables 25
2.2. Technical Instruments 26
2.3. Software 28
2.4. Buffers and solutions 28
2.5. Antibodies 30
2.6. Dyes and kits 31
3. Methods 32
3.1. Cells and cell culture 32
3.2. Drugs and treatments 33
3.2.1. Temozolomide 33
3.2.2. Natural and small molecule compounds 34
3.2.3. Ionizing radiation 35

3.3. Quantification of apoptosis 35
3.4. Quantification of senescent cells 36
3.5. Immunofluorescence 37
3.6. Preparation of cell lysates 38
3.7. Determination of protein concentrations by Bradford 38
3.8. SDS-PAGE and Western Blot analysis 39
3.9. Comet Assay 40
3.10. MTT assay 41
3.11. Immunohistochemistry and TUNEL staining 42
3.12. Patients and ethic statement 42
3.13. Statistical analysis 43
4. Results 44
4.1. Evaluation of TMZ-induced DSBs and DDR 44
4.1.1. Kinetics of TMZ-induced DSBs 45
4.1.2. Cell death and senescence induced by TMZ treatment 47
4.2. Characteristics of senescent cells 48
4.2.1. Morphological characteristics 48
4.2.2. Analysis of the DDR in senescent cells 52
4.2.3. Assessment of DNA damage repair in senescent cells 53
4.2.4. Detection of ROS in senescent cells 55
4.3. Identification of senescence maintaining pathways 56
4.3.1. Regulation of apoptosis 56
4.3.2. Role of the DDR 59
4.3.3. Role of DNA repair 62
4.3.4. Role of autophagy 66
4.4. Screening for improved treatment options 68
4.4.1. Combinatorial treatment of TMZ and IR 69
4.4.2. Effect of IR on TMZ-induced senescent cells 71
4.4.3. Combinatorial treatment of TMZ and CCNU 72
4.4.4. Combinatorial treatment of TMZ and methadone 73
4.4.4.1. Cyto- and genotoxicity of MTD 73
4.4.4.2. Influence of MTD on TMZ-induced cell death and senescence 77
4.5. Identification of senolytic agents 80
4.5.1. MCOPPB 80
4.5.2. Artesunate 81
4.5.3. Curcumin 82

4.5.3.1. Cyto- and genotoxic effects of curcumin 82
4.5.3.2. Effect of curcumin on TMZ-induced senescence 86
4.5.3.3. Fisetin 88
4.6. In situ analysis of senescence markers 90
5. Discussion 92
5.1. Senescence is the main trait induced by TMZ 93
5.2. Evaluation of DSBs following TMZ treatment 94
5.3. Senescent cells show an active DNA damage response 95
5.4. An active DNA damage response is necessary to maintain senescence 96
5.5. Senescence is maintained by inhibition of the intrinsic apoptotic pathway 97
5.6. Autophagy is essential for senescence maintenance 98
5.7. Senescent cells require DSBs repair 99
5.8. Timing is key in combinatorial treatment with TMZ and IR or CCNU 100
5.9. Can methadone be used as adjuvant for TMZ treatment? 101
5.10. Possible senolytic activity of curcumin 103
5.11. MCOPPB is not senolytic in GBM cells 104
5.12. Artesunate and fisetin are novel senolytic agents in GBM cells 104
6. Conclusions 106
7. Publication bibliography 107
8. Supplemental material 126
8.1. Supplemental figures 126
8.2. ImageJ coding 130
8.2.1. Macro for nuclei and foci counting 130
8.3. List of tables 132
8.4. List of figures 132
8.5. List of abbreviations 134
8.6. List of publications 138
8.7. Acknowledgement 139
8.8. Eidesstattliche Erklärung 140
8.9. Curriculum vitae 141

Abstract

The alkylating drug Temozolomide (TMZ) in combination with ionising radiation (IR) represents the first-line treatment in glioblastoma (GBM) therapy. While cancer treatment aims for triggering cell death to eliminate the tumour, cancer cells developed strategies to escape cell death: they activate cell survival pathways, including cellular senescence (CSEN) upon chemotherapeutic treatment. Over the past years *in vitro* and *in vivo* studies demonstrated that senescent cells could escape their senescent state and re-start proliferation, which may result in delayed tumour progression. Additionally, CSEN is accompanied by the senescence associated secretory phenotype (SASP), which includes pro-inflammatory cytokines, and drives senescence and tumorigenesis, rendering CSEN an unfavourable outcome of chemotherapy. A better understanding of the cellular responses to chemotherapy as well as strategies to eliminate senescent cells are therefore desirable.

Here, we focused on the effect of TMZ treatment regarding CSEN of the malignant brain tumour GBM. The following main questions were addressed: 1) What are the kinetics of TMZ-induced genotoxic, cytotoxic, and cytostatic effects and how are senescent cells characterised? 2) Which pathways are responsible for the maintenance of GBM cells in the TMZ-induced senescent state? 3) Which treatment options, including natural and synthetic compounds, can be used to reduce the load of TMZ-induced senescent cells in GBM?

To gain insight into the cellular processes following TMZ treatment, we analysed the formation of DSBs over time, and the induction of early and late apoptosis/necrosis (cell death) and CSEN. We found a significant level of DNA double-strand breaks (DSBs) 3 d after treatment which persisted up to 10 d following the onset of TMZ exposure. In line with the increase in DSBs, cell death and predominantly CSEN were provoked 3 d following TMZ treatment and increased up to day 5 and 8, respectively. We then analysed TMZ-induced senescent cells and identified pathways essentially involved in maintaining the senescent state. The DNA damage response (DDR) factors ATM, ATR, CHK1, CHK2, p53 and p21 were found to be active in TMZ-induced senescent cells. For senescence maintenance, the ATM/ATR-CHK1-p53-p21 axis as well was a pathway involving NF-kB were involved, as revealed from inhibitor experiments. Since the autophagy inhibitor chloroquine was senolytic, we conclude that activation of autophagy is required for keeping cells in the senescent state. To increase cell death levels following TMZ treatment, we co-treated LN229 and A172 cells with IR, N-(2-chloroethyl)-N'-cyclohexyl-N-nitrosourea (CCNU, lomustine) or methadone (MTD) and screened for natural compounds that specifically drive senescent cells into cell death, while proliferating cells are unharmed. No increase in cell death levels in the senescent cell population was observed upon co-treatment of GBM cells with TMZ and CCNU or MTD.

An additive effect on cell death was observed when GBM cells were first treated with TMZ and irradiated 3 h later, or first irradiated and treated with TMZ 6 h later.

Screening of natural compounds for their senolytic activity identified artesunate and fisetin, but not curcumin, as novel senolytic agents in GBM cells *in vitro* under the treatment conditions used. In a last step we identified senescent cells in patient derived tumour samples from matched primary and recurrent GBM via histochemistry staining. Increased DSBs combined with increased levels of trimethylated lysin on histone 3 (H3K27me3) served as senescence marker. Comparison of primary and recurrent tumour samples showed significantly higher DSBs and H3K27me3 but significantly lower cell death levels in the recurrent tumour samples. These results indicate that not only *in vitro* but also *in vivo* senescent cells accumulate following TMZ treatment of GBM.

Overall, the data presented in this study demonstrate that TMZ-induced CSEN is the main trait in GBM cells *in vitro* and very likely also *in vivo*. The identification of proteins involved in the TMZ-induced CSEN maintaining pathways in GBM cells might provide a reasonable support in the treatment of cancer. Also, the identification of novel senolytic agents and timing of the combination treatment with TMZ and IR in GBM cells *in vitro* can help to develop optimized treatment regiments for GBM.

Zusammenfassung

Das DNA-methylierende Zytostatikum Temozolomid (TMZ) in Kombination mit ionisierender Strahlung (IR) ist die erste Wahl bei der Behandlung des bösartigen Hirntumors Glioblastom (GBM). Während die Krebsbehandlung darauf abzielt, den Zelltod spezifisch in Tumorzellen auszulösen, um den Tumor zu beseitigen, haben die Krebszellen Strategien entwickelt, um dem Zelltod zu entgehen: Sie aktivieren Zellüberlebenswege, einschließlich die zelluläre Seneszenz (*engl. cellular senescence,* (CSEN)) bei chemotherapeutischer Behandlung. In den letzten Jahren haben In-vitro- und In-vivo-Studien gezeigt, dass seneszente Zellen ihrem seneszenten Zustand entkommen und sich wieder vermehren können, was zu einer verzögerten Tumorprogression führen kann. Darüber hinaus wird die CSEN von einem Seneszenz-assoziierten sekretorischen Phänotyp (SASP) begleitet, welches die Sekretion entzündungsfördernder Zytokine beinhaltet und die Seneszenz und Tumorigenese fördert, was CSEN zu einem ungünstigen Ergebnis der Chemotherapie macht. Ein besseres Verständnis der zellulären Reaktionen auf die Chemotherapie sowie Strategien zur Beseitigung seneszenter Zellen sind daher wünschenswert.

Hier haben wir uns auf die Auswirkungen der TMZ-Behandlung auf die CSEN des malignen Hirntumors GBM konzentriert. Die folgenden Hauptfragen wurden untersucht: 1) Wie ist die Kinetik der TMZ-induzierten genotoxischen, zytotoxischen und zytostatischen Effekte und wie werden seneszente Zellen charakterisiert? 2) Welche Signalwege sind für die Aufrechterhaltung des TMZ-induzierten seneszenten Zustands von GBM-Zellen verantwortlich? 3) Welche Behandlungsmöglichkeiten, einschließlich natürlicher und synthetischer Substanzen, können eingesetzt werden, um die Belastung durch TMZ-induzierte seneszente Zellen im GBM zu verringern?

Um einen Einblick in die zellulären Prozesse nach einer TMZ-Behandlung zu erhalten, analysierten wir die Bildung von DNA-Doppelstrangbrüchen (DSBs) im Zeitverlauf sowie die Induktion von früher und später Apoptose/Nekrose (Zelltod) und CSEN. Drei Tage nach der Behandlung mit TMZ fanden wir ein signifikantes Niveau von DSBs, welches bis zu 10 Tage nach Beginn der TMZ-Exposition anhielt. Im Einklang mit dem Anstieg der DSBs wurden 3 Tage nach der TMZ-Behandlung Zelltod und vor allem CSEN ausgelöst, die bis zum 5. bzw. 8. Tag nach Beginn der Behandlung zunahmen. Anschließend analysierten wir TMZ-induzierte seneszente Zellen und identifizierten Signalwege, die wesentlich an der Aufrechterhaltung des seneszenten Zustands beteiligt sind. Es wurde festgestellt, dass die DNA-Schadensreaktionsfaktoren ATM, ATR, CHK1, CHK2, p53 und p21 in TMZ-induzierten seneszenten Zellen aktiv sind. Durch Inhibitor-Experimenten wurde gezeigt, dass für die Aufrechterhaltung der Seneszenz die ATM/ATR-CHK1-p53-p21-Achse sowie ein NF-kB-Signalweg involviert sind.

Da der Autophagie-Hemmer Chloroquin senolytisch wirkte, schlussfolgern wir, dass die Aktivierung der Autophagie wesentlich für die Aufrechterhaltung des seneszenten Zustands der Zellen ist. Um den Zelltod nach einer TMZ-Behandlung zu erhöhen, behandelten wir LN229- und A172-Zellen gleichzeitig mit IR, N-(2-Chlorethyl)-N'-cyclohexyl-N-nitrosoharnstoff (CCNU, Lomustin) oder Methadon (MTD) und suchten nach natürlichen Verbindungen, die seneszente Zellen spezifisch in den Zelltod treiben, während proliferierende Zellen unversehrt bleiben. Bei der gleichzeitigen Behandlung von GBM-Zellen mit TMZ und CCNU oder MTD wurde kein Anstieg des Zelltods in der seneszenten Zellpopulation beobachtet. Ein additiver Effekt auf den Zelltod wurde beobachtet, als die GBM-Zellen erst mit TMZ behandelt und 3 Stunden später bestrahlt wurden, oder erst bestrahlt und 6 h später mit TMZ behandelt wurden. Beim Screening von Naturstoffen auf ihre senolytische Aktivität unter den verwendeten Versuchsbedingungen wurden Artesunat und Fisetin, jedoch nicht Curcumin, als neuartige senolytische Wirkstoffe in GBM-Zellen in vitro identifiziert.

In einem letzten Schritt identifizierten wir mittels histochemischer Färbung seneszente Zellen in von Patienten entnommenen Tumorproben von gematchten primären und rezidivierenden GBM. Erhöhte DSBs in Kombination mit erhöhten Werten von trimethyliertem Lysin auf Histon 3 (H3K27me3) dienten als Seneszenzmarker. Der Vergleich von primären und rezidivierenden GBM-Tumorproben ergab signifikant höhere DSBs und H3K27me3, aber signifikant niedrigere Zelltodwerte im Rezidiv. Diese Ergebnisse deuten darauf hin, dass sich nach einer TMZ-Behandlung von GBM nicht nur in vitro, sondern auch in vivo seneszente Zellen ansammeln.

Insgesamt zeigen die in dieser Studie präsentierten Daten, dass TMZ-induziertes CSEN das Hauptmerkmal in GBM-Zellen in vitro und sehr wahrscheinlich auch in vivo ist. Die Identifizierung von Proteinen, die an den TMZ-induzierten CSEN-Erhaltungswegen in GBM-Zellen beteiligt sind, könnte eine sinnvolle Unterstützung bei der Behandlung von Krebs sein. Auch die Identifizierung neuartiger senolytischer Wirkstoffe und die Untersuchung der zeitlichen Abfolge der Kombinationsbehandlung mit TMZ, IR und Senolytika an GBM-Zellen könnte dazu beitragen, optimierte Behandlungsschemata für die Therapie des GBM zu entwickeln.

1. Introduction

Cellular senescence (CSEN) has long been an accepted and even welcome side effect of chemotherapy that initially aims to destroy cancerous cells. Since senescent cells do not proliferate, they have been categorised as not harmful for the patient. Over the past few years, however, it became evident that senescent cells can escape from cell cycle arrest and re-start proliferation, leading to a delayed progression of the tumour following treatment (Saleh et al. 2019; Le Duff et al. 2018). Also, senescent cells secrete pro-inflammatory cytokines and interleukins, which is a hallmark of the senescence-associated secretory phenotype (SASP). The secretion of the SASP factors into healthy and cancerous tissue leads to inflammation, re-enforcement of senescence and, controversially, tumour progression (Faget et al. 2019). Understanding therapy induced CSEN in cancer and finding strategies to reduce it are desirable research goals.

Using the glioblastoma (GBM) cell lines LN229 and A172 as an *in vitro*-model system, we analysed cellular responses of GBM to the alkylating agent temozolomide (TMZ). This study aimed to better understand the induction of DNA double-strand breaks (DSBs), CSEN and early and late apoptosis/necrosis (cell death) upon treatment with TMZ. Also, analyses of senescent cell populations and the screening for natural compounds that specifically drive senescent cells into cell death, while leaving proliferating cells unharmed, was performed to help finding additional treatment options.

1.1. Brain Cancer: Glioblastoma

1.1.1. Classification

Brain tumours have first been discovered in 1873 and are defined as a mass or growth of abnormal cells in the brain (Shah and Kochar 2018). Depending on the origin of the cells causing the tumour, they are categorized as either primary or metastatic. While primary brain tumours have their origin in the brain or the direct surrounding tissue, metastatic brain tumours arise outside from the brain and later spread to the brain (Brain Tumors - Classifications, Symptoms, Diagnosis and Treatments 2021; Brain tumours | Cancer Research UK 2021; nhs.uk NaN). GBM are primary brain tumours that originate from glial cells in the brain.

The world health organization (WHO) further classifies tumours of the central nervous system into categories, families, and types. The categories depend on the origin of the tumour within the brain.

The families are differentiated by histological and immunohistochemical characteristics, as well as adult-type and paediatric-type. For classification of the tumour types, molecular diagnostics are consulted. They are subject to constant changes based on better understanding of specific tumour biology and increased utilisation of molecular markers.

The GBM is classified in the category of gliomas/glioneuronal tumours and neuronal tumours. It is further differentiated in the family of adult-type diffuse gliomas as glioblastoma with either isocitrate dehydrogenase 1 (IDH1) wild-type (wt) or IDH1 mutated (mt). If the IDH1 status cannot be determined, GBM is characterised as not otherwise specified (Louis et al. 2021). Other important diagnostic markers are the promoter methylation status of the O^6-methylguanine-DNA methyltransferase (MGMT) and the absence or presence of the phosphatase and tensin homolog (PTEN). A cohort study using 444 adult gliomas showed a worse outcome in GBM with IDH1 wt compared to IDH1 mt. *MGMT* promoter methylation, as well as PTEN deletion was associated with a better overall survival (OS) (Brito et al. 2019).

The grades of brain tumours, characterising how severe a tumour is, are based on cytological atypia, mitotic activity, microvascular proliferation, and necrosis. Benign brain tumours are graded as low-grade 1 or 2 tumours. They are slow-growing masses that do not tend to invade or damage the surrounding tissue, hence overall survival is high. While grade 1 tumours do not spread through the body and are unlikely to recur, grade 2 tumours might reoccur as high-grade tumours (Gupta and Dwivedi 2017; Louis et al. 2016). Malignant brain tumours are classified as high-grade 3 or 4 tumours. They grow faster than benign tumours, infiltrate the surrounding tissue and might spread through the body, e.g., by forming metastases. By restricting nutrients, space, and blood flow, they damage healthy tissue. Having removed the primary tumour, recurrences are common, often rapid, and overall survival is poor (Gupta and Dwivedi 2017; Louis et al. 2016). GBM is the most invasive and most aggressive brain tumour. It has a 5-year survival rate of less than 6 % and a median survival of 15 months. Recurrences occur about 5 months following resection of the tumour (Glioblastoma Multiforme – Symptoms, Diagnosis and Treatment Options 2021; Tan et al. 2020). It shows microvascular proliferation, many mitotic figures and is prone to necrosis (Wesseling et al. 1995; Jellinger 1978). Metastasis arising from GBM are rare but have been found in e.g., lymph nodes, lung, and pleura (Robert and Wastie 2008). Based on the beforementioned criteria, GBM is a grade 4 brain tumour according to the WHO classification.

1.1.2. Incidences and causes

GBM has rising incidence rates in several countries. According to the Central Brain Tumor Registry of the United States (CBTRUS), GBM had an incidence rate of 2.6 per 100,000 people-years between 1990 and 1994 (Surawicz et al. 1999). Between 2005 and 2009 it increased to 3.19 and then further to 3.21 in the years between 2011 and 2015 (Dolecek et al. 2012; Ostrom et al. 2018). The latest CBRTUS report states an incidence rate of 3.23 between 2014 and 2018 (Low et al. 2022). A study conducted in England shows an even higher increase in GBM incidences. In the 20 years between 1995 and 2015, the incidence rates almost doubled, from 2.4 to 5.0 per 100000 people-years (Philips et al. 2018). In Finland, an increase of 1.6 % was detected between 2000 and 2003 (Korja et al. 2019). According to the CBTRUS studies, gliomas account for about 78-81 % of malignant tumours, and about 54-57 % of gliomas are GBM (Surawicz et al. 1999; Dolecek et al. 2012; Ostrom et al. 2018; Low et al. 2022).

Risk factors known to have an impact on cancer development have been explored for their involvement in GBM development. So far, no substantial evidence has been conducted that life-style factors such as drug use, smoking and alcohol consumption are associated with GBM development. Also, increased usage of mobile phones does not seem to correlate with an increase in GBM development (Hochberg et al. 1990; Grochans et al. 2022; Brain tumour risk in relation to mobile telephone use: results of the INTERPHONE international case-control study 2010). Studies evaluating the effect of overweight and obesity on the risk of GBM development showed contrary results. While some studies found a correlation between a low body mass index and a lower risk, and obesity and a higher risk for GBM development in women, others could not demonstrate a connection between the two (Sergentanis et al. 2015; Wiedmann et al. 2017). Investigation of other environmental factors such as the exposure to pesticides on the risk of GBM development resulted in conflicting results. Exposure to chemicals and air pollution did not correlate with an increase in GBM development (Piel et al. 2019; Fallahi et al. 2017; Carles et al. 2017; Samanic et al. 2008; Andersen et al. 2018).

The only known relation to an increased risk for GBM development is age, gender, and hereditary predisposition. A correlation between age and diagnosis with GBM was demonstrated. While children are only rarely diagnosed, the incidences increase in age with a peak of newly diagnosed GBM at 75-84 years of age and a drop thereafter. The age of diagnosis is in elderly 64 years of age (Ostrom et al. 2013). Over the years GBM has been reported 1.12 – 2.59 times more often in men than in women worldwide, showing a clear gender predisposition (Grochans et al. 2022). Also, ethnicity seems to play a role. White seem to be more prone to GBM development than Hispanic, while Hispanic are more often diagnosed than Black, and Black more often than Asian

(Grochans et al. 2022). About 5 % of gliomas are familial and about 3.5 % are caused by neurofibromatosis type 1 and 2, demonstrating a genetic predisposition in some cases (Wrensch et al. 1997; Kamihara et al. 2017; Stefanaki et al. 2012). A prevalence of GBM development following ionising radiation (IR) has been demonstrated in 17 out of 100 analysed subjects, although, the latency between IR and GBM diagnosis varied between 3 and 37 years making a direct connection difficult (Hodges et al. 1992).

Overall, the studies demonstrate that even though GBM is the most common malignant brain tumour with increasing incidences and poor survival rates, the exact causes for GBM development have yet to be determined.

1.1.3. Diagnosis

As a primary brain tumour, GBM usually presents itself through symptoms like increased intracranial pressure, tissue destruction or compression of specialized regions within the brain. These further cause symptoms like severe headaches, seizures, unilateral weakness, personality changes, memory loss and others. Since they are not exclusive for brain tumours, a diagnosis is often difficult (Allen Perkins and Gerald Liu 2016; Hadidchi et al. 2019; Cahill et al. 2012). If a tumour is suspected, brain imaging is needed to confirm the diagnosis. The most used anatomical imaging tool is the magnetic resonance imaging (MRI) combined with computed tomography with and without contrast staining. To gain information about physiologic, metabolic, or functional tumour biology, positron emission tomography-MRI is used. These images can provide information about important characteristics, such as tumour cell proliferation, hypoxia and amino acid transport, helping to identify and treat brain tumours (Fink et al. 2015; Allen Perkins and Gerald Liu 2016). If, based on the imaging, a brain tumour is confirmed, a brain biopsy is taken to further specify the tumour classification according to the WHO using histopathological staining procedures (Allen Perkins and Gerald Liu 2016).

1.1.4. Treatment

The first step in GBM treatment is surgical removal of the tumour. Usually, surgical dissection of a tumour aims to remove all cancerous tissue from the brain while remaining complete nerve function. In GBM, however, complete resection of the tumour is impossible due to its highly infiltrative nature. Boundaries between tumour and healthy brain tissue often cannot be separated. Hence, following maximum safe resection of GBM, tumour cells remain within the brain (So et al. 2021; Seker-Polat et al. 2022). Nevertheless, surgical removal of the main tumour mass is important as it has been demonstrated by a significant positive correlation between longer progression free survival (PFS) and OS in patients with greater extend of resection (Keles et al. 1999; Stummer et al. 2006; Hentschel and Sawaya 2003).

Over the past years, the techniques for mapping the tumours' location within the brain, as well as the surgical removal have been greatly improved, leading to more extensive resections (Black et al. 1999; Mukherjee and Quinones-Hinojosa 2011). Cells that have infiltrated the healthy brain tissue and escaped surgical removal can recolonize and form recurrent tumours. Following surgery, the remaining cancer cells are therefore treated with chemotherapy and ionizing radiation (IR). Current standard treatment following surgery for GBM includes fractionated adjuvant radio-chemotherapy following the Stupp scheme. In this treatment schedule, patients are irradiated with fractionated doses of 2 Gy of γ-rays per day for 5 consecutive days per week for 6 weeks resulting in a total dose of 60 Gy. Concomitantly, patients receive oral administration of 75 mg TMZ per square meter of body surface (m^2) per day each day of the 6 weeks. These first 6 weeks of treatment are followed by a second 6-week treatment period, in which patients receive oral administration of 150-200 mg TMZ/m^2 per day for the first 5 days of every 28-day cycle (Stupp et al. 2005).

Although the improved treatment schedule for GBM has led to greater PFS and OS rates in patients (median survival without TMZ treatment was 10.2 month compared to 15 months with TMZ), recurrences occur in almost all GBM patients (Figure 1) and for now, no standardised treatment for recurrences exists (Seystahl et al. 2016). As for primary GBM tumours, the recurrences are usually surgically removed as best as possible. It delays symptom progression and improves the response to chemo- and radiotherapy. Also PFS and OS can be prolonged depending on the health condition of the patient (Barbagallo et al. 2008; Woernle et al. 2015). For a chemotherapeutic approach following surgery, nitrosoureas represent the widely accepted treatment option for recurrent GBM. Also, reirradiation is widely used and showing promising results (Seystahl et al. 2016; Minniti et al. 2021). Lately, the chloroethylating agent N-(2-chloroethyl)-N'-cyclohexyl-N-nitrosourea (CCNU, lomustine) is starting to develop a position as standard of care for recurrent GBM with *MGMT* promoter methylation (Weller and Le Rhun 2020).

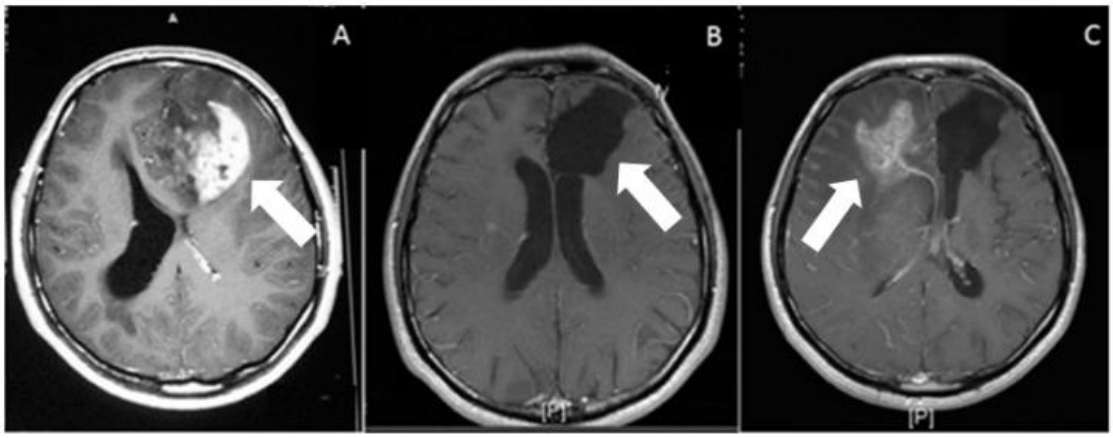

Figure 1: Exemplary MRI of re-occurring GBM.
MRI images show GBM pre (A) and post (B) tumour resection. 18 months following surgery, the tumour re-occurs on the opposite hemisphere (C) showing the infiltration capacity of GBM cells. Picture taken from (Seker-Polat et al. 2022)

1.2. Temozolomide

TMZ was first discovered in the 1980s during a project supervised by Malcolm Stevens at the Aston University in England (TEMOZOLOMIDE_ChemistryWorldJul09_tcm18-155909). It is a triazene analogue of dacarbazine, s used at this time in the treatment of Hodgkin disease and malignant melanoma (Stevens et al. 1984). In contrast to dacarbazine, TMZ does not have to be metabolically activated in the liver. Following oral administration, it is quickly absorbed in the gut (Jie et al. 2017; Saleem et al. 2003). Trials have been conducted to measure TMZ concentrations in plasma, spinal fluid, brain- and tumour tissue. In 2009, Rosso et. al. predicted TMZ concentrations via PET scan in combination with radio-labelled TMZ. Oral administration of 75-200 mg /m^2/d TMZ led to average peak concentrations of 2.9-6.7 µg/mL, corresponding to 15-35 µM TMZ in the tumour, while normal brain tissue reached 1.8-3.7 µg/mL, corresponding to 9-19 µM TMZ (Rosso et al. 2009). A second study published the same year measured TMZ concentrations following oral administration of 150 mg/m^2 TMZ in plasma and the brain interstitial fluid (BIF) using a catheter implanted during surgical removal of the GBM tumour. In plasma, average maximum concentrations of 5.5 µg/ml, corresponding to 28 µM TMZ, were measured, while the average maximum concentration in BIF reached 0.6 µg/ml, corresponding to 3 µM TMZ (Portnow et al. 2009). The same method was used in a study published in 2013, where intra-tumoral TMZ concentrations were measured in rats following a single oral dose of 50 mg/kg TMZ. Mean intra-tumoral TMZ concentrations of 0.59 µg/mL, corresponding to 3 µM TMZ were measured (Grossman et al. 2013).

TMZ is rather stable at acidic pH, with a half-live of about 1.82 h. At pH >7, however, TMZ is hydrolysed to 5-(3-methyltriazen-l-yl)-imidazole-4-carboxamide (MTIC), which is stable under these alkaline conditions. At acidic pH <7, MTIC has a half-life of about 2 min and decomposes to 5-aminoimidazole-4-carboxamid (AIC) and a highly reactive methyl diazonium ion, which is the active DNA-alkylating species (Figure 2) (Clark et al. 1995; Denny et al. 1994; Saleem et al. 2003; Newlands et al. 1992). This process occurs rapidly, as revealed by peak plasma concentrations 2.5 h after oral administration of TMZ (Baker et al. 1999).

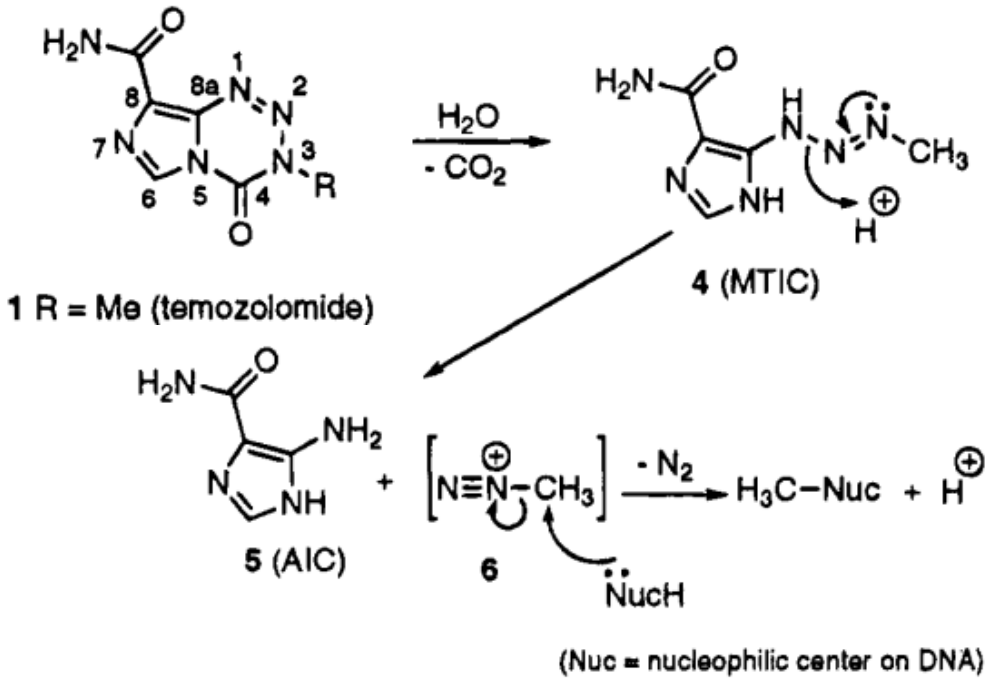

Figure 2: Conversion of TMZ to its active form.
TMZ is hydrolysed to MTIC, then further reduced to AIC and a methyl diazonium ion, which is the DNA alkylating species. The picture was adapted from (Clark et al. 1995)

1.2.1. Genotoxic effects of temozolomide

DNA-alkylating drugs, such as TMZ and CCNU exert their genotoxicity through alkylation of DNA bases and the induction of cross-links, respectively, and the subsequent induction of DNA single- and double-strand breaks (SSBs and DSBs) (Fu et al. 2012). As monofunctional alkylating agent, TMZ only transfers methyl groups to the DNA. Through a chemical S_N1-reaction it either methylates the cyclic nitrogen (N) or the extra-cyclic oxygen (O) atoms of DNA bases (Beranek 1990). It prevalently forms N7-methyl guanine (N7meG), and N3-methyl adenine (N3meA) adducts. while the O^6-methylguanine (O^6meG) adducts are a minor fraction. It has been shown, that TMZ preferentially methylates guanine in guanine-rich DNA sequences, yielding about 70-75 % N7meG, 8-11 % N3meA and 6-8 % O^6meG (Fu et al. 2012; Beranek 1990). Additionally, TMZ induces oxidative stress leading to oxidized bases, such as 8-Oxo-7,8-dihydroguanine (8-oxo-G) (Figure 3) (Wang et al. 2018). The N7meG adduct exerts its genotoxic effect through formation of apurinic-sites following spontaneous depurination. In contrast, N3meA, causes a genotoxic lesion itself, blocking the DNA polymerase and generating DSBs. This subsequently induces an S-phase blockage which, if not resolved, triggers the DNA damage response (DDR) and apoptosis pathways (Engelward et al. 1998). Additionally, the collision of replication with the base excision repair (BER) pathway, which is the main mechanism by which N-methylated adducts are repaired, leads to the induction of DSBs (Ensminger et al. 2014). The oxidised form of guanine (8-oxo-G) can mis-pair with adenine leading to mutations. The two major adducts N7meG and N3meA as well as 8-oxo-G are rapidly repaired by BER if the cell is BER competent. Since GBM is not known for mutations in BER, these DNA N-alkylation adduct play only a minor role in the induction of cytotoxic effects by TMZ, at least in the therapeutic dose range (Zhang et al. 2012; Fu et al. 2012).

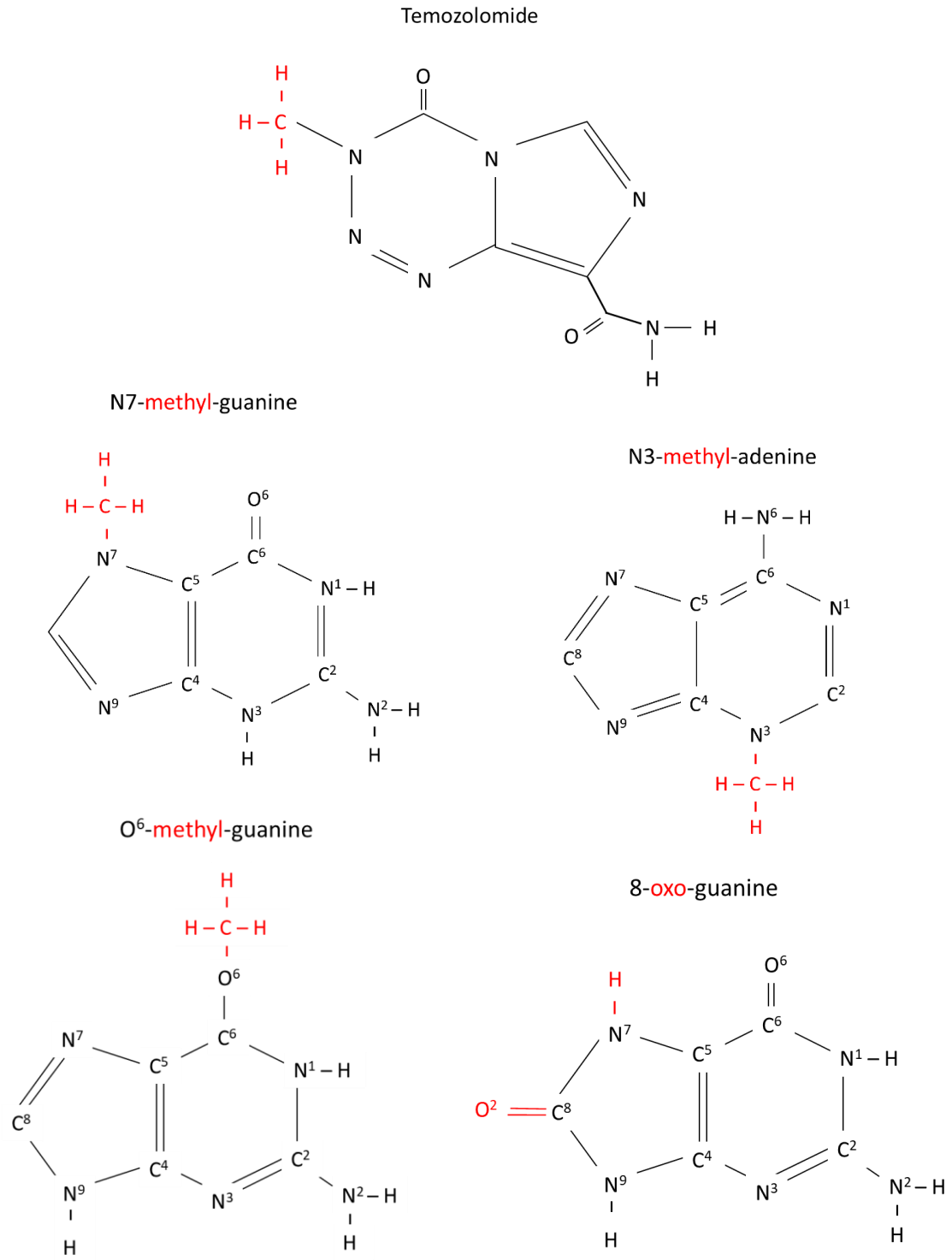

Figure 3: Molecular structures of TMZ and transformed DNA bases due to TMZ treatment.
The monofunctional alkylating agent TMZ primarily methylates guanine at the N7 and O^6 positions, as well as adenine at the N3 position. Oxidative damage induced by TMZ leads to formation of 8-oxo-guanine. Red indicates methylation directly by TMZ and oxidation through ROS induced by TMZ.

1.2.2. DNA damage induced by O^6methylguanine

The adduct that it is of most biological relevance in GBM treatment is O^6meG. Even though it is generated to a much lesser extent than all other adducts, it is responsible for almost all the cytotoxic and cytostatic effects provoked by TMZ. O^6meG is subject to direct repair via the suicide enzyme MGMT which restores the guanine base in a stoichiometric reaction. To this end, MGMT transfers the methyl group from the guanine onto a cysteine (Cys145) residue in its own active centre. Since the methyl-cysteine is not converted back, MGMT can act only once and is then subject to proteasomal degradation (Pegg et al. 1995; Xu-Welliver and Pegg 2002; Kaina et al. 2007). The protein expression level of MGMT varies between tumours and is highly regulated by epigenetic modifications, e.g., addition and removal of methyl groups at the promoter. Originally, the *MGMT* promoter is unmethylated, thus active, and MGMT is constantly expressed. Addition of a methyl group at the C5 position of the cytosine ring at cytosine-phosphate-guanine (CpG)- islands within the promoter region of *MGMT* leads to hypermethylation of the promoter and thus silencing of the gene, while de-methylation of the same leads to its (re-) activation (Illingworth and Bird 2009). Hence, the CpG methylation status of GBM is an important predictive and prognostic marker that can anticipate the efficacy of the TMZ treatment and thus the patient outcome (Weller et al. 2010; Weller et al. 2009). Even though it is rare, recurrent GBM tumours of TMZ treated primary GBM tumours can have an increased MGMT activity (Brandes et al. 2010). Also, in TMZ resistant xenografts, an increased MGMT expression was observed compared to the parental TMZ sensitive xenograft (Kitange et al. 2012). The studies propose that the *MGMT* gene might be regulated by TMZ itself, but studies performed in our lab could not confirm this hypothesis (Aasland et al. 2018; Christmann et al. 2011).

About 40 % of GBM have a hypermethylated *MGMT* promoter and, thus, lack the MGMT protein (Christmann et al. 2011; Taylor and Schiff 2015). In MGMT lacking cells, O^6meG can mis-pair with thymine (T) instead of cytosine (C) during replication since it has a higher affinity to thymine than to cytosine. If not recognised and removed by the mismatch repair (MMR) system, the mis-paired thymine is matched with adenine (A) in the next replication cycle, leading to a G-C to A-T transition mutation (Figure 4).

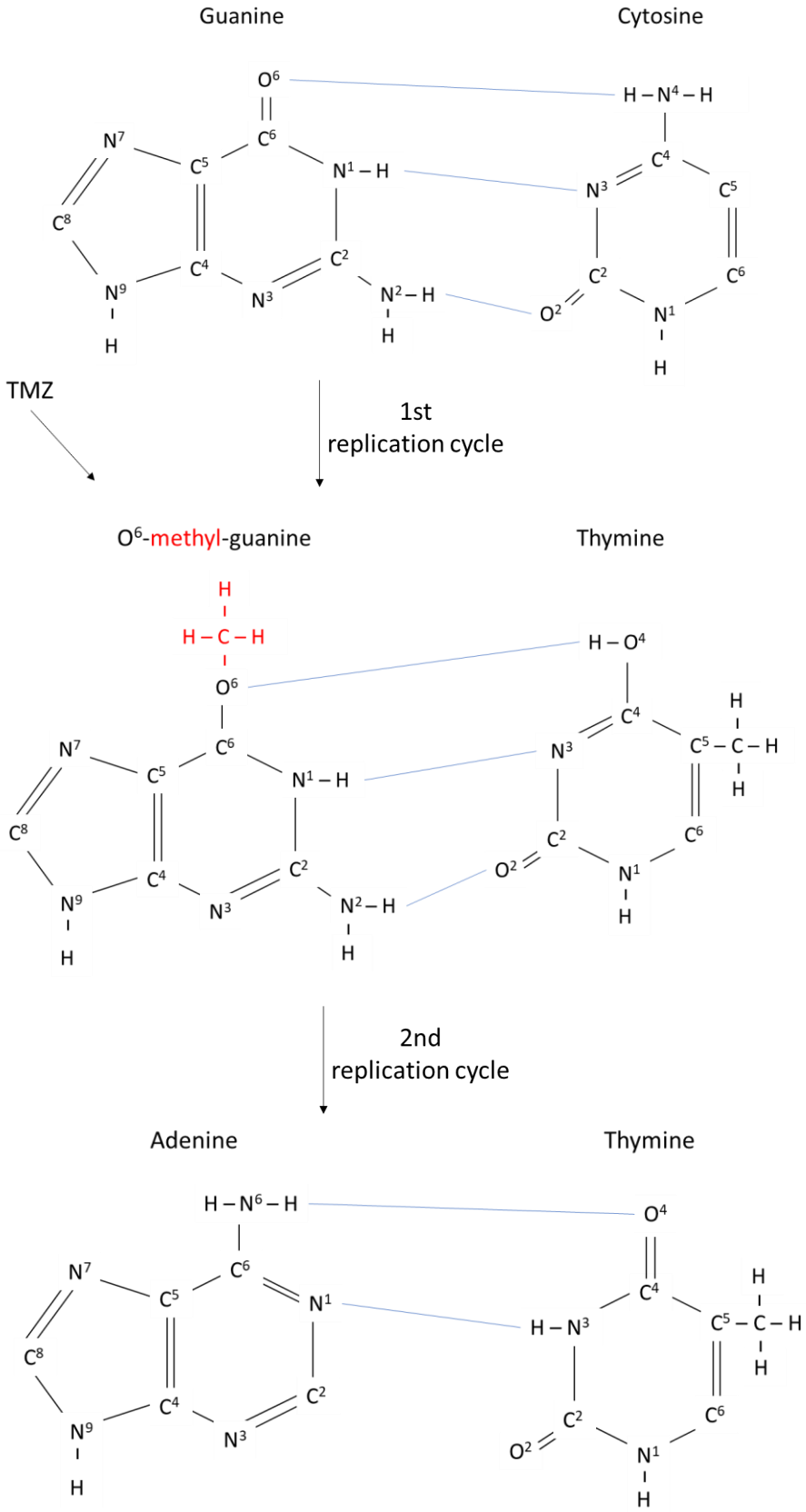

Figure 4: TMZ-induced transition mutations in MMR deficient cells.
In undamaged DNA, guanine pairs with cytosine. Treatment of TMZ leads to the methylation of guanine at the O^6 position. The guanine adduct has a higher affinity to thymine than cytosine, thus thymine is inserted opposite of guanine in the first replication cycle. In MMR deficient cells neither the O^6meG-cytosine nor the O^6meG-thymine pairing is recognised as faulty base pairing. Therefore, adenine is paired with thymine in the next replication cycle, leading to a G-C to A-T transition mutation. Red indicates methylation by TMZ. Blue indicates hydrogen bonds between the DNA bases.

If the cell is MMR competent, the O^6meG-C and the O^6meG-T pairs are recognised by MutSα and are excised (Duckett et al. 1996). Therefore, in a first step, either mismatch is recognized and bound by the MutSα complex, composed of MSH2 and MSH6. Phosphorylation of the complex ensures efficient binding (Christmann et al. 2002). Next, the undamaged strand needs to be identified. Hypotheses are currently discussed about how the MMR achieves this, but so far, the exact mechanisms remain unknown. However, upon recognition, the complex assembles with a second complex, the MutLα complex, which consist of the two proteins MLH1 and PMS2. Starting at a position situated 5' from the miss pair, the complex slides in 3' direction, stimulating exonuclease 1 (Exo1) to degrade the single stranded DNA (ssDNA) containing the mismatch. Several hundred nucleotides are degraded until the mismatch is reached and excised. Replication protein A (RPA) protects the remaining ssDNA from degradation. Once the mismatch is removed, the MutSα complex dissembles from the DNA and EXO1 is no longer stimulated and needed. The RPA protected gap is then synthesised by the polymerase pol δ (Figure 5) (Genschel and Modrich 2003; Bak et al. 2014).

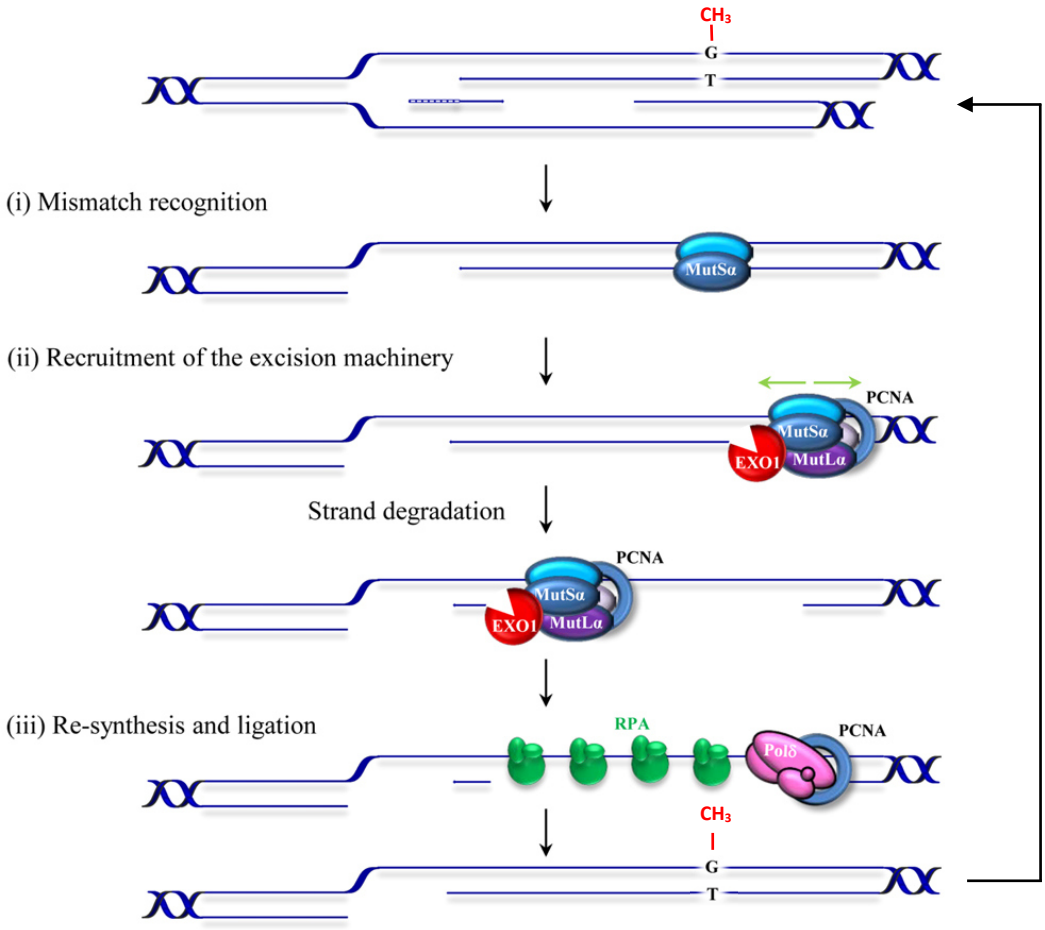

Figure 5: The mis-match repair system in human cells.
The MMR system includes three major steps. (i) Mis-match recognition by the MusSα complex. Thereafter (ii) strand separation, assembly of the MutLα complex and degradation of ssDNA including the mismatch by Exo1. RPA protects the ssDNA from further degradation. In a last step (iii), the DNA gap is closed by pol δ. The image was adapted from from (Kristiansen et al. 1981)

Since the O^6meG adduct is still in place and still has a higher affinity to thymine than cytosine, thymine is re-inserted during the next replication cycle. This re-occurring mismatch is again repaired by the MMR system resulting in repeated futile repair cycles. It has been hypothesised that the long ssDNA patches caused by MMR eventually collide with replication forks and are thus converted into DSBs. Studies performed in our lab showed that DSBs resulting from to the O^6meG adduct occur during the second replication cycle, indicating that the "futile MMR cycle" hypothesis is applicable (Quiros et al. 2010; Roos et al. 2004; Roos et al. 2007). Also, several studies proved the necessity of the MMR system in O^6meG triggered apoptosis (D'Atri et al. 1998; Kaina et al. 1997; Hickman and Samson 1999). Hence, the conversion of the O^6meG adduct into DSBs requires three items; Lack of MGMT to ensure persisting O^6meG adducts, a functioning MMR system, and DNA replication/proliferation.

1.2.3. Cytotoxicity induced by O^6methylguanine

Huge efforts have been made in elucidating the pathways that follow O^6meG induced DSBs in several cell systems, including GBM. So far, it has been shown that following TMZ treatment glioma cells activate the DDR and subsequently undergo apoptosis, autophagy and senescence (Knizhnik et al. 2013; He and Kaina 2019).

1.2.3.1. Induction of apoptosis

Apoptosis is a form of programmed cell death with vital roles in various processes, including embryonic development, maturing of the immune system and normal cell turnover. In cancer treatment the ability to induce apoptosis e.g., through induction of DNA damage (chemotherapy or IR), is recognized for its great therapeutic value. Cell death by apoptosis can be detected by morphological changes. In brief, during the early stage of apoptosis, cells detach from their surrounding cells and extracellular matrix attachments and start condensing the DNA in the nucleus. The nucleus is then segregated into several fragments and the cell membrane is pushed outwards, resulting in bulges. The last step of apoptosis includes the complete segregation of the cell into several apoptotic bodies (Figure 6) (Häcker 2000).

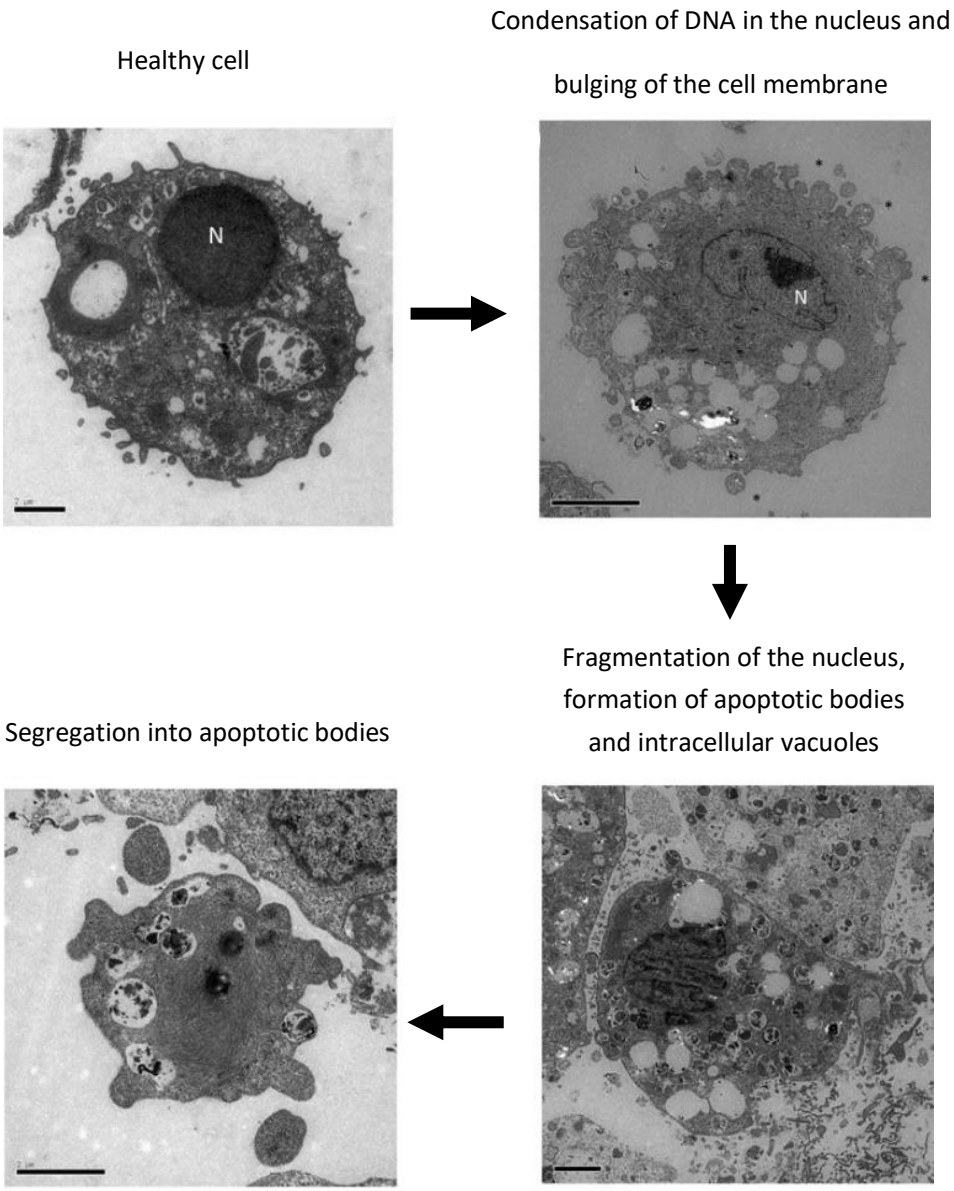

Figure 6: Representation of morphological changes during apoptosis.
Apoptotic cells condensate the DNA and then fragment the nucleus. The cell membrane is pushed outwards resulting in bulges. The cell then completely segregates into apoptotic bodies. The image was adapted from (Le et al. 2020)

The morphological changes during apoptosis are the result of biochemical changes within the cell. Those include protein cross-linking by tissue transglutaminases, protein cleavage by cysteine aspartyl proteases (caspases), DNA fragmentation through Ca^{2+}- and Mg^{2+}-dependent endonucleases and the expression of cell surface markers for phagocytic recognition (Hengartner 2000; Elmore 2007). Apoptosis can be induced via two major pathways; the death receptor (DR) mediated and the mitochondrial pathway. They are executed via the same pathway (activation of caspase-3 and -7) but have different initiation pathways.

The DR pathway relies on binding of DR ligands or cytotoxic stress, while the mitochondrial pathway results from signals within the cell, e.g., DNA damage or hypoxia, and the resulting stress. In GBM, both pathways are triggered by TMZ treatment.

Upon DNA damage induced by TMZ, GBM activate the stress kinases ataxia telangiectasia mutated (ATM) and ataxia telangiectasia mutated related (ATR) (Aasland et al. 2019b). It has recently been shown that activated ATM phosphorylates the E3 ubiquitin ligase seven in absentia homolog 1 (SIAH1), thereby inhibiting its activity. In undamaged cells, SIAH1 negatively regulates the homeodomain interacting protein kinase 2 (HIPK2) which marks homeodomain transcription factors for proteasomal degradation by ubiquitination. Upon phosphorylation of SIAH1, HIPK2 stabilizes and phosphorylates p53 at serine 46 which leads to stimulation of the Fas mediated apoptotic DR pathway (Figure 7) (He et al. 2019; Roos et al. 2007). In brief, the Fas ligand binds to the Fas receptor, leading to the recruiting of the adaptor protein FAS-associated death domain and pro-caspase-8. Together they form the death inducing signalling complex which induces the activation of caspase 8. The activated caspase-8 then cleaves and activates the executioner caspases that enforce apoptosis by degrading cellular components (Elmore 2007). By comparing p53wt with p53mt cells, it has been shown that this pathway triggering the induction of cell death was clearly stimulated in p53wt cells (He et al. 2019; Roos et al. 2007).

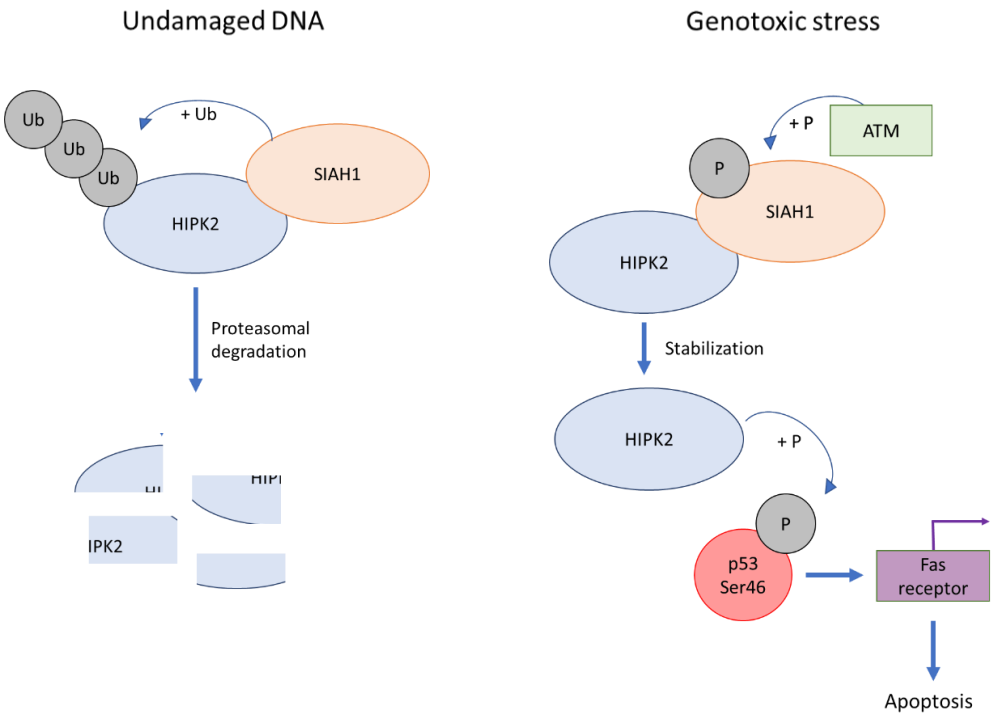

Figure 7: Activation of the Fas induced apoptotic pathway upon DNA damage.
In undamaged cells (left) SIAH1 continuously ubiquitinates (ub) HIPK2, which is then degraded. Upon DNA damage, ATM is activated and phosphorylates (p) SIAH1. The now inactive SIAH1 no longer marks HIPK2 for degradation. HIPK2 stabilizes and phosphorylates p53 at serin 46 (p53ser46). This leads to transcriptional activation of the fas receptor and induction of apoptosis.

A second pathway involved in apoptosis in glioma cells following TMZ, is the mitochondrial pathway. The mitochondrial pathway is mainly regulated by the B-cell lymphoma-2 (Bcl-2) protein family, which consists of pro-apoptotic and anti-apoptotic proteins. They regulate the cytochrome C release from the mitochondria. Once released, cytochrome C binds, together with dATP, to the cytosolic protein Apaf-1, forming of the apoptosome. The apoptosome serves as platform for the activation of initiator caspases which cleave and activate executioner caspases. They in turn carry out apoptosis by degrading cellular components. Thereby the Bcl-2 family regulates the induction or inhibition of apoptosis (Elmore 2007; Hengartner 2000). The role of the anti-apoptotic Mcl-1 protein in TMZ-induced apoptosis has been demonstrated. Following 50 µM TMZ treatment for 72 h, the Mcl-1 protein level was downregulated. Inhibition of Mcl-1 led to a significantly higher activation of caspases when cells were treated with 12.5 µM TMZ. Additionally, inhibition of the pro-apoptotic Bak protein led to a significant reduction in apoptosis. Inhibition of other pro- or anti-apoptotic Bcl-2 proteins had no effect (Gratas et al. 2014a). In U87 cells, a change in the Bcl-2:Bax ratio upon TMZ treatment was observed. While the Bcl-2 protein level stayed about the same in TMZ-treated cells, the level of the Bax protein level was increased, leading to an increase in the Bcl-2:Bax ration. Treatment of U87 cells with dexamethasone before the treatment with TMZ led to an abrogation of the increase in the Bax protein level. Concomitantly, the apoptosis levels were reduced. Thus, it has been proposed, that upon TMZ treatment a change in the Bcl-2:Bax ratio is induced that results in apoptosis. (Das et al. 2004; Ma et al. 2002). Overall, the beforementioned data suggest that upon TMZ treatment also Mcl-1 is downregulated in GBM cells to induce apoptosis via a change in the Mcl-1:Bak ratio.

1.2.3.2. Induction of senescence

As mentioned before, senescence is the second key response of glioma cells following TMZ treatment. It has long been thought to be a permanent cell cycle arrest, but recent studies demonstrate that senescent cells can escape their fate and re-start proliferation (Saleh et al. 2019). Thus, the definition of senescence is changing. There are different types of senescence, depending on their trigger. While oncogene-induced senescence is induced by oncogenes, age-related senescence is induced by telomer shortening, and DNA damage induced/therapy induced senescence is triggered by DNA damage occurring outside of telomeres. Depending on the type of senescence, cells can be arrested in either G1 or in G2/M phases of the cell cycle (Rayess et al. 2012; Aasland et al. 2019a). Taking together the results of several studies conducted on TMZ treated glioma cells, the induction of senescence appears to occur in the following way.

DSBs activate ATM and ATR, which phosphorylate their downstream targets checkpoint kinase 1 and 2 (CHK1 and CHK2). In turn, activated CHK1 and CHK2 phosphorylate the cell division cycle phosphatase CDC25c, which then no longer de-phosphorylates CDK1. The now active CDK1 blocks the G2/M transition and cells are arrested in G2/M. Additionally, CHK1 and CHK2 can phosphorylate p53 at serine 20 and 15, both leading to an activation of p21. The activated p21 then binds the CDK1/cyclin B1 complex, leading to its nuclear retention and inhibition, and cells are arrested in G2/M (Hirose et al. 2001; Eich et al. 2013; He and Kaina 2019; Aasland et al. 2019b). Another major pathway leading to senescence involves the SASP. In a pathway yet to be discovered, ATR downregulates the inhibitor of the nuclear factor kB (NF-kB), IkB. Increased levels of NF-kB lead to inhibition of apoptosis and transcription of SASP factors which re-enforce senescence (Figure 8).

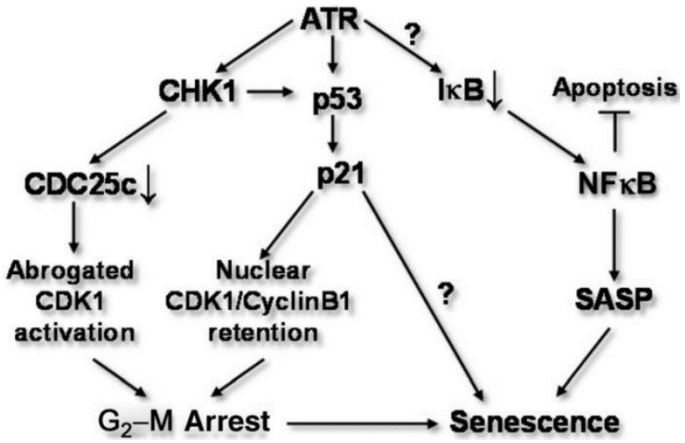

Figure 8: Schematic of TMZ-induced senescence in GBM cells.
Senescence is induced by several pathways starting from activation of ATM/ATR. Left: ATR phosphorylates and thereby activates CHK1, which phosphorylates and thereby inactivates CDC25c. CDK1, which is usually de-phosphorylated by CDC25c is now active and blocks the G2/M transition. Middle: ATR as well as active CHK1 phosphorylate p53 at ser20 and ser15 leading to induction of p21 and subsequent nuclear retention of the CDK1/cyclin B1 complex. This results in a G2/M arrest. Right: ATM reduced IkB levels by a yet unknown pathway. NK-kB can therefore stabilise and transcribe SASP factors that re-enforce senescence. The image was adapted from (Aasland et al. 2019b)

Interestingly, inhibition of autophagy leads to a reduction in senescence and an increase in apoptosis. Somehow, autophagy is needed to induce senescence in GBM cells following TMZ treatment but the exact pathway remains unknown (Knizhnik et al. 2013). However, it has been demonstrated in other cell systems that the high flux of recycled amino acids and other metabolites provided by autophagy are subsequently used for the massive synthesis of the SASP factors that facilitate CSEN (Kwon et al. 2017; Young et al. 2009). The SASP is additionally regulated by GATA, which in turn is regulated by p62 mediated selective autophagy. Upon senescence-inducing stimuli the interaction of p62 and GATA4 decreases. GATA4 protein levels increase, initiate activation of NF-kB and subsequently transcription of genes involved in the SASP (Kang et al. 2015).

Considering the unfavourable effects of senescence during GBM treatment and the important role of the SASP in maintaining and reinforcing senescence, the inhibition of the formation of the SASP, thus the autophagic pathway poses a target for eliminating senescent cells.

1.3. CCNU

The chloroethylating drug CCNU is, like TMZ, an alkylating agent. It preferentially forms adducts at the N7 position of guanine, resulting in N7-chloroethyl-guanine and N7-hydroxyethyl-guanine. As for TMZ, the adduct bearing the most cytotoxic effect is at the O^6 position of guanine. This adduct is highly unstable, thus, through intramolecular rearrangements, it quickly forms N1-O^6ethano-guanine (Figure 9) (Ludlum 1990).

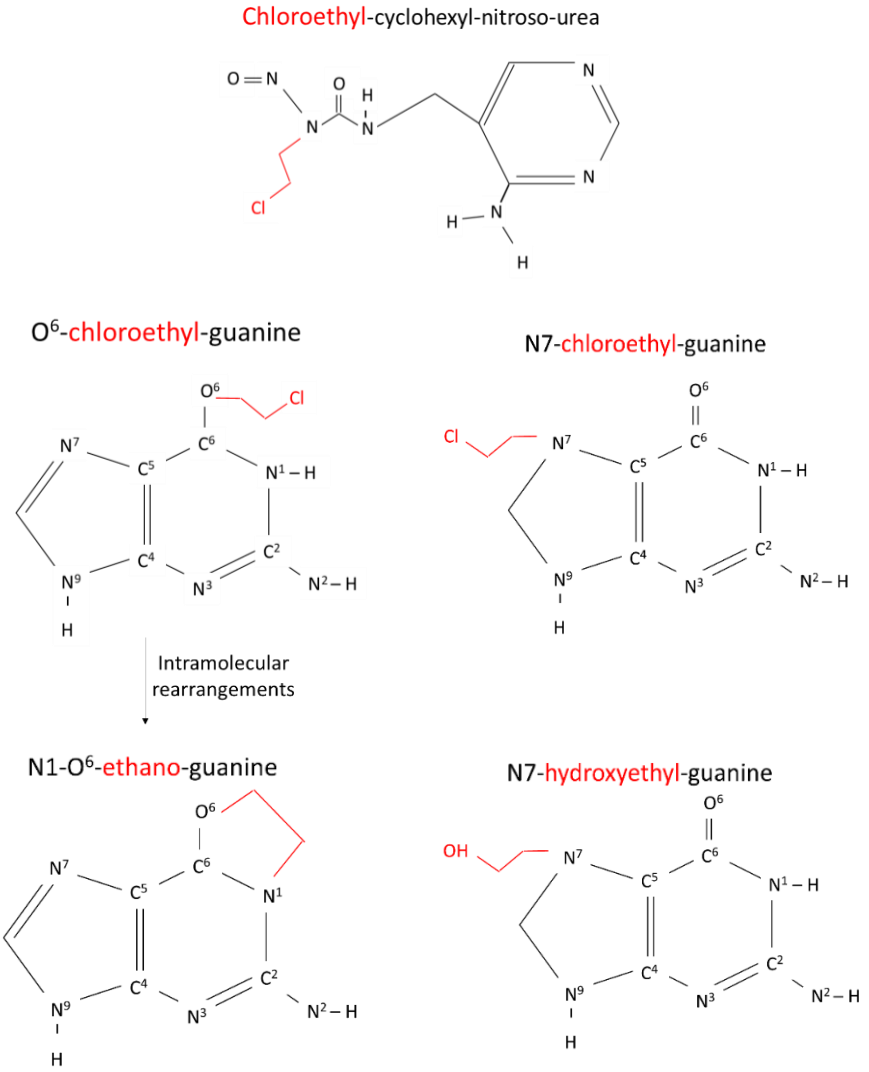

Figure 9: Molecular structures of CCNU and transformed DNA bases due to CCNU treatment.
CCNU transfers its chloroethyl group onto the O^6 or N7 positions of guanine. Following intramolecular rearrangements, the O^6chloroethyl-guanine is converted into N1-O^6-ethano-guanine.

The chloroethyl modified DNA bases can be recognised and repaired by the MGMT enzyme. Just like the repair of methylated bases following TMZ treatment, repair of chloroethylated bases following CCNU follows a stochiometric reaction. Therefore, MGMT transfers the chloroethyl group onto a cysteine residue (cys145) in its active site which leads to inactivation of MGMT and its proteasomal degradation (Coulter et al. 2007). In cells with CpG methylated and thus inactive *MGMT* promoter, the O^6- chloroethylated DNA bases are not repaired. As mentioned before, O^6-chloroethylguanine is highly unstable and is transformed to N1-O^6ethano-guanine following intramolecular rearrangements. The N1-O^6ethano-guanine then covalently binds to a cytosine of the complementary DNA strand, thus generating the stable N1-guanine-N3- cytosine interstrand cross link (ICL) DNA lesion (Figure 10) (Ludlum 1990).

N1-guanine-N3-Cytosine interstrand cross link

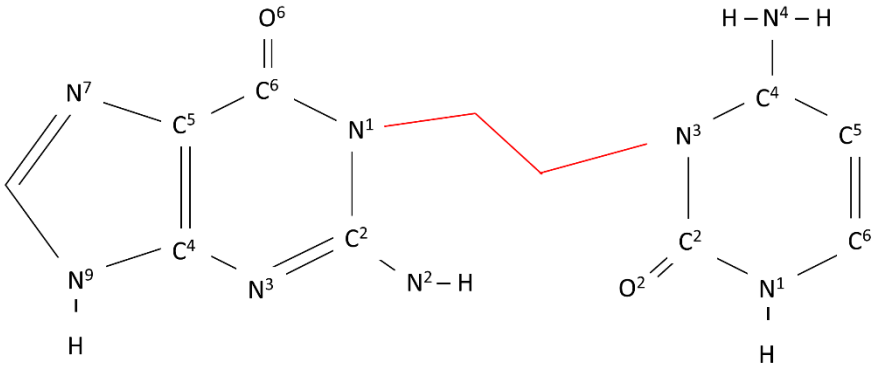

Figure 10: Interstrand cross link between guanine and cytosine.
The ethyl group of the N1-O^6-ethano-guanine forms and interstrand cross link (ICL) with the N3 of cytosine. The ICL is marked in red.

These ICLs lead to a block of replication as well as transcription, and later, if not repaired, induce cell death pathways. The exact mechanisms of ICLs recognition, repair and damage response are still being discovered. Two pathways have been suggested to be involved in ICLs repair. One hypothesis considers the repair of ICLs at stalled replication forks through generation of a one-ended DSB at the site of the ICL. During this repair mechanisms, the overhanging ssDNA could be recognised as DSBs and activate the DDR. A second hypothesis rests on the generation of a chicken-foot structure which is recognised as one ended DSBs. In both cases, the repair mechanisms would include NER to excise the corrupted DNA base, and HR to seal the generated overhanging ssDNA (Nikolova et al. 2017).

1.4. Methadone

Methadone (MTD) is a long-acting synthetic opioid, that was initially developed for treatment of opioid addiction, and serves as a second-line treatment for pain medication (Schuckit 2016; Palat and Chary 2018). As highly potent μ-opioid agonist, MTD binds to the G-protein coupled μ-opioid receptor (MOR), which is then activated. MOR is located at the cell membrane, the cytoplasm, or the nucleus of a variety of cells (Stein 2016). Depending on the cell, the activation of MOR leads to different events. In neurons, MOR activation mediates the analgesic effects of MTD, while in lymphocytes and macrophages MOR activation promotes immunosuppression and inflammation (Siuda et al. 2017; Brejchova et al. 2020).

The role of MTD in cancer development and cancer treatment is not clear, and contrary data have been provided. While some studies point towards tumour progression upon MOR activation, others showed the opposite. In non-small-cell lung cancer, colorectal cancer and breast cancer, MOR was shown to mediate tumour progression through several pathways. These include the phosphoinositide 3-kinases (PI3K)/Akt/STAT3 and the JNK pathways (Lennon et al. 2014; Lu et al. 2013). Activation of MOR was also shown to target the MAPK, COX2 and c-MYC, among others in hepatocellular carcinoma to promote tumour progression (Chen et al. 2019). Contrary, activation of MOR through morphine was shown to induce cell death and inhibit the migratory and invasion ability of hepatocellular carcinoma (Zhang et al. 2021). In glioblastoma cells, activation of MOR through MTD was proposed to improve the effectiveness of doxorubicin, thus have an anti-tumour effect. This hypothesis rests on the finding that the anti-apoptotic proteins XIAP and Bcl-X_L were downregulated upon activation of MOR through MTD treatment (Friesen et al. 2014). However, a study conducted by Brawanski et al. demonstrated a dose-dependent effect of MTD on glioblastoma cells. Thus, sole MTD treatment only induced apoptosis in glioblastoma cells at dosages above clinically achievable concentrations. The same was shown for the combinatorial treatment of MTD and TMZ (Brawanski et al. 2018). Taken together, these results show that the effect of MOR on tumour progression and cell death is highly cell type and dose dependent.

MTD is mostly administered orally and is absorbed quickly. Plasma peak concentrations of are reached within 2.5 h when administered in liquid form, and about 3 h when administered in tablet form. The bioavailability is in the range of 70 to 80 % (Kreutzwiser and Tawfic 2020). Plasma concentrations reached vary between oral and intravenous (i.v.) application an range from approximately 0.3 nM after oral administration to approximately 0.5 μM following i.v. application (Wolff et al. 1993; Meresaar et al. 1981). The MOR is located not only in the brain but also e.g., in the spinal cord and intestinal tract. Activation of MOR leads to a reduced release of the neurotransmitters in neurons, thus exerts its analgetic effect.

However, activation of MOR also leads to hypothermia, respiratory depression and reduced gastrointestinal motility. Therefore, the dosing of MTD needs to be carefully evaluated. The tolerable daily dose for humans was reported to be 100 mg with a maximum serum level between 0.3 and 1.3 µg/mL (Inturrisi et al. 1987; Kreutzwiser and Tawfic 2020).

1.5. Senolytic agents

There is increasing evidence that senescent cells can escape their senescent state and re-enter the cell cycle, leading to recurrent tumours month, sometimes years following treatment (Saleh et al. 2019; Olszewska et al. 2021; Le Duff et al. 2018). Additionally, senescent cells excrete the SASP factors into the surrounding healthy tissue, thereby promoting inflammation and tumour progression. These factors may contribute to shortening of PFS and OS (Demaria et al. 2017). Thus, reducing the senescent cell population is of major concern. One way of doing so is by inhibiting the induction of senescence. Another is treatment with senolytic agents, which specifically drive senescent cells into cell death while leaving proliferating cell unharmed. A few senolytic agents have already been identified or created, including the synthetic Bcl-2 inhibitors ABT-737 and ABT-263, the latter also known as Navitoclax (Yosef et al. 2016; Zhu et al. 2016). Also, some natural and synthetic compounds have been demonstrated to deplete senescent cells (Li et al. 2019b; L'Hôte et al. 2021). In this study, the three natural compounds artesunate, curcumin and fisetin, as well as the nociceptin receptor inhibitor 1-[1-(1-Methylcyclooctyl)-4-piperidinyl]-2-[(3R)-3-piperidinyl]-1H-benzimidazole (MCOPPB) were evaluated for their senolytic capacity in GBM.

1.5.1. Artesunate

Artesunate is a semisynthetic derivate of artemisinin, a natural sesquiterpene lactone extracted from the wormwood plant *Artemisia annua* (Haynes and Vonwiller 1994). In a two-step procedure artemisinin is first reduced to dihydroartemisinin and then further acylated to artesunate (Presser et al. 2017). Artesunate is highly water soluble, quickly absorbed in the gut and then hydrolysed to docosahexaenoic acid (Melendez et al. 1991; Nyunt and Plowe 2009). Artesunate has a long tradition in Chinese medicine for the treatment of malaria but nowadays its application exceeds this purpose (Kong and Tan 2015). There is considerable evidence that artesunate exerts anticancer effects in different types of cancer either as sole treatment or as adjuvant for chemotherapeutics.

Thus, sole artesunate treatment has proven to exert anticancer effects in colon and ovarian cancer (Jiang et al. 2018; McDowell et al. 2021). It also induces apoptosis in glioblastoma cells through sustained DSBs resulting from oxidative DNA damage (Berdelle et al. 2011). Also, a synergistic effect of artesunate and sorafenib was demonstrated in hepatocellular carcinoma and a sensitizing effect against TMZ in glioblastoma cells (Li et al. 2021; Berte et al. 2016). Hitherto, artesunate has not been evaluated as senolytic agent.

The molecular targets of artesunate are versatile, depending on the evaluated cell system and include several mechanisms. By activating caspase-3 and -9 and mediating the cytochrome C release from the mitochondria into the cytosol, artesunate effectively induces apoptosis via the mitochondria-dependent pathway. Additionally, artesunate has been shown to induced apoptosis by regulation of pro- and anti-apoptotic Bcl2- proteins, including Bcl-2, Bcl-X_L, Bax and Bak (Jiang et al. 2018; Qin et al. 2015). Various reports indicate that artesunate also induces autophagy and generates reactive oxygen species (ROS) (Jiang et al. 2018; Zhou et al. 2020). This effect has also been demonstrated in glioblastoma cells (Berdelle et al. 2011).

Clinical trials evaluated the safety and tolerability of artesunate. The observed adverse effects include leukopenia, neutropenia, and anaemia, as well as vertigo. However, those were no severe effects and the symptoms resolved after treatment was stopped. A dose-escalating study of intravenous artesunate on 3 consecutive days, showed no severe adverse effects even at the highest dose tested (8 mg/kg/d) (Louis Cantilena, Jr., MD, PhD 2018).

1.5.2. Curcumin

Curcumin is a naturally occurring polyphenol and one of the main substances found in the rhizome of *Curcuma spp*. It has a bright orange-yellow colour and is thus widely used as food colouring. Also, studies provided evidence for its beneficial effects. These include an increase in brain function, beneficial roles in the treatment of rheumatic diseases, diabetes and cancer, as well as anti-oxidative effects (Allegra et al. 2017; Bhat et al. 2019; Ghosh et al. 2015). Hence, it is also sold as food supplement. Recently, its role in cancer treatment as monotherapy and as adjuvant for chemotherapy has been exploited. Several studies provide evidence for the anti-cancer effects of curcumin in a variety of cancer, e.g., breast cancer, leukaemia and colorectal cancer (Kizhakkayil et al. 2010; Kuo et al. 1996; Pricci et al. 2020). In a glioblastoma mouse model curcumin induced apoptosis and repressed tumour growth by repressing angiogenesis. Curcumin also induced apoptosis via ROS and downregulation of Bcl-2 in a human leukaemia cell line (He et al. 2020; Kuo et al. 1996).

These results suggest that depending on the type of cancer, curcumin might be sufficient as monotherapy. Curcumin might also be used as adjuvant to potentiate the chemotherapeutic effects of paclitaxel as has been demonstrated in a rat glioblastoma cell model (Fratantonio et al. 2019). The effect of curcumin on senescent cells has also been investigated. Thus, in IR-induced senescent human fibroblasts curcumin induced apoptosis through upregulation of the proteasomal degradation of the anti-apoptotic Bcl-2 proteins Bcl-X_L and Mcl-1 (Li et al. 2019a). The molecular targets of curcumin are diverse and trigger several pathways. Known molecules regulated through curcumin treatment and involved in cancer development are NF-kB, p53, PI3K, NRF2, Bcl-2 and Bcl-X_L (Shehzad et al. 2010; Kasi et al. 2016).

A huge obstacle in curcumin usage is its administration. Curcumin is practically insoluble in water. Thus, plasma concentrations reach only trace amounts even after high dose oral administration of native curcumin. Reports of plasma concentrations reaching up to 1.7 µM following an oral dose of 8 g native curcumin underline this obstacle (Liu et al. 2016). Strategies to overcome these limitations have been investigated. Hitherto, packing curcumin into micelles has proven as best strategy. A single-blind study including 23 subjects demonstrated a 185-fold better bioavailability of micellized curcumin compared to native curcumin. Hence, administration of 500 mg micellar curcumin led to plasma levels of about 3.2 µM (Schiborr et al. 2014). The safety of native and micellar curcumin has been evaluated in feeding studies, demonstrating no adverse effects (Seiwert et al. 2021). Also, testing of synthetic curcumin via the Ames test, showed that this form of curcumin is not a mutagenic agent (Damarla et al. 2018). The German Federal Institute for Risk Assessment (*ger. Bundesinstitut für Risikobewertung* BfR) published a detailed risk assessment for native curcumin 2019. It specifies that a maximum of 3 mg/kg/d are an acceptable daily intake.

1.5.3. Fisetin

Fisetin is a polyphenol found in several fruits and vegetables, with the highest amount found in strawberries (Arai et al. 2000). It is investigated for its health supporting effects. Thus, fisetin has been demonstrated to have beneficial effects in Alzheimer's and Parkinson's disease and in the treatment of ischemic strokes (Nabavi et al. 2016; Wang et al. 2019). It also bears antioxidative properties (Khan et al. 2013). Recently, the role of fisetin in cancer treatment is exploited since several studies indicated that the anti-proliferative and apoptosis-inducing effect of fisetin specifically target cancer cells (Khan et al. 2008). Thus, cell death was induced in several cancer types, including lung-, colon-, prostate- and pancreatic cancer, as well as malignant melanoma (Khan et al. 2013).

Additionally, fisetin has been shown to target senescent cells, while leaving proliferating cells less affected. Hence, fisetin is a senolytic agents (Yousefzadeh et al. 2018; Zhu et al. 2017). The molecular targets of fisetin are versatile and differ depending on the cell line investigated. So far, targets of the PI3K-, mTOR and ERK/JNK-pathways have been shown to be inhibited by fisetin, while the NF-kB and AMPK pathways are activated (Khan et al. 2013). Like curcumin, fisetin has a low water solubility and thus a low bioavailability. However, data about plasma concentrations reached following oral administration of fisetin are lacking. In mice, a peak concentration of 2.5 µg/mL fisetin was reached 15 min following intraperitoneal administration of 223 mg/kg fisetin. The half-live was about 5 minutes (Touil et al. 2011). New delivery methods, such as encapsulation in lipids, are being developed to circumvent this obstacle in fisetin delivery. They could also be used for local treatment (Renault-Mahieux et al. 2021).

1.6. Aim of the study

In the first part of this study, we focused on TMZ-induced geno- and cytotoxic, and cytostatic effects in GBM cells. The following questions were addressed: a) What is the kinetic of TMZ-induced DSBs, cell death and CSEN? b) How is the distribution of TMZ-induced cell death and CSEN? c) Do TMZ-induced DSBs persist in senescent GBM cells? d) Do they trigger the DDR? e) Can DSBs in senescent GBM cells be repaired? f) What role does the DNA lesion O^6meG play in the repair of DSBs in senescent GBM cells?

Having established that CSEN is the main trait in GBM cells upon TMZ treatment (chapter 4.1.2), we focused on how the senescent state in GBM cells is maintained. The following questions were addressed: a) Does the DDR play a role in TMZ-induced senescence maintenance? b) What role does the mitochondrial apoptosis pathway play? c) How else is the TMZ-induced senescent state maintained?

In the last part, we focused on how the load of TMZ-induced senescent GBM cells can be reduced. The following questions were addressed: a) Do the natural compounds curcumin and fisetin bear senolytic activity in GBM cells? b) Are the synthetic/semisynthetic drugs artesunate, MCOPPB, CCNU and MTD senolytic agents in GBM cells? c) Is IR senolytic in GBM cells? d) Does the combination treatment of GBM cells with TMZ and MTD or TMZ and IR increase cell death levels?

2. Materials

2.1. Chemicals and consumables

If not stated otherwise, all chemicals used in this study were obtained from either Carl Roth GmbH & Co. KG (Karlsruhe, Germany) or from Sigma-Aldrich (Steinheim, Germany), while all plasticware, such as cell culture flasks and dishes, 15-, 50-ml and 1,5 ml sampling tubes, were purchased from Greiner BioOne GmbH (Frickenhausen, Germany), Eppendorf AG (Hamburg, Germany) or TPP Techno Plastic Products AG (Trasadingen, Switzerland).

Table 1: List of chemicals and consumables.

Chemical/consumable	Product number	Company
3-(4,5-dimethylthiazol-2-yl)-2,5-diphenyltetrazolium bromide (MTT)	15655	Biomol GmbH, Germany
Acrylamide 4K solution 40 % - Mix 37.5 : 1 BC (Acrylamide 40 %)	A1577	AppliChem GmbH, Germany
AnnexinV-FITC (AV)	130-093-060	Miltenyi Biotec B.V. & Co. KG, Germany
Blotting membrane	Amersham Protean 0.2 µM NC	GE Healthcare life Sciences, UK
C12FDG	M2888	Marker Gene Technlogies Inc., USA
C12FDG	ab273642	Abcam plc., UK
Centrifuge 15- and 50-ml falcon tubes	Megafuge 1.0	Heraeus Holding GmbH, Germany
Coverslips round, 18 mm	48380-046	VWR International, LLC, USA
Coverslips square, 22 mm	94-22222	CNA scientific Inc., USA
Diaminobenzidine	-	Lab Vision Cooperation, Fermont, CA, USA
Dulbecco's Modified Eagle Medium (DMEM) GlutaMax	61965059	Gibco, Thermo Fisher Scientific Inc, USA
EnVision FLEX Target Retrieval Solution, high pH	S2368	Dako, Glostrup, Demnark
Ethylenediaminetetraacetic acid (EDTA)	A2937	AppliChem GmbH, Germany
Foetal calf serum (FCS)	10270106	Gibco, Thermo Fisher Scientific Inc, USA
LI-COR stripping buffer	928 - 40030	LI-COR Inc., USA
Microscope slides	17234884	Thermo Fisher Scientific Inc, USA
peroxidase-blocking solution	-	Dako, Glostrup, Demnark
Phenylmethanesulfonyl fluoride (PMSF)	A0999	AppliChem GmbH, Germany
Phosphate buffered saline (PBS)	l 182-50	Merck KGaA, Germany

Pipette tip 1000 µl	I1011-2011	Starlap International GmbH, Germany
Pipette tip 20 µl	S1110-3000	Starlap International GmbH, Germany
Pipette tip 200 µl	70.760.012	Sarstedt AG & Co. KG, Germany
Potassium ferricyanide	A3883	AppliChem GmbH, Germany
Potassium ferrocyanide	A1867	AppliChem GmbH, Germany
Trypsin	15400054	Gibco, Thermo Fisher Scientific Inc, USA
Vectra shield	H-1000	Vector Laboratories, USA
Whatman paper	732-0591	VWR International GmbH, Germany
X-Gal	AG-CC1-0003-G001	BIOMOL GmbH, Germany

2.2. Technical Instruments

Table 2: List of technical instruments.

Instrument	Name	Company
Blotting chamber	TransBlot Cell	BioRad Laboratories GmbH, Germany
Casting Stand plus gaskets	Mini-Protean Tetra Cell Casting Stand	Bio Rad Laboratories GmbH, Germany
Chamber for sodium dodecyl sulphate polyacrylamide gel electrophoresis (SDS-PAGE) and Western blot	Mini Protean Tetra Cell	BioRad Laboratories GmbH, Germany
Chamber for single-cell gel electrophoresis (SCGE)	Tetra Vertical Electrophoresis Cell	Bio Rad Laboratories GmbH, Germany
Clean bench	NU 440-600, Class II	NuAire, Inc., USA
Clean bench	EN12469, Class II	Thermo Fisher Scientific Inc, USA
Comb for SDS-Gel preparation	Mini Protean Comb, 15-well	Bio Rad Laboratories GmbH, Germany
Confocal laser scanning microscope (LSM)	LSM 710	Carl Zeiss GmbH, Germany
Cooling Centrifuge 1.5 ml tubes	Refrigerated 5402	Eppendorf SE, GErmany
Dako Autostainer Plus	Immnostainer	Dako, Glostrup, Denmark
Flow cytometer	FACS Calibur	BD Biosciences, Germany
Flow cytometer	FACS Canto II	BD Biosciences, Germany
Fluorescence microscope	Nikon Microphot-FXA EPI-FL3	Nikon Corp., Japan

Freezer (-20 °C)	Premium, NoFrost	Liebherr AG, Szwitzerland
Freezer (-80 °C)	Forma 9000 series	Thermo Fisher Scientific Inc., USA
Freezing container	Mr. Frosty	Thermo Fisher Scientific Inc, USA
Fridge (+4 °C)	Premium, NoFrost	Liebherr AG, Szwitzerland
Gel electrophorese chamber for SCGE	DNA SUB CEL	Bio Rad Laboratories GmbH, Germany
Gel holders for WB	Mini Trans-Blot system	Bio Rad Laboratories GmbH, Germany
Glass plates for SDS-Gel preparation	Mini Protean short plate	Bio Rad Laboratories GmbH, Germany
Heating block and shaker	MHR 13	Andreas Hettich GmbH & Co.KG, Germany
Infrared imaging system	Odyssey 9120	LI-COR Inc., USA
Incubator	CO_2 incubator HeraCell	Thermo Fisher Scientific Inc, USA
Light microscope	Axiovert 35	Carl Zeiss GmbH, Germany
Light microscope	REB-01	Discover ECHO Inc., USA
Microplate reader	Multiskan EX	Thermo Fisher Scientific Inc, USA
Microplate reader	TriStar^2 Multimode Reader LB 942	GmbH & Co. KG, Germany
Microwave	Micromaxx MM 41580	Medion AG
Power supply	PowerPac HC	BioRad Laboratories GmbH, Feldkirchen, Germany
Rocker	Certomat TC2	B. Braun Biotech International GmbH, Sweden
Scale > 60 g	L-2200 P	Sartorius AG, Germany
Scale 0.01-60 g	TE64-0CE	Sartorius AG, Germany
Scale for genotoxic substances	XPR	Mettler-Toledo International Inc., USA
Shaking incubator	MaxQ 4000	Thermo Fisher Scientific Inc., USA
Sonifier	Branson Sonifier 250	Branson Ultrasonics Corporation, Danbury, USA
Spacing plates for SDS-gel preparation, 1.5 mm	Mini Protean Spacing plate	Bio Rad Laboratories GmbH, Germany
Table centrifuge	Sprout	Thermo Fisher Scientific Inc, USA

Thermal cycler	T100	Bio Rad Laboratories GmbH, Germany
Tube roller	Roller mixer SRT 9	Cole-Parmer GmbH, Germany
Vortex mixer	D-6013	neoLab Migge GmbH, Germany
Water bath	3044	Köttermann GmbH, Germany
Gammacell irradiator	GC-2000	Moolgard Medical Denmark, Denmark

2.3. Software

Table 3: Software list

Software	Company
Ascent Software for Multiskan	Thermo Fisher Scientific Inc, USA
Cell quest Pro	BD (Becton, Dickinson and Company) corporation, Germany
CellA Imaging Software	Olympus Soft Imaging Solutions, Germany
Citavi	Swiss Academic Software GmbH, Germany
Comet IV Software	Perceptive Instruments Ltd., UK
ECHO Rebel	Discover ECHO Inc., USA
FACSDiva	BD (Becton, Dickinson and Company) corporation, Germany
Flowing software 2.0	Perttu Terho, Turku Biosciences, Finland
GraphPad Prism	GraphPad Software, USA
ICE Software	Berthold Technologies, Germany
ImageJ	U.S. National Institutes of Health, USA
ImageJ Colocalization Plug-in	Pierre Bourdoncle, Institut Jacues Monod, France
ImageJ Macro for automatic foci and/or colocalization count	Edited from Wynand P. Roos, Institute for toxicology, University Medical Center Mainz, Germany
MS Office Version 365	Microsoft Corporation, Germany
Odyssey Version 3.0	LI-COR Inc., USA
ZEISS ZEN Imaging Software 2.1	Carl Zeiss GmbH, Germany

2.4. Buffers and solutions

Table 4: List of buffers and solutions.

Buffer/Solution	Recipe
Annexin binding buffer stock (10x), pH 7.4	100 mM HEPES 1.4 M NaCl 250 µM $CaCl_2$ 0.1 % BSA
Blocking solution for WB	5 % skim milk in TBS-T or 5 % BSA in TBS-T
Bradford	0.01 % Coomassie 4.7 % ethanol 8.5 % H_3PO_4

Cell extraction buffer	10 mM TRIS, pH 7.4 2 mM Na_3VO_4 100 mM NaCl 1 % Triton-X 1 mM EDTA 10 % glycerol 1 mM EGTA 0.1 % SDS mM Na_4P_2O7
Citric acid-$Na_2PO_412H_2O$ buffer, pH 6	126.4 mM Na2PO412H2O 36.85 mM Citric acid In ddH2O
Electrophoresis buffer for alkaline comet assay, pH >13	300 mM NaOH 1 mM EDTA
Electrophoresis buffer for neutral comet assay, pH 7.5	90 mM TRIS 90 mM boric acid 2 mM EDTA
Fixation buffer for X-gal staining (10x)	20 % formaldehyde 2 % glutaraldehyde In PBS
Fixation buffer LSM	Methanol:Aceton (7:3)
FPG-buffer, pH 8	40 mM HEPES 0.1 M KCl 0.5 mM EDTA 0.2 mg/ml BSA
Hypotonic buffer	20 mM TRIS 10 mM NaCl 3 mM $MgCl_2$
Laemmli stock (10x)	1.92 M glycine 0.25 M TRIS
LSM antibody solution	0.3% Triton X-100 In PBS
Lysis buffer MTT	0.04 N HCL
Lysis buffer for alkaline comet assay pH 10 for neutral comet assay pH 7.5	2.5M NaCl 100 mM EDTA 10 mM TRIS 1% Triton X-100
Neutralization buffer for alkaline comet assay, pH 7.5	0.4 M TRIS
PBS	137 mM NaCl 2.7 mM KCl 4.3 mM Na_2HPO_4 1.47 mM KH_2PO_4
Ponceau S	5 % Acetic acid 0.1 % Ponceau In ddH_2O

<table>
<tr><td>SDS-Gel</td><td>
<table>
<tr><td></td><td colspan="4">2x 1.5 mm Gel</td></tr>
<tr><td>Ingredient</td><td>stacking</td><td colspan="3">separating</td></tr>
<tr><td></td><td>5 %</td><td>7.5 %</td><td>10 %</td><td>15 %</td></tr>
<tr><td>Tris 1.5 M pH 8.8</td><td>-</td><td>5 ml</td><td>5 ml</td><td>5 ml</td></tr>
<tr><td>Tris 1.5 M pH 6.8</td><td>1 ml</td><td>-</td><td>-</td><td>-</td></tr>
<tr><td>Acrylamide (40 %)</td><td>0.98 ml</td><td>3.750 ml</td><td>5 ml</td><td>7.5 ml</td></tr>
<tr><td>ddH_2O</td><td>5.7 ml</td><td>10.88 ml</td><td>9.67 ml</td><td>7.12 ml</td></tr>
<tr><td>Temed (10 %)</td><td>20 µl</td><td>120 µl</td><td>80 µl</td><td>80 µl</td></tr>
<tr><td>SDS (20 %)</td><td>80 µl</td><td>100 µl</td><td>100 µl</td><td>100 µl</td></tr>
<tr><td>APS (100 ng/ml)</td><td>60 µl</td><td>150 µl</td><td>150 µl</td><td>200 µl</td></tr>
</table>
</td></tr>
<tr><td>SDS-PAGE running buffer</td><td>Laemmli stock 1x
0.1 % SDS</td></tr>
<tr><td>Staining solution for X-gal staining, pH 6</td><td>100 mM Na2PO412H2O
30 mM Citric acid
125 mM NaCl
1.7 mM $MgCl_2$
4.5 mM Potassium ferricyanide
4.5 mM Potassium ferrocyanide
0.31 % X-gal
In ddH_2O</td></tr>
<tr><td>Tris buffered saline (TBS) (10x), pH 7.6</td><td>200 mM Tris
1.5 M NaCl</td></tr>
<tr><td>TRIS buffer pH 8.8 and 6.8</td><td>1.5 M TRIS</td></tr>
<tr><td>Western blot blotting buffer</td><td>Laemmlie stock 1x
Methanol 20 %</td></tr>
<tr><td>Western blot washing buffer, pH 7.5
(TBS-T)</td><td>1x TBS
0.1 % Tween-20</td></tr>
</table>

2.5. Antibodies

Table 5: List of primary antibodies.

Primary antibodies	Product number	Host	Company
53BP1	MAB3802	Mouse	EMD Millipore Corp., USA
ATM pS1981 (10H11.E12)	4526	Mouse	Cell Signalging Technology Corporation, UK
ATR pThr1998	PA5-77873	Rabbit	Invitrogen AG, USA
Bcl-W (31H4)	2724S	Rabbit	Cell Signalging Technology Corporation, UK
Bcl-X_L	2764T	Rabbit	Cell Signalging Technology Corporation, UK

CHK1 pS345	2341	Rabbit	Cell Signalging Technology Corporation, UK
CHK2 pTyr68	2661	Rabbit	Cell Signalging Technology Corporation, UK
H3K27me3 (C36B11)	9733S	Rabbit	Cell Signalging Technology Corporation, UK
H3K27me3	9718S	-	Cell Signalging Technology Corporation, UK
HSP90 (F-8)	Sc-13119	Mouse	Santa Cruz Biotechnology Inc., USA
MGMT (9-Max)	inhouse production	Rabbit	Prof. Dr. Bernd Kaina (inhouse production)
P21 Waf1/Cip1 (12D1)	2947S	Rabbit	Cell Signalging Technology Corporation, UK
p53 (DO-1)	Sc-126	Mouse	Santa Cruz Biotechnology Inc., USA
p53 pS15	9284S	Rabbit	Cell Signalging Technology Corporation, UK
p53 pSer46	558245	Mouse	BD Pharmingen
Rad51	ab63801	Rabbit	Abcam plc., UK
TRF1	ab10579	Mouse	Abcam plc., UK
yH2AX pS139 (20E3)	9718S	Rabbit	Cell Signalging Technology Corporation, UK
yH2AX pS139 (JBW301)	05-636	Mouse	EMD Millipore Corp., USA
yH2AX pS139	9718S	-	Dako, Glostrup, Denmark

Table 6: List of secondary antibodies.

Secondary antibodies	Product number	Host	Company
Anti-goat-Alexa Fluor 488	A11078	Rabbit	Invitrogen AG, USA
Anti-mouse-Alexa Fluor 488	A11017	Goat	Invitrogen AG, USA
Anti-mouse-IRDye 680RD	925-68072	Donkey	LI-COR Inc., USA
Anti-mouse-IRDye 800cw	926-32212	Donkey	LI-COR Inc., USA
Anti-Rabbit-Alexa Fluor 488	ab150077	Goat	Abcam plc., UK
Anti-rabbit-Cy3	ab97075	Goat	Abcam plc., UK
Anti-Rabbit-IRDye 680RD	926-68073	Donkey	LI-COR Inc., USA
Anti-rabbit-IRDye 800cw	926-32213	Donkey	LI-COR Inc., USA

2.6. Dyes and kits

Table 7: List of dyes.

Dye	Product number	Company
Prestained Pageruler	26616	Thermo Fisher Scientific Inc, USA
Propidium iodide (PI)	81845	Sigma-Aldrich Corporation, USA
Spectra Multicolor Broad Range Protein Ladder	26634	Thermo Fisher Scientific Inc, USA
TO-PRO™-3 Iodide (642/661)	T3605	Invitrogen AG, USA
TUNEL Assay Kit – HRP-DAB	ab206386	Abcam plc., UK

3. Methods

3.1. Cells and cell culture

The human glioblastoma cell lines LN229 (Research resource identifier (RRID): CVCL_0393) and A172 (RRID: CVCL_0131) were obtained from the American Type Culture Collection (ATCC). The MGMT positive cell line LN229-MGMT-c12 was previously generated by our group through stable transfection with a pSV2MGMT vector and a pSV2neo plasmid for selection (Knizhnik et al. 2013; Roos et al. 2007). The MGMT inducible cell line LN229-MGMT^{ind}c12 was kindly provided by Prof. Monica Hegi (Neuroscience Research Center and Neurosurgery, Lausanne University Hospital and University of Lausanne, Switzerland), the human diploid telomerase-immortalized primary fibroblast cell line VH10T was kindly provided by Prof. L. Mullenders (Department of Toxicogenetics, Leiden University Medical Centre, the Netherlands). The cellular characteristics are summarised in *Table 8*. To induce the expression of MGMT in the LN229-MGMT^{ind}c12 cell line, the cells were treated with 100 ng/ml of doxycycline.

Table 8: Cell line characteristics.

Cell line		LN229	LN229-MGMT-c12	LN229-MGMT^{ing}c12	A172	VH10T
Cell type		GBM				fibroblast
Tissue		Brain				foreskin
Organism		homo sapiens				
Sex		female			male	male
Features	p53	+ (mutated but functional)			+	+
	PTEN	+	+	+	-	/
	p16	-	-	-	+	/
	p14	-	-	-	+	/
	MGMT	-	+	inducible	-	+
Doubling time		~27 h			~ 42 h	/

All cells were cultured in Dulbecco's Modified Eagle Medium (DMEM) GlutaMax, supplemented with 10 % foetal calf serum (FCS), and were kept in a 5 % CO_2 humidified atmosphere at 37 °C. To maintain the cell culture, cells were cultivated in T-25 cell culture flasks containing 5 ml of medium. They were routinely passaged to avoid confluency and were kept in culture for no longer than 4 months. Depending on the experiment, the cells were seeded into either 10- or 5 cm cell culture dishes or 6-, 12-, 24-, or 96-well plates. It was taken care to maintain sustained proliferation throughout the experiment or until proliferation was interrupted by the treatment. Thus, for short-term experiments which did not exceed 2 d, cells were treated at about 70 % confluency, while for long-term experiments, cell were treated at about 50 % confluency.

For cryopreservation, cells of one 10 cm dish were collected by trypsinization, resuspended in 7.5 % dimethyl sulfoxide (DMSO) in FCS and transferred into 4 cryo tubes. Cells were then frozen over night at -80 °C in a passive-freeze container, reducing the temperature by -1 °C per hour. The next day, they were transferred into the gas phase above liquid nitrogen for long term storage. To reduce cell death during thawing, DMEM GlutaMax medium supplemented with 10 % FCS was pre-heated to 37 °C and the frozen cells were resuspended until fully thawed. The cells were then centrifuged and resuspended in the pre-heated medium. For each cryo tube, the cells were split into two cell culture flasks.

All cell culture work was performed under sterile conditions while routinely tested for mycoplasma to ensure cell culture quality and safety.

3.2. Drugs and treatments

All drugs and compounds were prepared and stored according to the manufacturer's recommendation. To avoid thaw-freezing-cycles, aliquoted were prepared and every aliquot was used no more than 3 times. To ensure that the cells were in a proliferating phase when treated, they were seeded 2 d prior to treatment and visually checked for confluency. When senescent cells were treated, the old medium was removed, and the cells were treated in fresh medium.

3.2.1. Temozolomide

The drug used to induce senescence was TMZ, which was kindly provided by Prof. Geoff Margison (University of Manchester, UK). For long-term storage, TMZ was dissolved in DMSO to create a 150 mM stock and then stored at -80 °C. Each aliquot was used only once. Immediately before treatment, the stock solution was further diluted in sterile double-distilled water (ddH_2O) to create a 15 mM solution which was then administered to the medium to reach the final desired working concentration.

3.2.2. Natural and small molecule compounds

The natural compounds curcumin and fisetin, as well as the curcumin- and water-micelles were used no longer than 3 d following preparation and were stored in the dark. While ethanol dissolved curcumin, fisetin, artesunate and all inhibitors were stored at -20 °C, micelles were stored at 4 °C. For cytotoxicity and senolytic testing, proliferating and senescent cells were treated for 2 d with the respective compound. The exact concentrations used for treatment can be found in the results. All used components are listed in *Table 9*.

Table 9: List of natural and small molecule compounds.

Compound	CAS number	Product number	Company
ABT-263 (Navitoclax)	923564-51-6	S1001	Selleck Chemicals LLC, USA
ABT-737	852808-04-9	S1002	Selleck Chemicals LLC, USA
AZD1390 (ATM inhibitor)	2089288-03-7	HY-109566	Hycultec GmbH, Germany
BV-6	1001600-56-1	S7597	Selleck Chemicals LLC, USA
Artesunate	88495-63-0		
CHK2 inhibitor II	516480-79-8	C3742	Sigma-Aldrich Corporation, USA
Chloroquine	54-05-7	S6999	Selleck Chemicals LLC, USA
Curcumin (native)	458-37-7	08511	Sigma-Aldrich Corporation, USA
Curcumin (micelles)	-	EW0124/5	NovaSol A/S, India
Fisetin	528-48-3	Ab142429	Abcam plc., UK
KU0060648	KU0060648	S8045	Selleck Chemicals LLC, USA
MCOPPB trihydrochloride	108147-88-1	PZ0159	Sigma Aldrich Chemie GmbH
NF-kB inhibitor III	380623-76-7	481411	Sigma Aldrich Chemie GmbH
Pifithrin-a	63208-82-2	S2929	Selleck Chemicals LLC, USA
Pifithrin-μ	64984-31-2	S2930	Selleck Chemicals LLC, USA
PX866	502632-66-8	13055	Cell Signaling Technology Inc., USA
Ri1	415713-60-9	1885	Axon Medchem BV, The Netherlands
UC2288	1394011-91-6	5328130001	Merck KGaA, Germany
UCN-01	112953-11-4	U6508	Sigma Aldrich Chemie GmbH
Veliparib	912444-00-9	A 861695	Axon Medchem BV, The Netherlands
VE-821 (ATR inhibitor)	1232410-49-9	HY-14731	Hycultec GmbH, Germany
Water micelles	-	EWO0105/7/80/W	NovaSol A/S, India
3-Methyladenine	5142-23-4	189490	Merck KGaA, Germany

3.2.3. Ionizing radiation

To induce additional DNA damage, IR was used. Therefore, cells were irradiated with γ-rays at different doses, reaching from 2 to 10 Gy, using the Gammacell irradiator 2000 (GCi). For transportation, the cell culture dishes were sealed to reduce risk of contamination. To exclude effects from temperature changes during transportation to and from the GCi, control samples were transported along irradiated samples.

3.3. Quantification of apoptosis

During apoptosis, the membrane of the cells is bulged outward, making access to phosphatidylserine (PS), usually located at the cytoplasmic side of the membrane. The method used in this study to measure early apoptosis and late apoptosis/necrosis takes advantage of this mechanism by binding an fluorochrome-coupled annexin molecule to the outward bulged PS in a calcium dependent manner, thus identifying apoptotic cells.

To differentiate the early apoptotic from the late apoptotic/necrotic fraction, the DNA intercalator propidium iodide (PI) was added. Since during late apoptosis and necrosis, the cell membrane becomes permeable, PI can enter the cell and intercalate the DNA, staining only late apoptotic/necrotic cells. Hence, during flowcytometric analysis, living cells appear as unstained population, while early apoptotic cells show up as annexin positive but not DNA-intercalated (AV^+/PI^-), late apoptotic/necrotic cells as double-stained (AV^+/PI^+) populations (Vermes et al. 1995). To quantify early and late apoptosis/necrosis, the cells were treated and incubated according to the experiment. Since apoptotic/necrotic cells detach from the plate and accumulate in the medium, the supernatant was collected. The adherent cells were detached from the plate by trypsinization, pooled with the supernatant and then centrifuged at 1000 rounds per minute (rpm) for 5 min. The resulting cell pellets were resuspended in 50 µl annexin binding buffer, containing 2.5 µl AV. Following an incubation time of 15 min at room temperature (RT), the cells were transferred onto ice and 10 µl of a 50 µg/ml PI solution were added. Samples were kept in the dark after the addition of annexin-FITC until measurement. Depending on the experimental setup, measurements were executed using either the BD FACS Calibur or FACSCanto II flow cytometer, as well as the Cell quest pro or FACS Diva software. After measuring, the data were assessed using the Flowing Software 2. An untreated, stained control sample was used to determine the optimal gate parameters for a correct cell selection (for exemplary pictures see supplemental Supplemental figure S1).

3.4. Quantification of senescent cells

The senescent state has several widely accepted identification markers, one of which is the upregulation of the senescence associated β-galactosidase (SA-β-gal), which catalyses the hydrolysis of β-galactosidases. Thus, an upregulation can be detected via the β-galactose derivates 5-Dodecanoylaminofluorescein-di-β-D-galactopyranoside (C12FDG) or 5-Bromo-4-chloro-3-indoxyl-β-D-galactopyranoside (X-Gal). While cleavage of X-Gal forms an intensely blue product that can be detected by light microscopy, the cleavage of C12FDG produces a fluorescent product that can be detected using the UV-vis channel of the flow cytometer (Burn 2012; Haugland and Johnson 1993).

To determine the senescent population following treatment and incubation of the cells via C12FDG, the endogenous β-gal activity had to be inhibited. Therefore, the supernatant was removed, and cells were incubated with fresh medium containing 300 µM chloroquine (Clq) for 30 min in the incubator. Thereafter, 33 µM C12FDG were added to the medium and the cells were incubated for an additional 90 min in the incubator. The cells were then washed with cold phosphate buffered saline (PBS), collected by trypsinization, and centrifuged for 5 min at 6000 rpm at 4 °C.

For analysis, the resulting cell pellets were resuspended in an adequate amount of PBS and stored on ice until measurement. The samples were kept in the dark from the addition of Clq until analysis using the BD FACS calibur or FACSCanto II flow cytometer and the Cell quest pro or FACS Diva software, respectively. A stained, untreated control sample served as standard to determine the optimal gating parameters and to ensure correct determination of the senescent population in the treated samples (for exemplary pictures see supplemental Supplemental figure S1).

While for the analysis via C12FDG living cells can be measured, the analysis via X-gal staining requires cell fixation prior to the X-gal treatment and measurement. To achieve that, the prepared cells were washed with PBS twice, then fixed in 1x fixation buffer for 5 min at RT. Residual fixation buffer was removed by washing fixed cells three times with PBS. For staining, the PBS was removed, and the cells were incubated with the staining solution in the incubator under CO_2 exclusion over-night but for between at least 12 h and maximal 16 h. Longer incubation periods might lead to a staining of cells by endogenous β-gal activity. Pictures of the un-/stained cells were taken using the ECHO Rebel light microscope system and cell numbers were counted using the ImageJ software.

3.5. Immunofluorescence

To identify structures within the cell, high resolution microscopes are necessary. In this study, DNA damage and telomers were detected using a laser scanning microscope (LSM). Therefore, coverslips were pre-incubated in diethyl ether for 20 min, washed in decreasing concentrations of ethanol in ddH_2O (100 %, 70 %, 0 %) and then incubated in 1 M hydrogen chloride for further 20 min. The cover slips were stored in 70 % ethanol in ddH_2O. Before seeding, one coverslip per 24-well plate, or two to four coverslips per 5 cm dish were placed in the well/dish and air dried before the medium and cells were added. For staining, treated and incubated cells were washed with PBS twice, then dehydrated and permeabilized in a methanol and acetone buffer (7:3) for 6 min at -20 °C and fixed in 4 % paraformaldehyde (PFA) for 10 min at RT. The residual PFA was removed by washing the cells once with cold PBS. The cells were re-hydrated for 5 min with cold PBS three times (15 min total). Prior to the primary antibody incubation, the fixed cells were blocked with 3 % bovine serum albumin (BSA) in PBS over night at 4 °C. Primary antibodies were administered in 0.3 % Triton X-100 in PBS over-night at 4 °C, after which cells were washed three times with cold PBS. Incubation of the secondary antibody occurred in 0.3 % Triton X-100 in PBS for 1 h at RT in the dark. After three additional 5 min washing steps to remove residual secondary antibody, cells were stained with TO-PRO™-3 Iodide, mounted onto microscope slides using Vectashield, and sealed with clear nail polish.

Upon DNA damage, the histone 2AX surrounding the DSBs is phosphorylated (=γH2AX) by ATM or ATR and 53BP1 is recruited to the site of damage. This accumulation of γH2AX and 53BP1 results in the appearance of foci following binding of fluorescent antibodies (Kuo and Yang 2008). Pictures of one plane per cell were taken for γH2AX or 53BP1 staining. Telomers were detected via the telomeric repeat-binding factor 1 (Trf1), which is part of the shelterin complex, coating the telomers (Liu et al. 2004). Detection of Trf1 by a single plane per cell showed to be insufficient, thus, z-stacks (overlay of >5 planes) were taken for telomer staining. Both pictures and z-stacks were taken using the Carl Zeiss ZEN program and cells were analysed using the ImageJ software with a colocalization plug-in. Foci of γH2AX, 53BP1 and Trf1, as well as colocalizations of γH2AX and Trf1 were quantified using a macro for ImageJ (for coding see supplemental material).

3.6. Preparation of cell lysates

For the protein analysis by sodium dodecyl sulphate polyacrylamide gel electrophoresis (SDS-PAGE) and Western blot, the cells need to be lysed. Therefore, the cells were washed with PBS, detached from the plate, and incubated in cell-extraction buffer for 30 min on ice with 10 min vortex intervals. Lysates were then sonicated three times for 10 pulses each at a duty cycle of 40 % and an output control of 4 using the Branson Sonifier 250. To separate the proteins from the cell debris, lysates were centrifuged at 14,000 rpm for 15 min at 4 °C, and the supernatant was collected without disturbing the pellet. Parts from the lysates were analysed for their protein concentration using Bradford analysis, the rest was mixed with RotiLoad and boiled at 90-95°C for 5-10 min to reduce disulphide bridges and denature the proteins. Cell lysates were stored in aliquots at -20 °C.

3.7. Determination of protein concentrations by Bradford

The colorimetric quantification of protein concentrations was developed by Marion Bradford in 1976 and is based on the absorbance shift of the Coomassie brilliant blue G-250 (Coomassie) dye from 465 nm to 595 nm upon binding to a protein (Bradford 1976). In brief, the Coomassie dye is stored in a cationic state having an absorbance maximum of 465 nm, thus having a brownish colour. When combined with a protein, the Coomassie dye donates a free electron to the protein's amino group. The protein's carboxyl group is thereby exposed and noncovalently binds to the dye's non-polar region by Van der Waals force. Thus, the blue anionic sulfonate of the dye is stabilized and the absorption maximum shifts to 595 nm, resulting in a blue colour (Ninfa et al. 2010). The higher the blue ratio within the sample, the more protein the sample contains. For quantification of protein concentrations in the samples, a standard curve reaching from 4.5 µg/ml to 45 µg/ml BSA was prepared in ddH_2O. Water without BSA served as blank. Lysates for protein analysis were diluted 1:2 in ddH_2O. Then 10 µl of undiluted standard and 10 µl of diluted sample were added to 200 µl Bradford solution in a 96 well plate. Samples were mixed briefly and incubated for 15 min in the dark at RT. Absorption was measured at 595 nm, each sample was assessed in triplets.

3.8. SDS-PAGE and Western Blot analysis

A widely used technique to analyse proteins within cell populations is the SDS-PAGE combined with Western blot. During the SDS-PAGE, denatured proteins are separated on basis of their molecular mass using an electrical current. Therefore, their intrinsic charge needs to be removed. To achieve that, SDS is included in the SDS-PAGE buffer. Since SDS is negatively charged it masks the intrinsic charge of the protein upon binding. Additionally, the basic pH of the buffer reduced positive charges. About one SDS molecule binds per two amino acids, thus, all proteins are negatively charged in proportion to their molecular weight. Upon application of a constant electrical field the proteins migrate through the acrylamide matrix towards the anode, with small molecules migrating faster than large ones, thereby separating the proteins according to their molecular mass.

For gel casting, the Mini-Protean gel casters were assembled according to the manufacturer. The stacking gel was prepared according to the table in the material part (*Table 4*), filled between the spacer- and short plates and overlayed with 100 % isopropanol. Following polymerisation, the isopropanol was discarded, the stacking gel prepared according to *Table 4*, and poured on top of the separation gel. A 15-well comb was applied for each gel to form pockets for protein loading. The cast gels were stored in a humidified atmosphere at 4 °C overnight before usage but for no longer than one week. Right before usage, the comb was removed, and the ladder and 30-100 µg of protein per sample were loaded onto the gel. The SDS-PAGE was run at 70 V until the samples had passed the collection gel and then at 120 V until the end. Before protein detection, proteins were transferred onto an Amersham Protean 0.2 µM NC blotting membrane. During this method the negatively charged proteins are being transferred onto the blotting membrane using an electrical current. To avoid over-heating, pre-chilled (4 °C) blotting buffer was used. Before assembling of the Mini-Protean blotting chamber according to the manufacturer, the blotting membrane was soaked in pre-chilled blotting buffer for 30 min. The proteins were then transferred onto the membrane with an 80 mA current over-night at 4 °C.

Western blot analysis is based on antibody binding to the protein of interest. To reduce unspecific background staining, the membranes were blocked in either 5 % skim milk or BSA, each prepared in TBS-T. The blocking solutions were removed by three washing steps with TBS-T for 5 min each (total of 15 min). They were then incubated in the respective primary antibody over-night at 4 °C. Excessive primary antibodies were removed by three 5 min washing steps in TBS-T. The secondary antibodies were then prepared in TBS-T without supplement and incubated for 1 h at RT. The proteins were detected using the Odyssey infrared imaging system following washing of the membranes for 3x 5 min.

For detection of phosphorylated and total protein, membranes were stripped using the LI-COR stripping buffer according to the manufacturer's instructions and re-incubated with the respective antibodies following the mentioned protocol.

3.9. Comet Assay

The comet assay is a single cell gel electrophorese (SCGE), allowing the measurement of DNA damage, e.g., single- and double strand breaks (SSBs and DSBs, respectively), oxidative damage and a-basic sites among others. In principle, the mobility of DNA fragments in an electrical field is measured. While the supercoiled DNA is unable to move through the polymer structure, smaller fragments and loose DNA ends are pulled out, forming the comet tail. Depending on the pH-value of the lysis- and electrophoresis-buffer different DNA damages can be detected. While the neutral comet assay primarily detects SSBs, the alkaline conditions are necessary to cleave the hydrogen bonds between the base pairs of double stranded DNA, and therefore detects SSBs and DSBs. Additionally, the alkaline comet assay can detect DNA damage, that themselves do not induce strand breaks but are converted into such at the alkaline pH of the SCGE, e.g., AP-sites. Furthermore, oxidative damage, e.g., 8-oxo-guanine, can be detected using a modified version of the alkaline comet assay by adding the formamidopyrimidine glycosylase (FPG) (Collins et al. 1997; Klaude et al. 1996).

In this study, the neutral comet assay, as well as the alkaline comet assay, modified with the FPG were used and performed with the technical assistance of Anna Frumkina from the Institute of Toxicology of the University Medical Center Mainz. Therefore, microscope slides were covered in 1.5 % agarose and dried overnight, lysis buffer was pre-chilled at 4 °C for at least 1 h and low melting point (LMP) agarose was pre-heated to 37 °C for preparation. For the comet assay itself, cells treated and incubated according to the experiment, were washed in PBS, and collected by trypsinization. They were then resuspended in PBS, mixed with 0.5 % LMP agarose and spread onto the agarose-covered microscope slides that were then covered with a coverslip. The agarose was let polymerize for 5 min at 4 °C after which the coverslips were removed and cells were lysed in the pre-chilled alkaline or neutral lysis buffer, depending on the comet assay, for 50 min. For the FPG modified alkaline comet assay, microscope slides were then incubated for 5 min at RT in FPG-buffer, after which 50 µl of a 1 µg/ml FPG solution were added to each slide. They were immediately covered with a coverslip and incubated for 45 min at 37 °C.

From all slides (neutral or alkaline, with or without FPG) coverslips were removed and slides were transferred into the electrophoresis chamber, where they were covered in alkaline or neutral electrophoresis buffer, depending on the comet assay, and incubated for 20 min at 4 °C for denaturation. The SCGE was run at 25 V for the neutral, and 300 mA for the alkaline comet assay for 15 min at 4 °C. For the alkaline comet assays, slides were then neutralized by washing three times for 5 min each in neutralization buffer. All slides, irrespective of the comet assay, were washed briefly in ddH_2O, incubated for 5 min in 100 % ethanol, and airdried for at least 2 h at RT. Immediately before analysis, 50 µl of a 50 µg/ml PI solution were spread onto each slide and a coverslip was applied onto each slide. For each sample, at least 50 cells were analysed using a fluorescence microscope and the Comet IV Software. The amount of DNA damage was expressed as the tail fluorescence intensity in relation to the head fluorescence intensity in percent, which is calculated by the formular:

$$tail\ intensity\ [\%] = \frac{Tail\ fluorescence\ intensity}{head\ fluorescence\ intensity} x\ 100$$

3.10. MTT assay

Cell viability was measured using the 3-(4,5-dimethylthiazol-2-yl)-2,5-diphenyltetrazolium bromide (MTT) assay. Like the Bradford assay it is a colorimetric measurement, based on the metabolic conversion of MTT. Upon cleavage by a mitochondrial reductase, the yellow MTT is converted into an insolubilized blue formazan (Vistica et al. 1991). This colorimetric change can be measured at 570 nm using a microplate reader. To assess the viability, cells were seeded in 96-well plates and treated and incubated according to the experiment. The medium was then exchanged for 100 µl phenol red free DMEM including 0.5 mg/ml MMT. Following an incubation time of 2-3 h at RT, the MTT solution was removed, and formazan was solubilized by addition of 100 µl of a 0.04 N HCL in propanol. To ensure full solubilization, the plate was shaken at 200 rpm for 10 min. Cell viability was thereafter analysed using a microplate reader at 570 nm. All samples were measured in triplicates.

3.11. Immunohistochemistry and TUNEL staining

The patient derived primary and recurrent GBM tumour samples were resected by the Department of Neurosurgery from the University Medical Center Mainz. The tissue sections were kindly provided by Prof. Dr. Clemens Sommer and the immunohistochemistry staining and the terminal deoxynucleotidyl transferase (TdT), dUTP nick end labelling (TUNEL) were kindly performed by Dr. Petra Leukel from the Institute of Neuropathology from the University Medical Center Mainz. Matched primary and recurrent tumour samples of ten patients were included.

The tumour samples were routinely formalin-fixed, and paraffin embedded immediately after resection. The immunohistochemistry staining and TUNEL assay were performed on 4 µm thick de-waxed tissue sections. For the immunohistochemistry staining, the antigen retrieval was performed using the FLEX Target Retrieval Solution with high pH. To block the endogenous peroxidase the sections were treated with a peroxidase-blocking solution. The γH2AX and H3K27me3 staining was performed in an automated immunostainer using the γH2AX and the H3K27me3 primary antibodies in a 1:500 and 1:200 dilution, respectively. Using the universal immune-enzyme polymer method (Nichirei Biosciences, Tokyo, Japan), the immunoreactivity was thereafter visualised, and the sections were developed in diaminobenzidine.

For the detection of apoptotic cells in the tumour sections, the TUNEL Assay Kit - horseradish peroxidase (HRP) - diaminobenzidine (DAB) from Abcam was used according to the manufacturer. In brief, the de-waxed tissue was treated with proteinase K, permeabilised with H_2O_2 and then equilibrated. The labelling was performed with the TdT, and the sections were then blocked and further incubated with a conjugation solution. Visualisation was performed by DAB-HRP and methylene green.

For each tumour slide, ten sections were evaluated by light microscopy at a 100-fold magnification. The quantification of γH2AX, H3K27me3 and TUNEL positive cells was performed using the ImageJ software.

3.12. Patients and ethic statement

For the evaluation of γH2AX, H3K27me3 and TUNEL positive cells in GBM tumour samples, human material was used. The usage of these samples occurred in agreement with the declaration of Helsinki in the use of human material for research. The written informed consent of all patients or their legal guardians for the "scientific use of tumour tissue not required for histopathological diagnosis" was obtained in the admission contract of the University Medical Center Mainz.

This was in accordance with the ethics committee of Rhineland-Palatinate and the approval of the local ethics committee (No. 2020-15261).

3.13. Statistical analysis

All graphs were built, and statistics were performed using the GraphPad Prism software. Significance levels were calculated using the unpaired t-test and Welch's correction. All experiments were performed at least three times, if not stated otherwise.

4. Results

Despite all efforts, GBM still poses a threat to human life. The classical Stupp-schema for GBM treatment, consisting of maximum safe resection of the tumour followed by TMZ treatment concomitantly with IR, prolongs PFS and OS, but survival rates are still low, under 10 %, and the disease progresses rapidly, leading to the death of the patient within 15 months on average. Thus, a better understanding of cellular responses to TMZ is desirable to improve treatment schedules for GBM patients.

To get a better understanding of the mode of action of TMZ in GBM cells, we determined the kinetics of DSBs induction, early and late apoptosis/necrosis (cell death) and CSEN. Furthermore, we analysed senescent cells and identified pathways involved in CSEN maintenance. Next, we evaluated the treatment with IR or CCNU administered together with TMZ and screened for senolytic agents using three natural compounds, and a nociceptin receptor inhibitor, previously shown to bear senolytic activity.

4.1. Evaluation of TMZ-induced DSBs and DDR

We previously demonstrated that the induction of TMZ-induced DSBs is dose-dependent. We observed a linear correlation between the TMZ concentration in the medium and the number of DSBs and level of cell death and CSEN (Stratenwerth et al. 2021). To further investigate TMZ-induced DNA damage and cell responses, we analysed TMZ-induced DSBs as well as cell death and CSEN kinetics. Since the lesion responsible for cytotoxic and genotoxic effects of TMZ, O^6meG, is repaired by MGMT, cell lines deficient for MGMT were used in the following series of experiments. To ensure no expression of MGMT in the LN229 and A172 cell lines, we performed western blot analyses. As shown in Figure 11 neither the LN229 nor the A172 cell line expressed MGMT. The MGMT expressing cell line LN229-MGMT^{ind}c12 served as positive control.

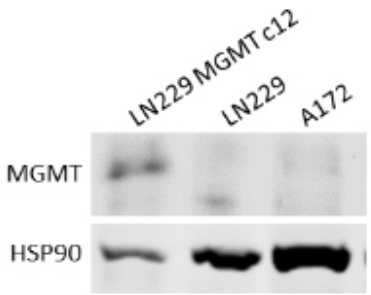

Figure 11: Western blot analysis of the MGMT protein expression.
The protein level of MGMT in proliferating LN229, A172 and LN229-MGMTc12 was detected by western blot analysis with subsequent immunostaining. For each lysate, 50 µg protein were loaded onto a 15 % polyacrylamide gel. Pictures are representative for one experiment. HSP90 served as loading control.

4.1.1. Kinetics of TMZ-induced DSBs

To analyse the kinetics of DSBs following TMZ treatment, LN229 cells in the exponential growth phase were treated with 20 µM TMZ for 2-120 h and fixed thereafter. DSBs were assessed using γH2AX and 53BP1 immunofluorescence staining. Antibody binding was detected by LSM and quantified using the ImageJ software. The foci in the green channel represent antibody binding to γH2AX, while the red channel detected 53BP1 antibody binding. The merged picture shows an overlap of both, γH2AX and 53BP1 foci. Colocalized foci appear in yellow (Figure 12).

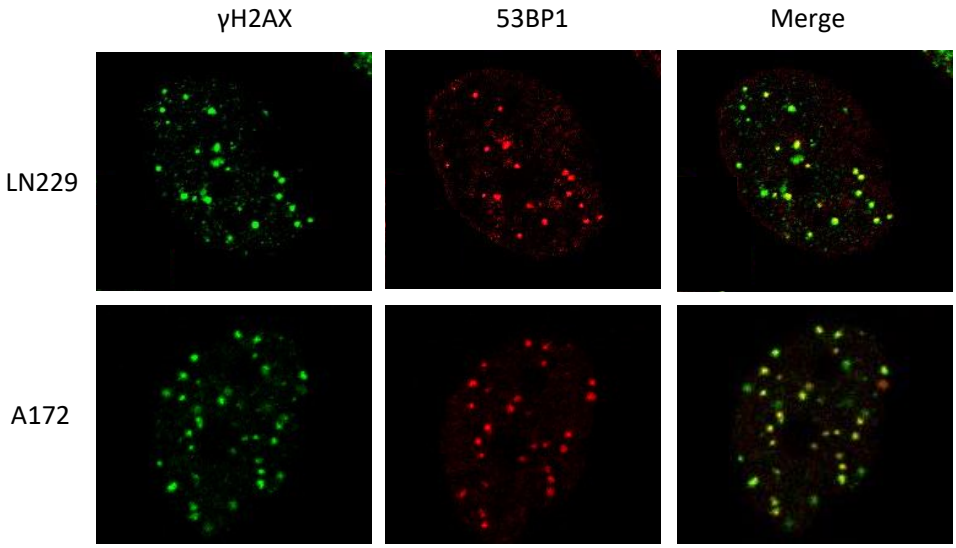

Figure 12: Representative images of γH2AX and 53BP1 foci detected via LSM in one nucleus.
LN229 cells were treated with 20 µM TMZ for 72 hrs. γH2AX and 53BP1 foci were stained by immunofluorescence and detected via LSM. The green channel represents γH2AX foci, the red channel 53BP1 foci. Overlaps between both foci are indicated in the merged picture and appear yellow. Pictures represent one plane from each nucleus and were taken using 64x magnification objective with immersion oil.

Foci within the nuclei, which were stained with ToPro3, were quantified using a macro for the ImageJ software with an installed colocalization plugin (for macro code see supplement). Hereafter, all foci were quantified using this method. As shown in Figure 13A, TMZ treated cells showed a significantly higher number of γH2AX foci than the untreated proliferating control cell populations (designated as CON) starting at 48 h following treatment, while 53BP foci arose later and were first detected 72 h after the onset of treatment. Both, the number of γH2AX and 53BP1 foci stayed significantly higher than the control level up to 120 h post treatment.

O^6meG is a minor adduct induced by TMZ, accounting for about 7 % of the lesions induced in the DNA. In higher quantity, N- and other O-alkylation lesions do occur, which are repaired via BER and the ALKBH-2 protein. It has recently been proposed that simultaneous repair of different alkylated DNA adducts in proximity can lead to early DSB induction without replication (Fuchs et al. 2021).

We were thus interested in the early induction of DSBs in our cell system. Both, LN229 and A172 cells treated with 50 µM TMZ showed a significant increase in γH2AX foci 2 h following treatment. Six h after treatment the amount of γH2AX foci returned to the control levels (designated as CON) in both cell lines (Figure 13B).

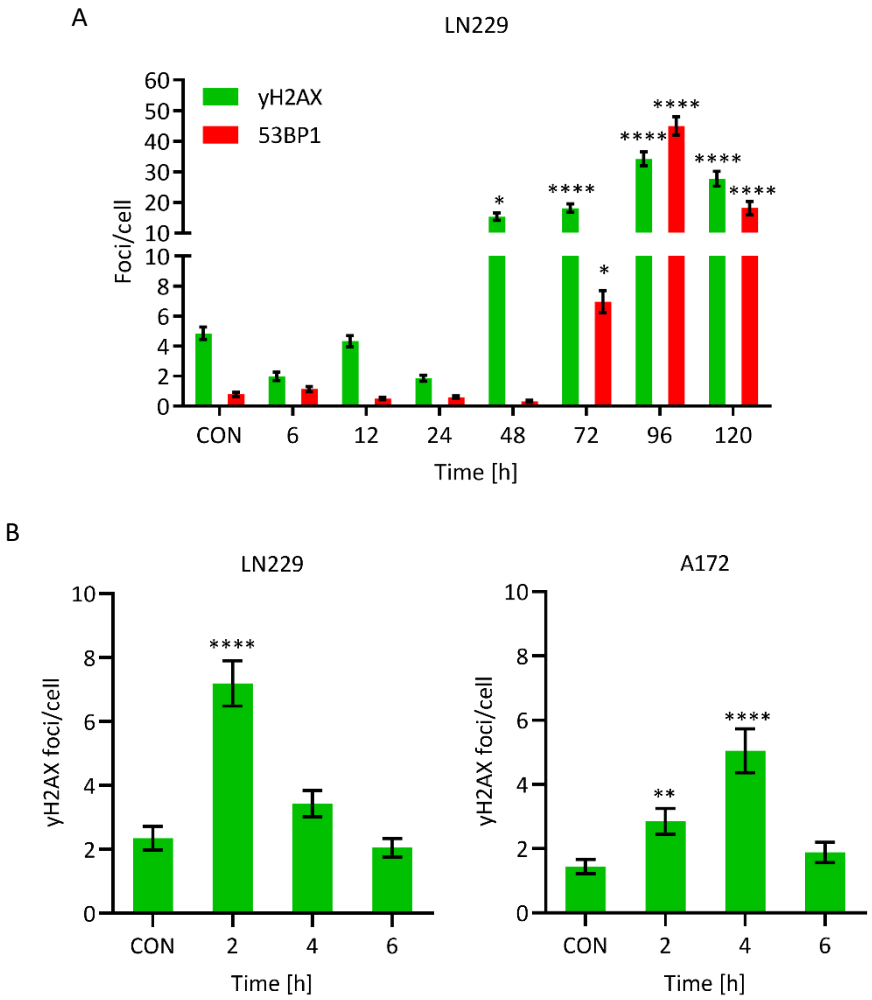

Figure 13: Kinetics of TMZ-induced DSBs.

LN229 and A172 cells were treated with (A) 20 µM or (B) 50 µM TMZ for the indicated time points. γH2AX and 53BP1 were stained using immunofluorescence and foci were detected via LSM Untreated proliferating cells served as control (CON). The data are given with the mean ± SEM of one representative experiment. *p<0.05, **p<0.01, ****p<0.0001.

4.1.2. Cell death and senescence induced by TMZ treatment

As previously demonstrated, the unrepaired DNA damage O^6meG can lead to cell death and CSEN in a dose-dependent manner (Stratenwerth et al. 2021). To get a better understanding of TMZ-induced cell responses, we analysed the kinetics of TMZ-induced cell death and CSEN following TMZ treatment. To this end, LN229 and A172 cells were treated with 50 µM TMZ and harvested at the indicated time points. Apoptotic and senescent cells were stained by AV/PI and C12FDG, respectively, and positively stained cells were detected by flow cytometry. Evaluation of the flow cytometry data was performed using the flowing software 2.0. As shown in Figure 14, cell death and CSEN both increased with time. While significantly higher levels of CSEN were first detected 3 d (72 h) following treatment, cell death increased later and was first significantly increased 4 d (96 h) post treatment. Also, cell death levels reached about 20-30 % after 10 d (240 h) of TMZ treatment, while CSEN levels increased up to 80 %. These results clearly demonstrate that the cell survival mechanisms based in the induction of CSEN is the main trait induced in GMB cells following TMZ treatment.

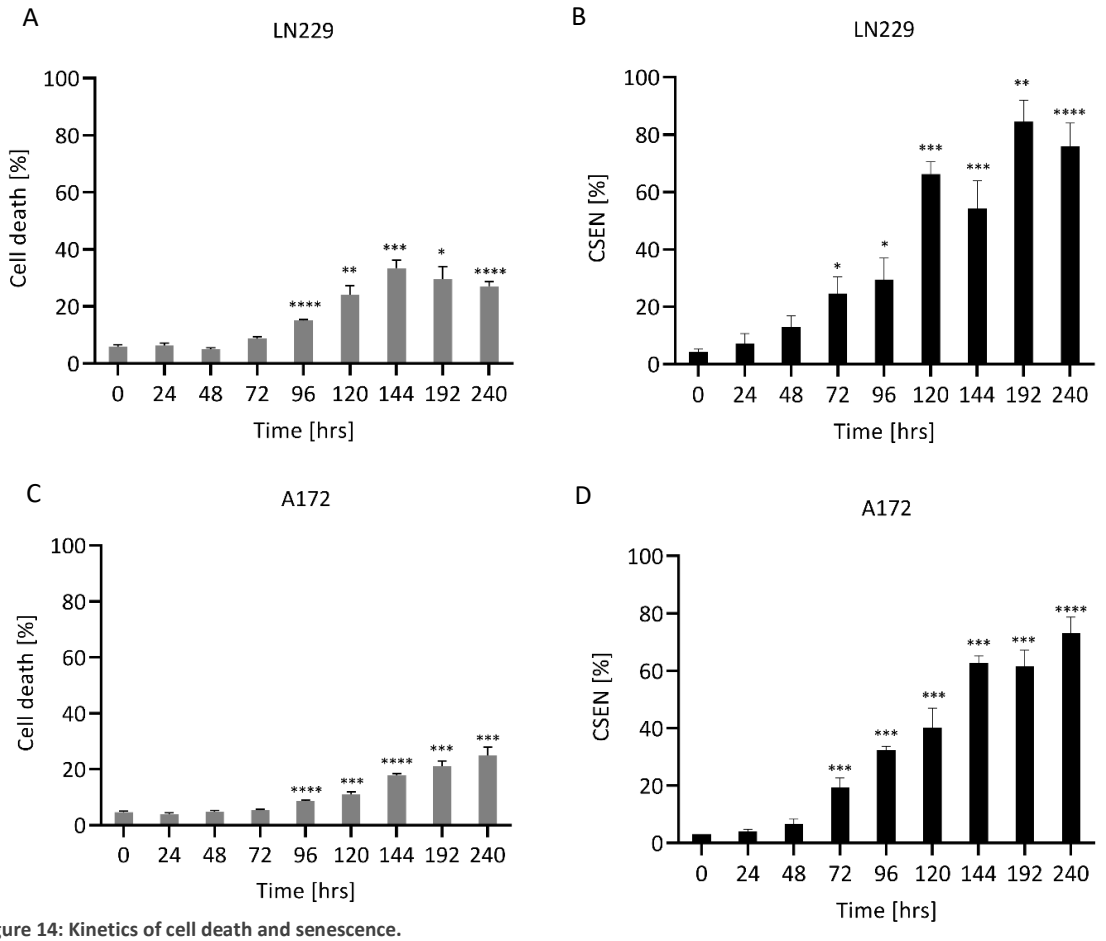

Figure 14: Kinetics of cell death and senescence.
Treatment of LN229 and A172 cells with 50 µM TMZ leads to a time-dependent increase in cell death (A and C) and CSEN (B, D), starting at 96 h and 72 h post treatment, respectively. Cell death and CSEN were detected by AV/PI and C12FDG staining, respectively. Untreated proliferating cells (0 h) served as control. The data is given with the mean ± SEM for three representative experiments. *p<0.05, **p<0.01, ***p<0.001, ****p<0.0001.

4.2. Characteristics of senescent cells

Senescent cells were shown to be able to escape their senescent state and start proliferating again (Saleh et al. 2019; Olszewska et al. 2021). It has therefore been hypothesized that these senescent cells lead to recurrences of GBM tumours (Demaria et al. 2017). A better understanding of CSEN could lead to treatment options reducing senescent cells in GBM patients, thus leading to a better patient outcome. Here, we used different methods to identify senescent cells, including morphology and detection of SA-β-gal. We then characterised senescent cells by identifying active pathways, analysing DSBs repair and ROS levels.

4.2.1. Morphological characteristics

Our previous results showed high amounts of senescent cells 8-10 d following TMZ treatment. Morphological analysis of TMZ treated LN229 and A172 cell populations and staining with X-gal, a substrate that turns into a blue dye when processed by SA-β-gal, were performed to confirm these results. As shown in Figure 15A, TMZ treated LN229 and A172 cells display a flat, enlarged morphology, typical for senescence, and are positively stained with X-gal, indicating the presence of SA-β-gal. Contrary, untreated proliferating cells were smaller and unstained. An overview of the cell populations clearly demonstrated a high number of senescent cells following TMZ treatment for 8 d (Figure 15B). Quantification of positively stained cells using a light microscope and the ImageJ software confirmed the increasing number of senescent cells over time, reaching about 80 % after 8 d (Figure 15C).

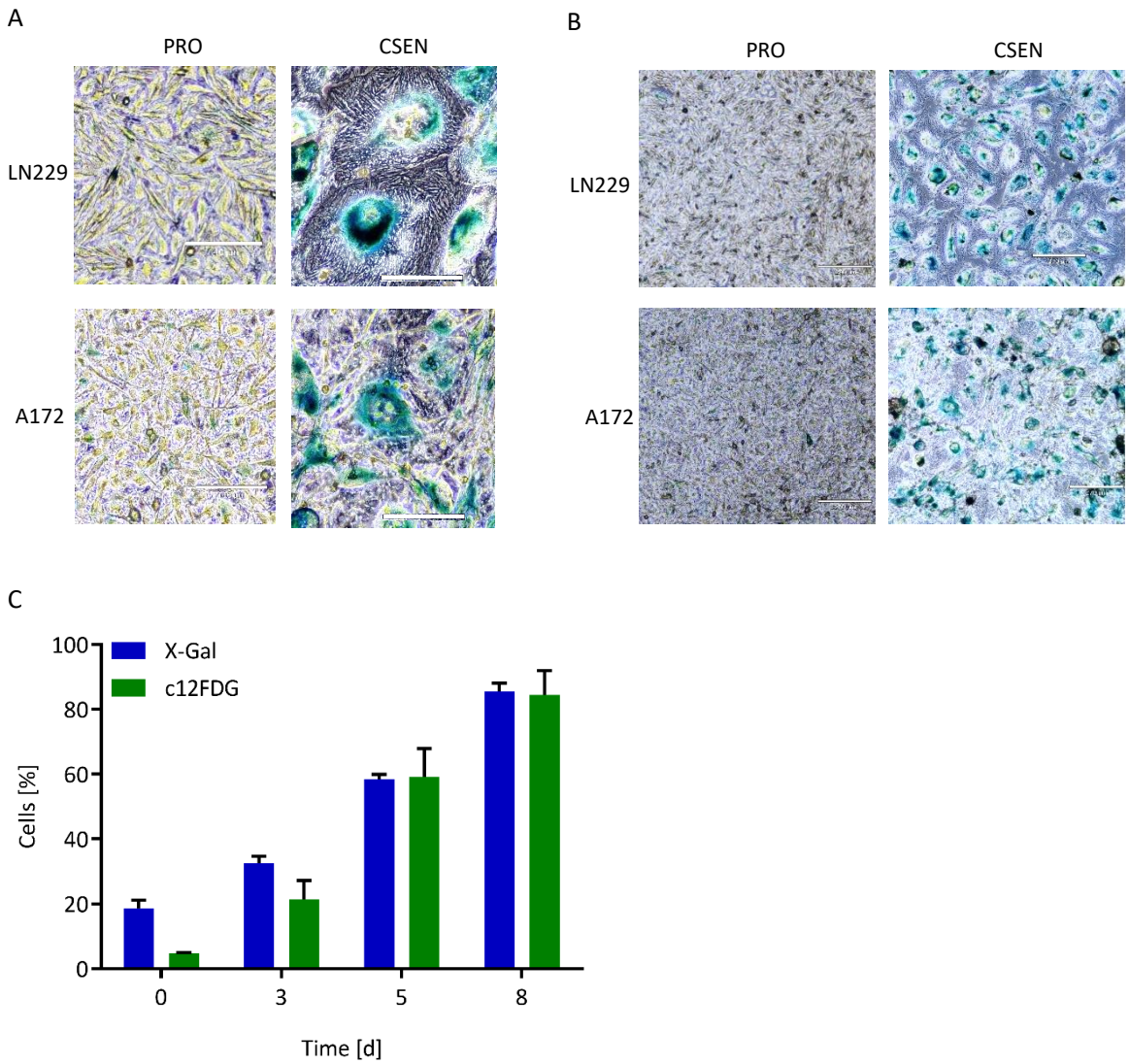

Figure 15: Morphological and bio-molecular characteristics of senescent cells.
(A) Senescent cells (CSEN) display enlarged, flat morphology and are stained blue, while proliferating cells (PRO) are smaller and unstained. Pictures were taken with 20x magnification objective, measuring bars display 140 µm. (B) Microscopical analysis of LN229 and A172 cell populations 8 d following 50 µM TMZ treatment show high number of X-gal-stained cells. Pictures were taken with 10x magnification objective, measuring bars display 270 µm. (C) Quantification of X-gal-stained cells confirms high number of senescent cells measured by flow cytometry. The data is given with the mean ± SEM for one representative experiment.

These results show that treatment of LN229 and A172 cells with 50 µM TMZ for 8 d is sufficient to produce a high percentage of senescent cells. Therefore, this treatment schedule was further used to generate a senescent cell population. Additionally, western blot analysis was used to detect γH2AX. This and all following neutral comet assays to detect DSBs were performed with support of the technical assistance from Anna Frumkina. In Figure 16A and B, the quantification of γH2AX and 53BP1 foci clearly show the presence of DSBs in senescent LN229 and A172 cells, while the proliferating control population (PRO) showed basal levels of DSBs. This was confirmed by elevated γH2AX protein levels in the senescent cell populations observed in the western blots (Figure 16C and D).

Also, the high tail intensities in senescent cells detected with the comet assay confirmed the presence of DSBs in the senescent cell populations (Figure 16E and F).

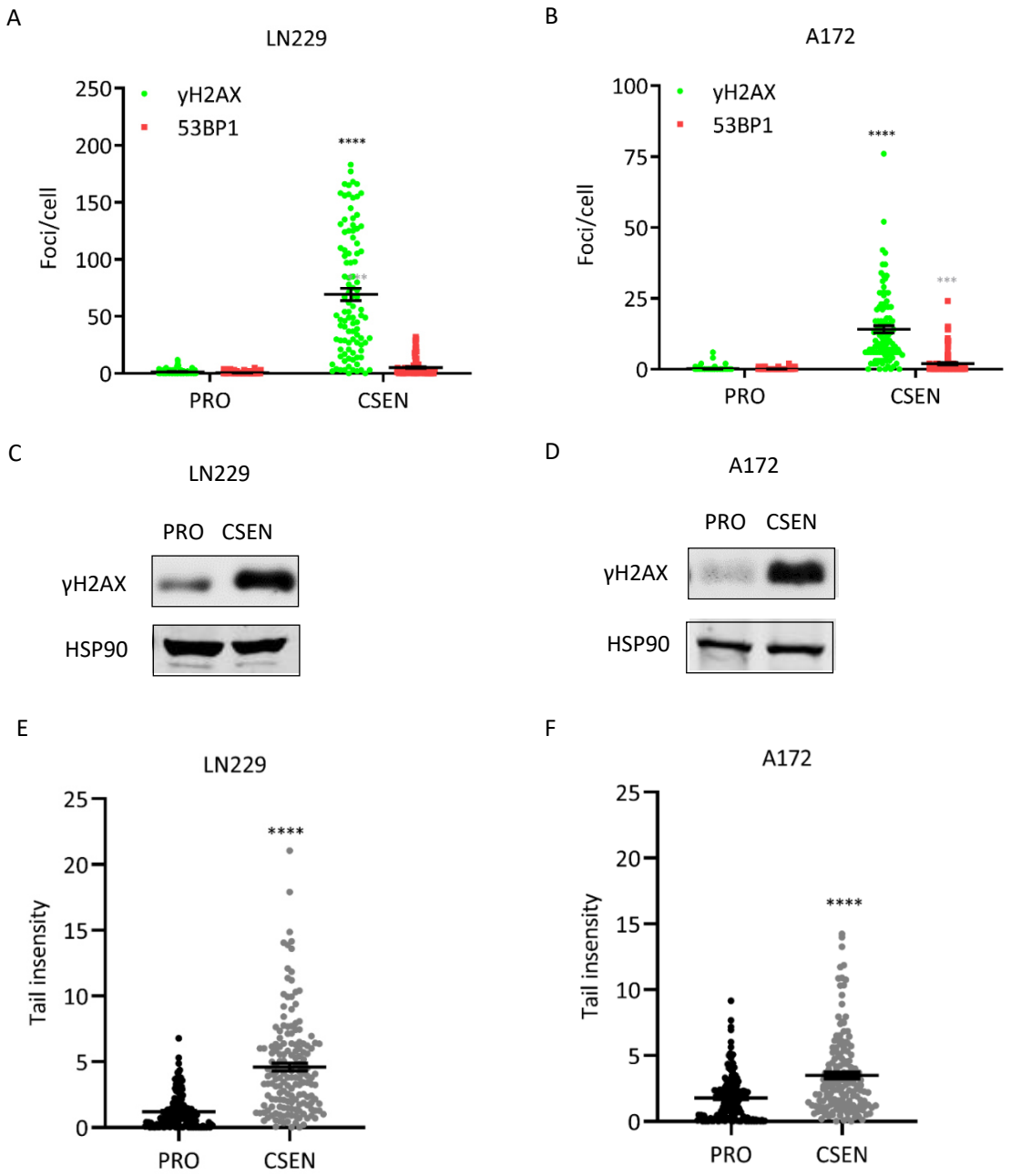

Figure 16: DSBs are present in senescent LN229 and A172 cells.

Senescent (CSEN) LN229 and A172 cells display a high number of DSBs compared to their proliferating (PRO) counterpart. (A and B) DSBs were detected by γH2AX and 53BP1 immunofluorescence staining, assessed by LSM. The data is given with the mean ± SEM for one representative experiment. (C and D) γH2AX protein levels were detected by western blot analysis with subsequent immunostaining. From each lysate, 50 µg protein were loaded onto a 15 % polyacrylamide gel. Pictures are representative for one experiment. HSP90 served as loading control. (E, F) DSBs were detected by elevated tail intensities in the neutral comet assay. Data are mean ± SEM for ≥ three independent experiments. *p<0.05, **p<0.01, ***p<0.001, ****p<0.0001.

During replicative senescence, DSBs occur at telomers due to telomer shortening, resulting in ATM recruitment and phosphorylation of histone 2AX (Arnoult and Karlseder 2015; Di d'Adda Fagagna 2008). To check whether this happens in the case of TMZ-induced senescence, we co-stained γH2AX with the Trf1. As part of the telomere's shelterin nucleoprotein complex, Trf1 is present at telomers throughout the cell cycle and is therefore a potent telomer marker (Liu et al. 2004). By merging the channels for γH2AX, shown in red, and Trf1, shown in green, co-localized foci appear in yellow. Visual analysis of the pictures shows the lack of co-localized foci (Figure 17A). The quantification of co-localizations between γH2AX and Trf1 foci in senescent LN229 and A172 cells showed no overlapping foci, demonstrating, that DSBs in TMZ-induced senescent LN229 and A172 cells occur mainly outside of telomers (Figure 17B).

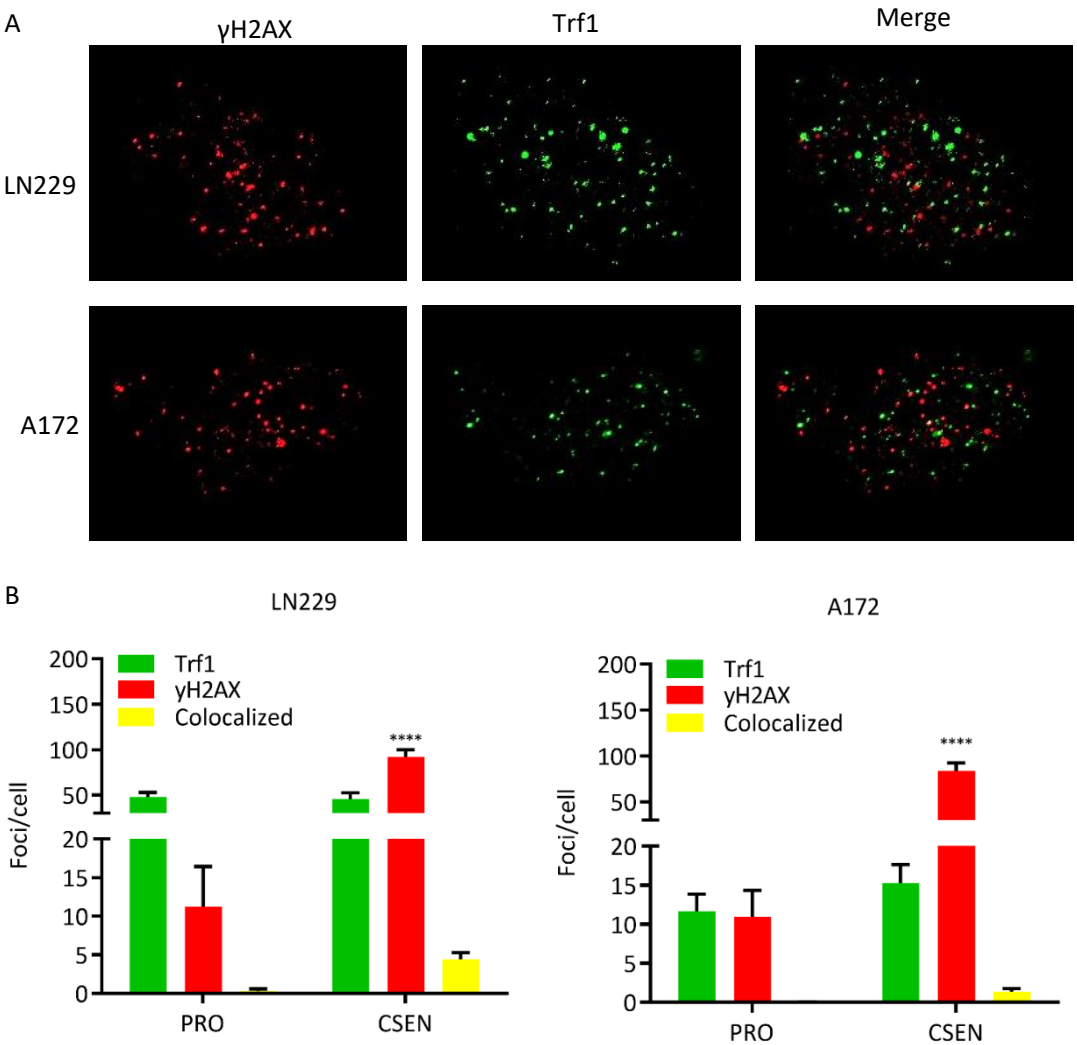

Figure 17: Representative images and quantitative analysis of γH2AX and Trf1 staining.

Senescent LN229 and A172 cells were co-stained for γH2AX and 53BP1 using immunofluorescence staining, detected by LSM. (A) Representative pictures. The red channel represents γH2AX foci, the green channel Trf1 staining (= telomers). The merged pictures identify overlapping γH2AX and Trf1 foci by yellow staining. The pictures represent one plane from each nucleus and were taken using a 64x magnification objective with immersion oil. (B) The number of γH2AX and Trf1 foci, as well as co-localisations were quantified using the ImageJ. Proliferating cells served as control (PRO). The data is given with the mean ± SEM for one representative experiment. ****p<0.0001.

4.2.2. Analysis of the DDR in senescent cells

The presence of DSBs in the senescent LN229 and A172 cell populations leads to the hypothesis that in senescent cells the DDR is permanently activated. To provide support for this hypothesis, we analysed the activation of the DDR factors ATM, ATR, CHK1, CHK2, p53 and p21 in senescent cells. In western blots of lysates obtained from proliferating and TMZ-induced senescent LN229 and A172 cell populations were compared. In line with the high number of DSBs in senescent cells shown earlier, we observed activation of the DDR. The active DDR was verified by phosphorylation of ATM at Ser1981 and ATR at Thr1989, CHK1 at Ser345 and CHK2 at Thr68, as well as phosphorylation of p53 at Ser15 and Ser46, and induction of p21 (Figure 18A-D). It is important to note that despite a mutation in the p53 gene in LN229 cells, the protein was still stabilized, phosphorylated, and able to transactivate p21 expression following TMZ treatment, hence p53 is functionally wild-type (Figure 18C and D). Comparing the activation of ATM and CHK2 in both cell lines, it is obvious that the activation was more prominent in LN229 cells (Figure 18A and B). Since senescence is a pro-survival pathway, we were wondering whether or not antiapoptotic pathways were active in order to to prevent cell death. Western blot analysis of Bcl-2 and Bcl-X_L showed different regulation patterns in LN229 and A172 cells. While in LN229 Bcl-2 was highly upregulated, Bcl-X_L showed only a slight induction. In A172 cells on the other hand, Bcl-X_L was highly upregulated, while Bcl-2 was even downregulated (Figure 18E and F). This data indicates that upon TMZ reatment, glioblastoma cells activate the DDR as well as anti-apoptotic pathways in order to circumvent cell death.

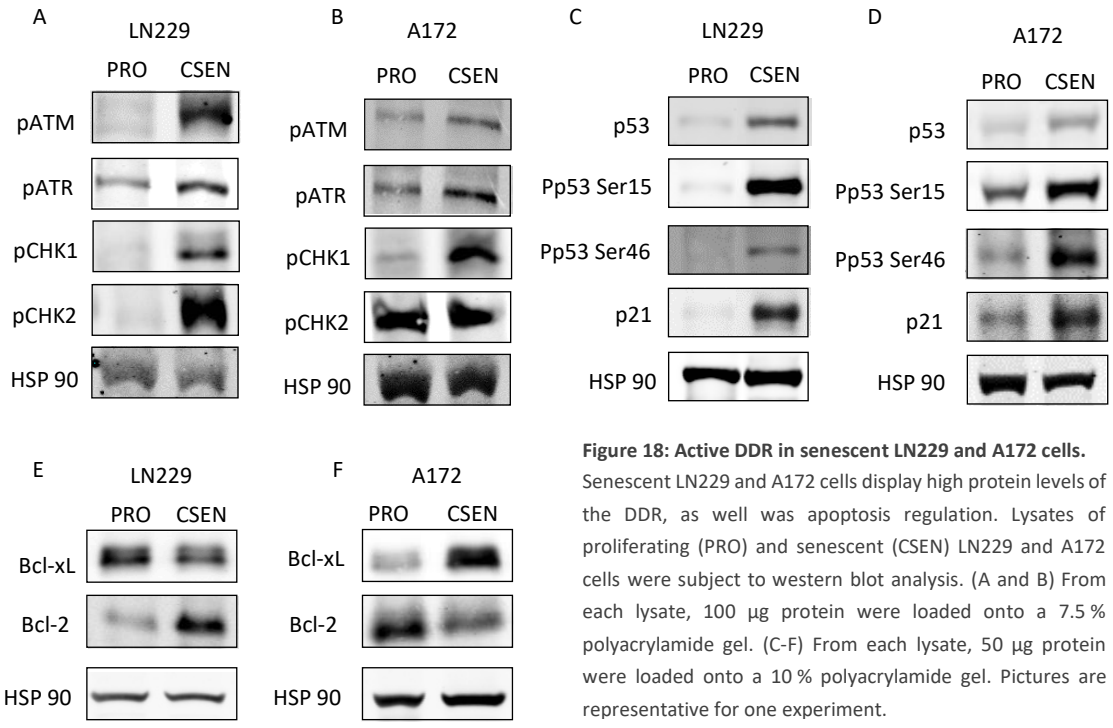

Figure 18: Active DDR in senescent LN229 and A172 cells. Senescent LN229 and A172 cells display high protein levels of the DDR, as well was apoptosis regulation. Lysates of proliferating (PRO) and senescent (CSEN) LN229 and A172 cells were subject to western blot analysis. (A and B) From each lysate, 100 µg protein were loaded onto a 7.5 % polyacrylamide gel. (C-F) From each lysate, 50 µg protein were loaded onto a 10 % polyacrylamide gel. Pictures are representative for one experiment.

4.2.3. Assessment of DNA damage repair in senescent cells

Although DSBs are still present in the senescent LN229 and A172 cell populations, an active DDR give reason to believe that additional DNA damage is recognised by the DDR which cannot be repaired in CSEN cells. To check this hypothesis, we irradiated proliferating and senescent LN229 and A172 cells with 6 Gy of γ-rays and measured the occurring DSBs by the neutral comet assay. If senescent cells repair the additional DNA damage, the tail intensities are expected to be reduced within a few hours. Indeed, a significant increase in DSBs immediately after irradiation (0.25 h) of proliferating and senescent cells was observed by high tail intensities. These decreased significantly after 3 h and even further after 6 h post-exposure, which indicates a repair of DSBs (Figure 19). Obviously, CSEN cells are capable of DSBs repair.

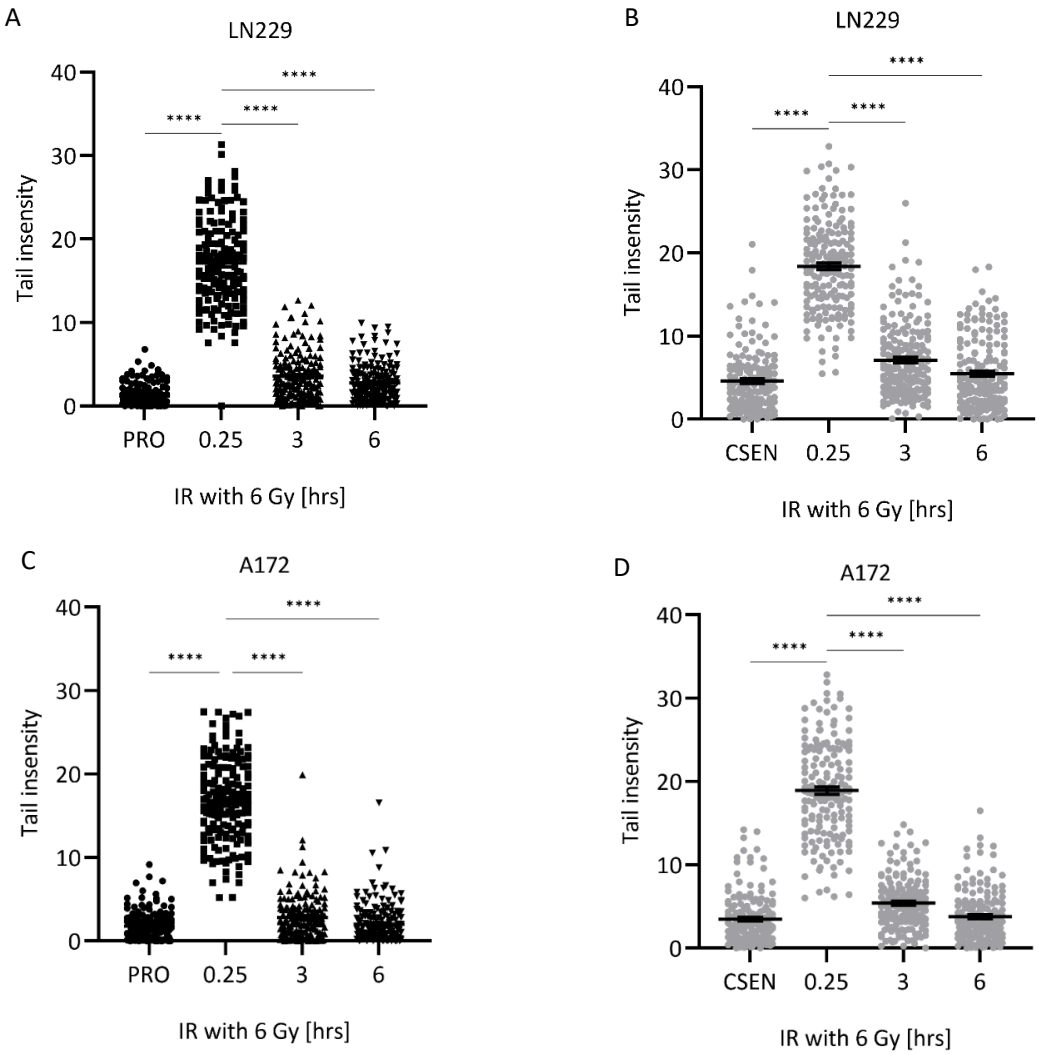

Figure 19: Active DNA repair in proliferating and senescent cells.
Proliferating (PRO) and senescent (CSEN) LN229 and A172 cells were irradiated with 6 Gy or left untreated as control. DSBs were detected by comet assay immediately after irradiation (0.25 h), 3 h and 6 h later. Senescent LN229 (B) and A172 (D) show the same level of DSBs repair than their proliferating counterparts (A and C, respectively). The data is given with the mean ± SEM for three representative experiments. $p<0.0001$.

These findings lead, however, to the question, why senescent cells display high numbers of DSBs. One could hypothesize that persisting O^6meG adducts hinder DNA repair, hence leading to persisting DSBs. To verify this theory, we treated used the LN229-MGMT^{ind}c12 cell line kindly provided by Prof. Monika E. Hegi from the Neuroscience Research Center and Neurosurgery of the Lausanne University Hospital and University of Lausanne, Switzerland. This cell line is naturally MGMT deficient. Upon treatment with doxycycline (dox), however, expression of MGMT is induced. Making use of this tet-on system, we treated LN229-MGMT^{ind}c12 cells with 50 µM TMZ for 8 d to induce high levels of senescence. We then induced MGMT expression in this population by dox treatment and measured DSBs by neutral comet assay 2 d later. Interestingly, expression of MGMT in senescent LN229 cells led indeed to a reduction in the tail intensity, hence reduced DSBs (Figure 20). This result indicates that at least a sub-fraction of unrepaired DSBs in senescent LN229 and A172 cells result from persisting O^6meG adducts in the DNA. Further analysis, e.g., through the determination of γH2AX and 53BP1 foci before and after MGMT expression should be performed to confirm these results.

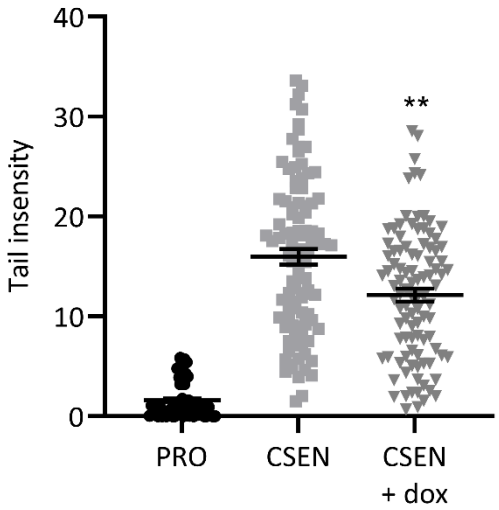

Figure 20: MGMT expression in senescent cells leads to DSBs repair.
MGMT expression was induced in senescent (CSEN) LN229-MGMT^{ind}c12 cells via 100 ng/ml dox treatment. A significant reduction in the tail intensity measured using the neutral comet assay and was detected 2 d later. Proliferating cells served as control (PRO). The data are given with the mean ± SEM of one representative experiment. **p<0.01.

4.2.4. Detection of ROS in senescent cells

ROS contributing to senescence lead to DSBs and activate cell death. They have long been associated with chemotherapy (Conklin 2004; Nair et al. 2015). Since TMZ treatment causes the induction of cell death and senescence, and senescent cells show high levels of DSBs, we measured ROS levels in proliferating and senescent LN229 and A172 cell populations. This was done via DCF detection in the flow cytometer. Additionally, we measured oxidative DNA damage by an FPG-modified alkaline comet assay with the help of the technical assistance of Anna Frumkina. Our results demonstrate an increase of ROS levels in senescent LN229 and A172 cells compared to proliferating cells (Figure 21A and B). Also, oxidative DNA damage increased significantly (Figure 21C and D), leading to the conclusion that senescent cells have increased ROS damage. Whether high ROS levels results directly from TMZ treatment or indirectly from DNA damage caused by TMZ is yet to be determined.

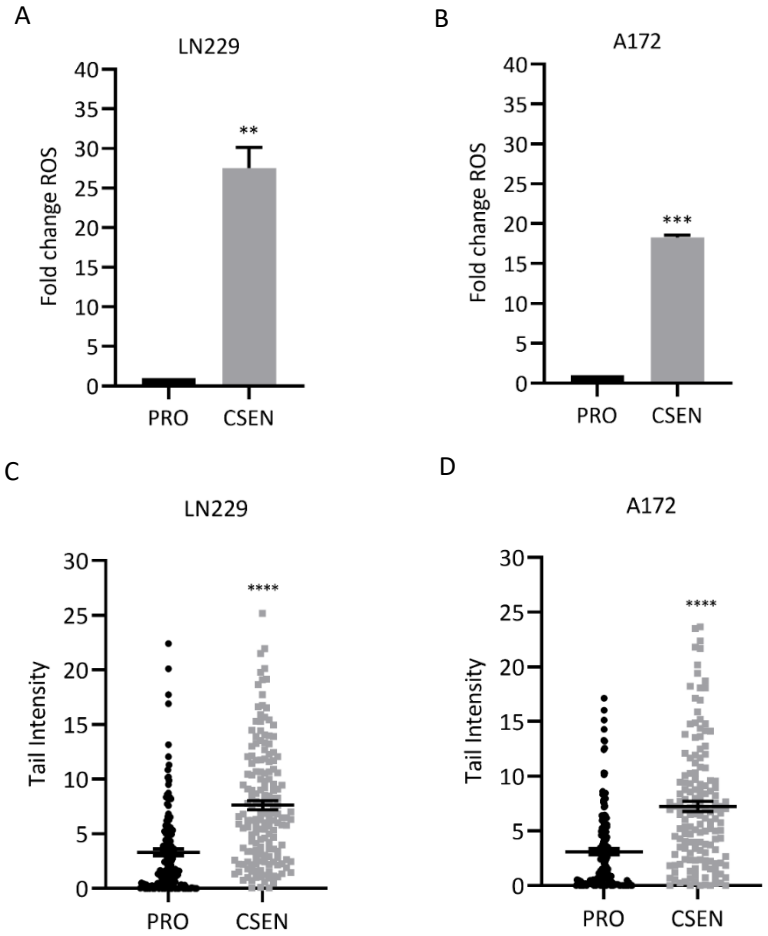

Figure 21: ROS and oxidative DNA damage in senescent cells.

Senescent (CSEN) LN229 and A172 cells show increased levels of ROS and oxidative DNA damage. (A, B) ROS was measured using DCF detection in the flow cytometer. (C and D) oxidative DNA damage was quantified in an FPG modified alkaline comet assay. Proliferating cells served as control (PRO). The data is given with the mean ± SEM for three representative experiments. **p<0.01, ***p<0.001, ****p<0.0001.

4.3. Identification of senescence maintaining pathways

In the past years, efforts to identify pathways that lead to cell death and senescence following TMZ treatment have shown that the activated DDR is mandatory to induce several pathways in GBM following TMZ treatment, including cell death, autophagy, and senescence. Additional studies demonstrated that the autophagic pathway is necessary to induce senescence in GBM cells (Knizhnik et al. 2013; Aasland et al. 2019a; He et al. 2019; Kanzawa et al. 2004; Sharma and Almasan 2021). Also, the anti- and pro-apoptotic Bcl2 family proteins have been proven to be involved in TMZ-induced senescence and apoptosis (Gratas et al. 2014a; Fan et al. 2020; Yosef et al. 2016; Choi et al. 2018). But still little is known about the maintenance of senescence. Understanding the molecular processes of senescence maintenance might help to improve GBM treatment. This led us to conduct further research. Thus, we inhibited know factors involved in senescence induction to assess if they are required for senescence maintenance.

4.3.1. Regulation of apoptosis

First, we inhibited two pro-apoptotic factors of the Bcl-2 family in senescent LN229 and A172 cells with the known senolytic agent ABT-737, a small molecule drug that specifically inhibits Bcl-2 and Bcl-xL (Yosef et al. 2016; Fan et al. 2020). Microscopic analysis of proliferating LN229 and A172 cells treated with 2.5 µM ABT-737 for 48 h had no indication of cell death, while senescent cells treated with the same concentration and time showed a reduction in cell density and signs of cell death (Figure 22). Therefore, we chose 48 h as the duration for the treatment with ABT-737 for the following experiments.

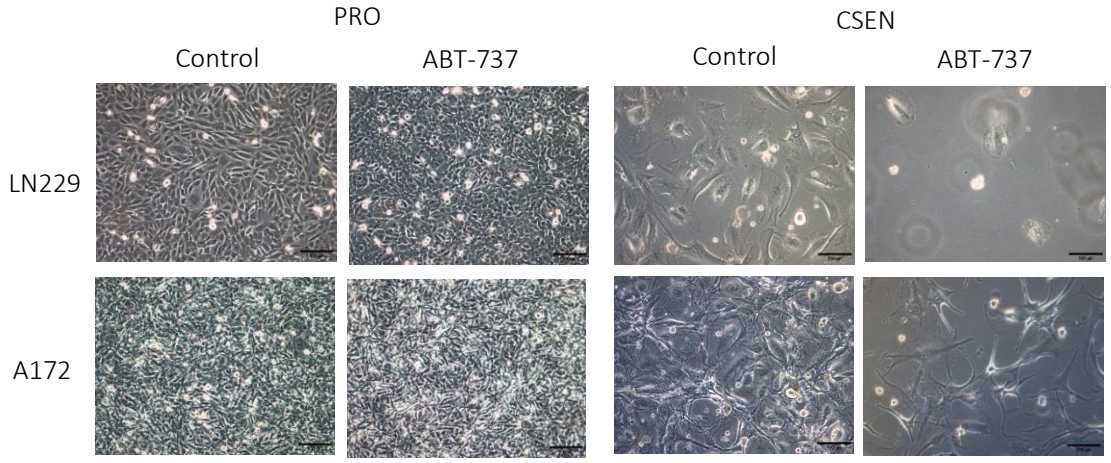

Figure 22: Microscopic analysis of the senolytic effect of ABT-737.
Proliferating (PRO) and senescent (CSEN) LN229 and A172 cells were treated with 2.5 µM ABT-737 for 48 h or kept untreated as control. Pictures were taken using a light microscope with an 20x objective and are representative for one experiment. Measuring bars (bottom right in each picture) refer to 100 µm.

The MTT assays display a dose-dependent reduction in viability of proliferating and senescent LN229 cells, with a higher viability reduction in the senescent cell population following treatment with ABT-737 (Figure 23A and B). To prove that the reduction in cell viability resulted from specific cell death of senescent cells, we measured CSEN as well as the cell death levels before and after treatment of senescent LN229 and A172 cells. This measurement was performed using 2.5 µM ABT-737 and cell death and CSEN was detected via C12FDG, and AV/PI staining that was measured by flow cytometry and quantified using the flowing software 2.0. A significant reduction in CSEN with a concomitant increase of cell death was detected (Figure 23C and D). Since treatment with ABT-737 for 48 h already showed strong effects in the MTT assay which was confirmed in the C12FDG and AV/PI assays, the 48-h duration was chosen for treatment with all other inhibitors thereafter.

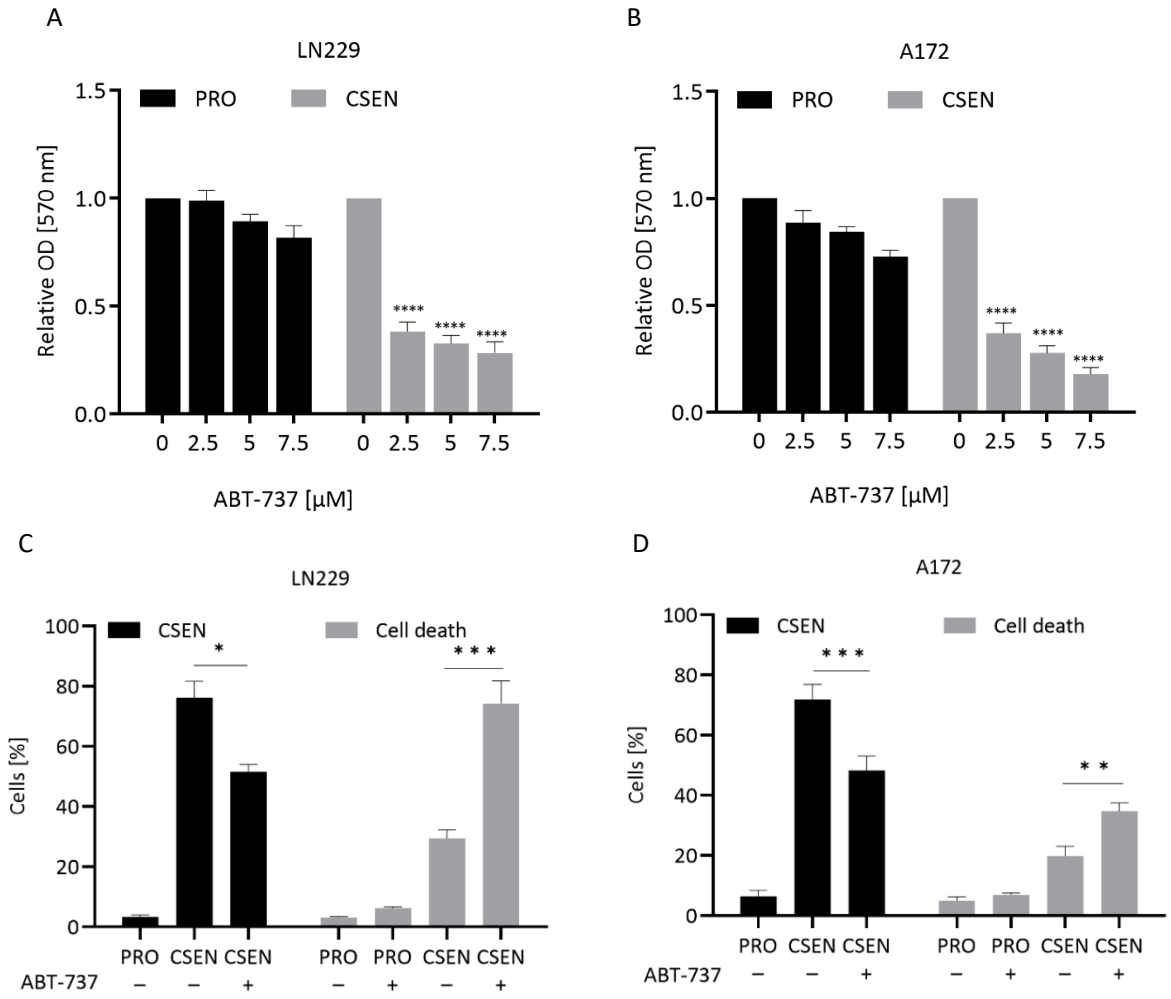

Figure 23: ABT-737 reduces CSEN in GBM cells.
Proliferating (PRO) and senescent (CSEN) LN229 and A172 cells were treated with the indicated concentrations of ABT-737 for 48 h. (A, B) MTT assay shows dose-dependent reduction in proliferating and senescent LN229 andA172 cells, with senescent cells reacting stronger than proliferating cells. (C and D) Treatment of senescent LN229 and A172 cells with ABT-737 at a concentration non-toxic on proliferating cells (2.5 µM) leads to a significant reduction in senescence, while concomitantly apoptosis increases significantly. Cell death and senescence were quantified by measurement of AV/PI staining. The data is given with the mean ± SEM for three representative experiments. *p<0.05, **p<0.01, ***p<0.001, ****p<0.0001.

To confirm the results and to prove that the assay for the identification of senescence maintaining players was working, we inhibited Bcl-2 and Bcl-X_L with ABT-263 (navitoclax), which is already in clinical use for the treatment of leukaemia. Also, navitoclax is currently under investigation for GBM treatment (Guerra et al. 2019; Lasica and Anderson 2021; Karpel-Massler et al. 2017). Interestingly, inhibition of Bcl-2 and Bcl-X_L with 2.5 µM navitoclax, a concentration non-toxic on proliferating cells, led to a significant reduction in CSEN in LN229 cells while only a minor reduction in A172 cells was observed. Cell death through apoptosis increased in both cell lines (Figure 24).

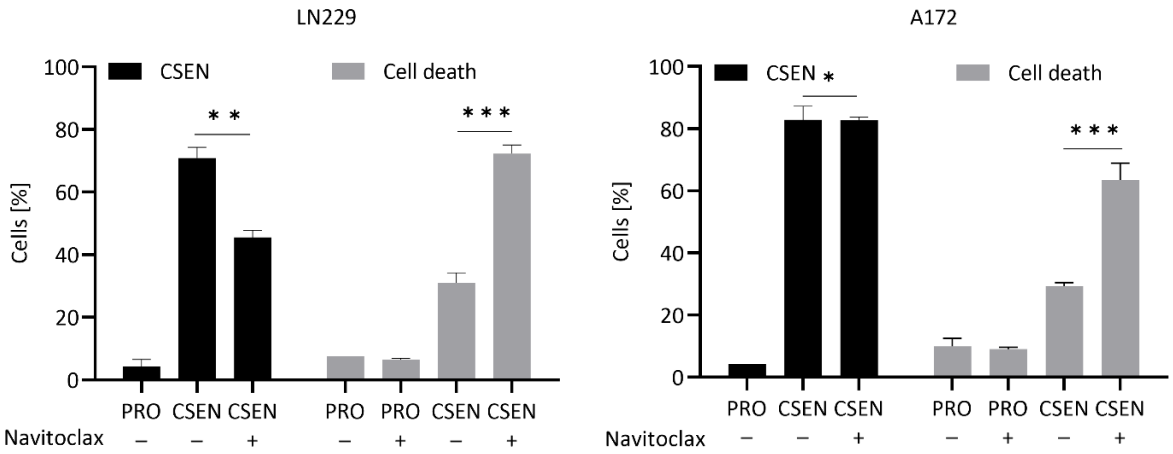

Figure 24: Navitoclax reduces senescence in LN229 but not A172 cells.
Treatment of senescent (CSEN) LN229 and A172 cells with 2.5 µM ABT 263 (Navitoclax) for 48 h led to a significant reduction of senescence levels in LN229 but not A172 cells. Concomitantly, cell death increased significantly in both cell lines. Senescent and dead cells were quantified by C12FDG and AV/PI staining, respectively. Proliferating cell served as control (PRO). The data is given with the mean ± SEM for three representative experiments. *p<0.05, **p<0.01, ***p<0.001.

Having shown that the experimental setup is reasonable for detecting senescence and senolysis, we further analysed the role of apoptosis in senescence maintenance by inhibiting the apoptosis inhibitors cIAP1/2 and XIAP with BV6, a smac mimetic and cIAP1/2, XIAP antagonist (Vanlangenakker et al. 2011; Varfolomeev et al. 2009). As shown in Figure 25, inhibition of cAIP1/2 and XIAP by 2.5 µM BV6 lead to a significant reduction in CSEN levels in both, LN229 and A172 cell lines. At the same time, cell death levels increased significantly, but more so in LN229 than in A172 cells. No significant increase in cell death was observed when proliferating cells were treated with the same concentration of BV6. In conclusion, glioblastoma cells seem to regulate anti-apoptotic factors upon TMZ treatment to circumvent cell death and increase survival.

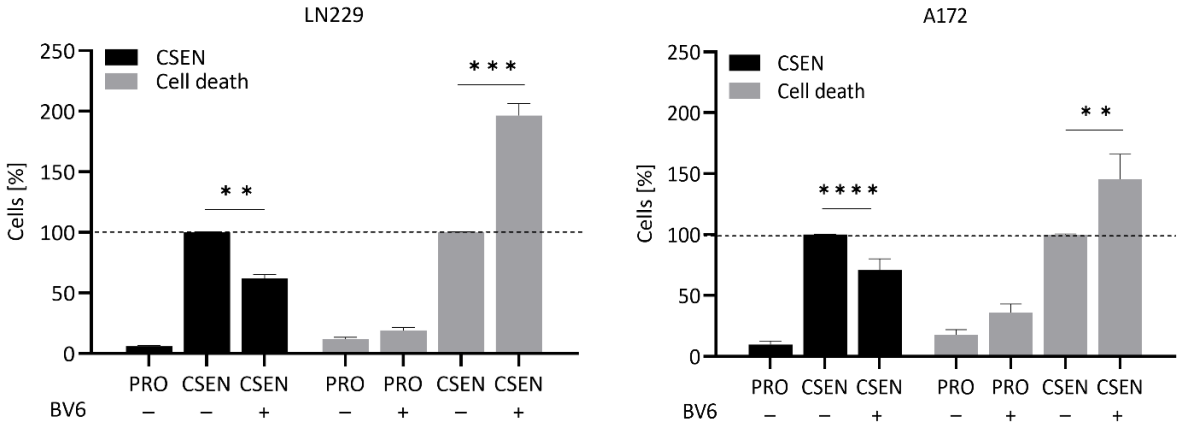

Figure 25: Inhibition of cIAP1/2 and XAIP reduces senescence.
LN229 and A172 cells were treated with 2.5 µM BV6 for 48 h. A significant reduction in CSEN and induction in cell death was observed in both cell lines. C12FDG and AV/PI staining were used for quantification of senescence and cell death, respectively. Proliferating cells served as control (PRO). The data is given with the mean ± SEM for three representative experiments. **p<0.01, ***p<0.001, ****p<0.0001.

4.3.2. Role of the DDR

Our previous results revealed the presence of DNA damage in form of DSBs and oxidative DNA damage as well as an activated DDR in senescent glioblastoma cells treated with TMZ. It is known that the DDR is necessary to induce CSEN (Aasland et al. 2019a), which led us to further investigate the role of the DDR in senescence maintenance. To this end, we inhibited major DDR players such as ATM (using 10 µM AZD1390), ATR (using 10 µM VE-821), CHK1 and 2 (using 50 nM UCN-01 and 10 µM CHK2 inhibitor II hydrate, respectively), p53 (using 10 µM pifithrin-α to inhibit the p53-dependent transactivation of p53-responsive genes and 10 µM pifithrin-µ to reduce the affinity of p53 to Bcl-X_L and Bcl-2) and p21 (using 5 µM UC2288). In all experiments, inhibitor concentrations non-toxic on proliferating cells were used. As shown in Figure 26, a significant reduction in the CSEN level was observed following treatment with ATM and ATR inhibitors in LN229 cells. Simultaneously, cell death levels increased significantly. The results were confirmed using the A172 cell line.

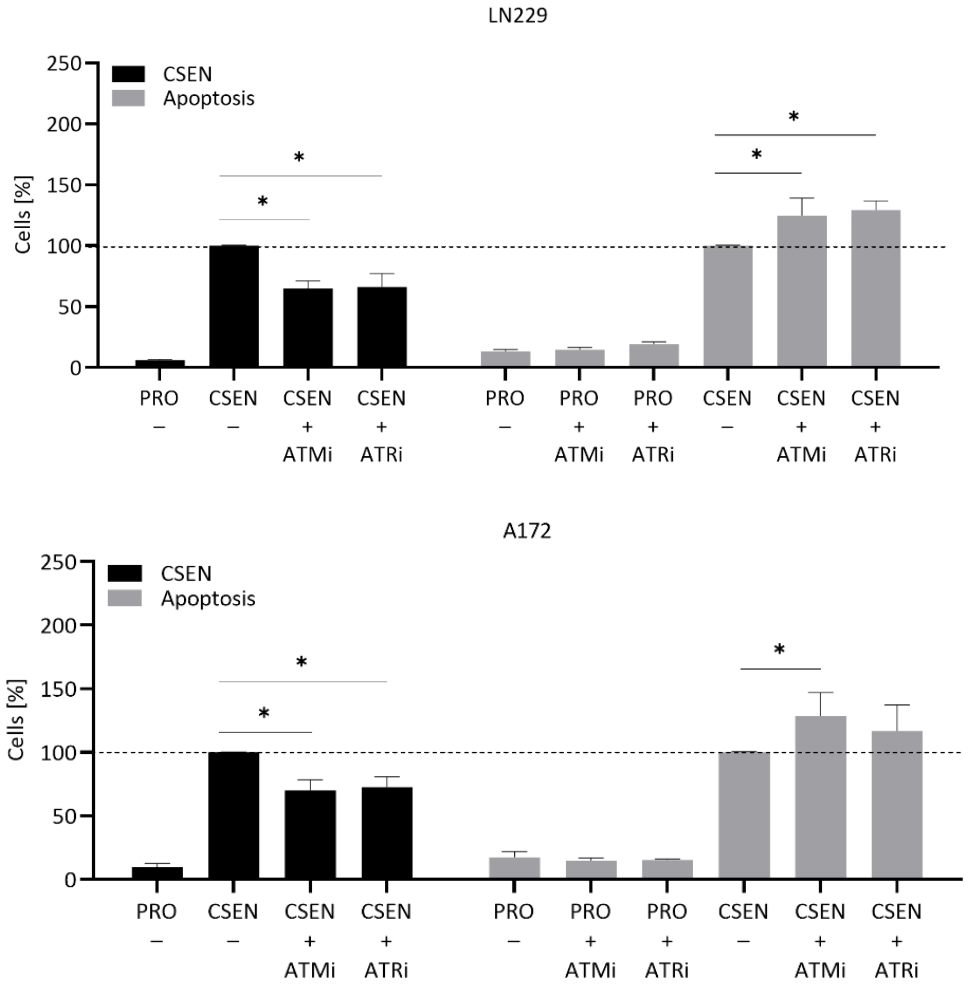

Figure 26: ATM and ATR are necessary for senescence maintenance.

LN229 and A172 cells were treated with inhibitors for ATM (AZD1390) and ATR (VE821) in concentrations non-toxic on proliferating cells (10 µM) for 2 d. CSEN and cell death were quantified using C12FDG and AV/PI staining, respectively, measured by flowcytometry. Proliferating cell served as control (PRO). The data is given with the mean ± SEM for three representative experiments. *p<0.05.

Following the DDR further downstream, we next targeted CHK1 and CHK2, p53 and p21 in senescent LN229 cells. No significant reduction in CSEN levels were observed upon inhibition of those DDR players. Interestingly, cell death levels still increased in CHK1 and p21 inhibited CSEN cell populations and following inhibition of p53 with either pifithrin-α or pifithrin-µ, while no induction of cell death was measured following inhibition of CHK2 (Figure 27). Since no reduction in senescence levels were observed, we conclude that these DDR factors do not play a role in senescence maintenance. The experiment was not repeated in A172 cells.

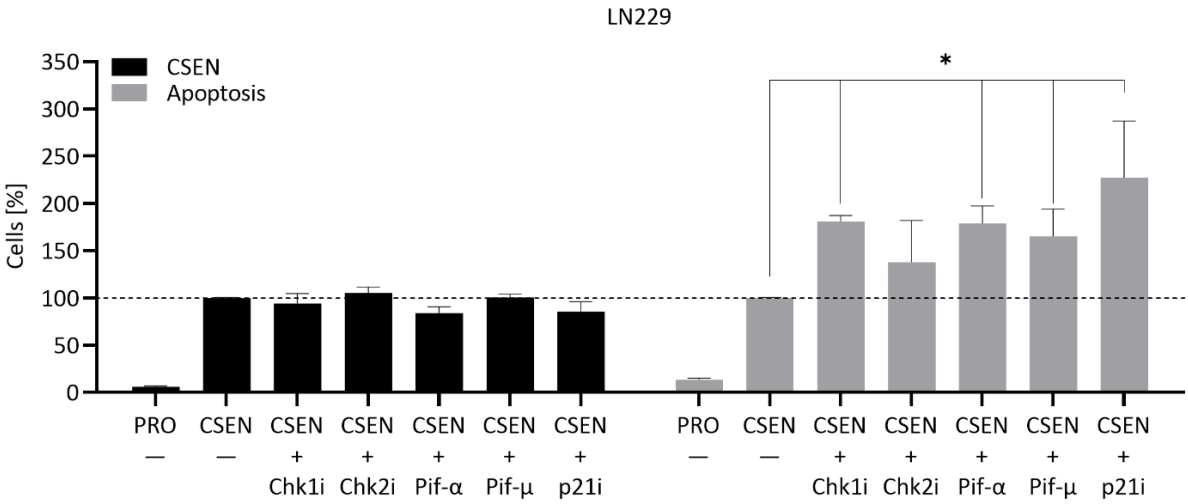

Figure 27: Inhibition of DDR in senescent GMB cells.

Senescent LN229 cells were treated with inhibitors of CHK1 (UCN-01, 50 nM), CHK2 (CHK2 inhibitor II hydrate, 10 μM), p53 (pifithrin-α and -μ, 10 μM each) and p21 (UC2288, 5 μM) in concentrations non-toxic on proliferating cells for 2 d. CSEN was measured by C12FDG staining and cell death levels by AV/PI staining using the flowcytometry. Proliferating cell served as control (PRO). The data is given with the mean ± SEM for three representative experiments. *p<0.05.

Beside the classic DDR, a pathway involving NF-kB has been shown to be activated by TMZ and to be necessary for senescence induction (Aasland et al. 2019a). NF-kB has long been known for its apoptosis inhibiting functions (van Antwerp et al. 1996). Being a transcription factor, it regulates the transcription of several proteins involved in the inhibition of apoptosis, including Bcl-X_L and cIAP1 and 2 (Naugler and Karin 2008; Karin and Lin 2002). To analyse the role of NF-kB in senescence maintenance in GBM cells, we inhibited NF-kB in senescent LN229 cells though treatment with 10 μM of the NF-kB inhibitor III. Interestingly, cell death levels increased significantly following treatment, without a reduction in CSEN levels (Figure 28). The missing reduction in CSEN levels following inhibition of NF-kB indicates that it is not necessary to maintain the senescent state in LN229 cells. The experiments were not repeated using A172 cells.

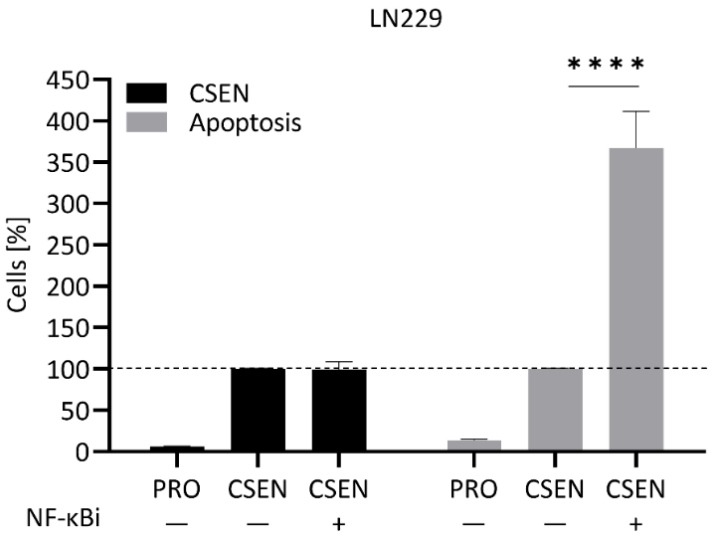

Figure 28: Role of NF-kB in senescence maintenance.
Senescent LN229 cells were treated for 2 d with 10 µM of the NF-kB inhibitor III. Cell death and senescence levels were quantified by AV/PI and C12FDG staining, respectively, measured by flowcytometry. Proliferating cell served as control (PRO). The data is given with the mean ± SEM for three representative experiments ****p<0.0001.

4.3.3. Role of DNA repair

We have now shown that senescent LN229 and A172 cells display a higher level of DSBs than their proliferating counterparts although they are able to perform DNA damage repair. Next, we analysed if DNA repair is active in senescent cells to circumvent cell death and thus maintain senescence. A major DNA repair enzyme is Rad51, which is needed for homologous recombination (HR) repair of DSBs, occurring mainly in S and G2 phases of the cell cycle (Budke et al. 2012). Since senescent cells are arrested in G2, HR might still be active. Another major player of DNA repair is poly [ADP-ribose] polymerase 1 (PARP1). Different from Rad51, PARP1 participates in several DNA repair mechanisms, such as NER, non-homologous end joining (NHEJ), HR and the MMR (Pascal 2018). Since senescence is a pro-survival mechanism, active DNA repair might be necessary to stay alive in the senescent state. To see whether inhibition of either of these pathways might trigger cell death in senescent cells, we inhibited Rad51 using 5 µM Ri1, and PARP1 using 10 µM veliparib. As indicated in Figure 29, inhibition of Rad51 or veliparib in non-toxic concentrations had an effect only through an increase in cell death while senescence levels stayed stable. These results suggest that the DNA damage repair mechanisms mediated through Rad51, or PARP1 are not required for senescence maintenance.

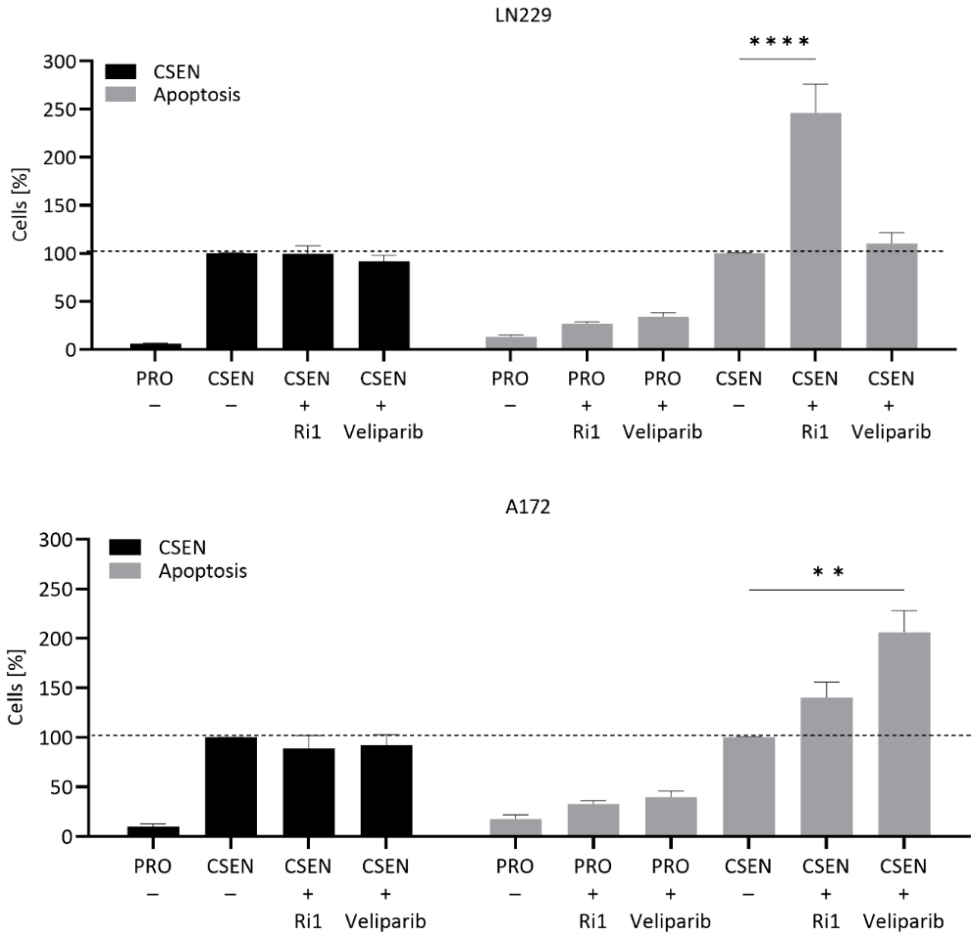

Figure 29: DNA repair mechanisms are not involved in senescence maintenance.

Senescent LN229 and A172 cells were treated with inhibitors of DSBs repair namely, Rad51 (Ri1, 5 µM) and PARP1 (veliparib, 10 µM) Proliferating cell served as control (PRO). Cell death and senescence levels were quantified using flowcytometric analysis of AV/PI and C12FDG staining. The data is given with the mean ± SEM for three representative experiments. *p<0.05, **p<0.01, ***p<0.001, ****p<0.0001.

Another important repair enzyme involved especially in the repair of O^6meG is MGMT. In GBM therapy with TMZ, MGMT promoter methylation is an important prognostic marker. Hypermethylation of the MGMT promoter leads to silencing of the MGMT gene, and this correlates with a better curative outcome. Contrary, unmethylated MGMT promoter leads to MGMT expression, which corelates with a shorter overall and progression free survival, as high MGMT levels lead to repair of the cytotoxic lesion O^6meG. Hence, little to no formation of DSBs occurs and TMZ cannot conduct its cytotoxicity. It has been shown that in recurrent GBM tumours following TMZ treatment *MGMT* promoter methylation is lower, thus MGMT expression is upregulated compared to the primary tumours (Christmann et al. 2010). This leads to the hypothesis that TMZ treatment might lead to de-methylation of hypermethylated MGMT promoters, hence an activation of MGMT expression in MGMT negative GBM.

If that is the case, the question remains if expression of MGMT following TMZ treatment and the resulting repair of O^6meG interferes with the cytotoxic effect of TMZ. In cooperation with Prof. Monika E. Hegi we used the LN229-MGMT^{ind}c12 cell line described above (chapter 4.2.3) to answer this question. Therefore, we treated LN229-MGMT^{ind}c12 cells with 50 µM TMZ at day 0 and with dox 1-7 d later in 24 h intervals. Cell death and CSEN levels were measured 5 d and 8 d following TMZ treatment, respectively. Beforehand, western blot analysis confirmed stable MGMT expression in proliferating and senescent dox treated LN229-MGMT^{ind}c12 cells (Figure 30A).

As shown in Figure 30B, induction of cell death was significantly reduced 5 d following TMZ treatment, when MGMT was expressed within 1 or 2 d following TMZ treatment. Thereafter, no significant difference was observed. The results were similar when CSEN was measured 8 d following TMZ treatment. If MGMT was induced up to 3 d following TMZ treatment, CSEN levels were significantly lower at day 8 compared to only TMZ treated LN229-MGMT^{ind}c12 cells. Expression of MGMT 4 d following TMZ treatment also resulted in a lower CSEN induction measured at day 8, although not at a significant level. Thereafter, no difference in CSEN levels independent of MGMT expression was observed (Figure 30C). When senescent LN229-MGMT^{ind}c12 cells were treated with dox to induce MGMT expression, no difference in CSEN and cell death levels were observed 2 d later (Figure 30D). These results suggest that repair of O^6meG by MGMT after the induction of DSBs (which occur starting at 2-3 d following TMZ treatment) does not lead to a reduction in cell death or CSEN levels. Overall, the data revealed that O^6meG mediated DSBs formation is necessary for the induction of senescence and cell death, however, O^6meG does not participate in senescence maintenance.

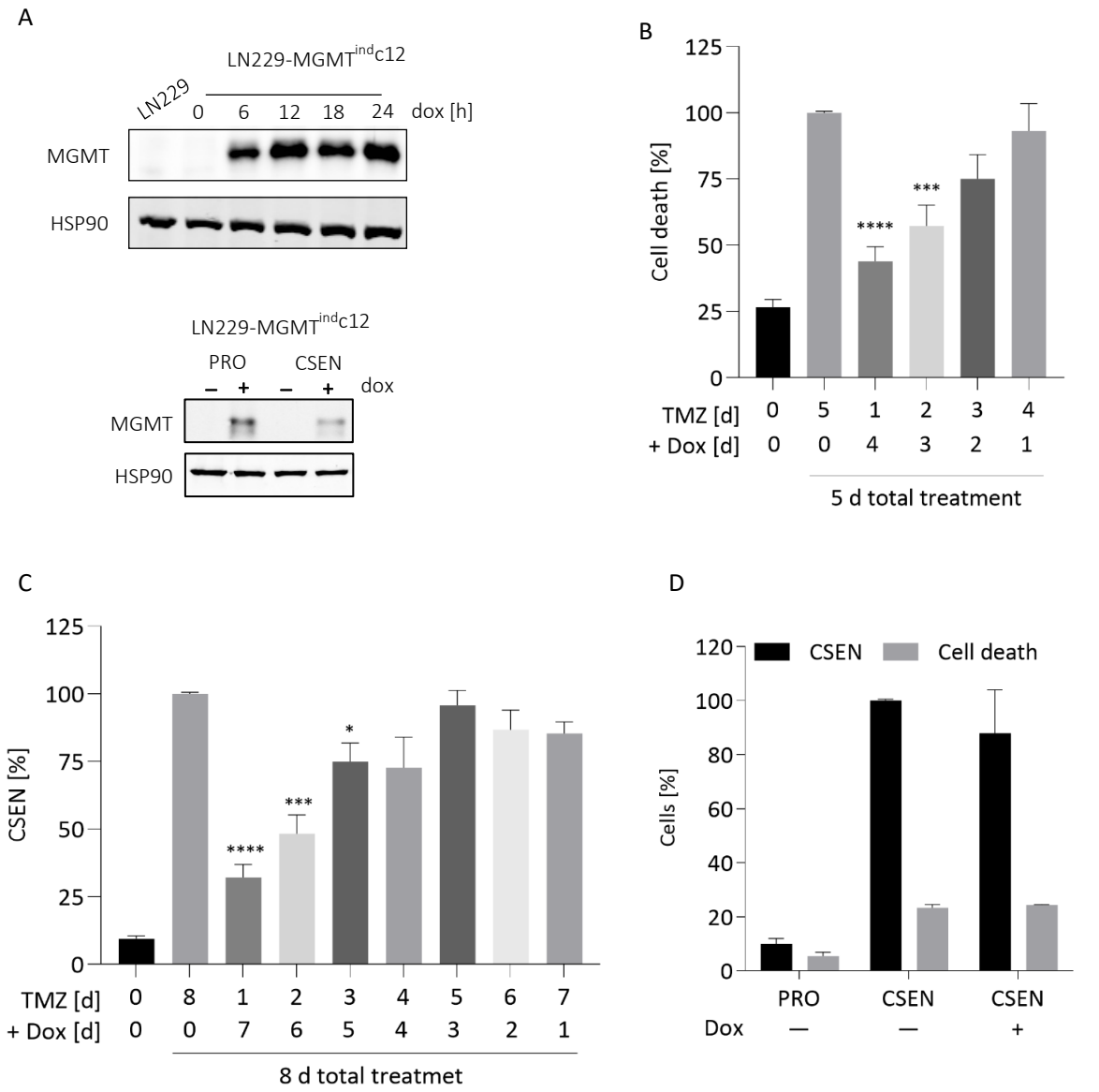

Figure 30: Induction of MGMT following TMZ treatment.

MGMT was induced in dox controlled LN229-MGMT^{ind}c12 cells by 100 ng/ml dox treatment. (A) Western bot analysis of MGMT expression in proliferating and senescent cells. Pictures are representative for one experiment; LN229 served as negative control. For each lysate 50 µg protein were loaded onto a 10% polyacrylamide gel. (B, C) LN229-MGMTindc12 were treated with 50 µM TMZ at day 0. Dox treatment followed 1-7 d thereafter in 24 h intervals. Cell death (B) and CSEN (C) were measured 5 and 8 d following TMZ treatment, respectively. Proliferating cells served as negative control (0/0), TMZ treated cells without dox treatment as positive control (5/0 for cell death and 8/0 for CSEN). (D) Senescent LN229-MGMT^{ind}c12 cells were treated with dox for 2 d. Cell death and CSEN were measured by AV/PI and C12FDG staining, respectively. The data is given with the mean ± SEM for three representative experiments. *p<0.05, ***p<0.001, ****p<0.0001.

4.3.4. Role of autophagy

Besides cell death and senescence, autophagy is induced in cells following treatment with DNA damaging agents, which was shown for GBM cells upon TMZ treatment (Knizhnik et al. 2013; Kanzawa et al. 2004; Katayama et al. 2007). Autophagy is a mechanism to control cellular homeostasis and it has recently been demonstrated to be associated with the induction of senescence (Knizhnik et al. 2013; Kanzawa et al. 2004; Katayama et al. 2007). Also, autophagy supports cell survival by eliminating dysfunctional organelles and turnover DNA damage repair proteins (Zhang et al. 2015). To see whether autophagy contributes to senescence maintenance, we either inhibited the fusion of the autophagosome and the lysosome using 20 µM chloroquine (Clq), or by blocking the autophagosome formation using 5 µM 3-methyladenine (3-MeA). Upon treatment of LN229 and A172 senescent cell populations with Clq, senescence was significantly reduced, while cell death increased simultaneously. The effect was greater in LN229 than in A172 cells. Similarly, treatment with 3-MeA led to a significant reduction in senescence, while cell death increased. Like Clq treatment, the effect was greater in LN229 cells (Figure 31).

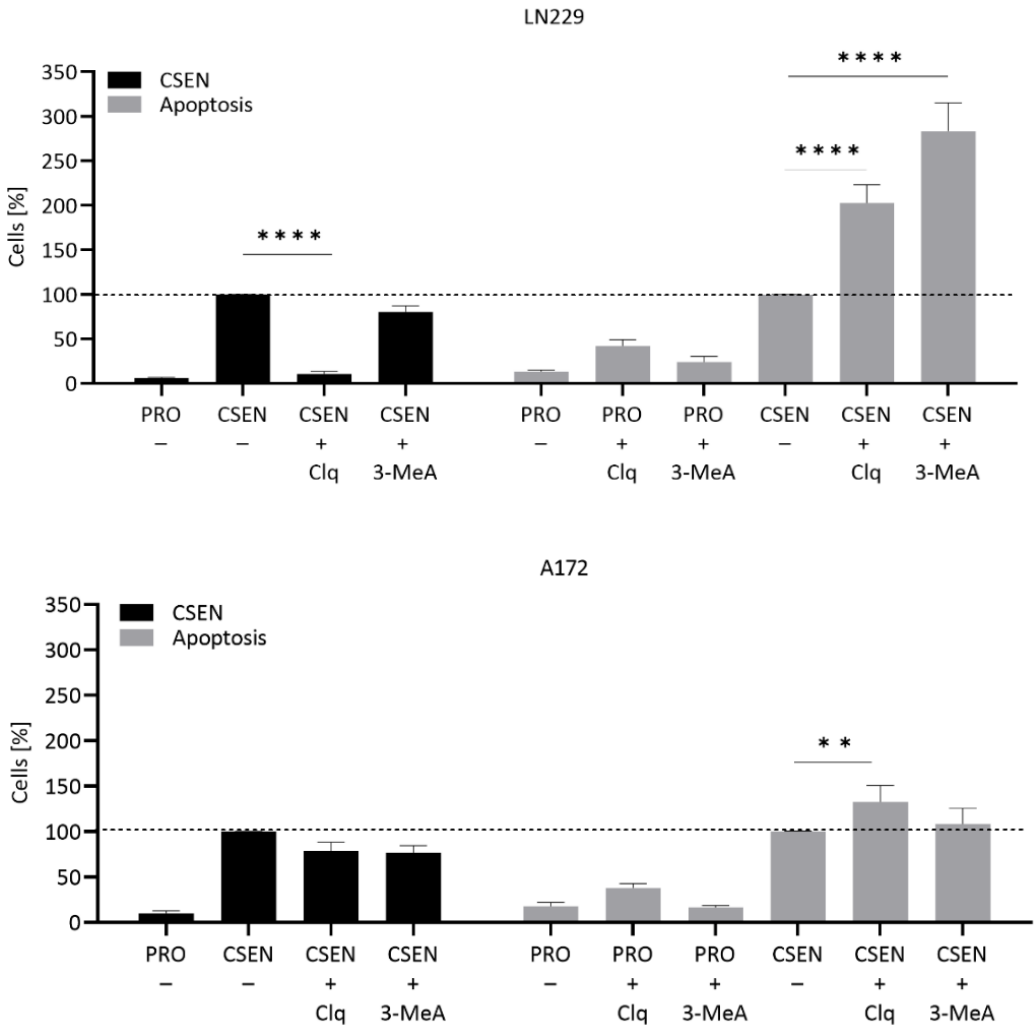

Figure 31: Autophagy maintains senescence in LN229 and A172 cells.

Senescent LN229 and A172 cells were treated with two individual inhibitors of autophagy (Clq, 20 µM and 3-MeA, 5 µM) for 2 d. Cell death was quantified by AV/PI staining; CSEN by C12FDG staining in the flow cytometer. Proliferating cell served as control (PRO). The data is given with the mean ± SEM for three representative experiments. **p<0.01, ****p<0.0001.

In our senescent glioblastoma cell system high levels of ROS were detected. It has been demonstrated that when high levels of ROS are present in the cell, autophagy can be induced through the PI3K pathway, leading to CSEN (Kma and Baruah 2022; Gao 2019). Autophagy on the other hand has been shown to be necessary for the SASP which reinforces CSEN (Kwon et al. 2017; Young et al. 2009). Hence, it can be hypothesised that the high ROS levels in our cell system activate autophagy though the PI3K axis to maintain the CSEN state. To test this supposition, we inhibited PI3K in our senescent LN229 and A172 cell populations through treatment with PX-866, a wortmannin derivative that is under investigation in clinical trials for the treatment of recurrent glioblastoma (Bowles et al. 2016; Hotte et al. 2019; Pitz et al. 2015).

Of note, treatment of GBM patients with TMZ with PX-866 alone and concomitantly with TMZ showed promising results (Harder et al. 2019; Koul et al. 2010). Interestingly, we observed that treatment of senescent LN229 and A172 cells with 1 µM of PX-866 resulted in a significant reduction in the CSEN levels in LN229 cells. Concomitantly, cell death increased in LN229 cells. There was no effect of PX-866 on A172 cells: The CSEN and cell death levels remained unaffected (Figure 32).

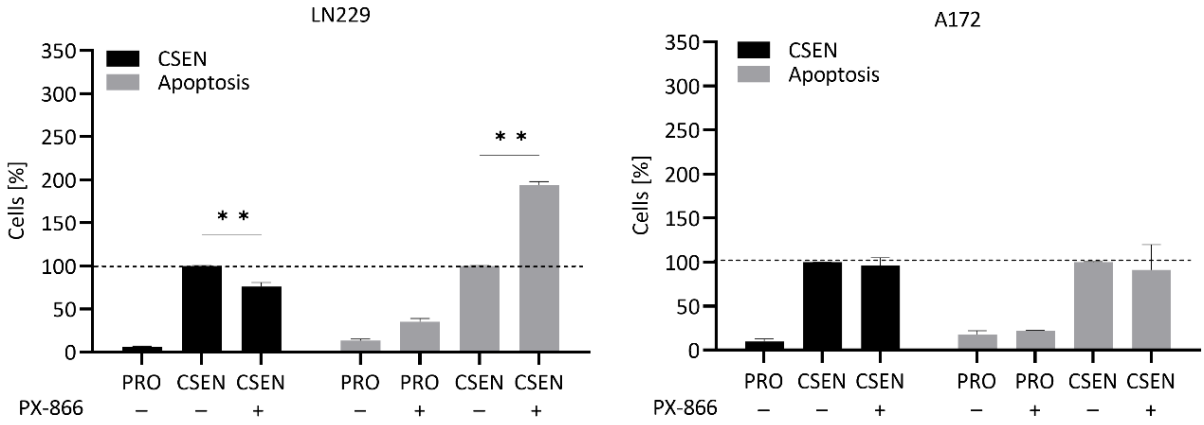

Figure 32: Effect of PI3K inhibition in senescent GBM cells.
Senescent LN229 and A172 cells were treated with 1 µM of the PI3K inhibitor PX-866 for 2 d. Cell death and senescence levels were quantified using AV/PI and C12FDG staining measured by flow cytometry. Proliferating cell served as control (PRO). The data is given with the mean ± SEM for three representative experiments. **p<0.01.

4.4. Screening for improved treatment options

In persuasion for a better outcome of GBM therapy, chemotherapeutics and other treatment options are often combined. Thus, for primary GBM treatment, TMZ is combined with IR according to the Stupp-protocol that is currently used in the clinical setup (Catarina Fernandes et al. 2017). In other treatment schedules, several chemotherapeutics are combined. This applies for TMZ and CCNU, which are administered in some protocols concomitantly (Herrlinger et al. 2019). Combined treatment regimens either aim to gain higher toxicity on tumour cells directly, or indirectly, e.g., though inhibition of cell survival pathways and DNA repair. Following sole TMZ treatment, GBM cells mainly enter the survival pathway of senescence. Treatment schedules that increase cell death levels are thus urgently needed. Here, we addressed the question whether the combination of IR, CCNU or methadone with TMZ leads to an increase in TMZ-induced cell death.

4.4.1. Combinatorial treatment of TMZ and IR

Within the clinical setup, GBM patients are treated with TMZ and IR the same time. Since IR induces DSBs, as does TMZ, this treatment might lead to more severe DNA damage, resulting in higher cell death levels. To investigate this possibility, LN229 cells were either pre-treated with TMZ before IR or pre-irradiated before TMZ treatment. A dose-response curve measured 3 d after irradiation, demonstrated a linear increase in cell death upon rising doses of IR. Doses < 4 Gy were insufficient to induce significant levels of cell death in GBM cells (Figure 33).

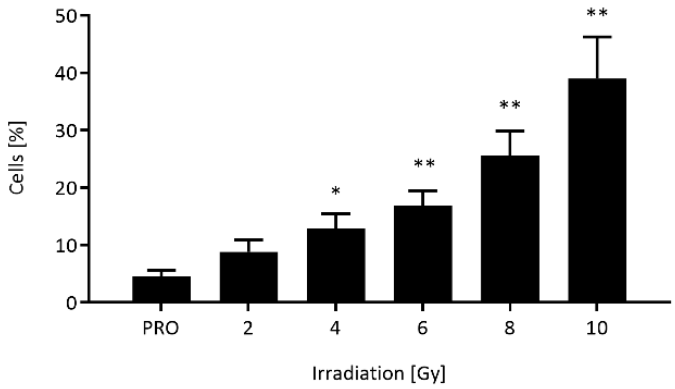

Figure 33: Dose-response of IR.
Proliferating cells were irradiated with rising dosages of γ-rays or left untreated as control (CON). Cell death, evaluated by AV/PI staining, was measured 3 d following irradiation. The data is given with the mean ± SEM for three representative experiments. *p<0.05, **p<0.01.

Thus, LN229 cell were treated with 20 µM TMZ for 3 h and irradiated with 6 Gy thereafter or were irradiated with 6 Gy for 6 h and subsequently treated with 20 µM TMZ. Cell death and CSEN levels were quantified 5 d and 8 d later, respectively. As shown in Figure 34A, cell death levels increased significantly following pre- or post-irradiation of TMZ treatment, compared to IR alone, but only pre-irradiation had a significant effect, compared to sole TMZ treatment. Although, post-irradiation also led to an increase in cell death. Senescence levels, shown in Figure 34B, increased significantly in both, pre- and post-irradiated LN229 cells, compared to either TMZ or IR treatment alone. The addition of the cell death levels of sole TMZ and sole IR treatment indicate the expected cell death values if the combined treatment of TMZ and IR has an additional effect. Indeed, comparing added and measured levels of cell death, no significant difference was observed (Figure 34C). The same was true for CSEN; no significant difference was detected, although the measured senescence levels were slightly lower than expected based on the added sole senescence level (Figure 34D).

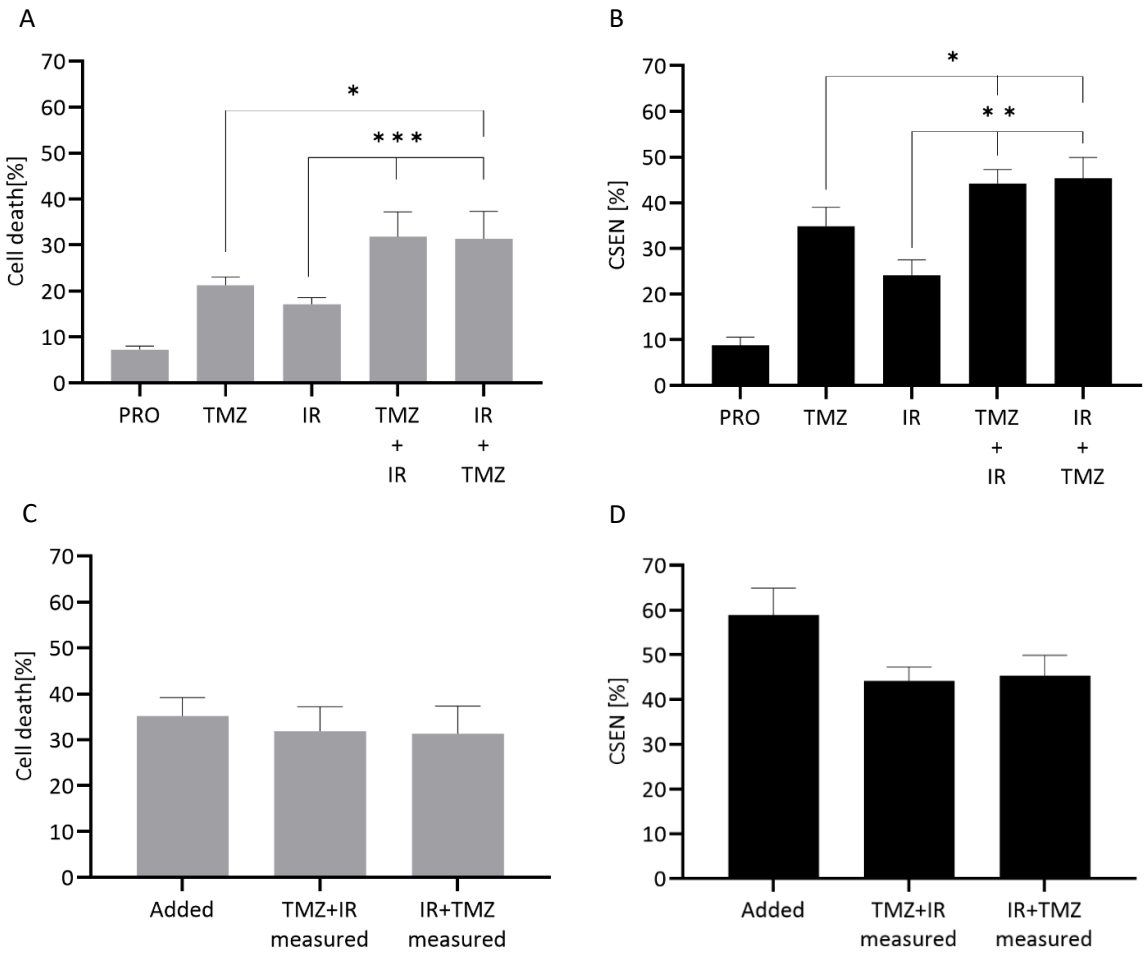

Figure 34: RT has an additive effect on TMZ treatment.

LN229 cells were either pre-treated with 20 µM TMZ for 3 h and then irradiated with 6 Gy or were pre-irradiated with 6 Gy for 6 h and then treated with 20 µM TMZ. Untreated proliferating (PRO) and sole TMZ and sole IR served as control. Cell death (A) and CSEN (B) were quantified via AV/PI 5d and C12FDG staining 8 d later, respectively. (C and D) Comparison of the added values of sole TMZ treatment and sole IR (added) to the measured values of combinatorial TMZ and IR treatment, The data is given with the mean ± SEM for three representative experiments. *p<0.05, **p<0.01, ***p<0.001.

4.4.2. Effect of IR on TMZ-induced senescent cells

According to the Stupp protocol, the combination of TMZ and IR is repeated for 6 weeks. We demonstrated previously that TMZ-induced senescence begins approximately one week following TMZ treatment. It is thus likely that senescent cells are treated with TMZ and IR. It is known that for TMZ-induced cytotoxicity DNA replication is necessary and results obtained in our lab show no induction of cell death when TMZ-induced senescent cells were treated with TMZ. However, IR induces DSBs independent of replication. Thus, IR-induced DSBs could still be cytotoxic to senescent cells. To see the effect of IR on TMZ-induced senescent cells, we irradiated a senescent LN229 cell population with dosages between 2 Gy and 10 Gy, representing sublethal and lethal dosages (Figure 35A), and measured cell death and senescence levels 2 d later. Following IR of senescent LN229 cells, a slight reduction in senescence levels was observed, while cell death levels increased slightly. The reduction was, however, not significant (Figure 35B). No reduction in CSEN levels was observed when 2 Gy were applied, indicating that at least a low dose of radiation cannot kill senescent cells.

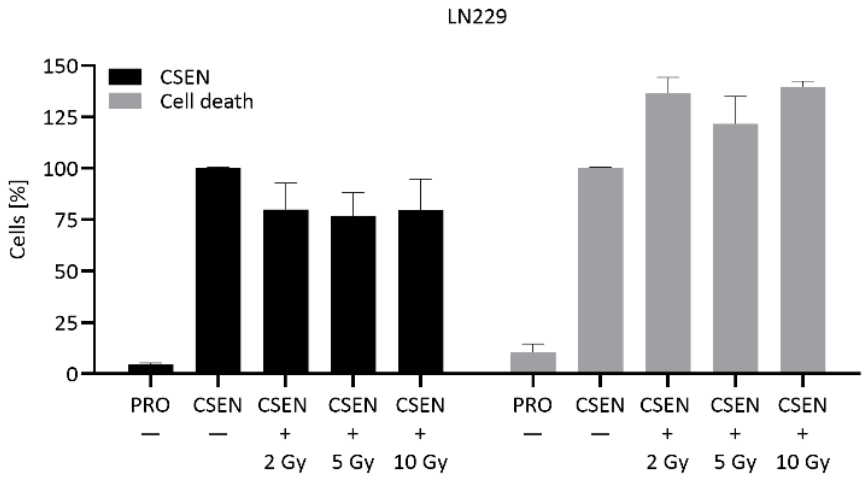

Figure 35: Effect of IR on senescent LN229 cells.
Proliferating and senescent cells were irradiated with rising dosages of γ-rays or left untreated as control (PRO). (A) Cell death, evaluated by AV/PI staining and CSEN, evaluated by C12FDG staining were measured by flowcytometry 2d following irradiation. The data is given with the mean ± SEM for three representative experiments. *p<0.05, **p<0.01.

These results demonstrate that the outcome of the addition of IR to TMZ treatment is time dependent. A beneficial effect of IR was seen when LN229 cell were treated with TMZ and IR concomitantly, while no effect was seen when TMZ-induced senescent cells were irradiated. These results should be verified *in vivo*. Also, the cytotoxic effect of the combinatorial treatment on the healthy tissue should be evaluated. Nevertheless, our results suggest that in the clinical setup a higher toxicity on proliferating GBM cells can be gained if TMZ and IR treatments are combined while irradiation of TMZ-induced senescent cells has no beneficial effect.

4.4.3. Combinatorial treatment of TMZ and CCNU

CCNU is part of the PCV schedule, a combination of the three alkylating agents procarbazine, CCNU and vincristine that is currently used for low grade glioma (LGG) and recurrent GBM, among others (Mehta et al. 2014). In 2006 a clinical phase I study demonstrated the beneficial effects of the addition of CCNU to TMZ treatment in GBM (Tafuto et al. 2006). To our best knowledge, for primary GBM treatment, CCNU is mainly given concomitantly with TMZ, resulting in higher toxicity not only for the tumour, but also for the patient, causing more severe side effects (Herrlinger et al. 2019). Here, we assessed the effect of CCNU on senescent GBM cells to see, whether the drug bears senolytic activity. The data presented in Figure 36 show that CCNU does not have senolytic activity which is evident by the missing reduction in CSEN. Of note, a slight increase in cell death was observed in the A172 cells which could be due to the cytotoxicity of CCNU on proliferating cells.

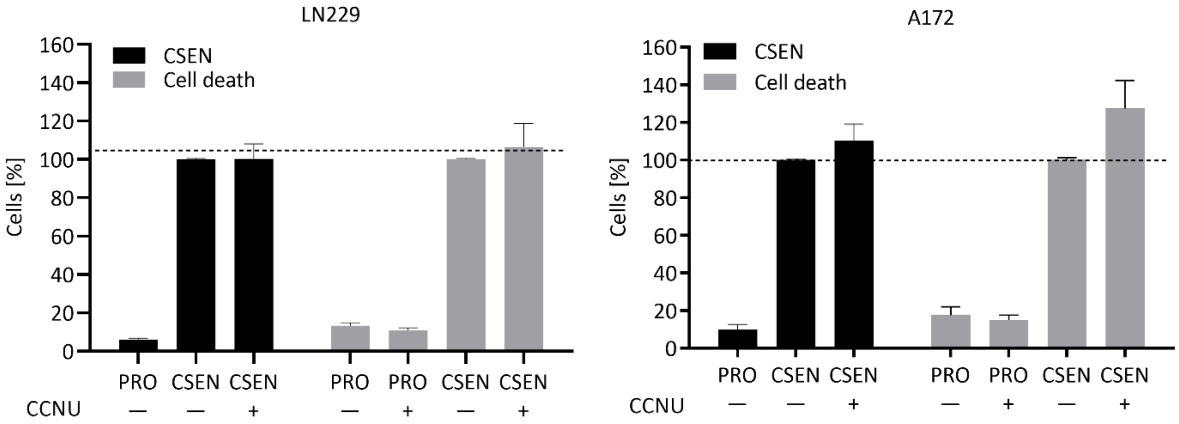

Figure 36: CCNU has no senolytic activity in GBM.

Senescent LN229 and A172 cells were treated with 10 µM CCNU and senescence and cell death levels were quantified by AV/PI and C12FDG staining 2d later. Proliferating cell served as control (PRO). The data is given with the mean ± SEM for three representative experiments.

4.4.4. Combinatorial treatment of TMZ and methadone

Methadone (MTD) is a μ-opioid receptor (MOR) agonist commonly known for its use in pain control and heroin substitution. It gained attention as an adjuvant for GBM chemotherapy (Brawanski et al. 2018). Recently, it has been shown that MTD induces apoptosis in leukaemia cells (Kua et al. 2019; Friesen et al. 2013). Promising results were obtained by combinatorial treatment of MTD with doxorubicin in GBM cell lines, where MTD increased apoptosis levels induced by doxorubicin (Friesen et al. 2014). It is important to note that in GBM treatment, TMZ and not doxorubicin is the main chemotherapeutic used in the clinic (Stupp et al. 2005). Having in mind the above-mentioned studies, we evaluated the geno- and cytotoxicity of MTD on GBM cells and human fibroblasts, analysed if combinatorial treatment of MTD with TMZ had beneficial effects and the senolytic activity of MTD.

4.4.4.1. Cyto- and genotoxicity of MTD

First, the cyto-and genotoxicity of MTD was assessed. Therefore, LN229 and A172 cells were treated with increasing concentrations of MTD, and cell death levels were measured 3 d later. In LN229 and VH10T cells cell death increased exponentially, while in A172 cells cell death stayed stable up to 20 μg/mL and then increased immediately to 60 %. In the LN229 and A172 cell lines, MTD levels were cytotoxic at >20 μg/mL, while the human fibroblast cell line VH10T tolerated concentrations up to 40 μg/mL (Figure 37). The results indicate, that MTD bears a higher cytotoxic activity in cancer than in non-cancer cells, although at concentrations well above the plasma levels achieved within patients which reach about 24 ng/ml and 0.6 μg/ml following an i.v. administration of 25 and 10 mg MTD, respectively (Inturrisi and Verebely 1972; Volavka et al. 1978).

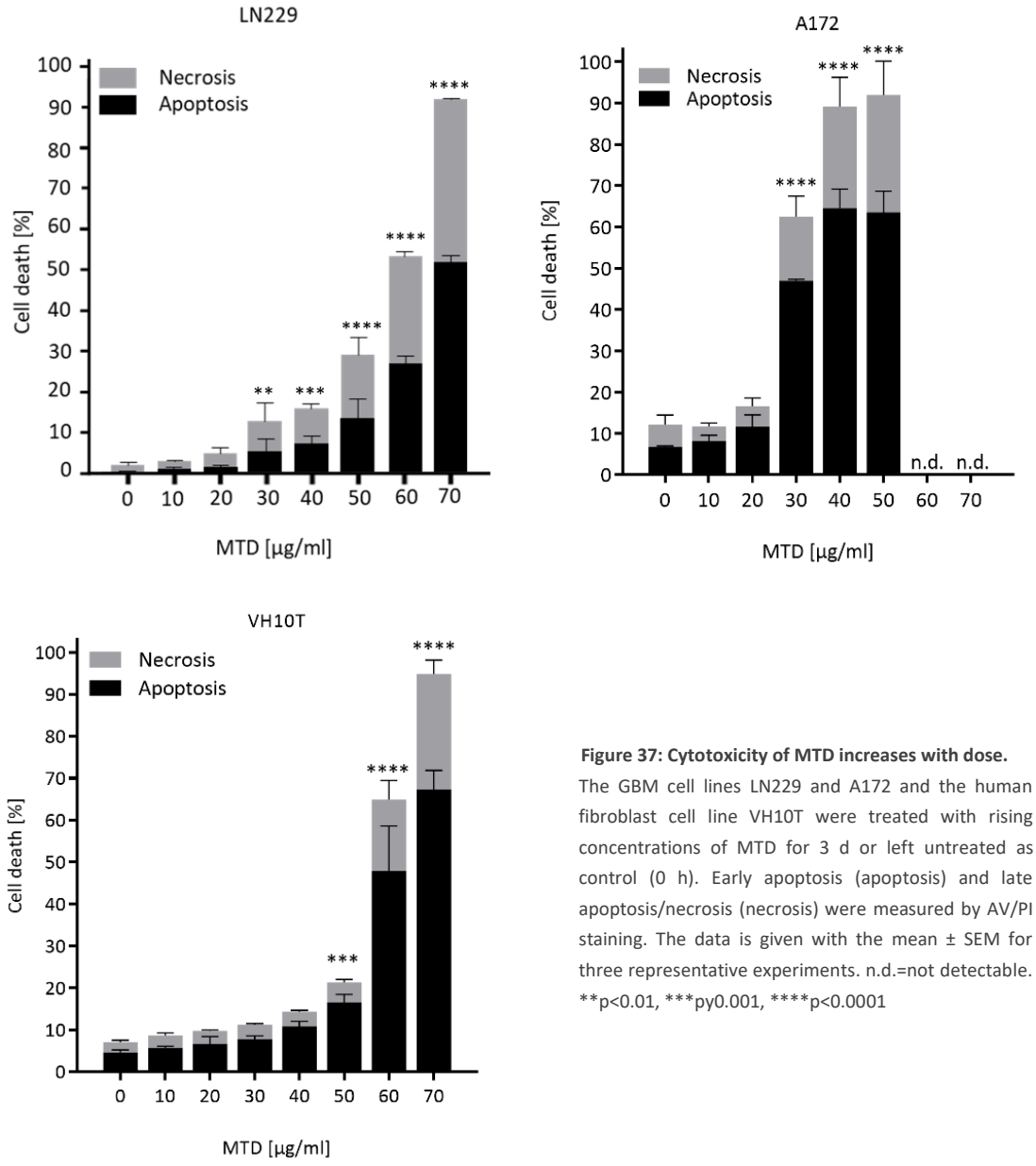

Figure 37: Cytotoxicity of MTD increases with dose.
The GBM cell lines LN229 and A172 and the human fibroblast cell line VH10T were treated with rising concentrations of MTD for 3 d or left untreated as control (0 h). Early apoptosis (apoptosis) and late apoptosis/necrosis (necrosis) were measured by AV/PI staining. The data is given with the mean ± SEM for three representative experiments. n.d.=not detectable. **p<0.01, ***py0.001, ****p<0.0001

Activation of MOR by MTD can reduce the anti-apoptotic proteins XIAP and Bcl-X_L (Friesen et al. 2014). Since treatment of GBM cells with MTD led to an induction of cell death, we were wondering if the apoptotic pathway was mediated by activation of MOR. Western blot analysis of LN229, A172 and VH10T cells showed expression of the receptor in all cell lines (Figure 38A). Additionally, previous Western blots demonstrated the expression of the anti-apoptotic factors Bcl-X_L and Bcl-2 in proliferating LN229 and A172 cells (chapter 4.2.2). The induction of cell death following MTD treatment might thus be initiated through the MOR-mediated downregulation of these anti-apoptotic proteins. To assess this hypothesis, we pre-treated LN229 and A172 cells with naloxone (Nalx), a MOR antagonist, 30 min before treatment with 50 µg/mL MTD.

Cell death levels were measured 3 d later. Treatment of LN229 and A172 cells with 200 µM Nalx alone was not cytotoxic, while treatment with 50 µg/mL MTD resulted again in about 20 % and 90 % cell death in LN229 and A172 cells, respectively. Pre-treatment with Nalx had no effect on cell death levels, indicating that the induction of cell death by MTD is not mediated by the MOR (Figure 38B).

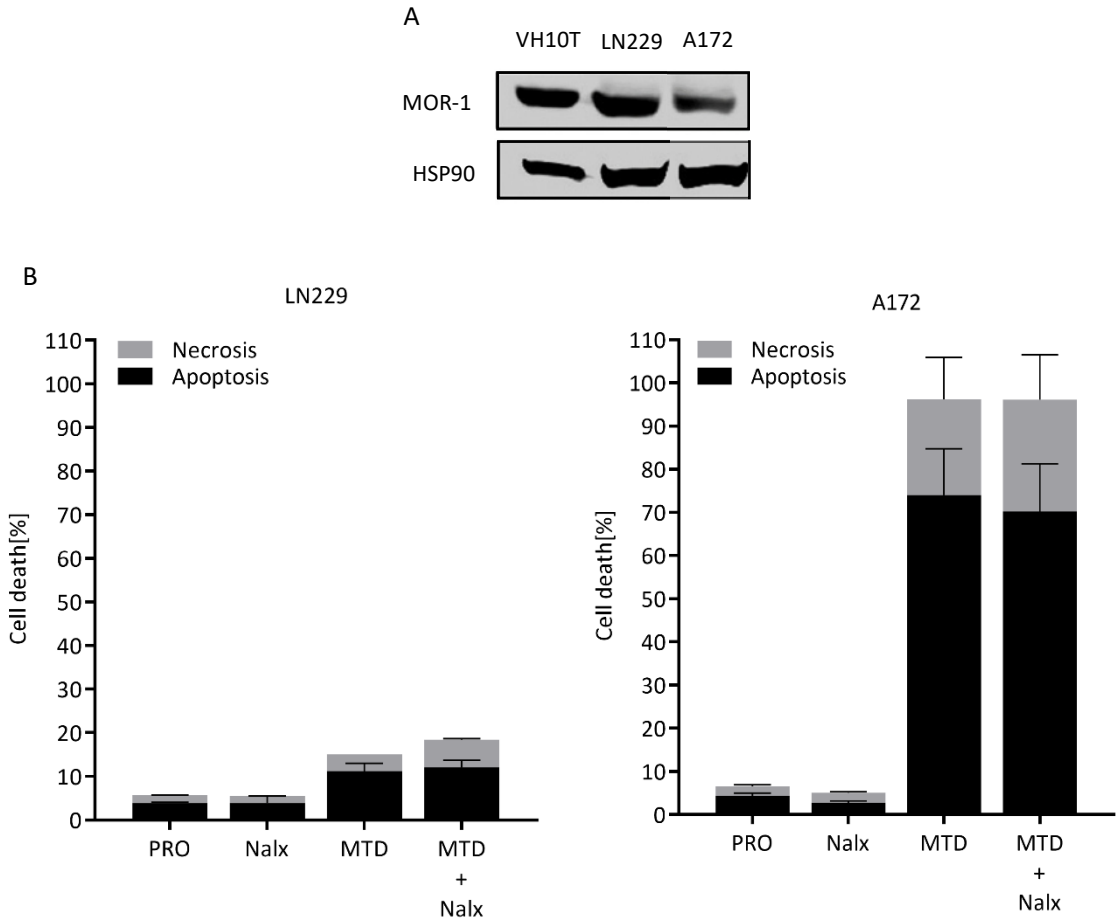

Figure 38: Role of MOR in MTD induced cell death.
(A) Cell lysates of proliferating LN229 and A172 cells were subject to western blot analysis. For each lysate, 30 µg of protein were loaded onto a 10 % polyacrylamide gel. The picture is representative for one experiment. (B) LN229 and A172 cells were pre-treated with 200 µM naloxone (Nalx) for 30 min, followed by treatment with 50 µg/mL MTD. Early apoptosis (apoptosis) and late apoptosis/necrosis (necrosis) were measured by AV/PI staining in the flow cytometer 3 d later. Proliferating (PRO) cells served as control. The data is given with the mean ± SEM for three representative experiments.

Since MTD was cytotoxic, we were wondering if it also bears genotoxic effects. To assess this possibility, we quantified the amount of DSBs in LN229 cells before and after MTD treatment with non-cytotoxic (10 µg/L) and cytotoxic (30 µg/mL) concentrations. The neutral comet assay analysis, performed with the support of the technical assistance of Anna Frumkina, showed no induction of DSBs following treatment of MTD for 24 h (Figure 39A and B). The results were confirmed by γH2AX immunofluorescence staining measured by LSM.

Quantification of foci showed no significant increase in γH2AX foci 24 h following a non-cytotoxic (20 µg/mL) and cytotoxic (40 µg/mL) treatment with MTD (Figure 39C and D). The results show that MTD is cytotoxic at concentrations too high to be reached within a patient (which under standard dosing is about 0.6 µg/ml) and that even at this dose level it does not bear genotoxic activity.

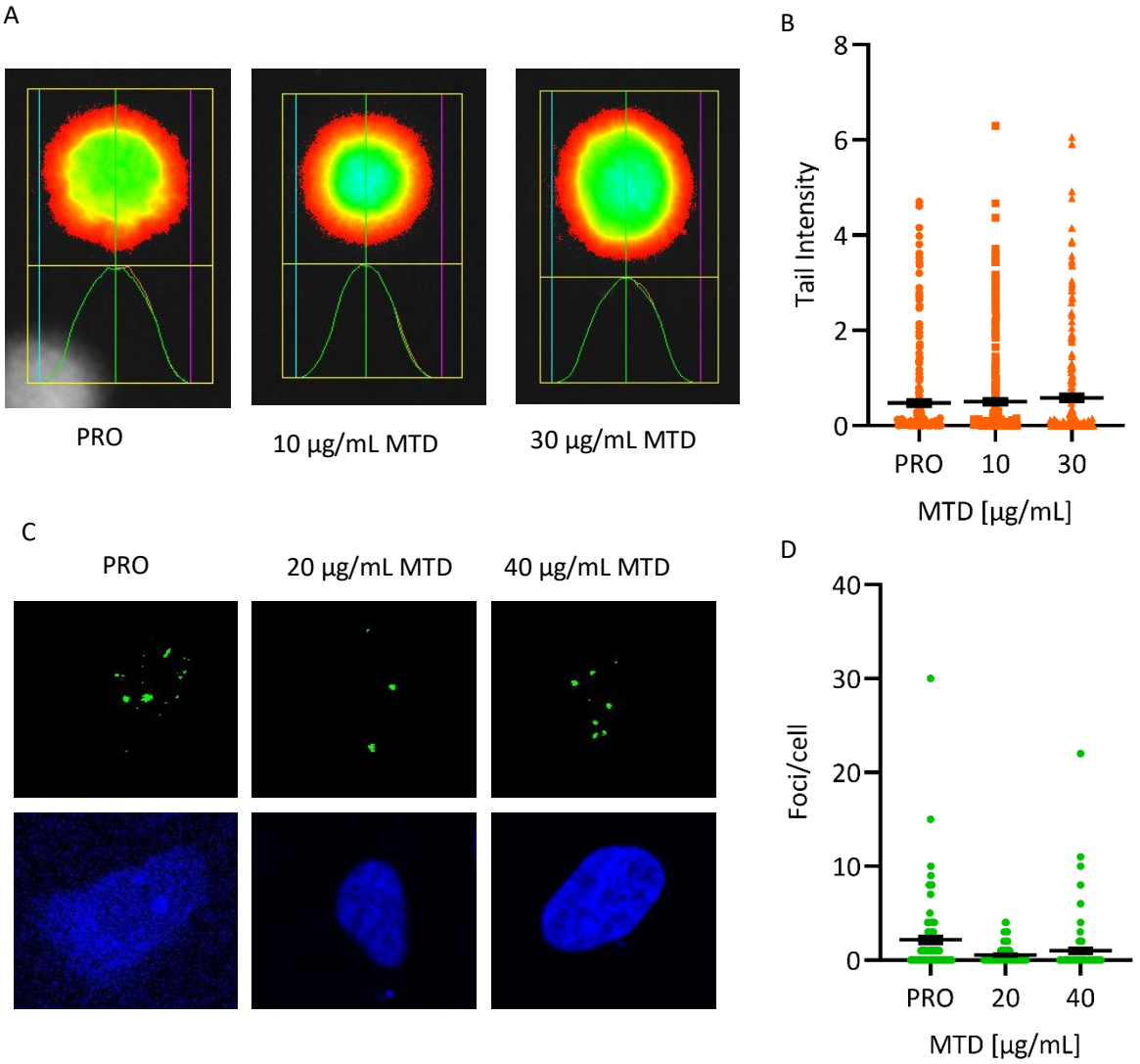

Figure 39: MTD does not induce DSBs.

LN229 cells were treated with non-cytotoxic and cytotoxic concentrations of MTD. DSBs were measured by Comet assay and γH2AY foci quantification. (A) Exemplary images of comet assay in LN229 cells. (B) Evaluation of comet assay tail intensity in control (PRO) and following MTD treatment in non-cytotoxic (10 µg/mL) and cytotoxic (30 µg/mL) concentrations of LN229 cells. (C) Exemplary pictures of γH2AX (green) and ToPro3 (blue) immunofluorescence staining in LN229 cells, taken with a 64x magnification objective using immersion oil. (D) Quantification of γH2AX foci in control (PRO) and following MTD treatment in non-cytotoxic (20 µg/mL) and cytotoxic (40 µg/ml) concentrations of LN229 cells. (B, C) Pictures are representative from one experiment. (B, D) The data is given with the mean ± SEM for three representative experiments.

4.4.4.2. Influence of MTD on TMZ-induced cell death and senescence

As mentioned before, simultaneous treatment with MTD and doxorubicin led to increased cell death levels in GBM cell lines compared to sole doxorubicin treatment (Friesen et al. 2014). Since TMZ and not doxorubicin is the state of the art chemotherapeutic for GBM treatment, we investigated the influence of MTD on TMZ-induced cell death. Therefore, LN229 and A172 cells were treated with 25 µM TMZ and post-treated with non-toxic concentrations of MTD (MTD 1=5 µg/mL and MTD 2=20 µg/mL) 3 h later. Cell death is a late response to TMZ, starting at day 3 and reaching a plateau at day 5 following treatment. Hence, 5 d were chosen as the timepoint to investigate the effect of MTD on TMZ-induced cell death. Proliferating cells served as control. As shown in Figure 40A and C, the addition of a low dose of MTD (5 µg/mL) had no effect, neither in LN229 nor in A172 cells, while the additional treatment of 20 µg/mL MTD 3 h following TMZ led to a significant increase of cell death in both cell lines compared to sole TMZ-induced cell death. It is important to note that in both cell lines, the observed effect of the combined treatment was slightly lower than the reference (expected) value obtained by addition of the sole TMZ- and MTD-induced cell death levels (Figure 40 B and D). The data clearly demonstrates that the simultaneous treatment of TMZ with MTD in low concentrations that might be reached within a patient has no cytotoxic effect on GBM cells. The addition of higher MTD doses showed a less than additive effect, and such high concentrations are not reached within the patient. Hence, we conclude that MTD is not suited as adjuvant for enhancing the curative effect of TMZ in GBM treatment.

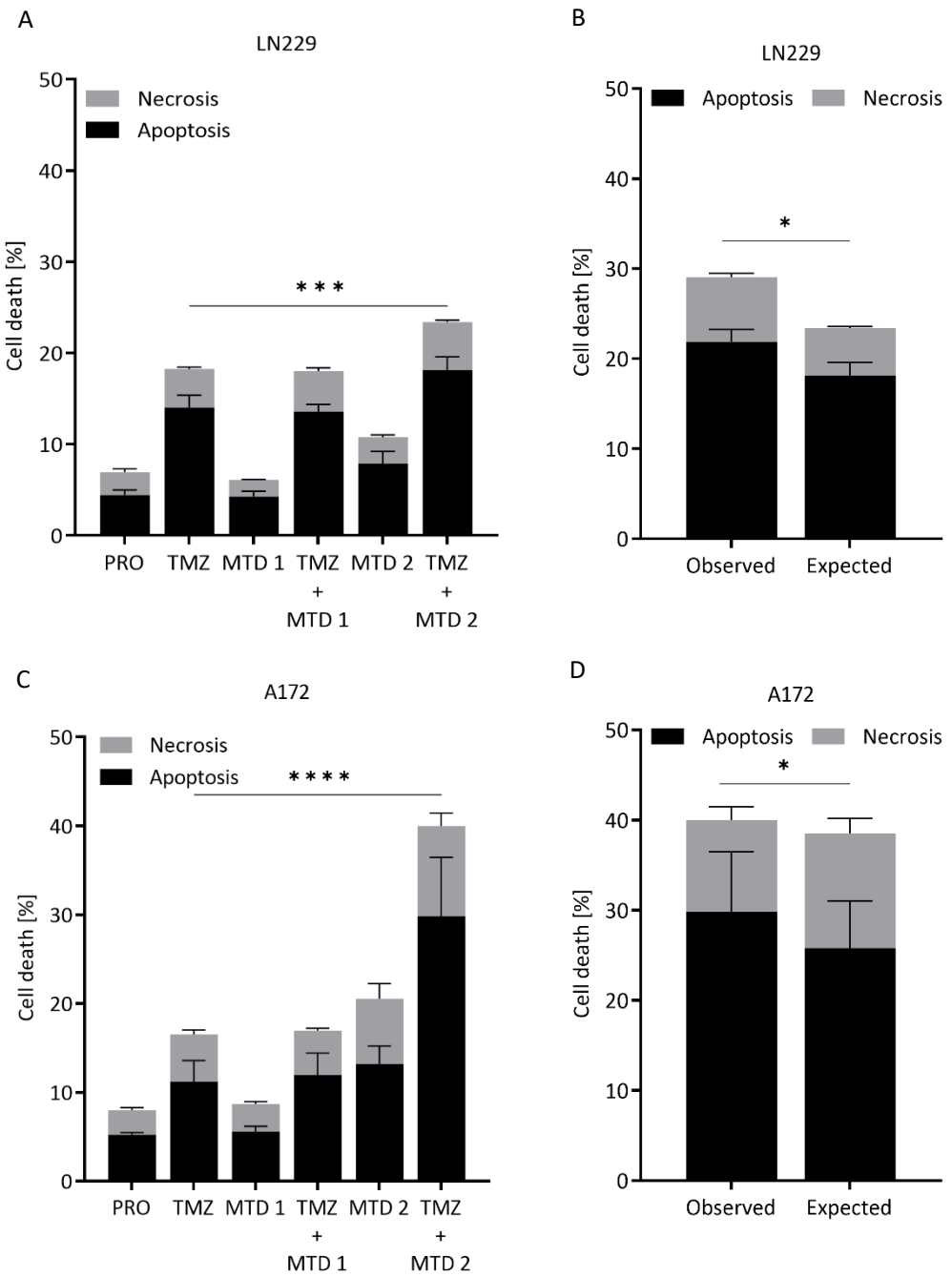

Figure 40: Effects of MTD on TMZ-induced cell death.

LN229 and A172 cells were treated with 25 µM TMZ followed by 5 µg/mL (MTD 1) and 20 µg/mL (MTD 2) MTD treatment 3 h later. Cell death levels (apoptosis and necrosis) were measured by annexin/PI staining in the flow cytometer 5 d following the addition of TMZ to the medium. Proliferating cell served as control (PRO). (A and C) Measured levels of apoptosis and necrosis in LN229 (A) and A172 (C) cells. (B and D) Comparison of added cell death values of sole TMZ and sole MTD treatments (Expected) with the measured cell death levels of combined treatment from A and C (Observed). The data is given with the mean ± SEM for three representative experiments. *p<0.05, ***p<0.001, ****p<0.0001.

As shown above (chapter 4.1.2), following TMZ treatment, cell death through apoptosis is a minor cellular response. The main proportion of the cell population activates cell survival pathways and finally enters the senescent state. Since the addition of MTD to the TMZ treatment resulted in an increase in cell death, the same could be true for the induction of senescence.

To test this hypothesis, LN229 cells were treated with 50 µM TMZ, followed by 5 µg/mL (MTD 1) and 20 µg/mL (MTD 2) MTD 3 h later. Senescence levels were measured by C12FDG staining with the flow cytometer 8d later. As shown in Figure 41A and CSEN levels remained constant, despite the addition of MTD to TMZ treatment. Thus, MTD does not interfere with the induction of senescence by TMZ.

MTD has been shown to downregulate XIAP and Bcl-X_L (Friesen et al. 2014). Senescent LN229 cells display high levels of Bcl-X_L (chapter 4.2.2), and we also demonstrated that inhibition of XIAP1 in senescent LN229 cells leads to a reduction in the CSEN levels (chapter 4.3.1). Thus, even though MTD does not reduce CSEN when used as adjuvant, the possibility remains that MTD kills senescent cells. To elucidate this possibility, senescent LN229 cells were treated with 5 µg/mL and 20 µg/mL MTD, and CSEN levels were measured 2 d later by C12FDG staining and flow cytometry. While 5 µg/mL MTD had no impact on CSEN levels, a significant reduction was measured following 20 µg/mL (Figure 41B). These results indicate that although MTD does not bear cyto- or genotoxic activity, it is not suitable as adjuvant for TMZ treatment or as a senolytic agent following TMZ therapy. It is, however, beneficial as pain medication, and no adverse effects were observed at these low treatment concentrations.

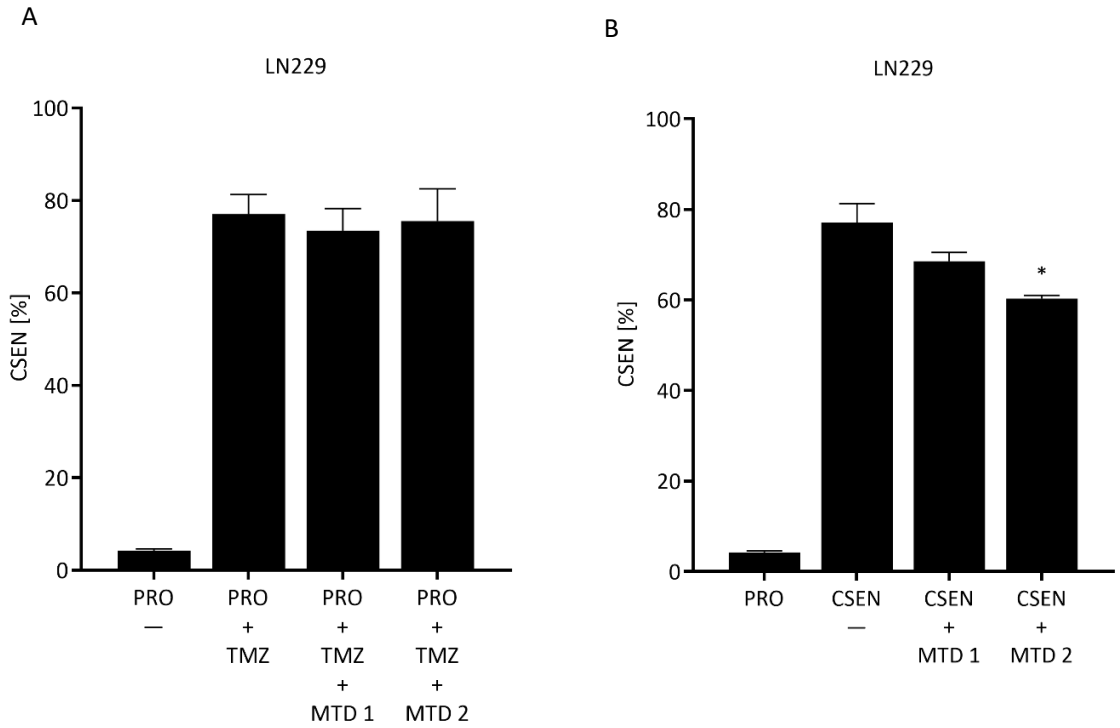

Figure 41: Effect of MTD on TMZ-induced senescence.

(A) LN229 cells were either treated with 50 µM TMZ alone or simultaneously with 5 µg/mL (MTD 1) or 20 µg/mL (MTD 2) MTD for 8 d. Proliferating cell served as control (PRO). (B) Senescent LN229 cells were treated with 5 µg/mL (MTD 1) or 20 µg/mL (MTD 2) MTD for 2 d. Senescence was quantified via C12FDG staining, measured in the flow cytometer. The data is given with the mean ± SEM for three representative experiments. *p<0.05

4.5. Identification of senolytic agents

Targeting pathways inducing or maintaining the senescent state is not the only option to eliminate senescent cells. Lately, more focus is laid on senolytic agents - compounds that specifically drive senescent cells into cell death, without affecting proliferating cells. They include synthetic as well as natural compounds. A few have already been identified in other cell systems including GBM. Here, we evaluated known senolytic agents for their senolytic activity in GBM and identified new options for eliminating senescent GBM cells.

4.5.1. MCOPPB

The nociceptin receptor FQ opioid receptor selective ligand MCOPPB has recently been identified as a possible senolytic agent in a library screen of pharmacologically active compounds (Raffaele et al. 2022). A subsequent study demonstrated that MCOPPB specifically kills doxorubicin-induced senescent hepatocellular carcinoma cells *in vitro* and reduced senescent cells *in vivo* in a mouse model (Raffaele et al. 2022). Thus, we considered the possibility that MCOPPB might also kill TMZ-induced senescent GBM cells. Treatment of proliferating LN229 cells with 1 µM MCOPPB led to a slight increase in cell death. Treatment of senescent LN229 cells led to a slight reduction in CSEN while senescence was reduced significantly in A172 cells. Interestingly, also cell death levels were reduced in both cell lines; slightly in the LN229 and significantly in the A172 cells (Figure 42). These data indicate that MCOPPB reduces both, the TMZ-induced cytotoxic and cytostatic effects in GBM cells. Since no increase in cell death was observed upon reduction in CSEN, MCOPPB does not bear senolytic activity in our GBM cell model.

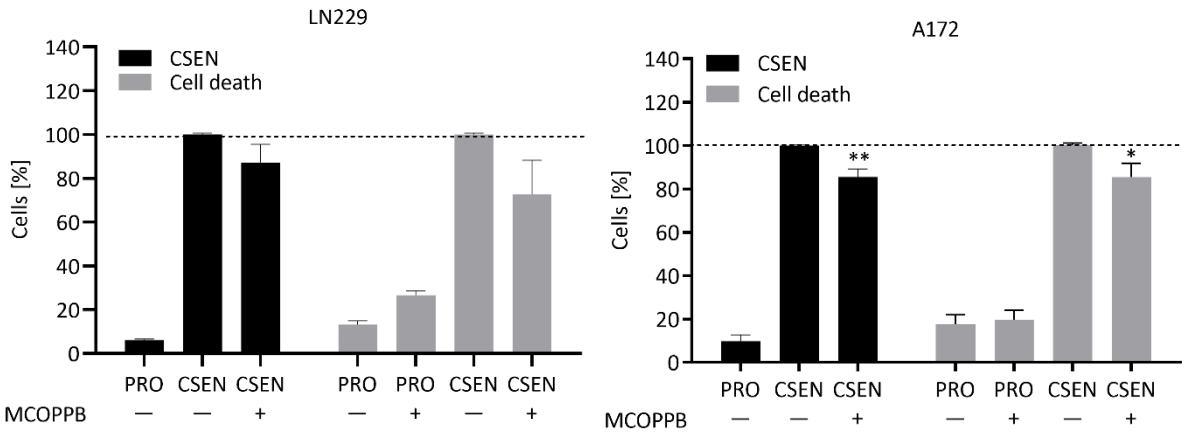

Figure 42: Effect of MCOPPB on senescent GBM cells.
Senescent LN229 and A172 cells were treated with 1 µM MCOPPB for 2 d. Proliferating cells (PRO) served as control. AV/PI and C12FDG positive cells were quantified by flow cytometer measurement for cell death and senescence evaluation, respectively. The data is given with the mean ± SEM for three representative experiments. *p<0.05, **p<0.01.

4.5.2. Artesunate

Artesunate is a semisynthetic derivative of artemisinin, a phytochemical found in *Artemisia annua*. It is widely used in the traditional Chinese medicine, mostly to treat malaria (Klayman 1985; Zhao et al. 1986). Starting in the 1990s, artemisinin and its derivatives, including artesunate, were evaluated as to their cytotoxic properties on cancer cells and found to be efficient apoptosis and autophagy inducing (Jiang et al. 2018). Since then, numerous studies have been performed on anti-cancer effects of artesunate but as to our best knowledge, no efforts have yet been made to identify the effect of artesunate on senescent (cancer) cells (Qin et al. 2015; Berdelle et al. 2011; Wei et al. 2020). Artesunate has been shown to regulate genes involved in DDR and DNA repair, regulation of apoptosis and proliferation, as well as oncogenes, tumour suppressor genes and genes coding for cytokines (Efferth et al. 2003). This background data led us to evaluate the senolytic effect of artesunate on GBM cells. As shown in Figure 43, treatment of senescent LN229 cell with 15 µM artesunate, which was non-toxic on proliferating cells, significantly reduced CSEN while increasing cell death. In A172 cells, the CSEN level was reduced not significantly, although cell death levels increased significantly. This indicates that artesunate has senolytic activity in the LN229 but not the A172 cell line.

Artesunate plasma peak concentrations within malaria patients reach 2.19 - 11.57 mM when given intravenously (Batty et al. 1996). Here, we demonstrate that 15 µM artesunate, which is well below the levels reached within patients, is already sufficient to induce cells death in senescent LN229 and A172 cells, and to reduce senescence in LN229 cells. It is important to note that the human fibroblast cell line VH10T showed no induction of cell death at this concentration (Supplemental figure S2). Artesunate can therefore be considered as a senolytic agent.

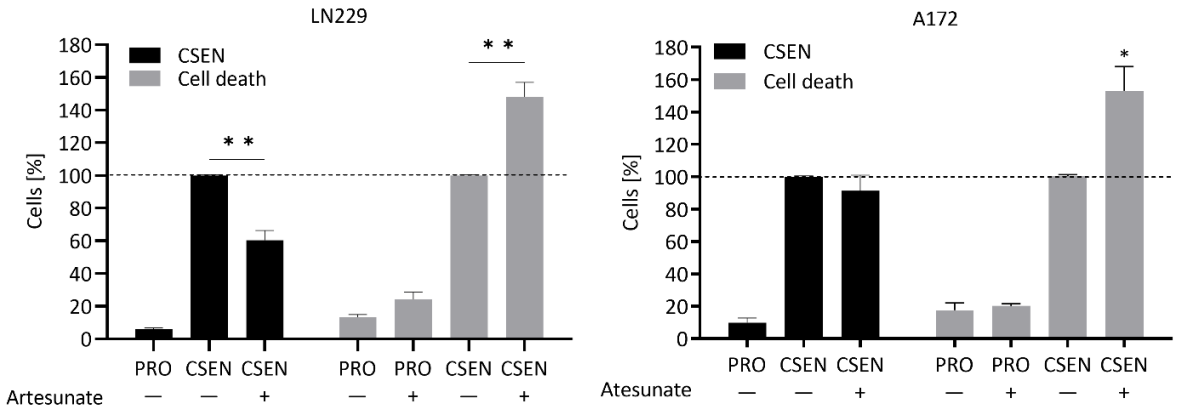

Figure 43: Senolytic effect of artesunate on GBM cells.
Senescent LN229 and a172 cells were treated with 15 µM artesunate for 2 d. Cell death and CSEN levels were quantified by positive annexin/VPI and C12FDG staining in the flow cytometer, respectively. Proliferating cells (PRO) served as control. The data is given with the mean ± SEM for three representative experiments. *p<0.05, **p<0.01.

4.5.3. Curcumin

Another phytochemical arising from the traditional Chinese medicine is curcumin, the principle curcuminoid responsible for the yellow colour in *curcuma longa*, also known as turmeric. Due to its colouring properties, it is widely used as food colouring and in cosmetics. It is widely sold as herbal food additive because of its beneficial roles in diabetes, several brain disorders, such as Alzheimer's disease and its anti-inflammatory effects (Bhat et al. 2019; Ghosh et al. 2015). It is supposed to have beneficial effect on health due to its anti-oxidative, anti-inflammatory, and anti-cancer effects (He et al. 2020; Kocaadam and Şanlier 2017). However, little is known abouts its cyto- and genotoxic effects. Considering the widespread usage of curcumin, analysis of these effects is essential. Thus, we assessed the dose-dependent induction of cell death and DNA damage following curcumin treatment and compared short-term vs long-term exposure. In a subsequent series of experiments, we also evaluated whether curcumin bears senolytic activity. Due to its low solubility in water, curcumin was either dissolved in ethanol (Cur-E) or packed into micelles (Cur-M) to be administered in aqueous solution.

4.5.3.1. Cyto- and genotoxic effects of curcumin

The effect of Cur-E and Cur-M on the cell viability was studied previously in our laboratory using the MTT assay, and showed a dose dependent decrease, stating at 5 µM 72 h post treatment. No difference between Cur-E and Cur-M was detected. Here, we confirmed these results by detection of cell death in LN229, A172 and VH10T cells 48 h following treatment. As shown in Figure 44, cell death was induced by curcumin starting at 20 µM in LN229 and A72 cells. No significant difference was observed between Cur-E and Cur-M in inducing apoptosis. Contrary, cell death in VH10T cells was induced at 20 µM when dissolved in ethanol, while curcumin packed in micelles started to be cytotoxic at 30 µM. Thereafter, no difference was observed between Cur-M and Cur-E induced cell death levels (Figure 44).

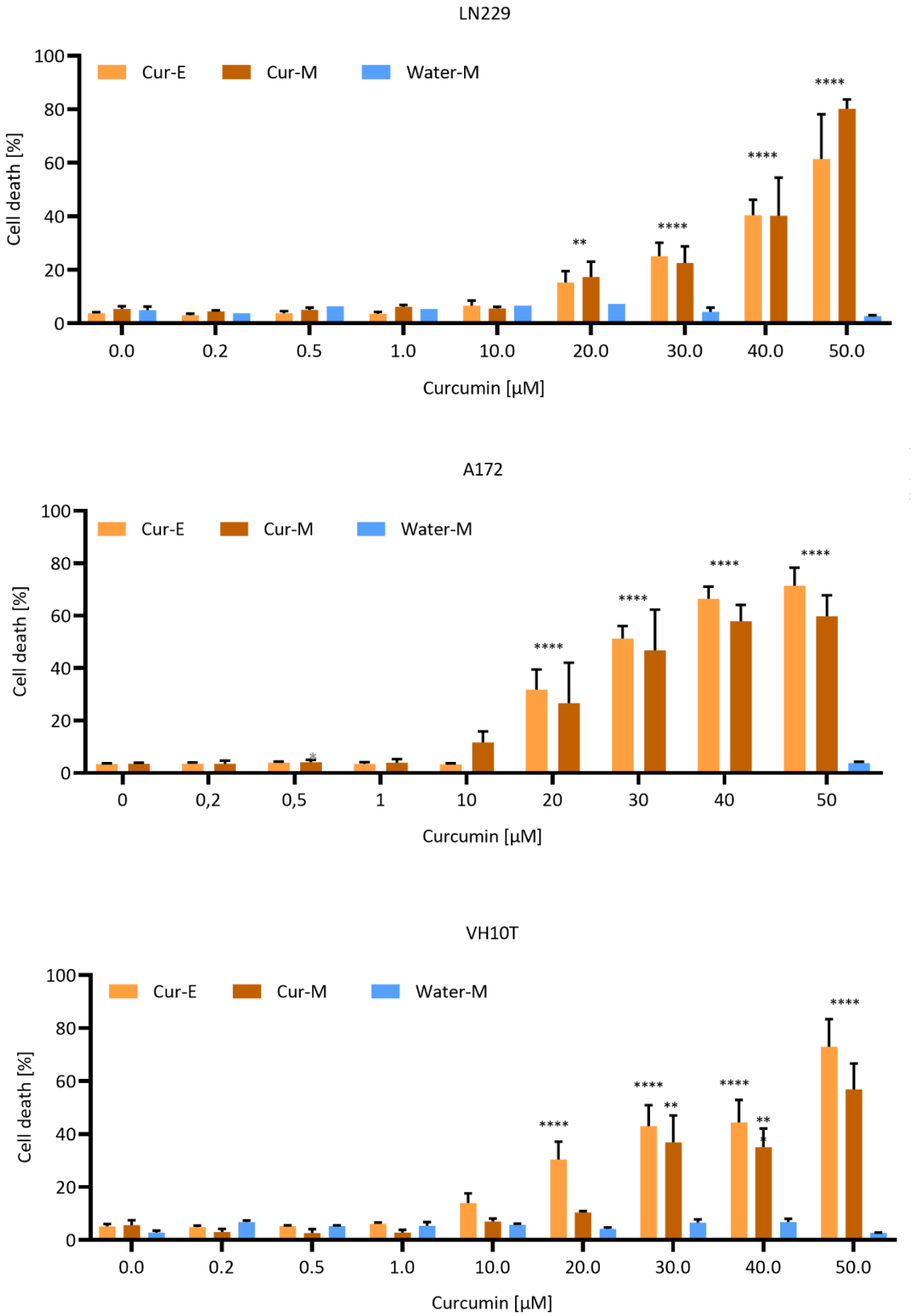

Figure 44: Curcumin induces cell death dose-dependently.

LN229, A172 and VH10T cells were treated with rising concentrations of curcumin dissolved in ethanol (Cur-E) or packed into micelles (Cur-M) for 2 d. Micelles packed with isotonic water (Water-M) served as control for cytotoxicity of micelles. Untreated cells served as control (0.0 µM curcumin). Cell death levels were quantified by AV/PI staining. The data is given with the mean ± SEM for three representative experiments. *p<0.05, **p<0.01.

Like the induction of cell death, DSBs were induced in a dose-dependent manner starting at 10 µM, measured by the neutral comet assay. No difference between Cur-E and Cur-M treated cells was observes. Interestingly, DSBs occurred as early as 1 h following treatment and were still present at 24 h post treatment (Figure 45). This and all following neutral comet assays were performed supported by the technical assistance of Anna Frumkina.

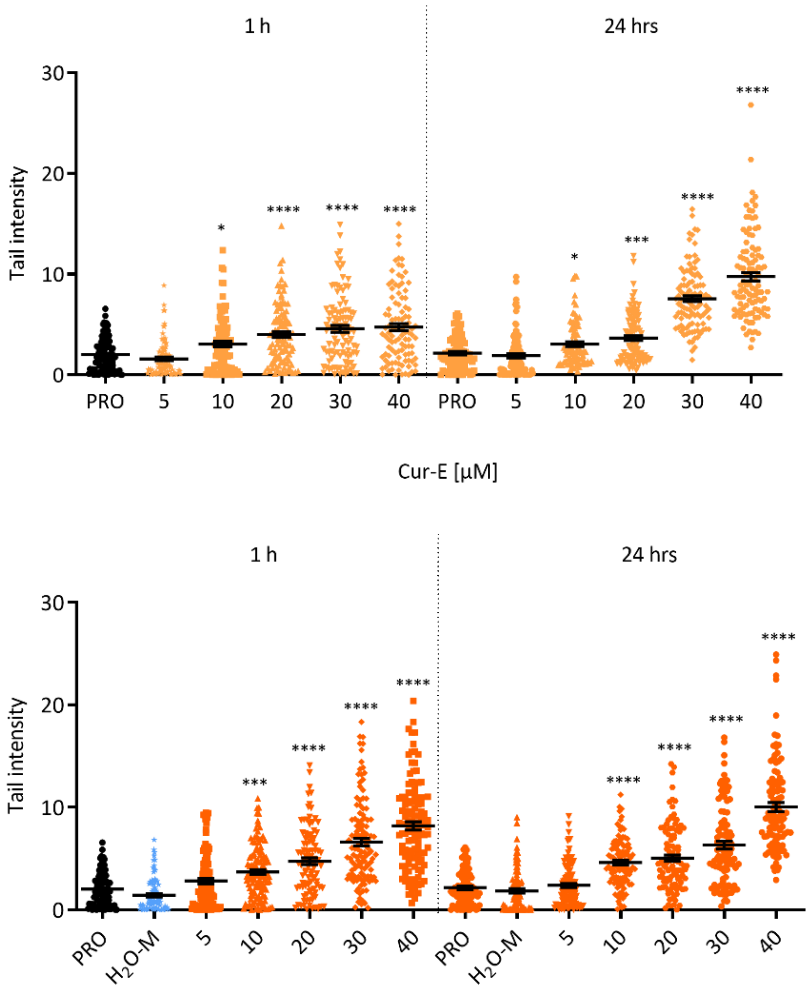

Figure 45: Induction of DSBs following curcumin treatment.
Proliferating LN229 cells were treated with the indicated concentrations of Cur-M and Cur-E for 1 h or 24 h or were left untreated as control (PRO). Water micelles served as control for micelle toxicity. The data was obtained through the neutral comet assay and is given with the mean ± SEM for three independent experiments. *p<0.05 ***p<0.001, ****p<0.0001.

Since curcumin was present in the medium throughout the experiment, the possibility remained that DSBs were not persisting, rather than being induced over and over. To assess this hypothesis, LN229 cells were treated with 40 µM Cur-E or 40 µM Cur-M for 1 h to induce high levels of DSBs. Thereafter the medium was renewed and DSBs were quantified immediately (0 h repair time) and in 1 h intervals for 4 h by comet assay. Tail intensity decreased significantly 1 h following removal of curcumin from the medium and was further reduced thereafter.

At 4 h after the medium change Cur-E treated cells reached tail intensity levels of the control, while in Cur-M treated cells DSBs were at the level of the water micelle treated cells. These results show that DSBs induced by curcumin are repaired within 4 h after the onset of curcumin treatment (Figure 46A). This finding led us to believe that short term treatment might also lead to a reduced level of cell death. Thus, we treated LN229 and A172 cells with 40 µM Cur-E or 40 µM Cur-M not permanently but for 1 h and evaluated cell death levels 48 h later. As shown in Figure 46B, short-term treatment of LN229, A172 and VH10T cells did not lead to induction of cell death. These results lead to the conclusion that curcumin must be present permanently to exert cytotoxic effects.

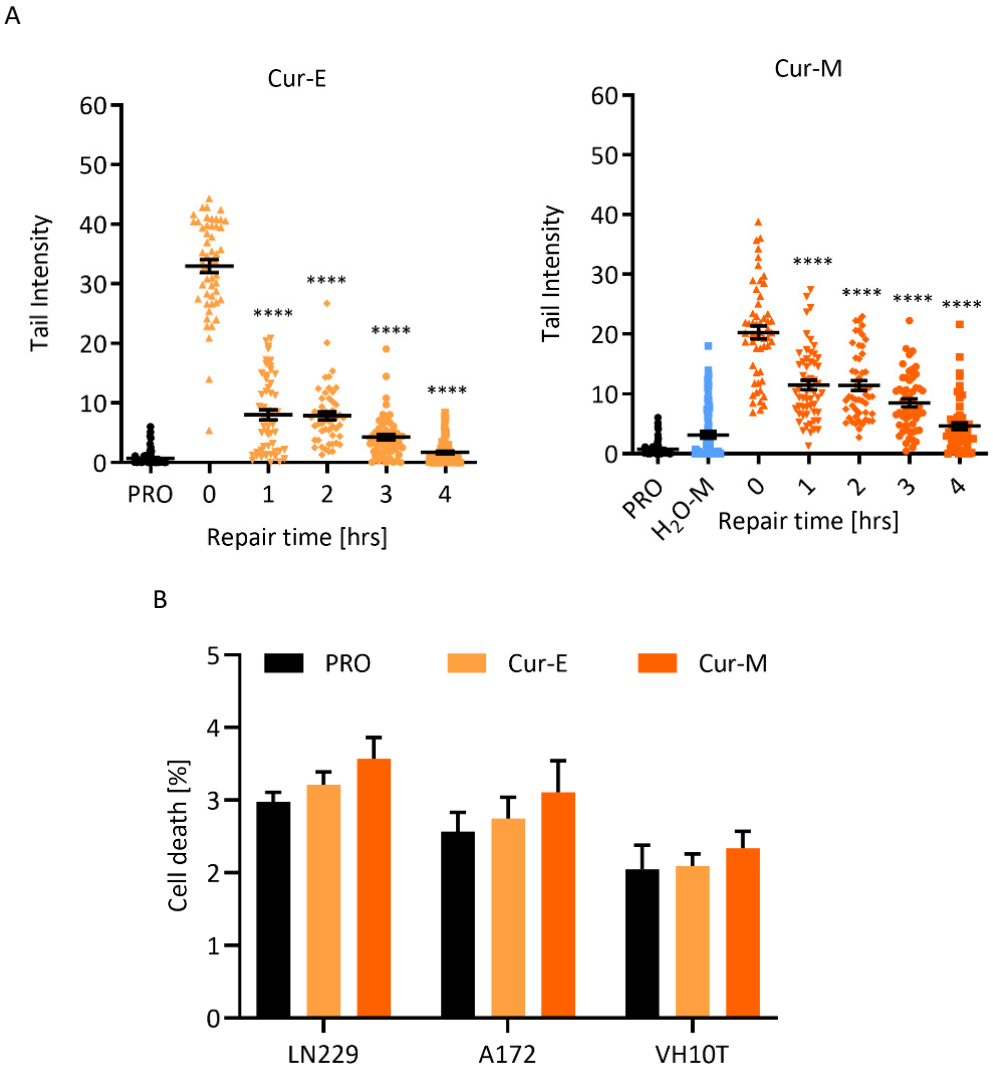

Figure 46: Effects of short-term treatment with curcumin.
Proliferating LN229 cells were treated with 40 µM of Cur-M or 40 µM of Cur-E for 1 h or were left untreated as control (PRO). Water micelles served as control for micelle toxicity. (A) The repair of DSBs was assessed by the comet assay in LN229 cells (B) Cell death levels in LN229, A172 and VH10T cells were measured 2 d following treatment with curcumin. The data is given with the mean ± SEM for three representative experiments. *p<0.05 ***p<0.001, ****p<0.0001.

4.5.3.2. Effect of curcumin on TMZ-induced senescence

The previous experiments demonstrated the cytotoxic effects of long-term curcumin treatment on proliferating GBM cells. In a subsequent series of experiments, we assessed the effect of curcumin on senescent GBM cells. First, the cell viability of senescent and proliferating LN229 cells was compared via MTT assay following increasing concentrations of curcumin. Interestingly, while in proliferating cells cell viability was significantly reduced starting at 10 µM curcumin, independent of administration, senescent cells were unaffected. Even at high concentrations of 40 µM curcumin, senescent cells did not display reduced cell viability (Figure 47A). These results were confirmed by evaluation of CSEN and cell death levels in senescent LN229 cells before and after curcumin treatment. While proliferating cells displayed a slight increase in cell death following 10 µM curcumin treatment, senescent cells showed a reduction in cell death and an increase in the senescence levels (Figure 47B). This indicates that curcumin is not a senolytic compound in our GBM cells.

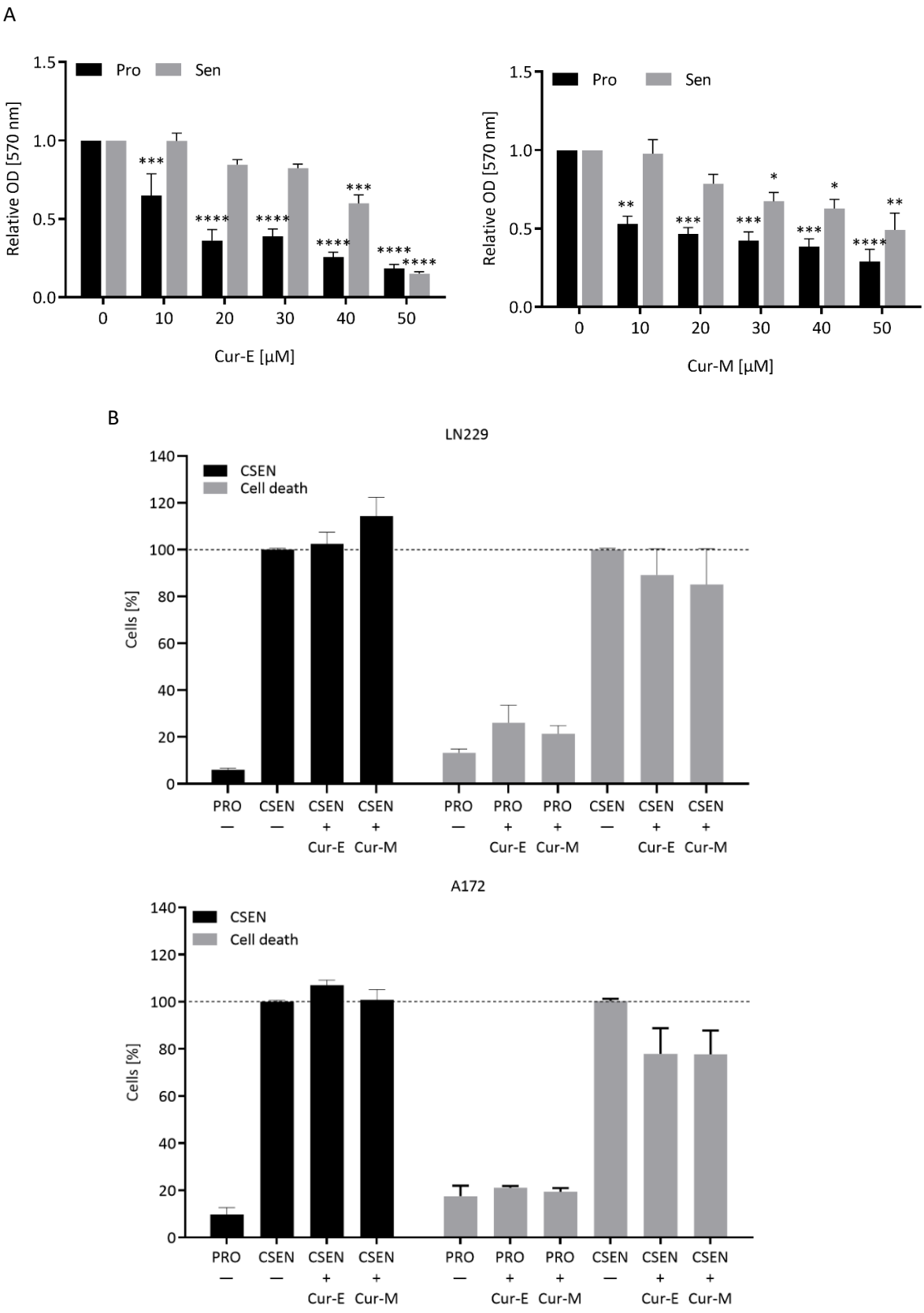

Figure 47: Effect of curcumin on senescent GBM cells.
Proliferating and senescent LN229 cells were treated with Cur-E and Cur-M and evaluated 2 d later. (A) Cell viability of proliferating and senescent LN229 cells following exposure to increasing concentrations of curcumin was measured by MTT assay. (B) Senescent LN229 cells were treated with 10 µM curcumin and cell death and CSEN levels were observed by AV/PI and C12FDG staining, respectively in the flow cytometer. The data is given with the mean ± SEM for three representative experiments.

4.5.3.3. Fisetin

Fisetin is a bioactive polyphenolic flavonoid that is found in many fruits e.g., strawberries, apples and persimmon, vegetables e.g., onions, and trees and flowers from the fabaceae family (Arai et al. 2000). Like curcumin, it serves as a yellow colouring agent. It has been shown in various studies to have a brought range of targets including the PI3K/AKT pathway, BCL-X_L and NF-kB. Inhibition of those targets by fisetin results in its anti-inflammatory and anti-cancer effects (Khan et al. 2008; Afroze et al. 2022). Additionally, fisetin acts as antioxidant, hypoglycaemic agent (Grynkiewicz and Demchuk 2019). Recently, fisetin has been shown to be a senolytic agent in HUVECs and to reduce replication-induced senescent cells in a mouse model (Zhu et al. 2017; Yousefzadeh et al. 2018). This prompted us to investigate its senolytic activity in GBM cells. Due to its low solubility in water, in our experiments fisetin was dissolved in ethanol. As shown in Figure 48, treatment of senescent LN229 and A172 cells with 20 µM fisetin resulted in a significant reduction in the CSEN level in LN229 cells. In A172 cells, CSEN reduction was also observes, which was, however, statistically not significant. Concomitantly, cell death levels increased significantly in LN229 cells and again non-significantly in A172 cells. Proliferating cells treated with 20 µM fisetin displayed no induction of cell death. Thus, we conclude that fisetin acts as senolytic agent in TMZ-induced senescent GBM cells.

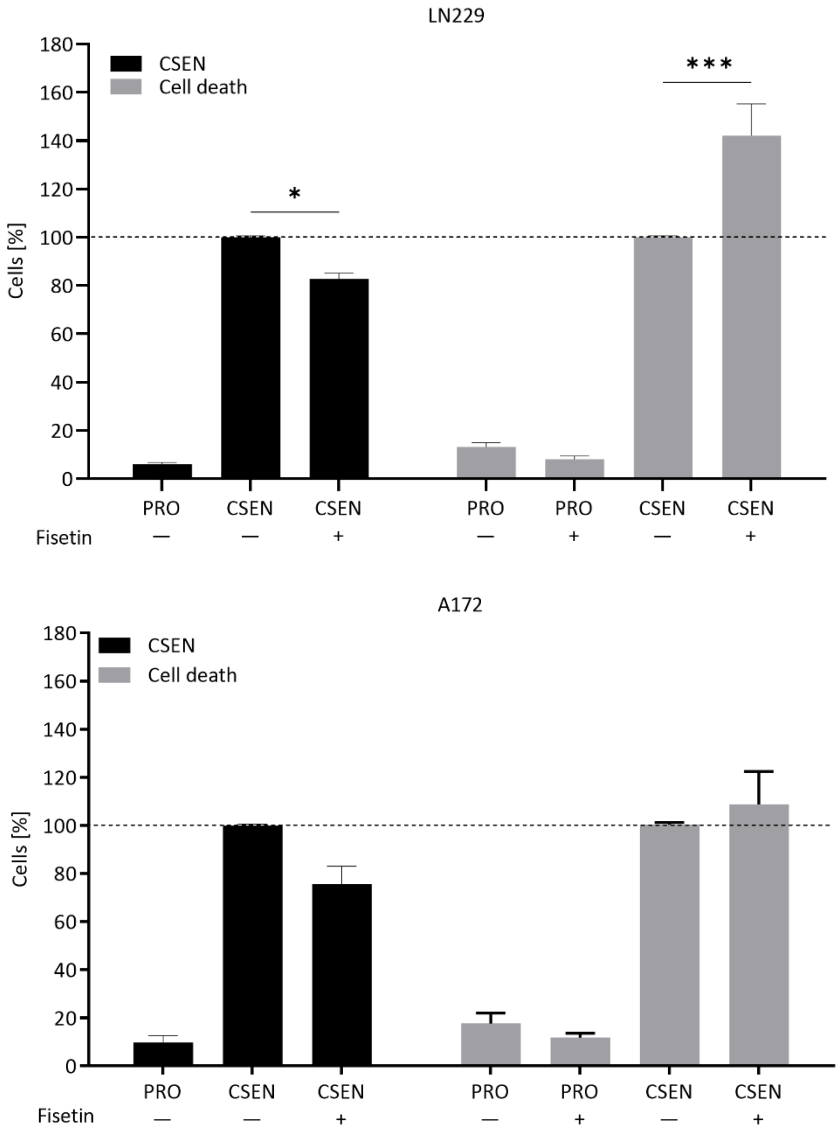

Figure 48: Senolytic activity of fisetin.

Senescent and proliferating LN229 and A172 cells were treated with 20 µM fisetin, dissolved in ethanol, for 2 d. Cell death and CSEN levels were assessed by AV/PI and C12FDG staining, respectively, in the flow cytometer. The data is given with the mean ± SEM for three representative experiments. *p<0.05 ***p<0.001.

4.6. In situ analysis of senescence markers

Our experiments demonstrated that following TMZ treatment, GBM cell mainly enter senescence and that cell death is only a minor trait (chapter 4.1.2). We also showed high numbers of DSBs in senescent LN229 and A172 cells. Another marker for senescence is tri-methylated lysin at histone 3 (H3K27me3). Our group recently showed that following TMZ treatment, senescent LN229 and A172 cells display high levels of H3K27me3. In the clinical setup, recurrent GBM tumours usually occur following treatment of primary GBM. One possible cause for the origin of recurrent tumours are senescent cells that overcome their senescent state and re-enter the cell cycle. To test this hypothesis, we stained patient derived matched primary and recurrent GBM tissue samples for senescent markers, namely γH2AX and H3K27me3, as well as apoptosis. The samples were kindly provided by Prof. Dr. Clemens Sommer and stained by Dr. Petra Leukel from the Institute of Neuropathology of the University Medical Center Mainz.

Visual analysis of primary tumours indicated low levels of γH2AX and H3K27me3 positive cells. In contrast, recurrent tumours displayed higher levels of DSBs and senescence. Contrary, the TUNEL assay indicated a high level of apoptosis in primary GBM tumours, while recurrent tumours were stained less for apoptosis (Figure 49).

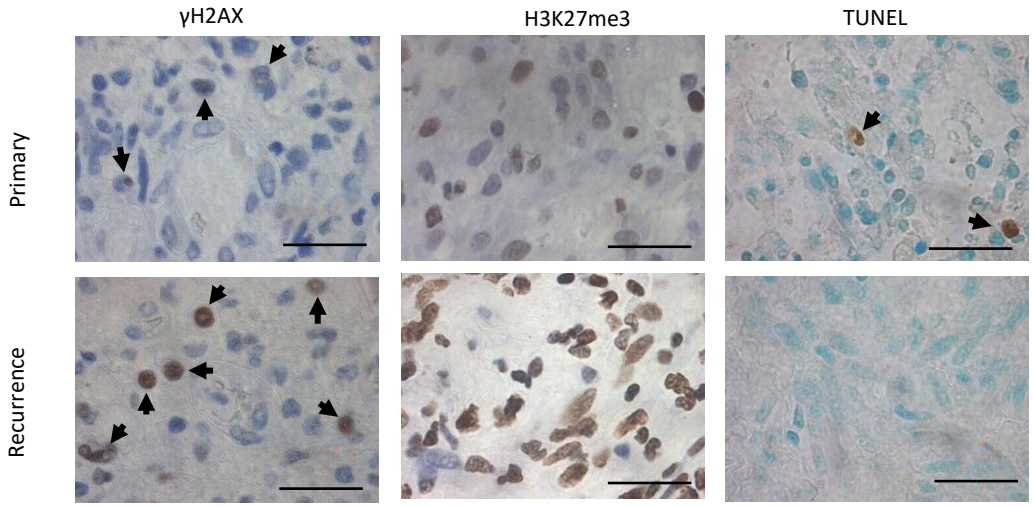

Figure 49: Exemplary pictures of primary and recurrent patient derived GBM tumour samples
Exemplary pictures of primary and recurrent GBM tissue stained for γH2AX, indicating DSBs and H3K27me3, indicating senescence. TUNEL assay staining indicates apoptosis. Pictures were taken using a 100-fold magnification objective and immersion oil. The measuring bar indicates 200 µM. The samples were kindly provided and stained by Prof. Dr. Clemens Sommer and Dr. Petra Leukel.

Quantitative evaluation of the microscopy pictures and comparison of overall primary and recurrent tumours confirmed the visual analysis. The CSEN marker H3K27me3 was increased in recurrent tissue. Significantly more γH2AX positive cells were present in the recurrent samples, indicating more DSBs.

Despite the high amount of DNA damage, significantly less cells stained positive for apoptosis in the recurrent tissues. (Figure 50A). This study included matched samples from 10 patients thus, tissue samples from more patients must be evaluated to confirm the results. Individual comparison of matched pairs showed that in all but one recurrent tumour the yH2AX level was increased compared to the primary tumour. For apoptosis and H3K27me3 all except two recurrent tumours showed lower levels than their primary match (Figure 50B). These results indicate that senescent GBM cells accumulate in brain tissue following treatment with TMZ and IR. The methylation status of the *MGMT* promotor for each tumour sample was evaluated; the tumour samples included five *MGMT*-promotor unmethylated and two *MGMT*-promotor methylated tumours. For one sample, the methylation status is unknown (Supplemental table S1). The methylations status did not correlate with the samples that showed different results in the yH2AX, TUNNEL and H3K27me3 staining.

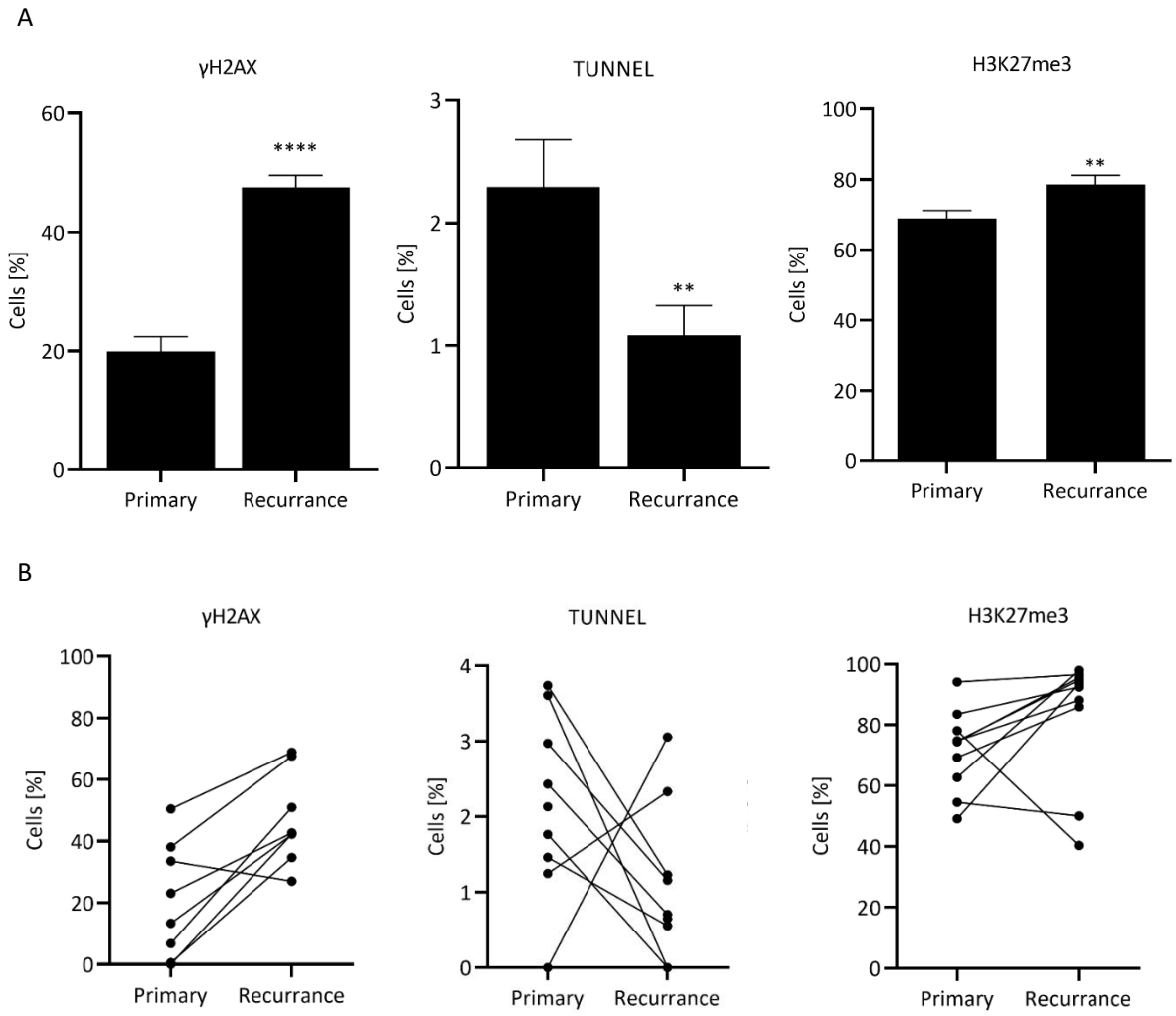

Figure 50: In situ analysis of senescence and apoptosis markers.

Levels of DSBs, indicated by yH2AX staining, apoptosis, detected by TUNNEL assay and senescence, indicated by H3K27me3 were evaluated in primary and recurrent GBM tissue of 10 patients. (A) Overall percentage of yH2AX and H3K27me positive as well as apoptotic cells, quantified from 10 sections per tumour slice from 10 tumour samples. (B) Comparison of the percentage of yH2AX and H3K27me positive as well as apoptotic cells from 10 sections per tumour in matched primary and recurrent tumour samples. **p<0.01 ***p<0.001.

5. Discussion

With about 40 % of all malignant brain tumours GBM is the most common one. The incidence rate is rising in several countries, reaching up to 5/100,000 people (Surawicz et al. 1999; Dolecek et al. 2012; Ostrom et al. 2018; Low et al. 2022; Philips et al. 2018). Until 2005, the standard of care for GBM was maximum safe resection combined with the alkylating agent TMZ. Since then IR was an additional treatment option, since administered concomitantly with TMZ, resulting in improved PFS and OS (Stupp et al. 2005). Although death rates are decreasing, GBM patients still have a low survival rate. Less than 6 % of all patients survive beyond 5 years following diagnosis, while the median survival is about 15 months. One cause for the poor prognosis are recurrent tumours occurring about 5 months following resection of the primary tumour (Glioblastoma Multiforme – Symptoms, Diagnosis and Treatment Options 2021; Tan et al. 2020; Korja et al. 2019). The rapid appearance of recurrencies is thought to result from drug and radiation resistant tumour stem cells (Safari and Khoshnevisan 2015; Frosina 2009). It has also been hypothesised that recurrences may arise from senescent cells that escaped their senescent state and re-entered the cell cycle (Saleh et al. 2019; Olszewska et al. 2021; Le Duff et al. 2018). The low therapy response of GBM underlines the importance of a better understanding of molecular mechanisms of TMZ treatment as well as the identification of improved treatment schedules and strategies to reduce CSEN. Here, we analysed the kinetics of DSBs formation, as well as the induction of early and late apoptosis/necrosis (cell death) and CSEN following TMZ treatment. We further analysed the senescent cell population and identified senescence maintaining proteins and pathways. To find improved treatment options for GBM, we co-treated GBM cell *in vitro* with TMZ and CCNU or IR and screened for senolytic agents.

In the clinical setup, TMZ is given daily in low doses to reduce side-effects. Hence, TMZ concentration levels in the tumour are low, reaching about 3-35 µM [1–3]. In the present work, however, cells were treated with 50 µM TMZ to analyse the CSEN and cell death levels, or with 20 µM to evaluate combinatorial treatment options. The question arises if the results obtained with high concentrations used *in vitro* can be transferred to the *in vivo* situation, where the TMZ concentration is much lower, and if the low concentrations reached within the patient are sufficient to induce the cytotoxic and cytostatic effects seen with higher TMZ concentration *in vitro*. We previously analysed the kinetics of TMZ-induced formation of O^6meG, DSBs, and the resulting cell responses, e.g., cell death and CSEN. The results show a linear dose-response with no threshold detected for the induction of cell death and CSEN (Stratenwerth et al. 2021). Additionally, daily treatment of LN229 and A172 cells with low doses of TMZ (5 µM), mimicking the clinical setup, resulted in an additive induction of cell death and CSEN equal to a single dose of 25 µM TMZ (Beltzig

et al. 2021). Based on these studies, we infer that it is justified to use experimental treatment concentrations of 50 µM and 20 µM TMZ. TMZ exerts its genotoxic und cytotoxic effects through methylation of guanine at the O^6 position (O^6meG). This adduct is quickly repaired by MGMT. If not repaired by MGMT, the adduct in converted into DSBs through futile MMR cycles that collide with replication (Quiros et al. 2010). To analyse the cytotoxic effects by TMZ, we used the MGMT deficient and MMR competent GBM cell lines LN229 and A172 and treated with TMZ when they were in the exponential growth phase.

5.1. Senescence is the main trait induced by TMZ

Analysis of TMZ-induced cell death and CSEN kinetics revealed an onset of CSEN parallel to the onset of cell death. In LN229 and A172 cells, significant levels of CSEN were detected 3 d following treatment. Cell death levels were significantly increasing starting at day 4. Both, CSEN and cell death increased up to 8 d and stayed stable thereafter. However, CSEN was the major response induced by TMZ since it occurred at a ~ 4-fold higher level than cell death (chapter 4.1.2). This was visually verified by detecting an enlarged, flat morphology and positive staining for SA-β-gal (Figure 15). The high number of senescent cells combined with the reporting of senescent cells escaping their cell cycle arrest may provide a possible explanation for the low response rate of patients to TMZ treatment as well as the high number of recurrences in GBM.

Cell death and CSEN are basic cellular processes. It is thus to be expected that these processes are not only induced in GBM cells *in vitro* but also relevant for the *in vivo* clinical setup. Therefore, in collaboration with Prof. Dr. Clemens Sommer and Dr. Petra Leukel from the Institute of Neuropathology of the University Medical Center Mainz, we stained patient derived GBM tumour samples for senescence markers and cell death (chapter 4.6). Primary and recurrent tumours were evaluated. Since GBM is a heterogenic tumour, different tumour sections for each tumour were evaluated. Quantification of DSBs harbouring cells showed a significant increase in the recurrent tumour. Simultaneously, cell death levels were significantly reduced. These results hint towards an accumulation of senescent cells in the recurrent tumour. An increase in trimethylated H3K27 (H3K27me3) in the recurrent tumour further strengthens these results (Figure 50A). Matched tumour samples of 10 patients were evaluated in total. To identify differences between the individual patients, we compared DSBs harbouring cells, cell death and the amount of H3K27me3 for the matched tumour samples. Interestingly, 9/10 samples showed an increase in DSBs, while 8 /10 had decreased cell death levels. H3K27me3 was highly increased in 3/10 samples and slightly increased in 3/10 samples, while 1/10 showed no change, 1/10 a slight reduction, and a 1/10 a high reduction (Figure 50B).

Although only 10 samples were evaluated, these results provide hints towards an accumulation of senescent cells in GBM tumours following TMZ treatment.

5.2. Evaluation of DSBs following TMZ treatment

An increase above the control level of DSBs was detected in LN229 cells as early as 3 d following TMZ treatment (Figure 13). LN229 cells have a doubling time of 24-27 h (Weller et al. 1998). The finding that DSBs occur first about 72 h following addition of TMZ to the cell culture medium are in line with the hypothesis that TMZ-induced DSBs occur after the second cell cycle when the repair of O^6meG by the MMR system eventually collides with replication forks (Quiros et al. 2010). It has recently been proposed, that DSBs can be induced independently from replication through simultaneous repair of base adducts in proximity (Fuchs et al. 2021). During BER as well as MMR, ssDNA is formed as an intermediate (Christmann et al. 2003). Therefore, it could be possible for DSBs to occur if ssDNA segments are in proximity on opposite DNA strands. To investigate this hypothesis, we measured DSBs induction 2, 4 and 6 h following TMZ treatment (4.1.1). Indeed, a significant increase in DSBs was observed 2 and 4 h following TMZ treatment in LN229 and A172 cells, respectively. However, these DSBs were repaired, and DSBs returned to control levels after 6 h (Figure 13). The short peak of DSBs detected 2 h following treatment could result from simultaneous repair of N- and O-alkylation by BER and procession by MMR in proximity. However, even though γH2AX detection showed a significant increase, only about 6-8 DSBs were detected, which is significantly lower than the 20 DSBs measured 48-72 h following treatment. Also, these DSBs were repaired within 3-4 h. Therefore, we conclude that DSBs that are induced early following TMZ treatment are irrelevant in TMZ-induced cytotoxicity.

It has been reported, that DSBs occurring in telomers that are not repaired can trigger drug-induced senescence (Fumagalli et al. 2012). Also, during replicative senescence, DSBs occur at telomers due to telomer shortening (Di d'Adda Fagagna 2008; Arnoult and Karlseder 2015). To see if TMZ induces DSBs at telomers, which are accompanied with senescence, we colocalised γH2AX and the Trf1 which is part of the telomer shelterin complex (Liu et al. 2004). Quantification of colocalization revealed that TMZ-induced DSBs do not occur significantly in telomers but rather randomly in the genome (Figure 17). Thus, TMZ-induced senescence differs from telomer-shortening induced replicative senescence (Di d'Adda Fagagna 2008; Arnoult and Karlseder 2015).

5.3. Senescent cells show an active DNA damage response

Active DSBs in senescent cells should constantly trigger the DNA damage response (DDR). Indeed, western blot analysis of the senescent LN229 and A172 cell populations revealed increased ATM and ATR phosphorylation, as well as CHK1 and CHK2 activation. Additionally, the p53 protein level was increased and p53 was phosphorylated at serine 15 and serine 46, indicating its activation. This was confirmed by the upregulation of p21, a downstream target of p53 (Figure 18). An active DDR indicates that DSBs in senescent cells can be repaired. By irradiating senescent cells and evaluating DSBs immediately after IR, 3 and 6 h later, we evaluated this hypothesis. A dosage of 6 Gy was sufficient to induce additional DSBs in senescent LN229 and A172 cells, as proven by neutral comet assay. A significant reduction was seen 3 h later. After an additional 3 h, the amount of DSBs returned to basic levels in both cell lines (Figure 19). These results clearly demonstrate that senescent cells are capable of DSBs repair.

In view of these findings, the question arises why senescent cell harbour persisting DSBs following TMZ treatment if they are capable of DNA repair. We previously demonstrated that O^6meG adducts are still present 24 h after treatment with TMZ (Stratenwerth et al. 2021). This indicates that in MGMT lacking cells, O^6meG lesions are not repaired and persist in senescent cells. We were therefore wondering if residual O^6meG adducts are the source of persisting DSBs, and if these had an impact on CSEN and cell death levels. In collaboration with Prof. Monica Hegi (Neuroscience Research Center and Neurosurgery, Lausanne University Hospital and University of Lausanne, Switzerland), we used an MGMT inducible cell line (LN229-MGMT^{ind}c12) to express MGMT at the desired timepoints to clarify these questions. Western blot analysis confirmed the stable induction of MGMT in proliferating and senescent cells following dox treatment. Comparison of tail intensities of senescent LN229-MGMT^{ind}c12 before and after dox treatment showed a significant reduction in the tail intensity following dox treatment (Figure 20). This data is based on one experiment and should be repeated to be confirmed. Still, the data indicate the DSBs repair upon MGMT expression. These results demonstrate that residual O^6meG adducts could be responsible for persisting DSBs in senescent cells. Interestingly, dox-mediated induction of MGMT expression in CSEN cells did not result in a reduction of the CSEN level. Although the amount of DSBs following dox-treatment was significantly lower than before the expression of MGMT, it was significantly higher than in the proliferating control. The reduction in DSBs might not have been enough to reduce the CSEN level. It could also mean that persisting DSBs and the resulting constantly active DDR are not required to maintain the senescent state. To clarify this question, we analysed the necessity of the DDR players in maintaining the senescent state.

5.4. An active DNA damage response is necessary to maintain senescence

The ATM/ATR-CHK1/CHK2-p53 axis has been shown to be required for the induction of CSEN following TMZ treatment (Aasland et al. 2019a). To elucidate if this signalling axis also played a role in senescence maintenance, we inhibited either one of the players involved in this pathway, namely ATM, ATR, CHK1, CHK2, p53 and p21 in senescent LN229 cells (chapter 4.3.2). Quantification of CSEN and cell death levels before and 2 d after inhibition were compared. It was taken care to use the inhibitors in concentrations that were non-toxic on proliferating cells. Inhibition of ATM or ATR led to a significant reduction in CSEN levels, which was joined by an increase in cell death levels. The results were confirmed in A172 cells. Next, we inhibited CHK1 and CHK2, as well as p53 and p21 in senescent LN229 cells. No reduction in CSEN levels was observed by either one, although cell death levels increased significantly upon CHK1, p53 and p21 inhibition. The reduction of CSEN upon ATM and ATR inhibition is in line with the activation of ATM and ATR following TMZ treatment. This concurs with the persisting DSBs and the hypothesis that sustained activation of the DDR is necessary to maintain the senescent state. The same results have been observed in HeLa cells, where substantial cell death was induced by ATM inhibition in senescent cells (Nair et al. 2015). Also, a screening study for kinase inhibitors that ameliorate CSEN also identified ATM inhibition to be sufficient to reduce CSEN levels in replicative, as well as genotoxic stress induced senescent human fibroblasts (Kang et al. 2017). Obviously, ATM and ATR are essential for senescence maintenance. How they participate in senescence maintenance remains unclear. It has been demonstrated that persistent ATM signalling is required to provoke the senescence-associated secretory phenotype (SAPS) (Rodier et al. 2009). Since senescent cells secrete the SAS-proteins, which has been shown to re-enforce CSEN, a reduced SASP could lead to reduced CSEN (Faget et al. 2019). During induction of senescence, ATM and ATR activate downstream the CHK1 and CHK2-p53-p21 axis resulting in the G2/M arrest. We observed no reduction in CSEN upon inhibition of these downstream players. However, a significant increase in cell death levels was observed upon inhibition of CHK1, p53 and p21. This cannot result from cell death of remaining proliferating cells within the cell culture because concentrations non-toxic on proliferating cells were used. Also, senescence levels reach about 80 % after 8 d. The remaining proliferating cells are not enough to induce such a high increase in cell death. A possible explanation could be that dying senescent cells are still positively stained for SA-β-gal and AV or AV and PI. In this case, the ATM/ATR-CHK1-p53-p21 axis would be involved in senescence maintenance. An additional experiment, measuring the oxylipin dihomo-15d-prostaglandin J2 as marker for senescent cell death should be performed to prove this theory (Wiley et al. 2021).

An alternative explanation for the missing reduction in CSEN following inhibition of CHK1 and CHK2 are the overlapping downstream pathways of these proteins. Both, CHK1 and CHK2 can phosphorylate p53 at serine 15, and both can directly act on CDC25c. Inhibition of either one might not be sufficient to see an effect because either one could compensate the inhibition of the other one. This would also explain the lack of CSEN reduction upon p53 or p21 inhibition, since CHK1 or CHK2 could directly act on CDC25c. Also, Wee1 could be involved, which has been shown to induce G2/M arrests in GBM through inactivation of the CDK1/cyclin B complex via CHK1 activation (O'Connell 1997).

Another pathway involved in the induction of senescence independent of the CHK1/2-p53-p21 axis is the ATM-p62-NF-kB pathway. It has been demonstrated in human fibroblasts that upon DNA damage, ATM blocks p62 dependent specific degradation of GATA4. The stabilized GATA4 activates NF-kB leading to senescence (Kang et al. 2015). Additionally, NF-kB has previously been shown to be essential for senescence induction (Aasland et al. 2019a). Inhibition of NF-kB in senescent GBM cells led to a significant induction of cell death, although no reduction in CSEN levels was observed. Again, this increase in cell death cannot be explained by cell death of remaining proliferating cells within the cell culture, but rather through cell death of senescent cells that still stain positively for SA-β-gal. Like the inhibition of CHK1, p53 and p21, an additional experiment, measuring the oxylipin dihomo-15d-prostaglandin J2 as marker for senescent cell death should clarify this question.

5.5. Senescence is maintained by inhibition of the intrinsic apoptotic pathway

Apoptosis and senescence are not only regulated by the DDR, but also through the mitochondrial pathway, involving the Bcl-2 family proteins. It has been proposed that the ration of the anti-apoptotic Bcl-2 and the pro-apoptotic Bax proteins is important in the regulation of apoptosis; if the ratio is towards Bax, apoptosis is induced (Das et al. 2004; Ma et al. 2002). Thus, upregulation of Bcl-2 is expected in case of maintenance of the senescence state. To verify if this is true in our cell system, we measured the Bcl-2 level in senescent LN229 and A172 cells. Interestingly, the senescent LN229 and A172 cells expressed different Bcl-2 protein patterns. In the LN229 cells, the Bcl-2 protein expression was indeed enhanced. Contrary, in A172 cells, Bcl-2 expression was reduced (Figure 18). A recent study demonstrated, that not only the Bcl-2:Bax ratio, but also the Mcl-1:Bak ratio is important to determine the cell fate by apoptosis (Gratas et al. 2014b). It might be that in A172 cells, not Bcl-2 but Mcl-1 is upregulated to prevent apoptosis.

Further analysis should be performed to check this possibility. To evaluate the role of Bcl-2 in the maintenance of GBM senescence, we treated senescent LN229 cells with ABT-737 and ABT-263 (navitoclax). Both are potent inhibitors for Bcl-2 and Bcl-X_L (Zhu et al. 2016). Upon treatment with either inhibitor, a significant reduction in CSEN was observed, concomitantly with a significant increase in cell death. These results were confirmed in A172 cells, although these cells did not express an increased Bcl-2 protein level (Figure 23 and Figure 24). They did, however express an increased amount of the Bcl-X_L protein compared to the proliferating control. Since both, ABT-737 and ABT-263 inhibit not only Bcl-2 but also Bcl-X_L, it is reasonable to assume that in LN229 cells, senescence is maintained by Bcl-2 upregulation, while in A172 senescence maintenance is regulated via Bcl-X_L upregulation. It is important to note that upon navitoclax treatment of senescent A172 cells, only a slight reduction in CSEN was observed, although cell death levels increased significantly. This supports the hypothesis, that apoptotic senescent cells still stain positive for SA-β-gal, and thus the reduction in senescence observed upon treatment of senescent cells with senolytic agents might not reflect the amount of dying senescent cells.

Another way to inhibit apoptosis is via cIAP and XIAP that directly inhibit the executioners of apoptosis; the caspases (Vanlangenakker et al. 2011; Varfolomeev et al. 2009). Inhibition of these proteins by BV-6 treatment in senescent LN229 cells led to a significant reduction in SCEN, while cell death levels increased significantly. The same was shown in A172 cells (Figure 25). Overall, it can be concluded that CSEN maintenance in GBM following TMZ treatment is regulated via the Bcl-2 and IAP proteins as well as some of the DDR proteins, as mentioned before.

5.6. Autophagy is essential for senescence maintenance

Senescent cells, even though they are not proliferating, still have an active metabolism as demonstrated by viability assays. This includes the repair of DNA damage, as proven by neutral comet assay analysis following IR of senescent cells (Figure 19). Autophagy is a mechanism to control cellular homeostasis and supports cell survival by eliminating dysfunctional organelles and turnover DNA damage repair proteins (Zhang et al. 2015; Katayama et al. 2007). Additionally, autophagy has previously been demonstrated to be essential for senescence induction and was shown to abrogate CSEN in human fibroblasts (Knizhnik et al. 2013; L'Hôte et al. 2021). We therefore assumed that autophagy also plays a crucial role in senescence maintenance. Indeed, inhibition of autophagy in senescent LN229 cells resulted in a shift from CSEN toward cell death. This was seen by inhibition of the late stages of autophagy through inhibition of the autophagosome and the lysosome fusion via clq as well as blocking the autophagosome formation by 3-meA. Of note, a greater effect was seen following clq treatment. Interestingly, these effects were not seen in A172 cells (Figure 31).

An explanation could be provided by the genetic differences between LN229 and A172 cells that regulate CSEN. LN229 cells lack p16 and p14, while A172 cells express these proteins. Additionally, LN229 cells are PTEN competent, while A172 cells are PTEN deleted.

The finding that senescent LN229, but not A172 cells are pushed into cell death following clq treatment indicates that the response might depend on PTEN, which has been linked to autophagy regulation in glioma cells (Errafiy et al. 2013). This example shows that the regulation of senescence maintenance is complex and depends on the genetic constitution of the cells in question. Nevertheless, autophagy has been identified as a senescence maintaining pathway.

When high levels of ROS are present in the cell, autophagy can be induced through the PI3K pathway, leading to the induction of CSEN (Kma and Baruah 2022; Gao 2019). TMZ-induced senescent LN229 and A172 cells displayed high levels of ROS, as revealed by DCFDA measurements. Therefore, we hypothesised that this pathway participates in maintaining the senescent state of GBM cells. Treatment of senescent LN229 cells with the PI3K inhibitor PX-866 did indeed reduce the CSEN level, while cell death was increased concomitantly. This effect, however, seems to be cell line specific as it was not seen in A172 cells (Figure 32). The differences between the two cell lines might result from different genetic backgrounds playing a role in autophagy regulation.

5.7. Senescent cells require DSBs repair

Following TMZ treatment, LN229 and A172 cells showed accumulation of DSBs (Figure 16). However, a decline in the level of DSBs that were induced by IR indicated that CSEN GBM cells are capable of DSBs repair (Figure 19). TMZ-induced senescent cells are arrested in the G2/M phase. During this cell cycle phase, HR repair is active, in which Rad51 plays a crucial role (Budke et al. 2012). Another protein involved in different DNA repair pathways, including NER, NHEJ, HR and MMR is PARP1 (Pascal 2018). It has been demonstrated that senescent cells eventually re-enter the cell cycle (Saleh et al. 2019; Olszewska et al. 2021; Le Duff et al. 2018). To see if active DNA repair is necessary to maintain senescence until the DNA is repaired, and cells can re-enter the cell cycle, we inhibited the HR protein Rad51 as well as PARP1 in senescent LN229 and A172 cells (chapter 4.3.2). Again, huge differences were observed between the cell lines. LN229 cells displayed significant increase in cell death following Rad51 inhibition which was not observed in A172 cells. Contrary, a significant increase was observed in A172 cells upon PARP inhibition, which was not seen in LN229 cells. Neither cell line showed a reduction in CSEN levels upon Rad51 or PARP inhibition. The same explanation applies as for the missing reduction in CSEN that was seen before. Studies conducted in mice models showed great response to PARP inhibition combined with TMZ treatment, especially if they were PTEN deficient (Lin et al. 2014).

Our results demonstrated an induction of cell death in the PTEN deleted A172 cells line, while no such effect was seen in the PTEN competent LN229 cell lines, which is in line with this study.

DSBs induced by TMZ in the low-dose range < 100 µM are due to the DNA adduct O^6meG. Our data indicated that repair of this lesion in senescent cells leads to a reduction of DSBs, which does not seem to result in abrogation of senescence. We were now wondering how long O^6meG mediated DSBs must persist to induce CSEN and cell death. To this end, we treated LN229-$MGMT^{ind}$-c12 cells with TMZ and activated MGMT expression in 24 h intervals for a total period of 5 d to measure cell death and for 8 d to measure CSEN (chapter 4.3.3). If MGMT was expressed, and thus O^6meG repaired, within the first 3 d following TMZ treatment, a significant reduction in cell death and CSEN levels was observed. Expression of MGMT thereafter had no significant effect on these cellular responses. These results fit the hypothesis that DSBs following TMZ are induced through futile MMR cycle and that O^6meG needs 2 cell cycle to be converted into DSBs. They also underline the results obtained by expression of MGMT in senescent cells, where repair of O^6meG led to reduced DSBs but not CSEN. Taken together, these results show that once CSEN or cell death is induced, repair of DSBs does not necessarily lead to an abrogation of the senescent state.

5.8. Timing is key in combinatorial treatment with TMZ and IR or CCNU

Besides inhibition of senescence maintaining pathways, additional damage to the cell might result in higher cell death levels. The current treatment schedule for GBM rests on TMZ concomitantly with fractionated IR. Each fraction has a dose of 2 Gy (Bolcaen et al. 2017). Here, we treated senescent LN229 cells with increasing dose of IR, including 2, 5 and 10 Gy. An increase in cell death levels was only observed upon high radiation doses, which are not used within the patient (Figure 34). Treatment of senescent cells with 2 Gy did not result in increased cell death levels (Figure 35). We demonstrated earlier that DSBs induced by IR in senescent LN229 and A172 cells are being repaired within 6 h. Additional inhibition of repair pathways in combination with IR of senescent glioma cells might therefore be beneficial. Since an increase of DNA damage in senescent cells did not lead to an increase in cell death, we were wondering, if an effect could be reached when IR induced DSBs were induced simultaneously with TMZ treatment. We demonstrated previously that O^6meG adducts are generated within 3 h following addition of TMZ to the cell culture medium (Stratenwerth et al. 2021). Therefore, we irradiated TMZ treated cells with 6 Gy 3 h following treatment to investigate if the additional DNA damage would cause additional cell death. Since senescence is the main trait induced by TMZ, we also measured CSEN levels (chapter 4.4.1).

Sole TMZ (20 µM) and sole IR (6 Gy) reached about 20 % and 15 % cell death, and 35 % and 25 % CSEN levels, respectively. TMZ pre-treatment of irradiated cells increased cell death levels to 32 %, and CSEN to 44 %.

We further analysed the effect of IR before the treatment with TMZ. The results were like pre-treatment of IR cells with TMZ. Combined treatment resulted in 31 % cell death and in 45 % CSEN. For cell death, these results are slightly lower as expected when sole TMZ and sole IR data are added (20 % from TMZ + 15 % from IR = 35 % combined calculated cell death vs. 32 % and 31 % combined measured cell death). Contrary, the results for CSEN were much lower than expected from addition of sole TMZ and sole IR values (35 % from TMZ + 25 % from IR = 60 % combined calculated CSEN vs. 44 % and 45 % combined measured CSEN). Given the fact that TMZ exerts its cytotoxic effects through MMR in proliferating cells, and IR induces cell cycle arrests, it is reasonable to assume that the reduced CSEN levels following combined treatment of TMZ and IR results from inhibition of TMZ-induced cytotoxicity.

A second approach to induce more damage in senescent GBM cells was treatment with the chloroethylating agent CCNU. This alkylating drug is currently used as alternative treatment option to TMZ and has been shown to have a beneficial effect on the median OS of GBM patients when combined with TMZ (Herrlinger et al. 2019; Nikolova et al. 2017). CCNU induces its cytotoxicity through crosslinking the DNA at the N1 position of guanine with the N3 position of cytosine at the complementary DNA strand. These ICLs block DNA replication and transcription, subsequently inducing the DDR and cell death pathways. Replication dependent repair of ICLs dependents on template DNA and is thus mainly performed during S-phase. Following TMZ treatment GBM cells are arrested in G2/M. Therefore, replication dependent repair of ICLs is not possible in this cell cycle stage. Thus, the additional DNA damage as well as blocking of DNA transcription might lead to abrogation of senescence. Treatment of senescent LN229 and A172 cells with CCNU did not results in reduced CSEN levels and cell death levels were not increased. Hence, the addition of CCNU after TMZ treatment is not suitable to reduce the CSEN level in GBM.

5.9. Can methadone be used as adjuvant for TMZ treatment?

Another compound that has been shown to exhibit beneficial effects in combinatorial treatment of GBM is MTD. Being a MOR agonist, it has been used for heroin substitution and pain medication, until studies demonstrated a sensitizing effect of MTD towards doxorubicin in leukaemia and GBM cells (Kua et al. 2019; Friesen et al. 2013). The effect of MTD was proposed to depend on the opioid receptor level that, in this case, regulates the influx and efflux of doxorubicin (Friesen et al. 2014). Based on these results a clinical trial was conducted that combined

TMZ and MTD in glioma treatment. Although the study included only 27 patients and conclusions drawn are rather preliminary, the results indicate that MTD is safe to be combined with TMZ (Onken et al. 2017). Here, we assessed the geno- and cytotoxicity of MTD alone and in combination with TMZ (chapter 4.4.4). We observed an induction of cell death at concentrations >20 µg/ml MTD for LN229 and VH10T cells, while the A172 cell line was more sensitive. However, contrary to the results obtained in leukaemia cells, the expression level of MOR in those cells did not correlate with the sensitivity of the cells towards MTD treatment (Friesen et al. 2013). Pre-treatment of the cells with naloxone, an antagonist of MOR did not result in reduced cell death levels, proving that MTD-induced cell death in GBM cell is not mediated though MOR-triggered pathways.

Previous studies demonstrated a sensitizing effect of MTD towards doxorubicin treatment of GBM cells (Friesen et al. 2014). Since TMZ, not doxorubicin, is the main chemotherapeutic used for GBM treatment, we were wondering whether the same is true for TMZ. Thus, in two experimental setups, we firstly pre-treated LN229 and A172 cells with non-toxic concentrations of MTD and subsequently with TMZ and measured cell death levels 5 d later. Secondly, we pre-treated with TMZ and subsequently with non-toxic concentrations of MTD and measured cell death levels 3 d later. The first experimental setup aimed to determine if MTD had a sensitizing effect on GBM cells towards TMZ. The second experiment was performed to elucidate the effect of TMZ on MTD induced cell death. Neither experiment showed an increase in cell death. When cells were pre-treated with toxic concentrations of MTD, TMZ treatment even resulted in less cell death than TMZ treatment alone. These data suggests that the pathways triggered by MTD and TMZ to induce cell death are not converging and involve different mechanisms.

Our previous experiments demonstrated that following TMZ treatment CSEN is the main trait induced (chapter 4.1.2). Since pre-treatment of LN29 and A172 cells with cytotoxic concentrations of MTD led to a decrease in TMZ-induced cell death, thus a benefit in cell survival, we were interested in the effect of MTD on the TMZ-induced cell survival pathway senescence. No increase in CSEN was observed upon concomitant treatment, which supports the notion that the signalling pathways triggered by MTD and TMZ are essentially different.

Since MTD induces cell death, we analysed its genotoxicity. Quantification of DSBs following MTD treatment did not indicate a genotoxic effect even at cytotoxic concentrations. We demonstrated that TMZ-induced DSBs. To see if MTD would interfere with these, we measured DSBs following combination treatment of MTD and TMZ. Even at cytotoxic concentrations MTD treatment did not increase TMZ-induced DSBs. The concentrations shown to be cytotoxic in our cell system (<20 µg/mL) are well above the concentrations reached within the patient (0.3-1.3 µg/mL) (Inturrisi and Verebely 1972; Volavka et al. 1978).

Since no cytotoxic or genotoxic effects were observed upon combination treatment <20 µg/mL, MTD can be considered safe to be used for pain relief in GBM patients treated with TMZ. As monotherapy or adjuvant for TMZ treatment in GBM, however, MTD does not seem to be beneficial.

5.10. Possible senolytic activity of curcumin

In Chinese traditional medicine, natural compounds are commonly used for treatment of all sorts of diseases. One of these compounds is the naturally occurring polyphenol curcumin. Several studies provided evidence for its beneficial role in cancer treatment, including glioma, leukaemia and colorectal cancer when combined with chemotherapy or administered alone (Fratantonio et al. 2019; He et al. 2020; Kuo et al. 1996; Pricci et al. 2020; Sminia et al. 2021). Here, we evaluated the effect of native curcumin dissolved in ethanol (Cur-E) and micellar curcumin (Cur-M) on GBM and human fibroblast cells (chapter 4.5.3). In dose-response experiments DSBs and cell death levels were measured 1 h, 1 d and 2 d following curcumin administration, respectively. Quantification of DSBs showed an early induction after 1 h of treatment starting at 10 µM. The same was found 24 h following treatment. In line with this, cell death increased at concentrations > 10 µM. These results are in line with the beforementioned reports where curcumin induced apoptosis in various cell lines at concentrations >10 µM within 48 h (Kuo et al. 1996; Anto et al. 2002; Kizhakkayil et al. 2010; Fratantonio et al. 2019). in these experiments, curcumin was administered constantly. Pharmacokinetic studies demonstrated a short half-life of curcumin; In rats, the measured plasma half-life of curcumin was about 30 min, while in human blood, the half-live was about 8 h (Gutierres et al. 2015; Wang et al. 1997). Thus, we repeated the experiments with short-time treatments. When cells were exposed to curcumin for 1 h, DSBs were induced immediately, but were repaired within 4 h. Cells exposed to curcumin for 1 h did not show increased cell death levels. Hence, curcumin is genotoxic, but needs to be administered permanently to harbour cytotoxic effects.

The molecular targets of curcumin include NF-kB, p53, PI3K, NRF2, Bcl-2 and Bcl-X_L (Shehzad et al. 2010; Kasi et al. 2016). We previously demonstrated that GBM activates pathways involving these molecules. Also, ROS levels increase following TMZ treatment, thus NRF2 might be involved. We were therefore interested on the effect of curcumin on senescent GBM cells. The colorimetric evaluation of cell viability via the MTT assay clearly demonstrated a protective effect of senescence against curcumin induced cytotoxicity: while the cell viability of proliferating GBM cell decreased starting from 10 µM curcumin, senescent cells were unaffected even at concentrations of 40 µM. These results were confirmed by CSEN and cell death measurements following treatment of senescent GBM cells with curcumin.

While proliferating cells showed a slight increase in cell death following curcumin treatment, senescent cells showed a slight decrease in cell death, while CSEN increased.

The increase in cell death is in line with previous experiments, where curcumin induced G2 arrests and senescence in cervical cancer and vascular smooth muscle cells (Wang et al. 2020; Grabowska et al. 2019). The protective effect of CSEN against the cytotoxic effects of curcumin might lie within the cell cycle arrest of CSEN cells. Curcumin induces its cytotoxicity through the induction of DSBs. Since CSEN are already arrested in G2/M and inhibit apoptosis induction the additional repairable DSBs is marginal.

The concentrations shown to be geno- and cytotoxic *in vitro* (>10 µM) are well below the serum levels that are reached in humans (native curcumin reached up to 1.8 µM upon 8 g of a single oral dosage, micellized curcumin reached 3.2 µM upon 500 mg single oral dosage (Liu et al. 2016; Schiborr et al. 2014)). Also, the genotoxic effects of curcumin were transient, since DSBs were repaired within a few hours. Thus, native curcumin, as well as micellized curcumin, can be considered a safe food supplement, when used in those concentrations. For GBM treatment, however, clinical trials are required.

5.11. MCOPPB is not senolytic in GBM cells

A recent screening study performed by Manlio Vinciguerra's group identified MCOPPB, a compound originally studied for its potential anxiolytic activity, as a senolytic agent in human fibroblasts (Raffaele et al. 2022). We were interested if the compound also has senolytic activity in glioma cells *in vitro*. Treatment of senescent LN229 and A172 cells with 1 µM MCOPPB resulted in only a very mild reduction of senescence and no increase in apoptosis. Therefore, MCOPPB seems to act cell type specific and cannot be considered senolytic, at least under the treatment conditions in LN229 and A172 glioma cells.

5.12. Artesunate and fisetin are novel senolytic agents in GBM cells

Lately, scientific research is increasing the focus on natural compounds for their anti-cancer and health improving properties. Several natural compounds were shown to have anti-angiogenic and anti-metastatic effects, and induce apoptosis in cancer cells (Muthu K. Shanmugam et al.; Chanvorachote et al. 2016; Yu et al. 2020). Some natural compounds were also shown to eliminate senescent cells *in vitro* and *in vivo*, thereby increasing health and lifespan (Li et al. 2019b). The natural compound fisetin and the semisynthetic compound artesunate are two of them.

Fisetin has been found to be cytotoxic in several types of cancer, including neuroblastoma and glioma (Kadari et al. 2017; Renault-Mahieux et al. 2021). It was also shown to reduce age related senescent cells *in vitro* and *in vivo* (Yousefzadeh et al. 2018). Artesunate has a long tradition in Chinese medicine for treatment of malaria (Kong and Tan 2015). Nowadays its applications exceed the treatment of malaria and studies for its usage in treatment of cancer are performed. Several reports indicate a beneficial role of artesunate in the treatment of e.g., colon cancer and hepatocellular carcinoma (Li et al. 2021; Jiang et al. 2018). It has previously been shown that artesunate inhibits HR in glioma cells and is thus beneficial for the treatment of glioma when combined with TMZ (Berte et al. 2016). To our best knowledge, fisetin and artesunate have not yet been evaluated for their senolytic activity in glioma cells. To provide an answer to this question we treated CSEN GBM cells with fisetin or artesunate (chapter 4.5). A significant reduction in the senescence levels parallel to an increase in apoptosis was observed upon treatment of LN229 cells with either fisetin or artesunate. Interestingly, in A172 cells only a slight reduction in CSEN was observed upon fisetin treatment and none upon treatment with artesunate. However, artesunate increased cell death levels significantly. As explained before, the increase in cell death cannot result from death of residual proliferating cells in the senescent cell population. The same concentrations used on proliferating glioma cells had no toxic effect. Fisetin and artesunate are therefore potent senolytic agents in glioma cells, although, the effect of fisetin seems to be cell type specific. This is in line with reporting that that fisetin had no impact on the CSEN level in an IR-induced senescent IMR90 cell system (Zhu et al. 2017).

Since artesunate is being used for the treatment of malaria and is considered a safe drug, artesunate should be considered for its application in the adjuvant treatment of glioblastoma. Contrary, fisetin is not used routinely in medicine. It was tested positive in the Aims test using the TA102 and the TA98 strains, detecting oxidative mutagens and frameshifts (Resende et al. 2012; Hardigree and Epler 1978; Levin et al. 1982). Also, induction of chromosomal male-segregation and formation of micronuclei upon treatment of human lymphoblastoid and human myeloid cells at concentrations between 9 -17 µM fisetin could be observed (Olaharski et al. 2005). This is lower than the concentrations used to induce a senolytic effect in GBM in our study. Before fisetin is considered as adjuvant for TMZ treatment, it should be tested if the geno- and cytotoxicity of fisetin observed in cancer cells also effects healthy tissue and if so, if repair mechanisms are present to protect the healthy tissue.

6. Conclusions

Our study provides insights into the cellular responses upon TMZ treatment. An in-depth analysis of the kinetic of DSBs upon MGMT induction demonstrated that O^6meG induced DSBs are responsible for cell death and CSEN induced by TMZ. Cell death and CSEN were induced simultaneously and had the same kinetics as the induction of DSBs. Importantly, CSEN was the main trait induced by TMZ, reaching 4-fold higher levels than cell death. Analysis of the long-term (> 8 d) TMZ treated population confirmed the high number of senescent cells, evident by high SA-β-gal levels, persistent DSBs, induction of p21 and methylated H3K27. Consequently, a high number of senescent cells is expected in the recurrent tumour. Indeed, comparison of matched primary and recurrent tumours revealed significantly more DSBs and tri-methylated H3K27 cells in the recurrent tumour, while apoptotic cells were reduced. Certainly, these results need to be confirmed in a larger tumour panel and with additional senescence markers, such as SA-β-gal. But these results combined with the reports of senescent cells re-starting proliferation, and the high occurrence of recurrent tumours indicate that CSEN is an important cellular process following TMZ treatment *in vivo*. Consequently, a better understanding of CSEN and strategies to reduce the CSEN load by elimination is of essence. In the present work, we also identified pathways involved in senescence maintenance and inhibition of apoptosis, including the DDR, DNA repair, autophagy, and the mitochondrial pathway. These results demonstrate the complexity of CSEN maintenance. For elimination of CSEN cells, inhibition of autophagy through chloroquine proved most efficient. A great reduction in CSEN was also seen following treatment with ABT-737 and ABT-263 (navitoclax), BV6, PX-866, inhibition of ATM and ATR, as well as treatment with fisetin and artesunate. The senolytic activity of ABT-737, navitoclax and PX-866, as well as chloroquine and artesunate are of particular interest. ABT-737, navitoclax and PX-866 are already used in clinical trials, thus treatment is considered safe and their application for adjuvant TMZ treatment should be explored. The same holds true for chloroquine and artesunate, which are commonly used as safe treatment options against malaria. Although fisetin showed great senolytic activity in GBM, subsequent geno-and cytotoxicity testing should be performed since it was positive in the Aims test. Out data indicate that CCNU and IR are not senolytic.

We previously demonstrated that at concentrations >25 µM TMZ a saturation of cellular responses is reached. Also, 5x 5 µM TMZ treatment resulted in an additive effect of 1x 25 µM TMZ treatment. Thus, although concentrations higher to those achieved in patients were used, the results are applicable for the in vivo situation. In the therapeutic situation, TMZ is administered concurrently with IR, while we treated with TMZ alone. However, since IR also induces SCEN, the use of senolytic agents may give new treatment options for GBM patients and help to prevent recurrences.

7. Publication bibliography

Aasland, Dorthe; Götzinger, Laura; Hauck, Laura; Berte, Nancy; Meyer, Jessica; Effenberger, Melanie et al. (2019a): Temozolomide Induces Senescence and Repression of DNA Repair Pathways in Glioblastoma Cells via Activation of ATR-CHK1, p21, and NF-κB. In *Cancer Res* 79 (1), pp. 99–113. DOI: 10.1158/0008-5472.CAN-18-1733.

Aasland, Dorthe; Götzinger, Laura; Hauck, Laura; Berte, Nancy; Meyer, Jessica; Effenberger, Melanie et al. (2019b): Temozolomide Induces Senescence and Repression of DNA Repair Pathways in Glioblastoma Cells via Activation of ATR-CHK1, p21, and NF-κB. In *Cancer research* 79 (1), pp. 99–113. DOI: 10.1158/0008-5472.CAN-18-1733.

Aasland, Dorthe; Reich, Thomas R.; Tomicic, Maja T.; Switzeny, Olivier J.; Kaina, Bernd; Christmann, Markus (2018): Repair gene O6 -methylguanine-DNA methyltransferase is controlled by SP1 and up-regulated by glucocorticoids, but not by temozolomide and radiation. In *Journal of neurochemistry* 144 (2), pp. 139–151. DOI: 10.1111/jnc.14262.

Afroze, Nazia; Pramodh, Sreepoorna; Shafarin, Jasmin; Bajbouj, Khuloud; Hamad, Mawieh; Sundaram, Madhumitha Kedhari et al. (2022): Fisetin Deters Cell Proliferation, Induces Apoptosis, Alleviates Oxidative Stress and Inflammation in Human Cancer Cells, HeLa. In *International journal of molecular sciences* 23 (3). DOI: 10.3390/ijms23031707.

Allegra, Alessandro; Innao, Vanessa; Russo, Sabina; Gerace, Demetrio; Alonci, Andrea; Musolino, Caterina (2017): Anticancer Activity of Curcumin and Its Analogues: Preclinical and Clinical Studies. In *Cancer investigation* 35 (1), pp. 1–22. DOI: 10.1080/07357907.2016.1247166.

Allen Perkins; Gerald Liu (2016): Primary Brain Tumors in Adults: Diagnosis and Treatment. In *AFP* 93 (3), pp. 211–217. Available online at https://www.aafp.org/afp/2016/0201/p211.html.

Andersen, Zorana J.; Pedersen, Marie; Weinmayr, Gudrun; Stafoggia, Massimo; Galassi, Claudia; Jørgensen, Jeanette T. et al. (2018): Long-term exposure to ambient air pollution and incidence of brain tumor: the European Study of Cohorts for Air Pollution Effects (ESCAPE). In *Neuro-oncology* 20 (3), pp. 420–432. DOI: 10.1093/neuonc/nox163.

Anto, Ruby John; Mukhopadhyay, Asok; Denning, Kate; Aggarwal, Bharat B. (2002): Curcumin (diferuloylmethane) induces apoptosis through activation of caspase-8, BID cleavage and cytochrome c release: its suppression by ectopic expression of Bcl-2 and Bcl-xl. In *Carcinogenesis* 23 (1), pp. 143–150. DOI: 10.1093/carcin/23.1.143.

Arai, Y.; Watanabe, S.; Kimira, M.; Shimoi, K.; Mochizuki, R.; Kinae, N. (2000): Dietary intakes of flavonols, flavones and isoflavones by Japanese women and the inverse correlation between quercetin intake and plasma LDL cholesterol concentration. In *The Journal of nutrition* 130 (9), pp. 2243–2250. DOI: 10.1093/jn/130.9.2243.

Arnoult, Nausica; Karlseder, Jan (2015): Complex interactions between the DNA-damage response and mammalian telomeres. In *Nature structural & molecular biology* 22 (11), pp. 859–866. DOI: 10.1038/nsmb.3092.

Bak, Sara Thornby; Sakellariou, Despoina; Pena-Diaz, Javier (2014): The dual nature of mismatch repair as antimutator and mutator: for better or for worse. In *Frontiers in genetics* 5, p. 287. DOI: 10.3389/fgene.2014.00287.

Baker, Sharyn D.; Wirth, Mark; Statkevich, Paul; Reidenberg, Pascale; Alton, Kevin; Sartorius, Susan E. et al. (1999): Absorption, Metabolism, and Excretion of 14C-Temozolomide following Oral Administration to Patients with Advanced Cancer. In *Clin Cancer Res* 5 (2), pp. 309–317.

Barbagallo, Giuseppe M. V.; Jenkinson, Michael D.; Brodbelt, Andrew R. (2008): 'Recurrent' glioblastoma multiforme, when should we reoperate? In *British journal of neurosurgery* 22 (3), pp. 452–455. DOI: 10.1080/02688690802182256.

Batty, Kevin T.; Davis, Timothy M.E.; Le Thu, Thi Anh; Quang Binh, Tran; Kim Anh, Trinh; Ilett, Kenneth F. (1996): Selective high-performance liquid chromatographic determination of artesunate and α- and β-dihydroartemisinin in patients with falciparum malaria. In *Journal of Chromatography B: Biomedical Sciences and Applications* 677 (2), pp. 345–350. DOI: 10.1016/0378-4347(95)00428-9.

Beltzig, Lea; Stratenwerth, Björn; Kaina, Bernd (2021): Accumulation of Temozolomide-Induced Apoptosis, Senescence and DNA Damage by Metronomic Dose Schedule: A Proof-of-Principle Study with Glioblastoma Cells. In *Cancers* 13 (24). DOI: 10.3390/cancers13246287.

Beranek, David T. (1990): Distribution of methyl and ethyl adducts following alkylation with monofunctional alkylating agents. In *Mutation Research/Fundamental and Molecular Mechanisms of Mutagenesis* 231 (1), pp. 11–30. DOI: 10.1016/0027-5107(90)90173-2.

Berdelle, Nicole; Nikolova, Teodora; Quiros, Steve; Efferth, Thomas; Kaina, Bernd (2011): Artesunate induces oxidative DNA damage, sustained DNA double-strand breaks, and the ATM/ATR damage response in cancer cells. In *Mol Cancer Ther* 10 (12), pp. 2224–2233. DOI: 10.1158/1535-7163.MCT-11-0534.

Berte, Nancy; Lokan, Stefanie; Eich, Marcus; Kim, Ella; Kaina, Bernd (2016): Artesunate enhances the therapeutic response of glioma cells to temozolomide by inhibition of homologous recombination and senescence. In *Oncotarget* 7 (41), pp. 67235–67250. DOI: 10.18632/oncotarget.11972.

Bhat, Abid; Mahalakshmi, Arehally M.; Ray, Bipul; Tuladhar, Sunanda; Hediyal, Tousif A.; Manthiannem, Esther et al. (2019): Benefits of curcumin in brain disorders. In *BioFactors (Oxford, England)* 45 (5), pp. 666–689. DOI: 10.1002/biof.1533.

Black, P. M.; Alexander, E.; Martin, C.; Moriarty, T.; Nabavi, A.; Wong, T. Z. et al. (1999): Craniotomy for tumor treatment in an intraoperative magnetic resonance imaging unit. In *Neurosurgery* 45 (3), 423-31; discussion 431-3. DOI: 10.1097/00006123-199909000-00001.

Bolcaen, Julie; Acou, Marjan; Descamps, Benedicte; Kersemans, Ken; Deblaere, Karel; Vanhove, Christian; Goethals, Ingeborg (2017): Glioblastoma. PET for Therapy Response Assessment in Glioblastoma. Edited by Steven de Vleeschouwer. Brisbane (AU).

Bowles, Daniel W.; Kochenderfer, Mark; Cohn, Allen; Sideris, Lucas; Nguyen, Nghia; Cline-Burkhardt, Vivian et al. (2016): A Randomized, Phase II Trial of Cetuximab With or Without PX-866, an Irreversible Oral Phosphatidylinositol 3-Kinase Inhibitor, in Patients With Metastatic Colorectal Carcinoma. In *Clinical colorectal cancer* 15 (4), 337-344.e2. DOI: 10.1016/j.clcc.2016.03.004.

Bradford, Marion M. (1976): A rapid and sensitive method for the quantitation of microgram quantities of protein utilizing the principle of protein-dye binding. In *Analytical Biochemistry* 72 (1-2), pp. 248–254. DOI: 10.1016/0003-2697(76)90527-3.

Brain Tumors - Classifications, Symptoms, Diagnosis and Treatments (2021). Available online at https://www.aans.org/Patients/Neurosurgical-Conditions-and-Treatments/Brain-Tumors, updated on 10/4/2021, checked on 10/4/2021.

Brain tumour risk in relation to mobile telephone use: results of the INTERPHONE international case-control study (2010). In *International journal of epidemiology* 39 (3), pp. 675–694.

Brain tumours | Cancer Research UK (2021). Available online at https://www.cancerresearchuk.org/about-cancer/brain-tumours, updated on 10/4/2021, checked on 10/4/2021.

Brandes, Alba A.; Franceschi, Enrico; Tosoni, Alicia; Bartolini, Stefania; Bacci, Antonella; Agati, Raffaele et al. (2010): O(6)-methylguanine DNA-methyltransferase methylation status can change

between first surgery for newly diagnosed glioblastoma and second surgery for recurrence: clinical implications. In *Neuro-oncology* 12 (3), pp. 283–288. DOI: 10.1093/neuonc/nop050.

Brawanski, Konstantin; Brockhoff, Gero; Hau, Peter; Vollmann-Zwerenz, Arabel; Freyschlag, Christian; Lohmeier, Annette et al. (2018): Efficacy of D,L-methadone in the treatment of glioblastoma in vitro. In *CNS oncology* 7 (3), CNS18. DOI: 10.2217/cns-2018-0006.

Brejchova, Jana; Holan, Vladimir; Svoboda, Petr (2020): Expression of Opioid Receptors in Cells of the Immune System. In *International journal of molecular sciences* 22 (1). DOI: 10.3390/ijms22010315.

Brito, Cheila; Azevedo, Ana; Esteves, Susana; Marques, Ana Rita; Martins, Carmo; Costa, Ilda et al. (2019): Clinical insights gained by refining the 2016 WHO classification of diffuse gliomas with: EGFR amplification, TERT mutations, PTEN deletion and MGMT methylation. In *BMC cancer* 19 (1), p. 968. DOI: 10.1186/s12885-019-6177-0.

Budke, Brian; Logan, Hillary L.; Kalin, Jay H.; Zelivianskaia, Anna S.; Cameron McGuire, William; Miller, Luke L. et al. (2012): RI-1: a chemical inhibitor of RAD51 that disrupts homologous recombination in human cells. In *Nucleic acids research* 40 (15), pp. 7347–7357. DOI: 10.1093/nar/gks353.

Burn, Sally F. (2012): Detection of β-Galactosidase Activity: X-gal Staining. In Odyssé Michos (Ed.): Kidney development. Methods and protocols / edited by Odyssé Michos. New York: Humana Press (Springer protocols, 886), pp. 241–250.

Cahill, Jennifer; LoBiondo-Wood, Geri; Bergstrom, Nancy; Armstrong, Terri (2012): Brain tumor symptoms as antecedents to uncertainty: an integrative review. In *Journal of nursing scholarship : an official publication of Sigma Theta Tau International Honor Society of Nursing* 44 (2), pp. 145–155. DOI: 10.1111/j.1547-5069.2012.01445.x.

Carles, Camille; Bouvier, Ghislaine; Esquirol, Yolande; Piel, Clément; Migault, Lucile; Pouchieu, Camille et al. (2017): Residential proximity to agricultural land and risk of brain tumor in the general population. In *Environmental research* 159, pp. 321–330. DOI: 10.1016/j.envres.2017.08.025.

Catarina Fernandes; Andreia Costa; Lígia Osório; Rita Costa Lago; Paulo Linhares; Bruno Carvalho; Cláudia Caeiro (2017): Current Standards of Care in Glioblastoma Therapy. In Catarina Fernandes, Andreia Costa, Lígia Osório, Rita Costa Lago, Paulo Linhares, Bruno Carvalho, Cláudia Caeiro (Eds.): Glioblastoma [Internet]: Codon Publications. Available online at https://www.ncbi.nlm.nih.gov/books/NBK469987/.

Chanvorachote, Pithi; Chamni, Supakarn; Ninsontia, Chuanpit; Phiboonchaiyanan, Preeyaporn Plaimee (2016): Potential Anti-metastasis Natural Compounds for Lung Cancer. In *Anticancer research* 36 (11), pp. 5707–5717. DOI: 10.21873/anticanres.11154.

Chen, D. T.; Pan, J. H.; Chen, Y. H.; Xing, W.; Yan, Y.; Yuan, Y. F.; Zeng, W. A. (2019): The mu-opioid receptor is a molecular marker for poor prognosis in hepatocellular carcinoma and represents a potential therapeutic target. In *British journal of anaesthesia* 122 (6), e157-e167. DOI: 10.1016/j.bja.2018.09.030.

Choi, Jae Yeon; Shin, Hyun Jin; Bae, In Hwa (2018): miR-93-5p suppresses cellular senescence by directly targeting Bcl-w and p21. In *Biochemical and biophysical research communications* 505 (4), pp. 1134–1140. DOI: 10.1016/j.bbrc.2018.10.010.

Christmann, Markus; Nagel, Georg; Horn, Sigrid; Krahn, Ulrike; Wiewrodt, Dorothee; Sommer, Clemens; Kaina, Bernd (2010): MGMT activity, promoter methylation and immunohistochemistry of pretreatment and recurrent malignant gliomas: a comparative study on astrocytoma and glioblastoma. In *Int. J. Cancer* 127 (9), pp. 2106–2118. DOI: 10.1002/ijc.25229.

Christmann, Markus; Tomicic, Maja T.; Kaina, Bernd (2002): Phosphorylation of mismatch repair proteins MSH2 and MSH6 affecting MutSalpha mismatch-binding activity. In *Nucleic acids research* 30 (9), pp. 1959–1966.

Christmann, Markus; Tomicic, Maja T.; Roos, Wynand P.; Kaina, Bernd (2003): Mechanisms of human DNA repair: an update. In *Toxicology* 193 (1-2), pp. 3–34. DOI: 10.1016/S0300-483X(03)00287-7.

Christmann, Markus; Verbeek, Barbara; Roos, Wynand P.; Kaina, Bernd (2011): O(6)-Methylguanine-DNA methyltransferase (MGMT) in normal tissues and tumors: enzyme activity, promoter methylation and immunohistochemistry. In *Biochimica et biophysica acta* 1816 (2), pp. 179–190. DOI: 10.1016/j.bbcan.2011.06.002.

Clark, A. S.; Deans, B.; Stevens, M. F.; Tisdale, M. J.; Wheelhouse, R. T.; Denny, B. J.; Hartley, J. A. (1995): Antitumor imidazotetrazines. 32. Synthesis of novel imidazotetrazinones and related bicyclic heterocycles to probe the mode of action of the antitumor drug temozolomide. In *Journal of medicinal chemistry* 38 (9), pp. 1493–1504. DOI: 10.1021/jm00009a010.

Collins, Andrew R.; Dobson, Victoria L.; Dušinská, Mária; Kennedy, Gayle; Štětina, Rudolf (1997): The comet assay: what can it really tell us? In *Mutation Research/Fundamental and Molecular Mechanisms of Mutagenesis* 375 (2), pp. 183–193. DOI: 10.1016/S0027-5107(97)00013-4.

Conklin, Kenneth A. (2004): Chemotherapy-associated oxidative stress: impact on chemotherapeutic effectiveness. In *Integrative cancer therapies* 3 (4), pp. 294–300. DOI: 10.1177/1534735404270335.

Coulter, Richard; Blandino, Maureen; Tomlinson, Jessica M.; Pauly, Gary T.; Krajewska, Magdalena; Moschel, Robert C. et al. (2007): Differences in the rate of repair of O6-alkylguanines in different sequence contexts by O6-alkylguanine-DNA alkyltransferase. In *Chemical research in toxicology* 20 (12), pp. 1966–1971. DOI: 10.1021/tx700271j.

Damarla, Sreenivasa Rao; Komma, Rajesh; Bhatnagar, Upendra; Rajesh, Navin; Mulla, Sadik Mohmad Abdulhamid (2018): An Evaluation of the Genotoxicity and Subchronic Oral Toxicity of Synthetic Curcumin. In *Journal of toxicology* 2018, p. 6872753. DOI: 10.1155/2018/6872753.

Das, Arabinda; Banik, Naren L.; Patel, Sunil J.; Ray, Swapan K. (2004): Dexamethasone protected human glioblastoma U87MG cells from temozolomide induced apoptosis by maintaining Bax:Bcl-2 ratio and preventing proteolytic activities. In *Molecular cancer* 3 (1), p. 36. DOI: 10.1186/1476-4598-3-36.

D'Atri, S.; Tentori, L.; Lacal, P. M.; Graziani, G.; Pagani, E.; Benincasa, E. et al. (1998): Involvement of the mismatch repair system in temozolomide-induced apoptosis. In *Molecular pharmacology* 54 (2), pp. 334–341. DOI: 10.1124/mol.54.2.334.

Demaria, Marco; O'Leary, Monique N.; Chang, Jianhui; Shao, Lijian; Liu, Su; Alimirah, Fatouma et al. (2017): Cellular Senescence Promotes Adverse Effects of Chemotherapy and Cancer Relapse. In *Cancer discovery* 7 (2), pp. 165–176. DOI: 10.1158/2159-8290.CD-16-0241.

Denny, B. J.; Wheelhouse, R. T.; Stevens, M. F.; Tsang, L. L.; Slack, J. A. (1994): NMR and molecular modeling investigation of the mechanism of activation of the antitumor drug temozolomide and its interaction with DNA. In *Biochemistry* 33 (31), pp. 9045–9051. DOI: 10.1021/bi00197a003.

Di d'Adda Fagagna, Fabrizio (2008): Living on a break: cellular senescence as a DNA-damage response. In *Nature reviews. Cancer* 8 (7), pp. 512–522. DOI: 10.1038/nrc2440.

Dolecek, Therese A.; Propp, Jennifer M.; Stroup, Nancy E.; Kruchko, Carol (2012): CBTRUS statistical report: primary brain and central nervous system tumors diagnosed in the United States in 2005-2009. In *Neuro-oncology* 14 Suppl 5, v1-49. DOI: 10.1093/neuonc/nos218.

Duckett, D. R.; Drummond, J. T.; Murchie, A. I.; Reardon, J. T.; Sancar, A.; Lilley, D. M.; Modrich, P. (1996): Human MutSalpha recognizes damaged DNA base pairs containing O6-methylguanine, O4-methylthymine, or the cisplatin-d(GpG) adduct. In *Proceedings of the National Academy of Sciences of the United States of America* 93 (13), pp. 6443–6447. DOI: 10.1073/pnas.93.13.6443.

Efferth, Thomas; Sauerbrey, Axel; Olbrich, Armin; Gebhart, Erich; Rauch, Pia; Weber, H. Oliver et al. (2003): Molecular modes of action of artesunate in tumor cell lines. In *Molecular pharmacology* 64 (2), pp. 382–394. DOI: 10.1124/mol.64.2.382.

Eich, Marcus; Roos, Wynand Paul; Nikolova, Teodora; Kaina, Bernd (2013): Contribution of ATM and ATR to the resistance of glioblastoma and malignant melanoma cells to the methylating anticancer drug temozolomide. In *Mol Cancer Ther* 12 (11), pp. 2529–2540. DOI: 10.1158/1535-7163.MCT-13-0136.

Elmore, Susan (2007): Apoptosis: a review of programmed cell death. In *Toxicologic pathology* 35 (4), pp. 495–516. DOI: 10.1080/01926230701320337.

Engelward, B. P.; Allan, J. M.; Dreslin, A. J.; Kelly, J. D.; Wu, M. M.; Gold, B.; Samson, L. D. (1998): A chemical and genetic approach together define the biological consequences of 3-methyladenine lesions in the mammalian genome. In *The Journal of biological chemistry* 273 (9), pp. 5412–5418. DOI: 10.1074/jbc.273.9.5412.

Ensminger, Michael; Iloff, Lucie; Ebel, Christian; Nikolova, Teodora; Kaina, Bernd; Löbrich, Markus (2014): DNA breaks and chromosomal aberrations arise when replication meets base excision repair. In *The Journal of cell biology* 206 (1), pp. 29–43. DOI: 10.1083/jcb.201312078.

Errafiy, Rajaa; Aguado, Carmen; Ghislat, Ghita; Esteve, Juan M.; Gil, Anabel; Loutfi, Mohammed; Knecht, Erwin (2013): PTEN increases autophagy and inhibits the ubiquitin-proteasome pathway in glioma cells independently of its lipid phosphatase activity. In *PloS one* 8 (12), e83318. DOI: 10.1371/journal.pone.0083318.

Faget, Douglas V.; Ren, Qihao; Stewart, Sheila A. (2019): Unmasking senescence: context-dependent effects of SASP in cancer. In *Nature reviews. Cancer* 19 (8), pp. 439–453. DOI: 10.1038/s41568-019-0156-2.

Fallahi, P.; Foddis, R.; Cristaudo, A.; Antonelli, A. (2017): High risk of brain tumors in farmers: a mini-review of the literature, and report of the results of a case control study. In *La Clinica terapeutica* 168 (5), e290-e292. DOI: 10.7417/T.2017.2022.

Fan, Ying; Cheng, Jiaoqi; Zeng, Huihong; Shao, Lijian (2020): Senescent Cell Depletion Through Targeting BCL-Family Proteins and Mitochondria. In *Frontiers in physiology* 11, p. 593630. DOI: 10.3389/fphys.2020.593630.

Fink, James R.; Muzi, Mark; Peck, Melinda; Krohn, Kenneth A. (2015): Multimodality Brain Tumor Imaging: MR Imaging, PET, and PET/MR Imaging. In *Journal of nuclear medicine : official publication, Society of Nuclear Medicine* 56 (10), pp. 1554–1561. DOI: 10.2967/jnumed.113.131516.

Fratantonio, Deborah; Molonia, Maria Sofia; Bashllari, Romina; Muscarà, Claudia; Ferlazzo, Guido; Costa, Gregorio et al. (2019): Curcumin potentiates the antitumor activity of Paclitaxel in rat glioma C6 cells. In *Phytomedicine : international journal of phytotherapy and phytopharmacology* 55, pp. 23–30. DOI: 10.1016/j.phymed.2018.08.009.

Friesen, Claudia; Hormann, Inis; Roscher, Mareike; Fichtner, Iduna; Alt, Andreas; Hilger, Ralf et al. (2014): Opioid receptor activation triggering downregulation of cAMP improves effectiveness of anti-cancer drugs in treatment of glioblastoma. In *Cell cycle (Georgetown, Tex.)* 13 (10), pp. 1560–1570. DOI: 10.4161/cc.28493.

Friesen, Claudia; Roscher, Mareike; Hormann, Inis; Fichtner, Iduna; Alt, Andreas; Hilger, Ralf A. et al. (2013): Cell death sensitization of leukemia cells by opioid receptor activation. In *Oncotarget* 4 (5), pp. 677–690. DOI: 10.18632/oncotarget.952.

Frosina, Guido (2009): DNA repair and resistance of gliomas to chemotherapy and radiotherapy. In *Molecular cancer research : MCR* 7 (7), pp. 989–999. DOI: 10.1158/1541-7786.MCR-09-0030.

Fu, Dragony; Calvo, Jennifer A.; Samson, Leona D. (2012): Balancing repair and tolerance of DNA damage caused by alkylating agents. In *Nature reviews. Cancer* 12 (2), pp. 104–120. DOI: 10.1038/nrc3185.

Fuchs, Robert P.; Isogawa, Asako; Paulo, Joao A.; Onizuka, Kazumitsu; Takahashi, Tatsuro; Amunugama, Ravindra et al. (2021): Crosstalk between repair pathways elicits double-strand breaks in alkylated DNA and implications for the action of temozolomide. In *eLife* 10. DOI: 10.7554/eLife.69544.

Fumagalli, Marzia; Rossiello, Francesca; Clerici, Michela; Barozzi, Sara; Cittaro, Davide; Kaplunov, Jessica M. et al. (2012): Telomeric DNA damage is irreparable and causes persistent DNA-damage-response activation. In *Nature cell biology* 14 (4), pp. 355–365. DOI: 10.1038/ncb2466.

Gao, Qi (2019): Oxidative Stress and Autophagy. In *Advances in experimental medicine and biology* 1206, pp. 179–198. DOI: 10.1007/978-981-15-0602-4_9.

Genschel, Jochen; Modrich, Paul (2003): Mechanism of 5'-Directed Excision in Human Mismatch Repair. In *Molecular Cell* 12 (5), pp. 1077–1086. DOI: 10.1016/S1097-2765(03)00428-3.

Ghosh, Shatadal; Banerjee, Sharmistha; Sil, Parames C. (2015): The beneficial role of curcumin on inflammation, diabetes and neurodegenerative disease: A recent update. In *Food and chemical toxicology : an international journal published for the British Industrial Biological Research Association* 83, pp. 111–124. DOI: 10.1016/j.fct.2015.05.022.

Glioblastoma Multiforme – Symptoms, Diagnosis and Treatment Options (2021). Available online at https://www.aans.org/Patients/Neurosurgical-Conditions-and-Treatments/Glioblastoma-Multiforme, updated on 10/4/2021, checked on 10/4/2021.

Grabowska, Wioleta; Mosieniak, Grażyna; Achtabowska, Natalia; Czochara, Robert; Litwinienko, Grzegorz; Bojko, Agnieszka et al. (2019): Curcumin induces multiple signaling pathways leading to vascular smooth muscle cell senescence. In *Biogerontology* 20 (6), pp. 783–798. DOI: 10.1007/s10522-019-09825-2.

Gratas, Catherine; Séry, Quentin; Rabé, Marion; Oliver, Lisa; Vallette, François M. (2014a): Bak and Mcl-1 are essential for Temozolomide induced cell death in human glioma. In *Oncotarget* 5 (9), pp. 2428–2435. DOI: 10.18632/oncotarget.1642.

Gratas, Catherine; Séry, Quentin; Rabé, Marion; Oliver, Lisa; Vallette, François M. (2014b): Bak and Mcl-1 are essential for Temozolomide induced cell death in human glioma. In *Oncotarget* 5 (9), pp. 2428–2435. DOI: 10.18632/oncotarget.1642.

Grochans, Szymon; Cybulska, Anna Maria; Simińska, Donata; Korbecki, Jan; Kojder, Klaudyna; Chlubek, Dariusz; Baranowska-Bosiacka, Irena (2022): Epidemiology of Glioblastoma Multiforme-Literature Review. In *Cancers* 14 (10). DOI: 10.3390/cancers14102412.

Grossman, Rachel; Tyler, Betty; Rudek, Michelle A.; Kim, Eugene; Zadnik, Patti; Khan, Ursalan et al. (2013): Microdialysis measurement of intratumoral temozolomide concentration after cediranib, a pan-VEGF receptor tyrosine kinase inhibitor, in a U87 glioma model. In *Cancer chemotherapy and pharmacology* 72 (1), pp. 93–100. DOI: 10.1007/s00280-013-2172-3.

Grynkiewicz, Grzegorz; Demchuk, Oleg M. (2019): New Perspectives for Fisetin. In *Frontiers in chemistry* 7, p. 697. DOI: 10.3389/fchem.2019.00697.

Guerra, Veronica A.; DiNardo, Courtney; Konopleva, Marina (2019): Venetoclax-based therapies for acute myeloid leukemia. In *Best practice & research. Clinical haematology* 32 (2), pp. 145–153. DOI: 10.1016/j.beha.2019.05.008.

Gupta, Anshu; Dwivedi, Tanima (2017): A Simplified Overview of World Health Organization Classification Update of Central Nervous System Tumors 2016. In *Journal of neurosciences in rural practice* 8 (4), pp. 629–641. DOI: 10.4103/jnrp.jnrp_168_17.

Gutierres, Vânia Ortega; Campos, Michel Leandro; Arcaro, Carlos Alberto; Assis, Renata Pires; Baldan-Cimatti, Helen Mariana; Peccinini, Rosângela Gonçalves et al. (2015): Curcumin Pharmacokinetic and Pharmacodynamic Evidences in Streptozotocin-Diabetic Rats Support the Antidiabetic Activity to Be via Metabolite(s). In *Evidence-based complementary and alternative medicine : eCAM* 2015, p. 678218. DOI: 10.1155/2015/678218.

Häcker, G. (2000): The morphology of apoptosis. In *Cell and tissue research* 301 (1), pp. 5–17. DOI: 10.1007/s004410000193.

Hadidchi, Shahram; Surento, Wesley; Lerner, Alexander; Liu, Chia-Shang Jason; Gibbs, Wende N.; Kim, Paul E.; Shiroishi, Mark S. (2019): Headache and Brain Tumor. In *Neuroimaging clinics of North America* 29 (2), pp. 291–300. DOI: 10.1016/j.nic.2019.01.008.

Harder, Bryan G.; Peng, Sen; Sereduk, Christopher P.; Sodoma, Andrej M.; Kitange, Gaspar J.; Loftus, Joseph C. et al. (2019): Inhibition of phosphatidylinositol 3-kinase by PX-866 suppresses temozolomide-induced autophagy and promotes apoptosis in glioblastoma cells. In *Molecular medicine (Cambridge, Mass.)* 25 (1), p. 49. DOI: 10.1186/s10020-019-0116-z.

Hardigree, A. A.; Epler, J. L. (1978): Comparative mutagenesis of plant flavonoids in microbial systems. In *Mutation Research/Genetic Toxicology* 58 (2-3), pp. 231–239. DOI: 10.1016/0165-1218(78)90014-9.

Haugland, R. P.; Johnson, I. D. (1993): Detecting enzymes in living cells using fluorogenic substrates. In *J Fluoresc* 3 (3), pp. 119–127. DOI: 10.1007/BF00862728.

Haynes, Richard K.; Vonwiller, Simone C. (1994): Extraction of artemisinin and artemisinic acid: preparation of artemether and new analogues. In *Transactions of the Royal Society of Tropical Medicine and Hygiene* 88, pp. 23–26. DOI: 10.1016/0035-9203(94)90466-9.

He, Yang; Kaina, Bernd (2019): Are There Thresholds in Glioblastoma Cell Death Responses Triggered by Temozolomide? In *International journal of molecular sciences* 20 (7). DOI: 10.3390/ijms20071562.

He, Yang; Roos, Wynand P.; Wu, Qianchao; Hofmann, Thomas G.; Kaina, Bernd (2019): The SIAH1-HIPK2-p53ser46 Damage Response Pathway is Involved in Temozolomide-Induced Glioblastoma Cell Death. In *Mol Cancer Res* 17 (5), pp. 1129–1141. DOI: 10.1158/1541-7786.MCR-18-1306.

He, Yihong; Wu, Cong; Duan, Jiayu; Miao, Junming; Ren, Hongyu; Liu, Jiagang (2020): Anti-Glioma Effect with Targeting Therapy Using Folate Modified Nano-Micelles Delivery Curcumin. In *Journal of biomedical nanotechnology* 16 (1), pp. 1–13. DOI: 10.1166/jbn.2020.2878.

Hengartner, M. O. (2000): The biochemistry of apoptosis. In *Nature* 407 (6805), pp. 770–776. DOI: 10.1038/35037710.

Hentschel, Stephen J.; Sawaya, Raymond (2003): Optimizing outcomes with maximal surgical resection of malignant gliomas. In *Cancer control : journal of the Moffitt Cancer Center* 10 (2), pp. 109–114. DOI: 10.1177/107327480301000202.

Herrlinger, Ulrich; Tzaridis, Theophilos; Mack, Frederic; Steinbach, Joachim Peter; Schlegel, Uwe; Sabel, Michael et al. (2019): Lomustine-temozolomide combination therapy versus standard temozolomide therapy in patients with newly diagnosed glioblastoma with methylated MGMT

promoter (CeTeG/NOA–09): a randomised, open-label, phase 3 trial. In *The Lancet* 393 (10172), pp. 678–688. DOI: 10.1016/S0140-6736(18)31791-4.

Hickman, M. J.; Samson, L. D. (1999): Role of DNA mismatch repair and p53 in signaling induction of apoptosis by alkylating agents. In *Proceedings of the National Academy of Sciences of the United States of America* 96 (19), pp. 10764–10769. DOI: 10.1073/pnas.96.19.10764.

Hirose, Yuichi; Berger, Mitchel S.; Pieper, Russell O. (2001): p53 Effects Both the Duration of G2/M Arrest and the Fate of Temozolomide-treated Human Glioblastoma Cells. In *Cancer Res* 61 (5), pp. 1957–1963. Available online at https://aacrjournals.org/cancerres/article/61/5/1957/508389/p53-Effects-Both-the-Duration-of-G2-M-Arrest-and.

Hochberg, F.; Toniolo, P.; Cole, P.; Salcman, M. (1990): Nonoccupational risk indicators of glioblastoma in adults. In *Journal of neuro-oncology* 8 (1), pp. 55–60. DOI: 10.1007/BF00182087.

Hodges, L. C.; Smith, J. L.; Garrett, A.; Tate, S. (1992): Prevalence of glioblastoma multiforme in subjects with prior therapeutic radiation. In *The Journal of neuroscience nursing : journal of the American Association of Neuroscience Nurses* 24 (2), pp. 79–83. DOI: 10.1097/01376517-199204000-00005.

Hotte, Sebastien J.; Chi, Kim N.; Joshua, Anthony M.; Tu, Donsheng; Macfarlane, Robyn J.; Gregg, Rirchard W. et al. (2019): A Phase II Study of PX-866 in Patients With Recurrent or Metastatic Castration-resistant Prostate Cancer: Canadian Cancer Trials Group Study IND205. In *Clinical genitourinary cancer* 17 (3), 201-208.e1. DOI: 10.1016/j.clgc.2019.03.005.

Illingworth, Robert S.; Bird, Adrian P. (2009): CpG islands--'a rough guide'. In *FEBS letters* 583 (11), pp. 1713–1720. DOI: 10.1016/j.febslet.2009.04.012.

Inturrisi, C. E.; Colburn, W. A.; Kaiko, R. F.; Houde, R. W.; Foley, K. M. (1987): Pharmacokinetics and pharmacodynamics of methadone in patients with chronic pain. In *Clinical pharmacology and therapeutics* 41 (4), pp. 392–401. DOI: 10.1038/clpt.1987.47.

Inturrisi, C. E.; Verebely, K. (1972): The levels of methadone in the plasma in methadone maintenance. In *Clinical pharmacology and therapeutics* 13 (5), pp. 633–637. DOI: 10.1002/cpt1972135part1633.

Jellinger, K. (1978): Glioblastoma multiforme: morphology and biology. In *Acta neurochirurgica* 42 (1-2), pp. 5–32. DOI: 10.1007/bf01406628.

Jiang, Feng; Zhou, Jin-Yong; Zhang, Dan; Liu, Ming-Hao; Chen, Yu-Gen (2018): Artesunate induces apoptosis and autophagy in HCT116 colon cancer cells, and autophagy inhibition enhances the artesunate-induced apoptosis. In *International journal of molecular medicine* 42 (3), pp. 1295–1304. DOI: 10.3892/ijmm.2018.3712.

Jie, Mingsha; Mao, Sifeng; Liu, Hanyang; He, Ziyi; Li, Hai-Fang; Lin, Jin-Ming (2017): Evaluation of drug combination for glioblastoma based on an intestine-liver metabolic model on microchip. In *The Analyst* 142 (19), pp. 3629–3638. DOI: 10.1039/C7AN00453B.

Kadari, Amrita; Gudem, Sagarika; Kulhari, Hitesh; Bhandi, Murali Mohan; Borkar, Roshan M.; Kolapalli, Venkata Ramana Murthy; Sistla, Ramakrishna (2017): Enhanced oral bioavailability and anticancer efficacy of fisetin by encapsulating as inclusion complex with HPβCD in polymeric nanoparticles. In *Drug Delivery* 24 (1), pp. 224–232. DOI: 10.1080/10717544.2016.1245366.

Kaina, Bernd; Christmann, Markus; Naumann, Steffen; Roos, Wynand P. (2007): MGMT: key node in the battle against genotoxicity, carcinogenicity and apoptosis induced by alkylating agents. In *DNA repair* 6 (8), pp. 1079–1099. DOI: 10.1016/j.dnarep.2007.03.008.

Kaina, Bernd; Ziouta, Aliki; Ochs, Kirsten; Coquerelle, Therese (1997): Chromosomal instability, reproductive cell death and apoptosis induced by O6-methylguanine in Mex−, Mex+ and methylation-tolerant mismatch repair compromised cells: facts and models. In *Mutation Research/Fundamental and Molecular Mechanisms of Mutagenesis* 381 (2), pp. 227–241. DOI: 10.1016/S0027-5107(97)00187-5.

Kamihara, Junne; Bourdeaut, Franck; Foulkes, William D.; Molenaar, Jan J.; Mossé, Yaël P.; Nakagawara, Akira et al. (2017): Retinoblastoma and Neuroblastoma Predisposition and Surveillance. In *Clinical cancer research : an official journal of the American Association for Cancer Research* 23 (13), e98-e106. DOI: 10.1158/1078-0432.CCR-17-0652.

Kang, Chanhee; Xu, Qikai; Martin, Timothy D.; Li, Mamie Z.; Demaria, Marco; Aron, Liviu et al. (2015): The DNA damage response induces inflammation and senescence by inhibiting autophagy of GATA4. In *Science (New York, N.Y.)* 349 (6255), aaa5612. DOI: 10.1126/science.aaa5612.

Kang, Hyun Tae; Park, Joon Tae; Choi, Kobong; Kim, Yongsub; Choi, Hyo Jei Claudia; Jung, Chul Won et al. (2017): Chemical screening identifies ATM as a target for alleviating senescence. In *Nature chemical biology* 13 (6), pp. 616–623. DOI: 10.1038/nchembio.2342.

Kanzawa, T.; Germano, I. M.; Komata, T.; Ito, H.; Kondo, Y.; Kondo, S. (2004): Role of autophagy in temozolomide-induced cytotoxicity for malignant glioma cells. In *Cell death and differentiation* 11 (4), pp. 448–457. DOI: 10.1038/sj.cdd.4401359.

Karin, Michael; Lin, Anning (2002): NF-kappaB at the crossroads of life and death. In *Nat Immunol* 3 (3), pp. 221–227. DOI: 10.1038/ni0302-221.

Karpel-Massler, Georg; Ishida, Chiaki Tsuge; Zhang, Yiru; Halatsch, Marc-Eric; Westhoff, M-Andrew; Siegelin, Markus D. (2017): Targeting intrinsic apoptosis and other forms of cell death by BH3-mimetics in glioblastoma. In *Expert opinion on drug discovery* 12 (10), pp. 1031–1040. DOI: 10.1080/17460441.2017.1356286.

Kasi, Pandima Devi; Tamilselvam, Rajavel; Skalicka-Woźniak, Krystyna; Nabavi, Seyed Fazel; Daglia, Maria; Bishayee, Anupam et al. (2016): Molecular targets of curcumin for cancer therapy: an updated review. In *Tumour biology : the journal of the International Society for Oncodevelopmental Biology and Medicine* 37 (10), pp. 13017–13028. DOI: 10.1007/s13277-016-5183-y.

Katayama, M.; Kawaguchi, T.; Berger, M. S.; Pieper, R. O. (2007): DNA damaging agent-induced autophagy produces a cytoprotective adenosine triphosphate surge in malignant glioma cells. In *Cell death and differentiation* 14 (3), pp. 548–558. DOI: 10.1038/sj.cdd.4402030.

Keles, G.Evren; Anderson, Brad; Berger, Mitchel S. (1999): The effect of extent of resection on time to tumor progression and survival in patients with glioblastoma multiforme of the cerebral hemisphere. In *Surgical Neurology* 52 (4), pp. 371–379. DOI: 10.1016/S0090-3019(99)00103-2.

Khan, Naghma; Afaq, Farrukh; Syed, Deeba N.; Mukhtar, Hasan (2008): Fisetin, a novel dietary flavonoid, causes apoptosis and cell cycle arrest in human prostate cancer LNCaP cells. In *Carcinogenesis* 29 (5), pp. 1049–1056. DOI: 10.1093/carcin/bgn078.

Khan, Naghma; Syed, Deeba N.; Ahmad, Nihal; Mukhtar, Hasan (2013): Fisetin: a dietary antioxidant for health promotion. In *Antioxidants & redox signaling* 19 (2), pp. 151–162. DOI: 10.1089/ars.2012.4901.

Kitange, Gaspar J.; Mladek, Ann C.; Carlson, Brett L.; Schroeder, Mark A.; Pokorny, Jenny L.; Cen, Ling et al. (2012): Inhibition of histone deacetylation potentiates the evolution of acquired temozolomide resistance linked to MGMT upregulation in glioblastoma xenografts. In *Clinical cancer research : an official journal of the American Association for Cancer Research* 18 (15), pp. 4070–4079. DOI: 10.1158/1078-0432.CCR-12-0560.

Kizhakkayil, Jaleel; Thayyullathil, Faisal; Chathoth, Shahanas; Hago, Abdulkader; Patel, Mahendra; Galadari, Sehamuddin (2010): Modulation of curcumin-induced Akt phosphorylation and apoptosis by PI3K inhibitor in MCF-7 cells. In *Biochemical and biophysical research communications* 394 (3), pp. 476–481. DOI: 10.1016/j.bbrc.2010.01.132.

Klaude, Maria; Eriksson, Stefan; Nygren, Jonas; Ahnström, Gunnar (1996): The comet assay: mechanisms and technical considerations. In *Mutation Research/DNA Repair* 363 (2), pp. 89–96. DOI: 10.1016/0921-8777(95)00063-1.

Klayman, D. L. (1985): Qinghaosu (artemisinin): an antimalarial drug from China. In *Science (New York, N.Y.)* 228 (4703), pp. 1049–1055. DOI: 10.1126/science.3887571.

Kma, Lakhan; Baruah, Taranga Jyoti (2022): The interplay of ROS and the PI3K/Akt pathway in autophagy regulation. In *Biotechnology and applied biochemistry* 69 (1), pp. 248–264. DOI: 10.1002/bab.2104.

Knizhnik, Anna V.; Roos, Wynand P.; Nikolova, Teodora; Quiros, Steve; Tomaszowski, Karl-Heinz; Christmann, Markus; Kaina, Bernd (2013): Survival and death strategies in glioma cells: autophagy, senescence and apoptosis triggered by a single type of temozolomide-induced DNA damage. In *PloS one* 8 (1), e55665. DOI: 10.1371/journal.pone.0055665.

Kocaadam, Betül; Şanlier, Nevin (2017): Curcumin, an active component of turmeric (Curcuma longa), and its effects on health. In *Critical reviews in food science and nutrition* 57 (13), pp. 2889–2895. DOI: 10.1080/10408398.2015.1077195.

Kong, Ling Yi; Tan, Ren Xiang (2015): Artemisinin, a miracle of traditional Chinese medicine. In *Natural product reports* 32 (12), pp. 1617–1621. DOI: 10.1039/c5np00133a.

Korja, Miikka; Raj, Rahul; Seppä, Karri; Luostarinen, Tapio; Malila, Nea; Seppälä, Matti et al. (2019): Glioblastoma survival is improving despite increasing incidence rates: a nationwide study between 2000 and 2013 in Finland. In *Neuro-oncology* 21 (3), pp. 370–379. DOI: 10.1093/neuonc/noy164.

Koul, Dimpy; Shen, Ruijun; Kim, Yong-Wan; Kondo, Yasuko; Lu, Yiling; Bankson, Jim et al. (2010): Cellular and in vivo activity of a novel PI3K inhibitor, PX-866, against human glioblastoma. In *Neuro-oncology* 12 (6), pp. 559–569. DOI: 10.1093/neuonc/nop058.

Kreutzwiser, Denise; Tawfic, Qutaiba A. (2020): Methadone for Pain Management: A Pharmacotherapeutic Review. In *CNS drugs* 34 (8), pp. 827–839. DOI: 10.1007/s40263-020-00743-3.

Kua, Vee May Dianne; Rasul, Azhar; Sreenivasan, Sasidharan; Rasool, Bilal; Younis, Tahira; Lai, Ngit Shin (2019): Methadone hydrochloride and leukemia cells: Effects on cell viability, DNA fragmentation and apoptotic proteins expression level. In *Pakistan journal of pharmaceutical sciences* 32 (4(Supplementary)), pp. 1797–1803.

Kuo, Linda J.; Yang, Li-Xi (2008): Gamma-H2AX - a novel biomarker for DNA double-strand breaks. In *In vivo (Athens, Greece)* 22 (3), pp. 305–309.

Kuo, Min-Liang; Huang, Tze-Sing; Lin, Jen-Kun (1996): Curcumin, an antioxidant and anti-tumor promoter, induces apoptosis in human leukemia cells. In *Biochimica et Biophysica Acta (BBA) - Molecular Basis of Disease* 1317 (2), pp. 95–100. DOI: 10.1016/S0925-4439(96)00032-4.

Kwon, Yoojin; Kim, Ji Wook; Jeoung, Jo Ae; Kim, Mi-Sung; Kang, Chanhee (2017): Autophagy Is Pro-Senescence When Seen in Close-Up, but Anti-Senescence in Long-Shot. In *Molecules and cells* 40 (9), pp. 607–612. DOI: 10.14348/molcells.2017.0151.

Lasica, Masa; Anderson, Mary Ann (2021): Review of Venetoclax in CLL, AML and Multiple Myeloma. In *Journal of personalized medicine* 11 (6). DOI: 10.3390/jpm11060463.

Le Duff, Mélanie; Gouju, Julien; Jonchère, Barbara; Guillon, Jordan; Toutain, Bertrand; Boissard, Alice et al. (2018): Regulation of senescence escape by the cdk4-EZH2-AP2M1 pathway in response to chemotherapy. In *Cell death & disease* 9 (2), p. 199. DOI: 10.1038/s41419-017-0209-y.

Lennon, Frances E.; Mirzapoiazova, Tamara; Mambetsariev, Bolot; Poroyko, Valeriy A.; Salgia, Ravi; Moss, Jonathan; Singleton, Patrick A. (2014): The Mu opioid receptor promotes opioid and growth factor-induced proliferation, migration and Epithelial Mesenchymal Transition (EMT) in human lung cancer. In *PloS one* 9 (3), e91577. DOI: 10.1371/journal.pone.0091577.

Levin, D. E.; Hollstein, M.; Christman, M. F.; Schwiers, E. A.; Ames, B. N. (1982): A new Salmonella tester strain (TA102) with A X T base pairs at the site of mutation detects oxidative mutagens. In *Proceedings of the National Academy of Sciences of the United States of America* 79 (23), pp. 7445–7449. DOI: 10.1073/pnas.79.23.7445.

L'Hôte, Valentin; Courbeyrette, Régis; Pinna, Guillaume; Cintrat, Jean-Christophe; Le Pavec, Gwenaëlle; Delaunay-Moisan, Agnès et al. (2021): Ouabain and chloroquine trigger senolysis of BRAF-V600E-induced senescent cells by targeting autophagy. In *Aging Cell* 20 (9), e13447. DOI: 10.1111/acel.13447.

Li, Wen; He, Yonghan; Zhang, Rongping; Zheng, Guangrong; Zhou, Daohong (2019a): The curcumin analog EF24 is a novel senolytic agent. In *Aging (Albany NY)* 11 (2), pp. 771–782. DOI: 10.18632/aging.101787.

Li, Wen; Qin, Lin; Feng, Rennan; Hu, Guangrong; Sun, Hui; He, Yonghan; Zhang, Rongping (2019b): Emerging senolytic agents derived from natural products. In *Mechanisms of ageing and development* 181, pp. 1–6. DOI: 10.1016/j.mad.2019.05.001.

Li, Zhong-jie; Dai, Hui-qi; Huang, Xiao-wei; Feng, Ji; Deng, Jing-huan; Wang, Zi-xuan et al. (2021): Artesunate synergizes with sorafenib to induce ferroptosis in hepatocellular carcinoma. In *Acta Pharmacologica Sinica* 42 (2), pp. 301–310. DOI: 10.1038/s41401-020-0478-3.

Lin, Fan; Gooijer, Mark C. de; Roig, Eloy Moreno; Buil, Levi C. M.; Christner, Susan M.; Beumer, Jan H. et al. (2014): ABCB1, ABCG2, and PTEN determine the response of glioblastoma to temozolomide and ABT-888 therapy. In *Clinical cancer research : an official journal of the American Association for Cancer Research* 20 (10), pp. 2703–2713. DOI: 10.1158/1078-0432.CCR-14-0084.

Liu, Dan; O'Connor, Matthew S.; Qin, Jun; Songyang, Zhou (2004): Telosome, a mammalian telomere-associated complex formed by multiple telomeric proteins. In *The Journal of biological chemistry* 279 (49), pp. 51338–51342. DOI: 10.1074/jbc.M409293200.

Liu, Weidong; Zhai, Yingjie; Heng, Xueyuan; Che, Feng Yuan; Chen, Wenjun; Sun, Dezhong; Zhai, Guangxi (2016): Oral bioavailability of curcumin: problems and advancements. In *Journal of drug targeting* 24 (8), pp. 694–702. DOI: 10.3109/1061186X.2016.1157883.

Louis, David N.; Perry, Arie; Reifenberger, Guido; Deimling, Andreas von; Figarella-Branger, Dominique; Cavenee, Webster K. et al. (2016): The 2016 World Health Organization Classification of Tumors of the Central Nervous System: a summary. In *Acta neuropathologica* 131 (6), pp. 803–820. DOI: 10.1007/s00401-016-1545-1.

Louis, David N.; Perry, Arie; Wesseling, Pieter; Brat, Daniel J.; Cree, Ian A.; Figarella-Branger, Dominique et al. (2021): The 2021 WHO Classification of Tumors of the Central Nervous System: a summary. In *Neuro-oncology* 23 (8), pp. 1231–1251. DOI: 10.1093/neuonc/noab106.

Louis Cantilena, Jr., MD, PhD (2018): Study of the Safety of Intravenous Artesunate. With assistance of U.S. Army Medical Research and Development Command. Available online at https://clinicaltrials.gov/ct2/show/results/NCT00292942, updated on 10/25/2018, checked on 9/28/2022.

Low, Justin T.; Ostrom, Quinn T.; Cioffi, Gino; Neff, Corey; Waite, Kristin A.; Kruchko, Carol; Barnholtz-Sloan, Jill S. (2022): Primary brain and other central nervous system tumors in the United States (2014-2018): A summary of the CBTRUS statistical report for clinicians. In *Neuro-oncology practice* 9 (3), pp. 165–182. DOI: 10.1093/nop/npac015.

Lu, Jin; Liu, Zefeng; Zhao, Lingling; Tian, Huimin; Liu, Xiuhua; Yuan, Changji (2013): In vivo and in vitro inhibition of human liver cancer progress by downregulation of the μ-opioid receptor and relevant mechanisms. In *Oncology reports* 30 (4), pp. 1731–1738. DOI: 10.3892/or.2013.2640.

Ludlum, David B. (1990): DNA alkylation by the haloethylnitrosoureas: Nature of modifications produced and their enzymatic repair or removal. In *Mutation Research/Fundamental and Molecular Mechanisms of Mutagenesis* 233 (1-2), pp. 117–126. DOI: 10.1016/0027-5107(90)90156-X.

Ma, Jianguo; Murphy, Maureen; O'Dwyer, Peter J.; Berman, Eric; Reed, Karin; Gallo, James M. (2002): Biochemical changes associated with a multidrug-resistant phenotype of a human glioma cell line with temozolomide-acquired resistance. In *Biochemical Pharmacology* 63 (7), pp. 1219–1228. DOI: 10.1016/s0006-2952(02)00876-6.

McDowell, Anthony; Hill, Kristen S.; McCorkle, J. Robert; Gorski, Justin; Zhang, Yilin; Salahudeen, Ameen A. et al. (2021): Preclinical Evaluation of Artesunate as an Antineoplastic Agent in Ovarian Cancer Treatment. In *Diagnostics (Basel, Switzerland)* 11 (3). DOI: 10.3390/diagnostics11030395.

Mehta, M. P.; Won, M.; Shaw, E. G.; Buckner, J.; Gilbert, M.; Barger, G. et al. (2014): Mature Survival Data from RTOG 9802: A Phase III Study of Radiation Therapy (RT) With or Without Procarbazine, CCNU, and Vincristine (PCV) for Adult Patients with High-Risk Low-Grade Glioma (LGG). In *International Journal of Radiation Oncology*Biology*Physics* 90 (1), S37-S38. DOI: 10.1016/j.ijrobp.2014.05.153.

Melendez, V.; Peggins, J. O.; Brewer, T. G.; Theoharides, A. D. (1991): Determination of the antimalarial arteether and its deethylated metabolite dihydroartemisinin in plasma by high-performance liquid chromatography with reductive electrochemical detection. In *Journal of pharmaceutical sciences* 80 (2), pp. 132–138. DOI: 10.1002/jps.2600800209.

Meresaar, U.; Nilsson, M. I.; Holmstrand, J.; Anggård, E. (1981): Single dose pharmacokinetics and bioavailability of methadone in man studied with a stable isotope method. In *European journal of clinical pharmacology* 20 (6), pp. 473–478. DOI: 10.1007/BF00542102.

Minniti, Giuseppe; Niyazi, Maximilian; Alongi, Filippo; Navarria, Piera; Belka, Claus (2021): Current status and recent advances in reirradiation of glioblastoma. In *Radiation oncology (London, England)* 16 (1), p. 36. DOI: 10.1186/s13014-021-01767-9.

Mukherjee, Debraj; Quinones-Hinojosa, Alfredo (2011): Impact of Extent of Resection on Outcomes in Patients with High-Grade Gliomas. In M. A. Hayat (Ed.): Tumors of the Central Nervous System, Volume 2. Dordrecht: Springer Netherlands, pp. 173–179.

Muthu K. Shanmugam; Sudha Warrier; Alan P. Kumar; Gautam Sethi; Frank Arfuso: Potential Role of Natural Compounds as Anti-Angiogenic Agents in Cancer. In *Current Vascular Pharmacology* 15 (6), pp. 503–519. Available online at http://www.eurekaselect.com/article/84745.

Nabavi, Seyed Fazel; Braidy, Nady; Habtemariam, Solomon; Sureda, Antoni; Manayi, Azadeh; Nabavi, Seyed Mohammad (2016): Neuroprotective Effects of Fisetin in Alzheimer's and Parkinson's Diseases: From Chemistry to Medicine. In *Current topics in medicinal chemistry* 16 (17), pp. 1910–1915. DOI: 10.2174/1568026616666160204121725.

Nair, Raji R.; Bagheri, Meisam; Saini, Deepak Kumar (2015): Temporally distinct roles of ATM and ROS in genotoxic-stress-dependent induction and maintenance of cellular senescence. In *J Cell Sci* 128 (2), pp. 342–353. DOI: 10.1242/jcs.159517.

Naugler, Willscott E.; Karin, Michael (2008): NF-kappaB and cancer-identifying targets and mechanisms. In *Current opinion in genetics & development* 18 (1), pp. 19–26. DOI: 10.1016/j.gde.2008.01.020.

Newlands, E. S.; Blackledge, G. R.; Slack, J. A.; Rustin, G. J.; Smith, D. B.; Stuart, N. S. et al. (1992): Phase I trial of temozolomide (CCRG 81045: M&B 39831: NSC 362856). In *British journal of cancer* 65 (2), pp. 287–291. DOI: 10.1038/bjc.1992.57.

nhs.uk (NaN): Brain tumours - NHS. Available online at https://www.nhs.uk/conditions/brain-tumours/, updated on 10/4/2021, checked on 10/4/2021.

Nikolova, Teodora; Roos, Wynand P.; Krämer, Oliver H.; Strik, Herwig M.; Kaina, Bernd (2017): Chloroethylating nitrosoureas in cancer therapy: DNA damage, repair and cell death signaling. In *Biochimica et biophysica acta. Reviews on cancer* 1868 (1), pp. 29–39. DOI: 10.1016/j.bbcan.2017.01.004.

Ninfa, Alexander J.; Ballou, David P.; Benore, Marilee (2010): Fundamental laboratory approaches for biochemistry and biotechnology. 2nd ed. / Alexander J. Ninfa, David P. Ballou, Marilee Benore. Hoboken, N.J.: Wiley; Chichester.

Nyunt, Myaing; Plowe, Christopher V. (2009): MALARIA. In : Pharmacology and Therapeutics: Elsevier, pp. 1141–1170.

O'Connell, M. J. (1997): Chk1 is a wee1 kinase in the G2 DNA damage checkpoint inhibiting cdc2 by Y15 phosphorylation. In *The EMBO Journal* 16 (3), pp. 545–554. DOI: 10.1093/emboj/16.3.545.

Olaharski, A. J.; Mondrala, S. T.; Eastmond, D. A. (2005): Chromosomal malsegregation and micronucleus induction in vitro by the DNA topoisomerase II inhibitor fisetin. In *Mutation Research/Fundamental and Molecular Mechanisms of Mutagenesis* 582 (1-2), pp. 79–86. DOI: 10.1016/j.mrgentox.2005.01.002.

Olszewska, Aleksandra; Borkowska, Agata; Granica, Monika; Karolczak, Justyna; Zglinicki, Bartosz; Kieda, Claudine; Was, Halina (2021): Escape From Cisplatin-Induced Senescence of Hypoxic Lung Cancer Cells Can Be Overcome by Hydroxychloroquine. In *Frontiers in oncology* 11, p. 738385. DOI: 10.3389/fonc.2021.738385.

Onken, Julia; Friesen, Claudia; Vajkoczy, Peter; Misch, Martin (2017): Safety and Tolerance of D,L-Methadone in Combination with Chemotherapy in Patients with Glioma. In *Anticancer research* 37 (3), pp. 1227–1235. DOI: 10.21873/anticanres.11438.

Ostrom, Quinn T.; Gittleman, Haley; Farah, Paul; Ondracek, Annie; Chen, Yanwen; Wolinsky, Yingli et al. (2013): CBTRUS statistical report: Primary brain and central nervous system tumors diagnosed in the United States in 2006-2010. In *Neuro-oncology* 15 Suppl 2, ii1-56. DOI: 10.1093/neuonc/not151.

Ostrom, Quinn T.; Gittleman, Haley; Truitt, Gabrielle; Boscia, Alexander; Kruchko, Carol; Barnholtz-Sloan, Jill S. (2018): CBTRUS Statistical Report: Primary Brain and Other Central Nervous System Tumors Diagnosed in the United States in 2011-2015. In *Neuro-oncology* 20 (suppl_4), iv1-iv86. DOI: 10.1093/neuonc/noy131.

Palat, Gayatri; Chary, Srini (2018): Practical Guide for Using Methadone in Pain and Palliative Care Practice. In *Indian journal of palliative care* 24 (Suppl 1), S21-S29. DOI: 10.4103/IJPC.IJPC_186_17.

Pascal, John M. (2018): The comings and goings of PARP-1 in response to DNA damage. In *DNA repair* 71, pp. 177–182. DOI: 10.1016/j.dnarep.2018.08.022.

Pegg, Anthony E.; Dolan, M. Eileen; Moschel, Robert C. (1995): Structure, Function, and Inhibition of O6-Alkylguanine-DNA Alkyltransferase. In, vol. 51: Elsevier (Progress in Nucleic Acid Research and Molecular Biology), pp. 167–223.

Philips, Alasdair; Henshaw, Denis L.; Lamburn, Graham; O'Carroll, Michael J. (2018): Brain Tumours: Rise in Glioblastoma Multiforme Incidence in England 1995-2015 Suggests an Adverse Environmental or Lifestyle Factor. In *Journal of environmental and public health* 2018, p. 7910754. DOI: 10.1155/2018/7910754.

Piel, Clément; Pouchieu, Camille; Migault, Lucile; Béziat, Béatrix; Boulanger, Mathilde; Bureau, Mathilde et al. (2019): Increased risk of central nervous system tumours with carbamate insecticide use in the prospective cohort AGRICAN. In *International journal of epidemiology* 48 (2), pp. 512–526. DOI: 10.1093/ije/dyy246.

Pitz, Marshall W.; Eisenhauer, Elizabeth A.; MacNeil, Mary V.; Thiessen, Brian; Easaw, Jacob C.; Macdonald, David R. et al. (2015): Phase II study of PX-866 in recurrent glioblastoma. In *Neuro-oncology* 17 (9), pp. 1270–1274. DOI: 10.1093/neuonc/nou365.

Portnow, Jana; Badie, Behnam; Chen, Mike; an Liu; Blanchard, Suzette; Synold, Timothy W. (2009): The neuropharmacokinetics of temozolomide in patients with resectable brain tumors: potential implications for the current approach to chemoradiation. In *Clinical cancer research : an official journal of the American Association for Cancer Research* 15 (22), pp. 7092–7098. DOI: 10.1158/1078-0432.CCR-09-1349.

Presser, Armin; Feichtinger, Andrea; Buzzi, Silke (2017): A simplified and scalable synthesis of artesunate. In *Monatshefte fur chemie* 148 (1), pp. 63–68. DOI: 10.1007/s00706-016-1865-9.

Pricci, Maria; Girardi, Bruna; Giorgio, Floriana; Losurdo, Giuseppe; Ierardi, Enzo; Di Leo, Alfredo (2020): Curcumin and Colorectal Cancer: From Basic to Clinical Evidences. In *International journal of molecular sciences* 21 (7). DOI: 10.3390/ijms21072364.

Qin, Guiqi; Wu, Liping; Liu, Hongyu; Pang, Yilin; Zhao, Chubiao; Wu, Shengnan et al. (2015): Artesunate induces apoptosis via a ROS-independent and Bax-mediated intrinsic pathway in HepG2 cells. In *Experimental cell research* 336 (2), pp. 308–317. DOI: 10.1016/j.yexcr.2015.07.004.

Quiros, Steve; Roos, Wynand P.; Kaina, Bernd (2010): Processing of O6-methylguanine into DNA double-strand breaks requires two rounds of replication whereas apoptosis is also induced in subsequent cell cycles. In *Cell cycle (Georgetown, Tex.)* 9 (1), pp. 168–178. DOI: 10.4161/cc.9.1.10363.

Raffaele, Marco; Kovacovicova, Kristina; Biagini, Tommaso; Lo Re, Oriana; Frohlich, Jan; Giallongo, Sebastiano et al. (2022): Nociceptin/orphanin FQ opioid receptor (NOP) selective ligand MCOPPB links anxiolytic and senolytic effects. In *GeroScience* 44 (1), pp. 463–483. DOI: 10.1007/s11357-021-00487-y.

Rayess, Hani; Wang, Marilene B.; Srivatsan, Eri S. (2012): Cellular senescence and tumor suppressor gene p16. In *Int. J. Cancer* 130 (8), pp. 1715–1725. DOI: 10.1002/ijc.27316.

Renault-Mahieux, Morgane; Vieillard, Victoire; Seguin, Johanne; Espeau, Philippe; Le, Dang Tri; Lai-Kuen, René et al. (2021): Co-Encapsulation of Fisetin and Cisplatin into Liposomes for Glioma Therapy: From Formulation to Cell Evaluation. In *Pharmaceutics* 13 (7). DOI: 10.3390/pharmaceutics13070970.

Resende, Flavia Aparecida; Vilegas, Wagner; Dos Santos, Lourdes Campaner; Varanda, Eliana Aparecida (2012): Mutagenicity of flavonoids assayed by bacterial reverse mutation (Ames) test. In *Molecules (Basel, Switzerland)* 17 (5), pp. 5255–5268. DOI: 10.3390/molecules17055255.

Robert, Mc; Wastie, Ml (2008): Glioblastoma multiforme: a rare manifestation of extensive liver and bone metastases. In *Biomedical imaging and intervention journal* 4 (1), e3. DOI: 10.2349/biij.4.1.e3.

Rodier, Francis; Coppé, Jean-Philippe; Patil, Christopher K.; Hoeijmakers, Wieteke A. M.; Muñoz, Denise P.; Raza, Saba R. et al. (2009): Persistent DNA damage signalling triggers senescence-

associated inflammatory cytokine secretion. In *Nature cell biology* 11 (8), pp. 973–979. DOI: 10.1038/ncb1909.

Roos, W. P.; Batista, L. F. Z.; Naumann, S. C.; Wick, W.; Weller, M.; Menck, C. F. M.; Kaina, B. (2007): Apoptosis in malignant glioma cells triggered by the temozolomide-induced DNA lesion O6-methylguanine. In *Oncogene* 26 (2), pp. 186–197. DOI: 10.1038/sj.onc.1209785.

Roos, Wynand; Baumgartner, Manuela; Kaina, Bernd (2004): Apoptosis triggered by DNA damage O6-methylguanine in human lymphocytes requires DNA replication and is mediated by p53 and Fas/CD95/Apo-1. In *Oncogene* 23 (2), pp. 359–367. DOI: 10.1038/sj.onc.1207080.

Rosso, Lula; Brock, Cathryn S.; Gallo, James M.; Saleem, Azeem; Price, Patricia M.; Turkheimer, Federico E.; Aboagye, Eric O. (2009): A new model for prediction of drug distribution in tumor and normal tissues: pharmacokinetics of temozolomide in glioma patients. In *Cancer Res* 69 (1), pp. 120–127. DOI: 10.1158/0008-5472.CAN-08-2356.

Safari, Mojdeh; Khoshnevisan, Alireza (2015): Cancer Stem Cells and Chemoresistance in Glioblastoma Multiform: A Review Article. In *Journal of stem cells* 10 (4), pp. 271–285.

Saleem, Azeem; Brown, Gavin D.; Brady, Frank; Aboagye, Eric O.; Osman, Safiye; Luthra, Sajinder K. et al. (2003): Metabolic Activation of Temozolomide Measured in Vivo Using Positron Emission Tomography. In *Cancer Res* 63 (10), pp. 2409–2415. Available online at https://aacrjournals.org/cancerres/article/63/10/2409/509961/Metabolic-Activation-of-Temozolomide-Measured-in#F1.

Saleh, Tareq; Tyutyunyk-Massey, Liliya; Murray, Graeme F.; Alotaibi, Moureq R.; Kawale, Ajinkya S.; Elsayed, Zeinab et al. (2019): Tumor cell escape from therapy-induced senescence. In *Biochemical Pharmacology* 162, pp. 202–212. DOI: 10.1016/j.bcp.2018.12.013.

Samanic, Claudine M.; Roos, Anneclaire J. de; Stewart, Patricia A.; Rajaraman, Preetha; Waters, Martha A.; Inskip, Peter D. (2008): Occupational exposure to pesticides and risk of adult brain tumors. In *American journal of epidemiology* 167 (8), pp. 976–985. DOI: 10.1093/aje/kwm401.

Schiborr, Christina; Kocher, Alexa; Behnam, Dariush; Jandasek, Josef; Toelstede, Simone; Frank, Jan (2014): The oral bioavailability of curcumin from micronized powder and liquid micelles is significantly increased in healthy humans and differs between sexes. In *Molecular nutrition & food research* 58 (3), pp. 516–527. DOI: 10.1002/mnfr.201300724.

Schuckit, Marc A. (2016): Treatment of Opioid-Use Disorders. In *The New England journal of medicine* 375 (4), pp. 357–368. DOI: 10.1056/NEJMra1604339.

Seiwert, Nina; Fahrer, Jörg; Nagel, Georg; Frank, Jan; Behnam, Dariush; Kaina, Bernd (2021): Curcumin Administered as Micellar Solution Suppresses Intestinal Inflammation and Colorectal Carcinogenesis. In *Nutrition and cancer* 73 (4), pp. 686–693. DOI: 10.1080/01635581.2020.1771384.

Seker-Polat, Fidan; Pinarbasi Degirmenci, Nareg; Solaroglu, Ihsan; Bagci-Onder, Tugba (2022): Tumor Cell Infiltration into the Brain in Glioblastoma: From Mechanisms to Clinical Perspectives. In *Cancers* 14 (2). DOI: 10.3390/cancers14020443.

Sergentanis, Theodoros N.; Tsivgoulis, Georgios; Perlepe, Christina; Ntanasis-Stathopoulos, Ioannis; Tzanninis, Ioannis-Georgios; Sergentanis, Ioannis N.; Psaltopoulou, Theodora (2015): Obesity and Risk for Brain/CNS Tumors, Gliomas and Meningiomas: A Meta-Analysis. In *PloS one* 10 (9), e0136974. DOI: 10.1371/journal.pone.0136974.

Seystahl, Katharina; Wick, Wolfgang; Weller, Michael (2016): Therapeutic options in recurrent glioblastoma--An update. In *Critical reviews in oncology/hematology* 99, pp. 389–408. DOI: 10.1016/j.critrevonc.2016.01.018.

Shah, Viral; Kochar, Pratiksha (2018): Brain Cancer: Implication to Disease, Therapeutic Strategies and Tumor Targeted Drug Delivery Approaches. In *Recent patents on anti-cancer drug discovery* 13 (1), pp. 70–85. DOI: 10.2174/1574892812666171129142023.

Sharma, Arishya; Almasan, Alexandru (2021): Autophagy and PTEN in DNA damage-induced senescence. In *Advances in cancer research* 150, pp. 249–284. DOI: 10.1016/bs.acr.2021.01.006.

Shehzad, Adeeb; Wahid, Fazli; Lee, Young Sup (2010): Curcumin in cancer chemoprevention: molecular targets, pharmacokinetics, bioavailability, and clinical trials. In *Archiv der Pharmazie* 343 (9), pp. 489–499. DOI: 10.1002/ardp.200900319.

Siuda, Edward R.; Carr, Richard; Rominger, David H.; Violin, Jonathan D. (2017): Biased mu-opioid receptor ligands: a promising new generation of pain therapeutics. In *Current opinion in pharmacology* 32, pp. 77–84. DOI: 10.1016/j.coph.2016.11.007.

Sminia, Peter; van den Berg, Jaap; van Kootwijk, Arthur; Hageman, Eline; Slotman, Ben J.; Verbakel, Wilko F. A. R. (2021): Experimental and clinical studies on radiation and curcumin in human glioma. In *Journal of Cancer Research and Clinical Oncology* 147 (2), pp. 403–409. DOI: 10.1007/s00432-020-03432-2.

So, Jae-Seon; Kim, Hyeono; Han, Kyung-Seok (2021): Mechanisms of Invasion in Glioblastoma: Extracellular Matrix, Ca2+ Signaling, and Glutamate. In *Frontiers in cellular neuroscience* 15, p. 663092. DOI: 10.3389/fncel.2021.663092.

Stefanaki, Kalliopi; Alexiou, George A.; Stefanaki, Christina; Prodromou, Neofytos (2012): Tumors of central and peripheral nervous system associated with inherited genetic syndromes. In *Pediatric neurosurgery* 48 (5), pp. 271–285. DOI: 10.1159/000351546.

Stein, Christoph (2016): Opioid Receptors. In *Annual review of medicine* 67, pp. 433–451. DOI: 10.1146/annurev-med-062613-093100.

Stevens, M. F.; Hickman, J. A.; Stone, R.; Gibson, N. W.; Baig, G. U.; Lunt, E.; Newton, C. G. (1984): Antitumor imidazotetrazines. 1. Synthesis and chemistry of 8-carbamoyl-3-(2-chloroethyl)imidazo5,1-d-1,2,3,5-tetrazin-4(3 H)-one, a novel broad-spectrum antitumor agent. In *Journal of medicinal chemistry* 27 (2), pp. 196–201. DOI: 10.1021/jm00368a016.

Stratenwerth, Björn; Geisen, Susanne M.; He, Yang; Beltzig, Lea; Sturla, Shana J.; Kaina, Bernd (2021): Molecular Dosimetry of Temozolomide: Quantification of Critical Lesions, Correlation to Cell Death Responses, and Threshold Doses. In *Mol Cancer Ther* 20 (10), pp. 1789–1799. DOI: 10.1158/1535-7163.MCT-21-0228.

Stummer, Walter; Pichlmeier, Uwe; Meinel, Thomas; Wiestler, Otmar Dieter; Zanella, Friedhelm; Reulen, Hans-Jürgen (2006): Fluorescence-guided surgery with 5-aminolevulinic acid for resection of malignant glioma: a randomised controlled multicentre phase III trial. In *The Lancet Oncology* 7 (5), pp. 392–401. DOI: 10.1016/S1470-2045(06)70665-9.

Stupp, Roger; Mason, Warren P.; van den Bent, Martin J.; Weller, Michael; Fisher, Barbara; Taphoorn, Martin J. B. et al. (2005): Radiotherapy plus concomitant and adjuvant temozolomide for glioblastoma. In *The New England journal of medicine* 352 (10), pp. 987–996. DOI: 10.1056/NEJMoa043330.

Surawicz, T. S.; McCarthy, B. J.; Kupelian, V.; Jukich, P. J.; Bruner, J. M.; Davis, F. G. (1999): Descriptive epidemiology of primary brain and CNS tumors: results from the Central Brain Tumor Registry of the United States, 1990-1994. In *Neuro-oncology* 1 (1), pp. 14–25.

Tafuto, Salvatore; Muto, Paolo; Tortoriello, Anna; Pisano, Agata; Comella, Pasquale; Formato, Roberta et al. (2006): Phase I study of temozolomide and lomustine in the treatment of high grade malignant glioma. In *Frontiers in bioscience : a journal and virtual library* 11, pp. 502–505. DOI: 10.2741/1814.

Tan, Aaron C.; Ashley, David M.; López, Giselle Y.; Malinzak, Michael; Friedman, Henry S.; Khasraw, Mustafa (2020): Management of glioblastoma: State of the art and future directions. In *CA: a cancer journal for clinicians* 70 (4), pp. 299–312. DOI: 10.3322/caac.21613.

Taylor, Jennie W.; Schiff, David (2015): Treatment considerations for MGMT-unmethylated glioblastoma. In *Current neurology and neuroscience reports* 15 (1), p. 507. DOI: 10.1007/s11910-014-0507-z.

TEMOZOLOMIDE_ChemistryWorldJul09_tcm18-155909. Available online at https://www.rsc.org/images/TEMOZOLOMIDE_ChemistryWorldJul09_tcm18-155909.pdf, checked on 3/31/2022.

Touil, Yasmine S.; Auzeil, Nicolas; Boulinguez, François; Saighi, Hanane; Regazzetti, Anne; Scherman, Daniel; Chabot, Guy G. (2011): Fisetin disposition and metabolism in mice: Identification of geraldol as an active metabolite. In *Biochemical Pharmacology* 82 (11), pp. 1731–1739. DOI: 10.1016/j.bcp.2011.07.097.

van Antwerp, D. J.; Martin, S. J.; Kafri, T.; Green, D. R.; Verma, I. M. (1996): Suppression of TNF-alpha-induced apoptosis by NF-kappaB. In *Science (New York, N.Y.)* 274 (5288), pp. 787–789. DOI: 10.1126/science.274.5288.787.

Vanlangenakker, N.; Vanden Berghe, T.; Bogaert, P.; Laukens, B.; Zobel, K.; Deshayes, K. et al. (2011): cIAP1 and TAK1 protect cells from TNF-induced necrosis by preventing RIP1/RIP3-dependent reactive oxygen species production. In *Cell death and differentiation* 18 (4), pp. 656–665. DOI: 10.1038/cdd.2010.138.

Varfolomeev, Eugene; Alicke, Bruno; Elliott, J. Michael; Zobel, Kerry; West, Kristina; Wong, Harvey et al. (2009): X chromosome-linked inhibitor of apoptosis regulates cell death induction by proapoptotic receptor agonists. In *The Journal of biological chemistry* 284 (50), pp. 34553–34560. DOI: 10.1074/jbc.M109.040139.

Vermes, István; Haanen, Clemens; Steffens-Nakken, Helga; Reutellingsperger, Chris (1995): A novel assay for apoptosis Flow cytometric detection of phosphatidylserine expression on early apoptotic cells using fluorescein labelled Annexin V. In *Journal of immunological methods* 184 (1), pp. 39–51. DOI: 10.1016/0022-1759(95)00072-I.

Vistica, D. T.; Skehan, P.; Scudiero, D.; Monks, A.; Pittman, A.; Boyd, M. R. (1991): Tetrazolium-based assays for cellular viability: a critical examination of selected parameters affecting formazan production. In *Cancer Res* 51 (10), pp. 2515–2520.

Volavka, J.; Verebey, K.; Resnick, R.; Mulé, S. (1978): Methadone dose, plasma level, and cross-tolerance to heroin in man. In *The Journal of nervous and mental disease* 166 (2), pp. 104–109. DOI: 10.1097/00005053-197802000-00004.

Wang, Limin; Di Cao; Wu, Huijun; Jia, Hongning; Yang, Chaoping; Zhang, Lihua (2019): Fisetin Prolongs Therapy Window of Brain Ischemic Stroke Using Tissue Plasminogen Activator: A Double-Blind Randomized Placebo-Controlled Clinical Trial. In *Clinical and Applied Thrombosis/Hemostasis* 25, 1076029619871359. DOI: 10.1177/1076029619871359.

Wang, Ruoxi; Li, Chunshuang; Qiao, Ping; Xue, Yaoyao; Zheng, Xu; Chen, Hongyu et al. (2018): OGG1-initiated base excision repair exacerbates oxidative stress-induced parthanatos. In *Cell death & disease* 9 (6), p. 628. DOI: 10.1038/s41419-018-0680-0.

Wang, Tuan; Wu, Xia; Al Rudaisat, Mus'ab; Song, Yinjing; Cheng, Hao (2020): Curcumin induces G2/M arrest and triggers autophagy, ROS generation and cell senescence in cervical cancer cells. In *Journal of Cancer* 11 (22), pp. 6704–6715. DOI: 10.7150/jca.45176.

Wang, Ying-Jan; Pan, Min-Hsiung; Cheng, Ann-Lii; Lin, Liang-In; Ho, Yuan-Soon; Hsieh, Chang-Yao; Lin, Jen-Kun (1997): Stability of curcumin in buffer solutions and characterization of its degradation

products. In *Journal of Pharmaceutical and Biomedical Analysis* 15 (12), pp. 1867–1876. DOI: 10.1016/S0731-7085(96)02024-9.

Wei, Shupei; Liu, Lili; Chen, Zhiyu; Yin, Wenli; Liu, Yingzi; Ouyang, Qianying et al. (2020): Artesunate inhibits the mevalonate pathway and promotes glioma cell senescence. In *Journal of cellular and molecular medicine* 24 (1), pp. 276–284. DOI: 10.1111/jcmm.14717.

Weller, Michael; Felsberg, Jörg; Hartmann, Christian; Berger, Hilmar; Steinbach, Joachim P.; Schramm, Johannes et al. (2009): Molecular predictors of progression-free and overall survival in patients with newly diagnosed glioblastoma: a prospective translational study of the German Glioma Network. In *Journal of clinical oncology : official journal of the American Society of Clinical Oncology* 27 (34), pp. 5743–5750. DOI: 10.1200/JCO.2009.23.0805.

Weller, Michael; Le Rhun, Emilie (2020): How did lomustine become standard of care in recurrent glioblastoma? In *Cancer treatment reviews* 87, p. 102029. DOI: 10.1016/j.ctrv.2020.102029.

Weller, Michael; Rieger, Johannes; Grimmel, Cornelia; van Meir, Erwin G.; Tribolet, Nicolas de; Krajewski, Stanislaw et al. (1998): Predicting chemoresistance in human malignant glioma cells: The role of molecular genetic analyses. In *Int. J. Cancer* 79 (6), pp. 640–644. DOI: 10.1002/(SICI)1097-0215(19981218)79:6<640::AID-IJC15>3.0.CO;2-Z.

Weller, Michael; Stupp, Roger; Reifenberger, Guido; Brandes, Alba A.; van den Bent, Martin J.; Wick, Wolfgang; Hegi, Monika E. (2010): MGMT promoter methylation in malignant gliomas: ready for personalized medicine? In *Nature reviews. Neurology* 6 (1), pp. 39–51. DOI: 10.1038/nrneurol.2009.197.

Wesseling, P.; Schlingemann, R. O.; Rietveld, F. J.; Link, M.; Burger, P. C.; Ruiter, D. J. (1995): Early and extensive contribution of pericytes/vascular smooth muscle cells to microvascular proliferation in glioblastoma multiforme: an immuno-light and immuno-electron microscopic study. In *Journal of neuropathology and experimental neurology* 54 (3), pp. 304–310. DOI: 10.1097/00005072-199505000-00003.

Wiedmann, Markus K. H.; Brunborg, Cathrine; Di Ieva, Antonio; Lindemann, Kristina; Johannesen, Tom B.; Vatten, Lars et al. (2017): The impact of body mass index and height on the risk for glioblastoma and other glioma subgroups: a large prospective cohort study. In *Neuro-oncology* 19 (7), pp. 976–985. DOI: 10.1093/neuonc/now272.

Wiley, Christopher D.; Sharma, Rishi; Davis, Sonnet S.; Lopez-Dominguez, Jose Alberto; Mitchell, Kylie P.; Wiley, Samantha et al. (2021): Oxylipin biosynthesis reinforces cellular senescence and allows detection of senolysis. In *Cell metabolism* 33 (6), 1124-1136.e5. DOI: 10.1016/j.cmet.2021.03.008.

Woernle, Christoph Michael; Péus, Dominik; Hofer, Silvia; Rushing, Elisabeth Jane; Held, Ulrike; Bozinov, Oliver et al. (2015): Efficacy of Surgery and Further Treatment of Progressive Glioblastoma. In *World neurosurgery* 84 (2), pp. 301–307. DOI: 10.1016/j.wneu.2015.03.018.

Wolff, K.; Hay, A. W.; Raistrick, D.; Calvert, R. (1993): Steady-state pharmacokinetics of methadone in opioid addicts. In *European journal of clinical pharmacology* 44 (2), pp. 189–194. DOI: 10.1007/BF00315479.

Wrensch, M.; Lee, M.; Miike, R.; Newman, B.; Barger, G.; Davis, R. et al. (1997): Familial and personal medical history of cancer and nervous system conditions among adults with glioma and controls. In *American journal of epidemiology* 145 (7), pp. 581–593. DOI: 10.1093/oxfordjournals.aje.a009154.

Xu-Welliver, Meng; Pegg, Anthony E. (2002): Degradation of the alkylated form of the DNA repair protein, O(6)-alkylguanine-DNA alkyltransferase. In *Carcinogenesis* 23 (5), pp. 823–830. DOI: 10.1093/carcin/23.5.823.

Yosef, Reut; Pilpel, Noam; Tokarsky-Amiel, Ronit; Biran, Anat; Ovadya, Yossi; Cohen, Snir et al. (2016): Directed elimination of senescent cells by inhibition of BCL-W and BCL-XL. In *Nature communications* 7, p. 11190. DOI: 10.1038/ncomms11190.

Young, Andrew R. J.; Narita, Masako; Ferreira, Manuela; Kirschner, Kristina; Sadaie, Mahito; Darot, Jeremy F. J. et al. (2009): Autophagy mediates the mitotic senescence transition. In *Genes & development* 23 (7), pp. 798–803. DOI: 10.1101/gad.519709.

Yousefzadeh, Matthew J.; Zhu, Yi; McGowan, Sara J.; Angelini, Luise; Fuhrmann-Stroissnigg, Heike; Xu, Ming et al. (2018): Fisetin is a senotherapeutic that extends health and lifespan. In *EBioMedicine* 36, pp. 18–28. DOI: 10.1016/j.ebiom.2018.09.015.

Yu, Jie; Zhong, Bingling; Xiao, Qingwen; Du, Lida; Hou, Ying; Sun, Hong-Shuo et al. (2020): Induction of programmed necrosis: A novel anti-cancer strategy for natural compounds. In *Pharmacology & therapeutics* 214, p. 107593. DOI: 10.1016/j.pharmthera.2020.107593.

Zhang, Dan; Tang, Bo; Xie, Xia; Xiao, Yu-Feng; Yang, Shi-Ming; Zhang, Jian-Wei (2015): The interplay between DNA repair and autophagy in cancer therapy. In *Cancer biology & therapy* 16 (7), pp. 1005–1013. DOI: 10.1080/15384047.2015.1046022.

Zhang, Hao-Wen; Wang, Fei; Zhou, Ya-Qun; Xu, San-Ping; Yu, Shi-Ying; Zhang, Zhan-Guo (2021): Morphine Suppresses Liver Cancer Cell Tumor Properties In Vitro and In Vivo. In *Frontiers in oncology* 11, p. 666446. DOI: 10.3389/fonc.2021.666446.

Zhang, Jihong; Stevens, Malcolm F. G.; Bradshaw, Tracey D. (2012): Temozolomide: mechanisms of action, repair and resistance. In *Current molecular pharmacology* 5 (1), pp. 102–114. DOI: 10.2174/1874467211205010102.

Zhao, Y.; Hanton, W. K.; Lee, K. H. (1986): Antimalarial agents, 2. Artesunate, an inhibitor of cytochrome oxidase activity in Plasmodium berghei. In *Journal of natural products* 49 (1), pp. 139–142. DOI: 10.1021/np50043a018.

Zhou, Xuejian; Chen, Yu; Wang, Feifan; Wu, Hongshen; Zhang, Yan; Liu, Jiaxin et al. (2020): Artesunate induces autophagy dependent apoptosis through upregulating ROS and activating AMPK-mTOR-ULK1 axis in human bladder cancer cells. In *Chemico-biological interactions* 331, p. 109273. DOI: 10.1016/j.cbi.2020.109273.

Zhu, Yi; Doornebal, Ewald J.; Pirtskhalava, Tamar; Giorgadze, Nino; Wentworth, Mark; Fuhrmann-Stroissnigg, Heike et al. (2017): New agents that target senescent cells: the flavone, fisetin, and the BCL-XL inhibitors, A1331852 and A1155463. In *Aging (Albany NY)* 9 (3), pp. 955–963. DOI: 10.18632/aging.101202.

Zhu, Yi; Tchkonia, Tamara; Fuhrmann-Stroissnigg, Heike; Dai, Haiming M.; Ling, Yuanyuan Y.; Stout, Michael B. et al. (2016): Identification of a novel senolytic agent, navitoclax, targeting the Bcl-2 family of anti-apoptotic factors. In *Aging Cell* 15 (3), pp. 428–435. DOI: 10.1111/acel.12445.

8. Supplemental material

8.1. Supplemental figures

Quantification of cell death was performed by adding early apoptosis and late apoptosis/necrosis levels. Early apoptosis levels were determined by annexinV-FITC (aV) staining, while late apoptosis/necrosis levels were determined by aV and propidium iodine (PI) double-staining. First, a stained and untreated sample was measured for each cell line to adjust the gate settings. Treated samples were measured thereafter. Cell debris was removed by gating the forward scatter (FSC) and the side scatter (SSC). The same procedure was performed for the measurement of senescent cells. Supplemental figure S1 gives an example for a control sample (A), and a TMZ treated sample (B).

A

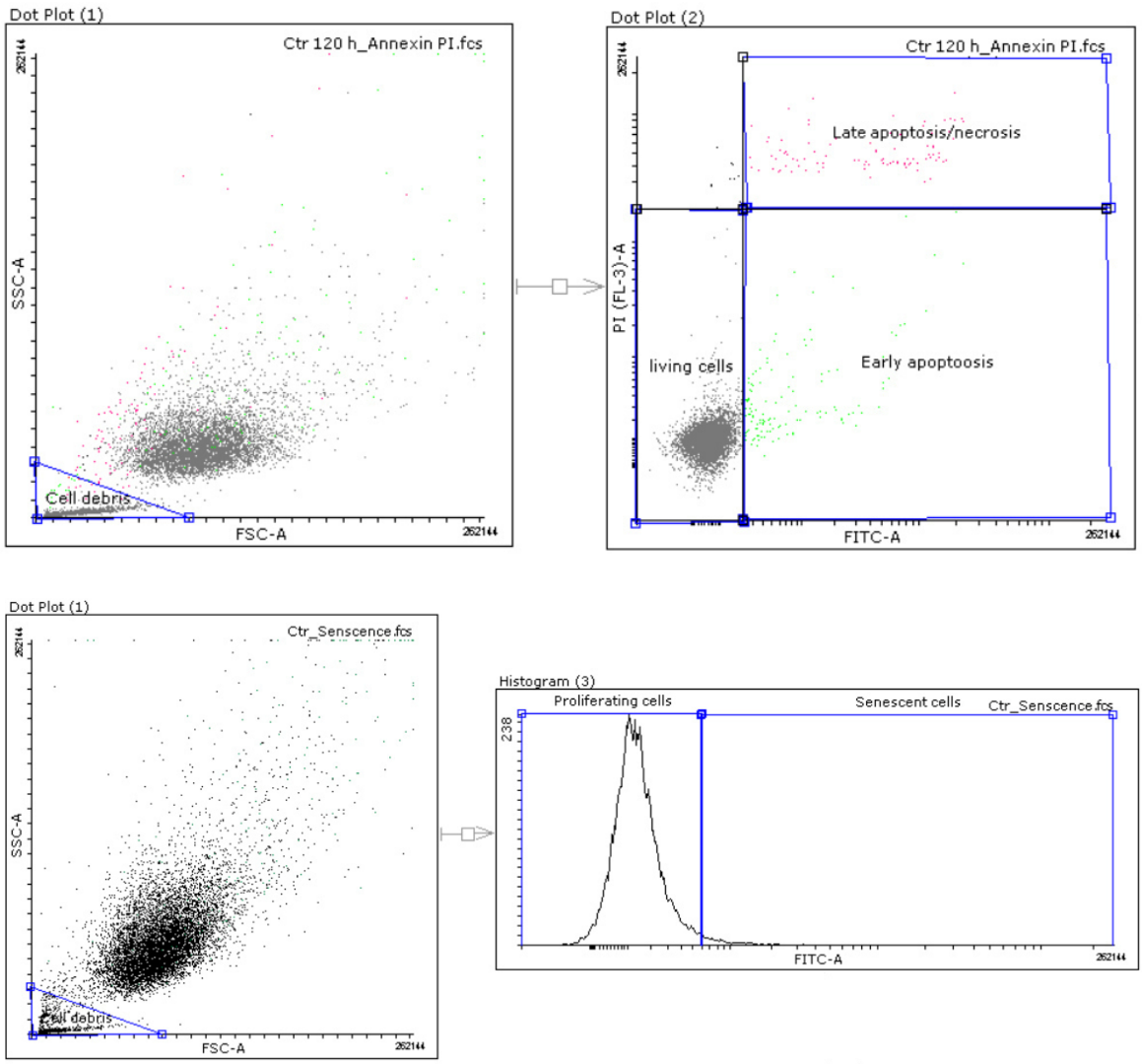

B

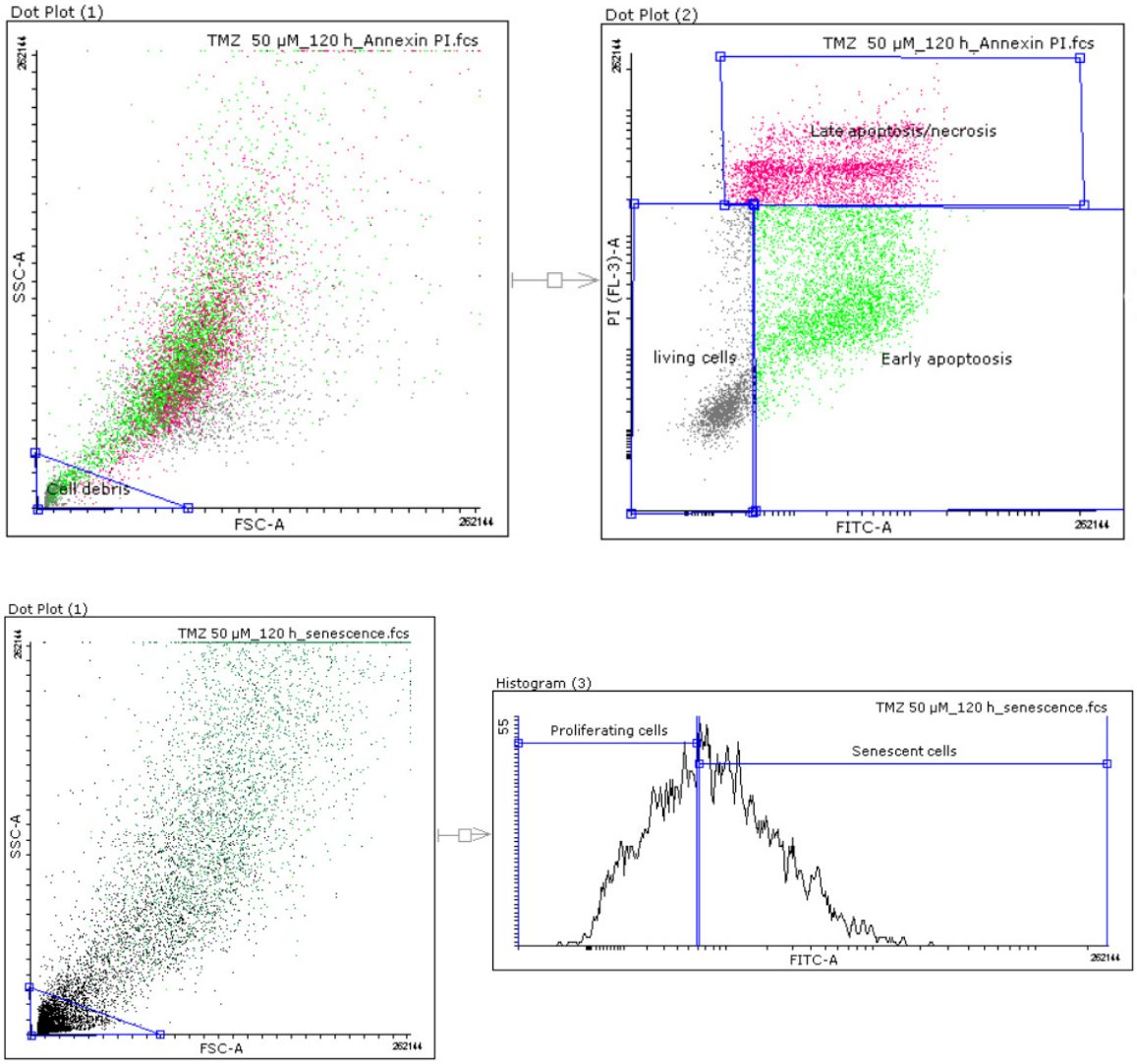

Supplemental figure S1: Gating for flowcytometric analysis of cell death and CSEN.

For the treatment with the inhibitors and natural components, we took care to use concentrations non-toxic on proliferating cells. The following graphs (Supplemental figure S2) demonstrate the non-toxic effect on proliferating GBM cells.

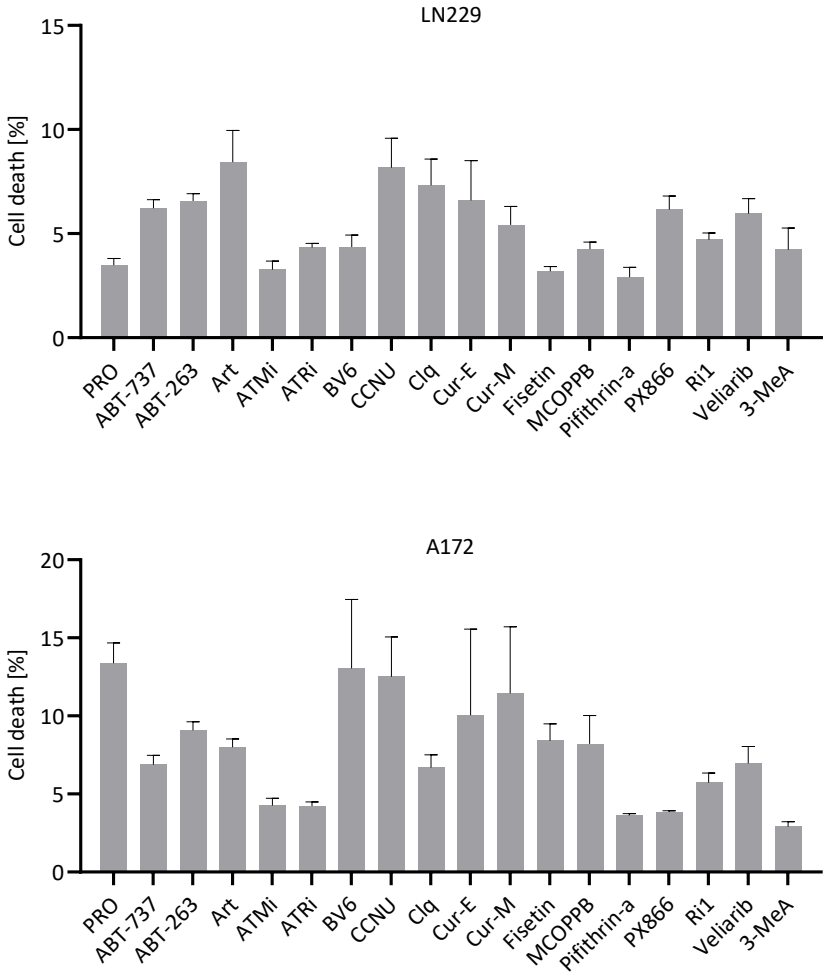

Supplemental figure S2: Cytotoxicity testing on proliferating cells.

The patient derived GBM tumours were tested for the methylation status of the MGMT-promotor through methylation-specific PCR, performed and kindly provided by Dr. Petra Leukel. The results are listed in the following table.

Supplemental table S1: Promotor methylation status of patient derived GBM tumours.

26-1	not tested
26-2	
35-1	UM
35-2	
36-1	UM
36-2	
44-1	M
44-2	
48-1	M
48-2	
51-1	UM
51-2	
57-1	UM
57-2	
58-1	UM
58-2	
59-1	M
59-2	
62-1	M
62-2	

8.2. ImageJ coding

For the quantification of foci following immunofluorescence staining, detected via LSM, a macro for automated nuclei and foci counting was used. For the assessment of colocalization, a colocalization plugin was installed and colocalizations were counted with the macro. The colocalization plugin can be downloaded on the website of the national institutes of health (https://imagej.nih.gov/ij/plugins/colocalization.html). It is provided by Pierre Bourdoncle from the Institut Jacques Monod, Service Imagerie, Paris.

8.2.1. Macro for nuclei and foci counting

```
macro "Finding Nuclei [q]" {
tit=getTitle();
run("Duplicate...", "title=Nuclei duplicate");
selectWindow("Nuclei");
run("Split Channels");
selectWindow("C1-"+"Nuclei");
close();
selectWindow("C2-"+"Nuclei");
close();
selectWindow("C3-"+"Nuclei");
run("8-bit");
run("Gaussian Blur...", "Sigma=3");
setAutoThreshold("Default");
run("Make Binary");
run("Invert");
run("Fill Holes");
run("Watershed");
run("Analyze Particles...", "size=0.00-Infinity circularity=0.00-1.00 show=Outlines add exclude include
in_situ");
rename("Nuclei_"+tit);
}


macro "Colocalization [w]"{
setBatchMode(true); //batch mode on
lo=1;                 //change parameters here
hi=20;
t=getTitle();
run("Duplicate...", "title=lo duplicate");
run("Duplicate...", "title=hi duplicate");
selectWindow("hi");
run("8-bit");
run("Gaussian Blur...", "radius="+hi+" stack");       //these settings will work for diffraction-limited
spots

selectWindow("lo");
run("8-bit");
run("Gaussian Blur...", "radius="+lo+ " stack");      //less noise if r=1, for example
imageCalculator("Subtract create stack", "lo","hi");
```

```
selectWindow("lo");
close();
selectWindow("hi");
close();
selectWindow("Result of lo");
rename("DoG_"+lo+"-"+hi+"_"+t);

//run("Enhance Contrast", "saturated=.1 normalize normalize_all use"); //this is optional !!


title = getTitle();
run("Split Channels");
selectWindow("C3-"+title);
close();

selectWindow("C1-"+title);
run("8-bit");
setThreshold(53,255);
run("Analyze Particles...", "size=0.00-200 circularity=0.00-1.00 show=Masks summarize");

selectWindow("C2-"+title);
run("8-bit");
setThreshold(107,255);
run("Analyze Particles...", "size=0.00-200 circularity=0.00-1.00 show=Masks summarize");


close("Results");
close("C1-"+title);
close("C2-"+title);
close("Mask of C1-"+title);
close("Mask of C2-"+title);

setBatchMode(false); //exit batch mode

selectWindow("ROI Manager");
}
```

8.3. List of tables

TABLE 1: LIST OF CHEMICALS AND CONSUMABLES. 25
TABLE 2: LIST OF TECHNICAL INSTRUMENTS. 26
TABLE 3: SOFTWARE LIST 28
TABLE 4: LIST OF BUFFERS AND SOLUTIONS. 28
TABLE 5: LIST OF PRIMARY ANTIBODIES. 30
TABLE 6: LIST OF SECONDARY ANTIBODIES. 31
TABLE 7: LIST OF DYES. 31
TABLE 8: CELL LINE CHARACTERISTICS. 32
TABLE 9: LIST OF NATURAL AND SMALL MOLECULE COMPOUNDS. 34

SUPPLEMENTAL TABLE S1: PROMOTOR METHYLATION STATUS OF PATIENT DERIVED GBM TUMOURS. ... 129

8.4. List of figures

FIGURE 1: EXEMPLARY MRI OF RE-OCCURRING GBM. 6
FIGURE 2: CONVERSION OF TMZ TO ITS ACTIVE FORM. 7
FIGURE 3: MOLECULAR STRUCTURES OF TMZ AND TRANSFORMED DNA BASES DUE TO TMZ TREATMENT. .. 9
FIGURE 4: TMZ-INDUCED TRANSITION MUTATIONS IN MMR DEFICIENT CELLS. 11
FIGURE 5: THE MIS-MATCH REPAIR SYSTEM IN HUMAN CELLS. 12
FIGURE 6: REPRESENTATION OF MORPHOLOGICAL CHANGES DURING APOPTOSIS. 14
FIGURE 7: ACTIVATION OF THE FAS INDUCED APOPTOTIC PATHWAY UPON DNA DAMAGE. 15
FIGURE 8: SCHEMATIC OF TMZ-INDUCED SENESCENCE IN GBM CELLS. 17
FIGURE 9: MOLECULAR STRUCTURES OF CCNU AND TRANSFORMED DNA BASES DUE TO CCNU TREATMENT. 18
FIGURE 10: INTERSTRAND CROSS LINK BETWEEN GUANINE AND CYTOSINE. 19
FIGURE 11: WESTERN BLOT ANALYSIS OF THE MGMT PROTEIN EXPRESSION. 44
FIGURE 12: REPRESENTATIVE IMAGES OF ΓH2AX AND 53BP1 FOCI DETECTED VIA LSM IN ONE NUCLEUS. .. 45
FIGURE 13: KINETICS OF TMZ-INDUCED DSBS. 46
FIGURE 14: KINETICS OF CELL DEATH AND SENESCENCE. 47
FIGURE 15: MORPHOLOGICAL AND BIO-MOLECULAR CHARACTERISTICS OF SENESCENT CELLS. 49
FIGURE 16: DSBS ARE PRESENT IN SENESCENT LN229 AND A172 CELLS. 50
FIGURE 17: REPRESENTATIVE IMAGES AND QUANTITATIVE ANALYSIS OF ΓH2AX AND TRF1 STAINING. 51
FIGURE 18: ACTIVE DDR IN SENESCENT LN229 AND A172 CELLS. 52
FIGURE 19: ACTIVE DNA REPAIR IN PROLIFERATING AND SENESCENT CELLS. 53
FIGURE 20: MGMT EXPRESSION IN SENESCENT CELLS LEADS TO DSBS REPAIR. 54
FIGURE 21: ROS AND OXIDATIVE DNA DAMAGE IN SENESCENT CELLS. 55
FIGURE 22: MICROSCOPIC ANALYSIS OF THE SENOLYTIC EFFECT OF ABT-737. 56
FIGURE 23: ABT-737 REDUCES CSEN IN GBM CELLS. 57
FIGURE 24: NAVITOCLAX REDUCES SENESCENCE IN LN229 BUT NOT A172 CELLS. 58
FIGURE 25: INHIBITION OF CIAP1/2 AND XAIP REDUCES SENESCENCE. 59
FIGURE 26: ATM AND ATR ARE NECESSARY FOR SENESCENCE MAINTENANCE. 60
FIGURE 27: INHIBITION OF DDR IN SENESCENT GMB CELLS. 61

FIGURE 28: ROLE OF NF-KB IN SENESCENCE MAINTENANCE. 62
FIGURE 29: DNA REPAIR MECHANISMS ARE NOT INVOLVED IN SENESCENCE MAINTENANCE. 63
FIGURE 30: INDUCTION OF MGMT FOLLOWING TMZ TREATMENT. 65
FIGURE 31: AUTOPHAGY MAINTAINS SENESCENCE IN LN229 AND A172 CELLS. 67
FIGURE 32: EFFECT OF PI3K INHIBITION IN SENESCENT GBM CELLS. 68
FIGURE 33: DOSE-RESPONSE OF IR. 69
FIGURE 34: RT HAS AN ADDITIVE EFFECT ON TMZ TREATMENT. 70
FIGURE 35: EFFECT OF IR ON SENESCENT LN229 CELLS. 71
FIGURE 36: CCNU HAS NO SENOLYTIC ACTIVITY IN GBM. 72
FIGURE 37: CYTOTOXICITY OF MTD INCREASES WITH DOSE. 74
FIGURE 38: ROLE OF MOR IN MTD INDUCED CELL DEATH. 75
FIGURE 39: MTD DOES NOT INDUCE DSBS. 76
FIGURE 40: EFFECTS OF MTD ON TMZ-INDUCED CELL DEATH. 78
FIGURE 41: EFFECT OF MTD ON TMZ-INDUCED SENESCENCE. 79
FIGURE 42: EFFECT OF MCOPPB ON SENESCENT GBM CELLS. 80
FIGURE 43: SENOLYTIC EFFECT OF ARTESUNATE ON GBM CELLS. 81
FIGURE 44: CURCUMIN INDUCES CELL DEATH DOSE-DEPENDENTLY. 83
FIGURE 45: INDUCTION OF DSBS FOLLOWING CURCUMIN TREATMENT. 84
FIGURE 46: EFFECTS OF SHORT-TERM TREATMENT WITH CURCUMIN. 85
FIGURE 47: EFFECT OF CURCUMIN ON SENESCENT GBM CELLS. 87
FIGURE 48: SENOLYTIC ACTIVITY OF FISETIN. 89
FIGURE 49: EXEMPLARY PICTURES OF PRIMARY AND RECURRENT PATIENT DERIVED GBM TUMOUR SAMPLES 90
FIGURE 50: IN SITU ANALYSIS OF SENESCENCE AND APOPTOSIS MARKERS. 91

SUPPLEMENTAL FIGURE S1: GATING FOR FLOWCYTOMETRIC ANALYSIS OF CELL DEATH AND CSEN. 127
SUPPLEMENTAL FIGURE S2: CYTOTOXICITY TESTING ON PROLIFERATING CELLS. 128

8.5. List of abbreviations

8-oxo-G	8-Oxo-7,8-dihydroguanine
AIC	5-aminoimidazole-4-carboxamid
ATCC	American type culture collection
ATM	Ataxia telangiectasia mutated
ATR	Ataxia telangiectasia and Rad3-related protein
AV	AnnexinV-FITC
Bcl-2	B-cell lymphoma-2
BER	Base excision repair
BIF	Brain interstitial fluid
BSA	Bovine serum albumin
C12FDG	5-Dodecanoylaminofluorescein-di-β-D-galactopyranoside
Caspase	Cysteinyl-aspartate specific protease
CBTRUS	Central brain tumour registry of the United States
CCNU	N-(2-chloroethyl)-N'-cyclohexyl-N-nitrosourea (Lomustine)
CDC25c	Cell division cycle phosphatase 25c
CHK1	Checkpoint kinase
Clq	Chloroquine
CpG	Cytosine-phosphate-guanine
CSEN	Cellular senescence
ddH_2O	double-distilled water
DDR	DNA damage response
DMEM	Dulbecco's Modified Eagle Medium
DMSO	Dimethyl sulfoxide
DNA	Deoxyribonucleic acid
Dox	Doxycycline
DR	Death receptor
DSB	DNA double-strand break
DTIC	5-(3,3-Dimethyl-1-triazenyl)imidazole-4108-carboxamid
DTT	Dithiothreitol
EDTA	Ethylenediaminetetraacetic acid

Exo1	Exonuclease 1
FCS	foetal calf serum
FITC	Fluorescein-isothiocyanate
FPG	Formamidopyrimidine glycosylase
GBM	Glioblastoma
GCi	Gammacell irradiator
HIPK2	homeodomain interacting protein kinase 2
HR	Homologous recombination
ICL	Inter-strand cross link
IDH1	Isocitrate dehydrogenase 1
IR	Ionizing radiation
i.v.	Intravenous
LMP	Low melting point
LSM	Laser scanning Microscope
MCOPPB	1-[1-(1-Methylcyclooctyl)-4-piperidinyl]-2-[(3R)-3-piperidinyl]-1H-benzimidazole
MGMT	O^6-methylguanine-DNA methyltransferase
MMR	Mismatch repair
MOR	µ-opioid receprot
MRI	magnetic resonance imaging
MRN	MRE11, RAD51, NBS1
mt	Mutated
MTD	Methadone
MTIC	3-methyl-(triazen-1-yl)imidazole-4-carboximide
MTT	3-(4,5-dimethylthiazol-2-yl)-2,5-diphenyltetrazolium bromide
N3meG	N3-methyl adenine
N7meG	N7-methyl guanine
Nalx	Naloxone
NER	Nucleotide excision repair
NF-kB	Nuclear factor-kB
NHEJ	Nonhomologous-end-joining

NRF2	Nuclear factor erythroid 2-related factor 2
O^6meG	O^6-methylguanine
OS	Overall survival
PAGE	Polyacrylamide gel electrophoresis
PBS	Phosphate buffered saline
PFA	Paraformaldehyde
PFS	Progression free survival
PI	Propidium iodide
PI3K	Phosphoinositide 3-kinases
Pif-α	Pifithrin-α
Pif-μ	Pifithrin-μ
PMSF	Phenylmethanesulfonylfluoride
PS	Phosphatidylserine
PTEN	Phosphatase and tensin homolog
ROS	Reactive oxygen species
RPA	Replication protein A
rpm	Rounds per minute
RT	Room temperature
SASP	Senescence associated secretory phenotype
SA- β-gal	Senescence associated β-galactosidase
SCGE	Single cell gel electrophoresis
SDS	Sodium dodecyl sulphate
SEM	Standard error of the mean
SIAH1	E3 ubiquitin ligase seven in absentia homolog 1
SSBs	Single-strand breaks
ssDNA	Single-stranded DNA
TBS	TRIS-buffered saline
TBS-T	TBS with 0.1 % Tween-20
TEMED	Tetramethyl ethylenediamine
TMZ	Temozolomide
Trf1	Telomeric repeat-binding factor 2

TRIS	Tris(hydroxymethyl)aminomethane
UV	Ultraviolet
WHO	World health organization
wt	wild type
X-Gal	5-Bromo-4-chloro-3-inodyl galactopyranoside
γH2AX	Phosphorylated histone 2AX

8.6. List of publications

The data presented in this thesis and additional data were published in the following journals:

Kaina B, **Beltzig L**, Piee-Staffa A, Haas B. Cytotoxic and Senolytic Effects of Methadone in Combination with Temozolomide in Glioblastoma Cells. Int J Mol Sci. 2020 Sep 23;21(19):7006. doi: 10.3390/ijms21197006 . PMID: 32977591 ; PMCID: PMC7582495.

Beltzig L, Frumkina A, Schwarzenbach C, Kaina B. Cytotoxic, Genotoxic and Senolytic Potential of Native and Micellar Curcumin. Nutrients. 2021 Jul 13;13(7):2385. doi: 10.3390/nu13072385 . PMID: 34371895 ; PMCID: PMC8308652.

Schwarzenbach C, Tatsch L, Brandstetter Vilar J, Rasenberger B, **Beltzig L**, Kaina B, Tomicic MT, Christmann M. Targeting c-IAP1, c-IAP2, and Bcl-2 Eliminates Senescent Glioblastoma Cells Following Temozolomide Treatment. Cancers (Basel). 2021 Jul 17;13(14):3585. doi: 10.3390/cancers13143585. PMID: 34298797; PMCID: PMC8306656.

Stratenwerth B, Geisen SM, He Y, **Beltzig L**, Sturla SJ, Kaina B. Molecular Dosimetry of Temozolomide: Quantification of Critical Lesions, Correlation to Cell Death Responses, and Threshold Doses. Mol Cancer Ther. 2021 Oct;20(10):1789-1799. doi: 10.1158/1535-7163.MCT-21-0228. Epub 2021 Jul 12. PMID: 34253592.

Beltzig L, Stratenwerth B, Kaina B. Accumulation of Temozolomide-Induced Apoptosis, Senescence and DNA Damage by Metronomic Dose Schedule: A Proof-of-Principle Study with Glioblastoma Cells. Cancers (Basel). 2021 Dec 14;13(24):6287. doi: 10.3390/cancers13246287. PMID: 34944906; PMCID: PMC8699541.

Beltzig L, Schwarzenbach C, Leukel P, Frauenknecht KBM, Sommer C, Tancredi A, Hegi ME, Christmann M, Kaina B. Senescence Is the Main Trait Induced by Temozolomide in Glioblastoma Cells. Cancers (Basel). 2022 Apr 29;14(9):2233. doi: 10.3390/cancers14092233 PMID: 35565362; PMCID: PMC9102829.

Kaina B, **Beltzig L**, Strik H. Temozolomide - Just a Radiosensitizer? Front Oncol. 2022 Jun 16;12:912821. doi: 10.3389/fonc.2022.912821 Titel anhand dieser DOI in Citavi-Projekt übernehmen. PMID: 35785203 Titel anhand dieser Pubmed-ID in Citavi-Projekt übernehmen; PMCID: PMC9246413.

Beltzig L, Christmann M, Kaina B. Abrogation of Cellular Senescence Induced by Temozolomide in Glioblastoma Cells: Search for Senolytics. Cells. 2022 Aug 19;11(16):2588. doi: 10.3390/cells11162588 PMID: 36010664; PMCID: PMC9406955.

8.7. Acknowledgement

In this way I would like to acknowledge everyone who participated in the completion of my doctoral thesis.

First, I would like to thank Prof. Dr. Bernd Kaina for assigning the fascinating research topic I was allowed to work on, and the opportunity to perform my doctoral thesis at the Institute of Toxicology. His valuable suggestions and expertise have helped me to successfully complete my work. The constant effort he showed gave me the motivation I needed to persevere, and his understanding of my sports activities helped me to get through stressful periods. I will always remember his dedication to science, and I am deeply grateful to have worked under his supervision.

My gratitude also goes to Prof. Dr. Thomas Hofmann, for his support without which it would not have been possible for me to perform my doctoral thesis at the Institute of Toxicology.

I would also like to thank my second supervisor Prof. Dr. Bernhard Lieb for his valuable advice and the time he invested in my doctoral thesis. I also thank our cooperation partners Prof. Dr. Clemens Sommer and Dr. Petra Leukel from the Institute of Neuropathology of the University Medical Center Mainz for providing and staining the patient derived tumour samples, as well as Prof. Dr. Monika Hegi and her co-worker Alessandro Tancredi from the Neuroscience Research Center and Neurosurgery of the Lausanne University for providing the MGMT inducible cell lines.

I also thank Dr. Wynand Roos and Prof. Dr. Markus Christmann who (almost) always had an answer for my questions and who shared not only expertise but also lab resources. With friendly conversations in between work, they made the institute a pleasant working place. I will never forget this special support that helped me to complete my experiments successfully.

Special thanks goes to Birgit Rasenberger, who always shared her practical experience, and through it supported me in my experiments, and to Anna Frumkina for her excellent work with the comet assays. I also thank our institute manager Paula Vinhais who relentlessly took care of purchase orders and stationery requests and found time for all other requests, and Guiseppina Etari who continuously took care of cleaning, preparing, and sterilising all the hardware needed for completing my experiments.

My colleagues and friends, I would like to thank for the lunch sessions, coffee breaks and all the sportive activities after work. They gave me the necessary breaks to recharge and endure. With their mental support and motivation, they helped me through this tough time.

Finally, I would like to express my deepest gratitude to my family for all the love and dedication, the support, and the trust they have shown me. Without them I would never have been able to get so far and to complete my doctoral thesis.

8.8. Eidesstattliche Erklärung

Die in der vorliegenden Arbeit vorgestellten Daten wurden experimentell am Institut für Toxikologie der Universitätsmedizin der Johannes-Gutenberg-Universität Mainz im Zeitraum vom 01.10.2018 bis 30.04.2022 unter der Betreuung von Prof. Dr. Bernd Kaina erhoben.

Die Daten der vorliegenden Arbeit, sowie weiterführende Daten wurden bereits in Publikationen veröffentlich. Eine Liste der Publikationen finden sich in Kapitel 8.6 dieser Arbeit.

Hiermit versichere ich, dass ich die vorliegende Arbeit selbstständig verfasst, und alle verwendeten Quellen und Hilfsmittel, sowie Kooperations-Partner angegeben habe.

_____ _____

Ort, Datum Lea Beltzig

Lea C. Beltzig

M. Sc. Biologie

lea.beltzig@uni-mainz.de
+4915730887416
Forsterst. 40, 55118 Mainz
07.12.1991, Seeheim-Jugenheim

FÄHIGKEITEN

Deutsch ■■■■■
Englisch ■■■■□

MS Office ■■■■□
SAP ■■□□□

Teamleiter ■■□□□

METHODEN

Zellkultur
Durchflusszytometrie
Western Blot
LSM
PCR
Comet Assay
IPMA
Tierexperimentelle Arbeiten

STÄRKEN

Selbstständiges und eigenverantwortliches Arbeiten

Konflikt-Fähigkeit

Positives Mindset

Anpack-Mentalität

INTERESSEN

Teamarbeit

Arbeit mit

Ehrenamt

Sport

Reisen

Ausbildung und Praktische Erfahrung

Seit 12/2022
Fortbildung Life Science Manager
Gesundheitsakademie Hessen
Pharmakoökonomie, QMB

Seit 10/2018
Doktorand in Biologie
Institut für Toxikologie an der Universitätsmedizin der JGU, Mainz

05/2018
Abschluss M. Sc. Biologie
JGU, Mainz

01 – 12/2017
Arbeiten im Service:
Teamleitererfahrung, Arbeiten in 5-Sterne Hotels, Betreuung von Firmenjubiläen, politische Veranstaltungen, Hochzeiten

06/2016 – 09/2017
Arbeiten im Service:
Teamleitererfahrung, Schichtenplanung, Ansprechpartner für Probleme und Fragen

07 – 10/2016
Werkstudent
Abteilung Bioanalytik, Biotest AG, Dreieich
Arbeiten im GMP regulierten Bereich

08/2015 – 03/2016
Auslandsaufenthalt
Work and travel

08/2015
Abschluss B. Sc. Biologie
Universität Konstanz

03/2015 – 05/2015
Werkstudent
Abteilung Bioanalytik, Biotest AG, Dreieich
Arbeiten im GMP regulierten Bereich

Mainz, 01.02.2023